eman ta zabal zazu
Universidad del País Vasco
Euskal Herriko Unibertsitatea

# *Combined micropatterning of cells, biosensors and nanomaterials: towards integrated microsystems for cell monitoring*

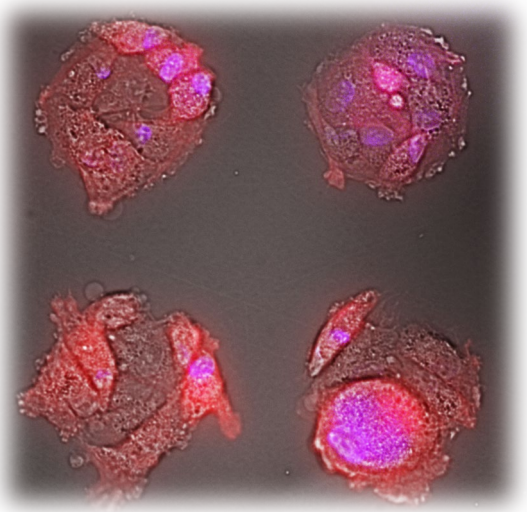

Enrique Azuaje Hualde

Vitoria-Gasteiz, 2021

Microfluidics Cluster UPV/EHU

eman ta zabal zazu
Universidad del País Vasco
Euskal Herriko Unibertsitatea

# Combined micropatterning of cells, biosensors and nanomaterials: towards integrated microsystems for cell monitoring

**Enrique Azuaje Hualde**

Vitoria-Gasteiz, 2021

**Agradecimientos**

Tras todos estos años de esfuerzo por llegar aquí, me gustaría agradecer a aquellas personas que me han ayudado y apoyado durante este viaje.

Me gustaría comenzar agradeciendo a mis directoras, Marian y Lourdes, por la confianza puesta en mí y todo lo que me habéis enseñado. Marian, siempre te agradeceré el que apostases por mí cuando más lo necesitaba, y el apoyo y los ánimos constantes que he recibido por tu parte durante todo el doctorado. Lourdes, agradecerte primero la paciencia que has tenido conmigo todo este tiempo. Gracias por guiarme y preocuparte de que explotase mi potencial. Pero sobretodo, gracias por enseñarme que las ideas que consideraba locas e imposibles no eran tan locas e imposibles. Esta tesis no sería igual sin esa visión tuya, gracias por seguir apostando en mí.

Seguidamente, me gustaría agradecer a mis compañeros de viaje, el Cluster de Microfluídica. Empezar por mi tercer co-director no oficial, Fernando. Gracias por todo el asesoramiento técnico y científico, por todas las cuestiones que me has sabido responder, por meterme en el mundo de la microfluídica de papel y por la emoción que trasfieres cuando hablamos de ciencia. Gracias a aquellas con las que empecé este viaje, Maite, Jaione, Janire y Tugçe, y a los PostDoc que vivieron y se fueron, Javi y Edi. Mucho ha llovido desde entonces, pero todos a vuestra manera habéis dejado vuestro granito de arena en el grupo. Gracias a Susana por soportarme como supervisor, tienes el cielo ganado. Gracias a los que han ido llegando, Jon, Raquel, Udara y Vahid, os deseo lo mejor en vuestro doctorado. Me gustaría dar las gracias especialmente a las que pasaron de compañeras a amigas durante estos años. Sandra, Alba y Yara, apenas tengo palabras para agradeceros todo lo que habéis sido para mí. Gracias por toda la ayuda personal y profesional. Gracias por hacerme reír tantísimas veces y no matarme cada vez que me dejo un guante sin tirar o me llevo las llaves a casa. Habéis sido mis compañeras de risas y lágrimas, y sin duda una de las partes más fundamentales de estos últimos años. Simplemente, gracias a las tres por haber estado ahí.

Por otro lado, me gustaría agradecer a los demás grupos de investigación con los que he podido trabajar durante esta tesis. Primero, gracias al grupo

BIOS por darme la oportunidad de hacer mis estancias predoctorales en sus instalaciones, incluso en tiempos de pandemia. I would like to thank Professors Andries van der Meer and Albert van den Berg for inviting to be a part of their group during my secondment. Job, thank you very much all your support and for caring about my well-being during my stay. Gracias al grupo de BIOMICS, en especial a Maite y a Eva, por todo el asesoramiento científico ofrecido durante esta tesis. Me gustaría agradecer también a todos los investigadores e investigadoras que me han acompañado fuera del laboratorio durante este periodo. A todos los que comíamos los jueves juntos, gracias por cada comida, cena, café... En especial, dar las gracias a Julen, Itziar y Mónica. Me habéis dado algunos de los momentos más divertidos de mi vida. Pero sobretodo, gracias por animarme cuando más lo necesitaba.

Gracias a todos los que, sin entender mucho lo que es un doctorado, habéis estado ahí apoyándome. Tía Gema, Izarchu, Abril, Vicky, Ángel y Rubén, aunque me consideréis el eterno estudiante, gracias por estar ahí cuando lo he necesitado. Gracias a mi familia de la carrera, David, Joseba, Maixa, Alba y Laura, por soportar tantos años oyéndome hablar de que quería hacer un doctorado y apoyarme siempre en mi camino. Gracias a mis amigos de toda la vida, Floren, Gerardo, Isabel y Harold, por sacarme fuera de mi burbuja, preocuparos por mi bienestar y estar incluso más emocionados que yo de esta etapa final.

Finalmente, me gustaría agradecer a aquellas personas sin las cuales no me habría sido posible llegar a donde estoy.

Ainho, gracias por todo. Has sido mi guía científica, administrativa y personal. Eres la persona más especial que me llevo de mi vida investigadora. Recordar mi tesis es recordar viajes, conciertos y salas de escape contigo, que espero podamos repetir muchas veces más en el futuro. Sergio y tú me hicisteis sentir Vitoria no como la ciudad donde vivía si no como mi hogar. Iñigo, gracias por estar ahí. Llegaste en un momento difícil y decidiste quedarte y apoyarme. Gracias por acompañarme en este viaje, por darme más de lo imaginable y aguantarme cuando no lo merecía. Gracias por quedarte cuando lo necesitaba. Pero sobretodo, gracias por seguir motivándome cada día a que siga adelante.

Arantza, aunque no siempre entiendas lo que hago, gracias por apoyarme a mí y a la familia y permitirme cumplir mi sueño. Papá, por muy dura que fuese esta primera etapa sin ti, gracias por seguir aquí guiándome con todo lo que me enseñaste. Mamá, gracias por inculcarme el querer superarme y que el saber no ocupa lugar. Gracias por motivarme a que siempre siga la lucha por conseguir lo que quiero y enorgullecerte de lo conseguido.

Muchísimas gracias a todos.

*Let me feel proud when it's over*

# Index

# Section 1

## Thesis overview

# Introduction

## General introduction

Cells are the most fundamental biological structures present in all living forms, being the core of the most simplistic organisms as well as the individual and differentiated building units of greater structures in multicellular beings. For such reason, understanding and replicating the intricate physiological and pathological pathways cells undergo in a lifespan as well as the different ways cells interact with their surroundings is of key importance in sight of the research in several areas, including cellular, molecular, developmental and biomedical biology [1].

While complex living beings such as mammals present several layers of cell distribution and arrangement, including the formation of cellular tissues and whole organs, sometimes it is desirable to study a specific cell type on its own. As a result, cell culture raised as the most acknowledged and optimal methodology to achieve these goals. In brief, this process is based on the growth of cells isolated from living tissues on suitable vessels made of materials presenting good biocompatibility and cell adherence characteristic in controlled conditions of nutrients, growth factors, $O_2$ and $CO_2$ supply. This has proven to be an excellent tool to study cell behavior, allowing the analysis of cell growth, proliferation and migration as well as biochemical changes inside of the cell, with direct applicability on a wide range of research areas including but not limited to toxicology, medicine and pharmaceutics [2].

However, cell culture on its core presents a series of limitations that are usually oversighted but carry a big importance in the study of cells. To begin with, regular cell cultures do not achieve a great level of control regarding the binding or spreading of the cells to the substrate, leading to cell studies where the cell shape, size or orientation may not be representative of the state of the cell in physiological conditions. More importantly, regular cell cultures lack a good control of the specific interactions a cell produces with its surroundings, which greatly affect cell behavior. In physiological conditions, cells are in constant interaction with the extracellular matrix (ECM) around them and with other cells trough both soluble chemical signals and physical cell-cell contact. While complementary *in vivo* studies are carried out to study

cell response in physiological conditions and as part of the whole organism, there is still potential in the development of novel cell culture platforms and methodologies that allow greater control over cell interactions. This could lead to an approximation of *in vitro* cell studies to real, physiological conditions [3].

In that sense, over the past years several strategies and research areas have arisen as possible solutions to the limitations previously listed. One of the most important areas in these regards have been the development and research on materials and biomaterials alike for the fabrication of cell culture systems with improved control over cell deposition and cell interactions. This mostly includes the development of novel gel-like materials for the imitation of the ECM, primary used for the generation of cell capsules and scaffolds, and the biochemical functionalization and modifications of solid materials aimed to control cell interactions [4]. This has led to the development of several platforms with very distinct applications, including the control of growth, differentiation and stimulation of cells and the controlled release of drugs and factors, among others [5]. Another hot area of research includes the patterning of cells for the controlled deposition of the cells in the substrate, subsequently allowing to control the distance between cells and their interactions, their orientation and the isolation of them if desirable. This is usually achieved by the patterning of cell adhesion proteins, enabling the control over the cell-material interactions, although other physical methods have also been widely used to generate a cell pattern. Furthermore, the patterning functions as a method to generate a high number of isolated cell culture events, making it possible to increase the analytical data obtained from a single sample [6].

While the aforementioned research areas are constantly evolving, the use of novel materials and analytical devices is minimal in comparison with the use of regular methodologies for cell culture. Furthermore, novel methods usually only address specific shortcomings regarding the control of the cell culture and still present some degree of complexity, downgrading the benefits for its day-to-day use [7]. On top of that, most cell and cell secretion monitoring methodologies, i.e. immunocytochemistry, ELISA and flow cytometry, are end-of-assay techniques and are not truly implemented within the cell culture, usually requiring cell fixation, cell detachment or cell medium removal which

by definition alter the state of the culture [8]. This generates a disjunctive between the control aimed for the culture and the active interruption of the controlled conditions for the analysis. In this regard, a potential area of research arises with the aim to obtain biosensors that can be adapted to controlled cell culture (integrated sensors), that reduce the number of invasive steps required for the analysis of the cells and their secretion (label-free sensors) and that enable the continuous monitoring of the outcome through the entirety of the assay (real-time sensors) [9]. However, there are very few examples of fully integrated platforms so far that allow both the monitoring of cell processes, especially cell secretion, and the control of cell microenvironments. Furthermore, the recent monitoring systems that have arisen have focused on very specific cell models, barely considering other factors that influence cell behaviors, and are not customizable and adaptable to varied cell contexts. For the future, it is desirable to concentrate the efforts on the development of multifunctional devices and platforms that will overcome the limitations present in conventional cell cultures, giving both good control over the state of the cells and their interactions and a well-integrated and not invasive monitoring and analysis.

# State of the art

## Background

Cells interact with a complex microenvironment, as in the case of mammal and human cells. This generates an interest in upgrading current methodologies for cell culture research and in developing new technologies that allow better replication of cell microenvironments, in order to approximate *in vitro* studies to the real physiological conditions [10]. The generation of novel, versatile cell culture systems designed to provide tight control over cell microenvironments is expected to have a huge impact on a wide variety of areas. The approximation of the *in vitro* models to *in vivo* models would lead to a reduction on the animal use for experimentation, a milestone highly looked after in near future [11,12]. Furthermore, these new technologies are key components in the progress of personalized medicine. From applying complex cell environments in drug testing to the manipulation of patient derived cells for diagnosis and therapy development, the possibilities are nearly endless [13,14].

On one side of this quest, many technologies have arisen that aim to improve the control over cell culture microenvironments and the numerous cell interactions. Isolation of cells for the single cell analysis of heterogeneous samples, patterning of cells for the control of cell-material and cell-cell interactions, generation of 3D cultures using novel biomaterials or the replication of whole physiological systems on chips are only a glimpse of what has been achieved so far and what is to come [5,6,10,15,16]. On the other side of this, new analytical methodologies and technologies developed for the monitoring of cell cultures are also a hot topic. Generating label-free, real-time cell monitoring techniques is a goal in this area. It is when these two sides meet where complexity heavily increases. For the most part, conventional methodologies for cell monitoring are highly invasive or end-of-assay. Incorporating sensors within a platform that do not interfere with the microenvironment control is enormously changeling. Furthermore, the complexity of the technologies proposed so far prevents its daily use in the clinical and research fields [9,17–19].

Not all cell processes offer the same level of challenge in prospect of the incorporation of their monitoring into a cell culture platform. Physical changes that can be observed in the cell, such as cell morphology, size or motility, among others, can be easily implemented as long as the materials selected and the design of the device allow the optical observation of the cells [20–23]. Monitoring of internal cell processes, while more challenging due to the requirement of dyes or electrochemical setups, has also been regularly accomplished in complex systems in a non-invasive, non-destructive way. DNA transcription and replication, protein expression, enzymatic activity, organelles and microtubules behavior and even intracellular mobilization of cations can all be easily monitored, once again, by the proper adaptation of the device [24–29]. When it comes to the detection and monitoring of cell secreted molecules, technical difficulties rapidly appear. The complexity of the sensoring elements required for the capture, recognition and transduction of a biomolecule into a signal hinders their implementation inside of a multifactorial microenvironment. Furthermore, localizing each sensor on the proximity of the desired secretor and achieving the sensitivity required for the detection of very low concentrations of each biomolecule is not an easy task. All of this generates important barriers on the development of integrated monitoring methods and technologies on complex, controlled microenvironments.

*Understanding cell secretion of signaling biomolecules*

Cells are in constant interaction with their surroundings and shape them in one form or another. One way the cells directly affect their microenvironment is through the emission of molecules generated intracellularly into the extracellular space. This can function as the removal of waste and other metabolic derivative products, process commonly known as excretion. However, cells also produce a massive number of biomolecules that participate at different levels in the construction, maintenance and regulation of the physiological system. This constitutes cell secretion, and is made of a wide variety of different chemical compounds with a varied range of functions.

Cell secretion can be classified following two principles. The first one depends on the distance the secreted biomolecule needs to travel, differentiating between autocrine secretion (the same cell will receive the secreted molecule), paracrine secretion (short distance outside the cell) or endocrine secretion (long distance inside of the organism). The second classification is based on the function that the biomolecule will take part off. Some biomolecules only serve structural purposes, others serve a regulatory roles on the organism, while others serve as signals for cell-cell communication [30].

This last group include a series of sub-groups of cell-secreted signaling biomolecules such as cytokines, growth factors and hormones, which play critical roles in controlling the cells' behaviors and regulating full systems on the organisms. The interest in being able to monitor cell secretion under controlled environments that replicate physiological conditions is clear, as the amount and nature of information that studying and analyzing cell secretion can offer is huge. Proper typifying and characterization of cell's secretion can offer a lot of insight on cell's mechanism, especially when it is subdue to a wide variety of stimuli. In practice, the detection, identification and quantification of cell secretion in the form of biomarkers is essential for diagnosis, prognosis and evaluation of pathological behaviors in cells [31,32].

*The concept of biosensor*

Conventional non-cell-destructive methodologies for monitoring of cell culture secreted signaling molecules include, but are not limited to, fluorescence immunoassays and mass spectroscopy. In most cases, analysis of cell secretion is carried out in completely separated units, removing cell supernatant from the culture vessels and analyzing it in the materials and equipment required for each methodology. This presents a series of limitations, including the incapability to address the secretion dynamics of specific cells in complex cell cultures and the large volume in which the analyte is diluted. Taking all into account, the core of the current investigations lies in the development of biosensors that can be fully integrated within a cell culture platform, showcasing high specificity and

sensitivity for the target molecule, and that neither interfere nor get affected by the complex nature of the cell's microenvironment [18,33].

A biosensor is a device that measures biological or chemical reactions by generating signals proportional to the concentration of an analyte in the reaction. It consist of a formed system that enables the capture of an analyte, in this case a cell secreted biomolecule, and the production of an appreciable and, quantifiable signal that can be correlated with the presence and the quantity of the biomolecule. From the conventional biosensing techniques to the most novel analytical devices, biosensors usually requires the use of similar modules whether they come as separated components and equipment or are integrated on a single unit. For the capture of the biomolecule, a bioreceptor is regularly required in some capacity. This part, usually another biochemical compound, binds specifically to the target analyte. After capture, the production of a signal is required to mark the presence of the successfully bound biomolecule. This can be achieved either by the interaction between the analyte and the bioreceptor itself or by the addition of secondary labels. Once a signal is produced, a transducer component (which converts the signal produced into a measurable signal), a display component (which presents the user the results of the analysis) and an electronic component that binds both are commonly required to complete the biosensor [34].

The amount and variety of elements used and implemented differ considerably between modules. Bioreceptors used in newer detection technologies are still very similar to those applied in conventional methodologies. When it comes to monitoring of signaling biomolecules, for example cytokines and growth factors, antibodies are used in the majority of cases. The easiness in their production, their market availability, and the confidence in their specificity makes them the gold standard as bioreceptors even today [35]. Other types of bioreceptors based on specific protein-protein, protein-enzyme and protein-lectin interactions have been thoughtfully explored. Their advantages include their reduced molecular weight in comparison to antibodies, which allows a higher density of receptors in the same place and the reduced cost of their production [34,36,37]. However, finding bioreceptors with specificity for each secreted signaling biomolecule is not an

easy task, and vastly undermines their use. In the recent years, synthetic DNA probes such as aptamers have arisen as potential bioreceptors. They have proven to be very specific for a wide range of chemical and biochemical molecules, comparing their binding capacities to that of the antibodies. They also present a series of advantages that no other type of bioreceptor does, including their low molecular weight, their low-cost and easy production, the easy manipulation of their sequence in order to control their specificity and the higher stability they present in comparison to proteins [38–40].

When it comes to the production of the signal that indicates the recognition and capture of the biomolecule, the focus has drifted into different perspectives. Directly coming from conventional cell culture monitoring technologies, fluorescence based detection systems have been heavily used in cell secretion biosensors. The easiness in differentiating between fluorescence presence and intensities related to the different quantities of the biomolecules allows their simple detection and quantification [41,42]. In the look-out for label-free biosensors, new methodologies have arisen. Optical label-free detection has been widely explored, which includes but is not limited to Surface Plasmon Resonance and Surface Enhanced Raman Spectroscopy. These methods are based on the observation of specific changes of physical phenomena such as light scattering or molecular vibration that can be correlated with the presence and quantity of an analyte [43,44]. Electrochemical detection has also been heavily explored for the new age of cell secretion biosensing. They are based on the transduction of the biochemical event into an electrical signal, which can be a change in current, voltage or impedance, among others [33,45]. Finally, calorimetric-based and magnetic-based detection methods have also been proposed and explored to a lesser degree [46].

Depending on the most desirable outcome when monitoring complex cell cultures, different combinations of the previously presented bioreceptors and signals can be applied, as no one of them is ideal. While antibodies are a safe choice as bioreceptors, especially in platforms aimed for multiplexed analysis of a wide variety of cell secreted biomolecules, synthetic DNA probes, such as DNAzymes and Structure Switching Signaling Aptamers [47,48], may potentially be a better option as they do not require the addition of a

secondary label to produce a quantifiable signal. However, when looking for label-free monitoring in general, electrochemical and optical biosensing arise as better approaches, as they, by definition, allow the label-free recognition of secreted biomolecules just by measuring the physical phenomena that occur when the analyte is captured in the sensing component. Yet, these methods present their own set of limitations, including the difficulty on detecting multiple analytes on a confined space [49,50]. This may explain why fluorescence and luminescence based detection methods remain the most suitable detection strategies to incorporate into a multifactorial cell culture platform. In all, a consensus has not been reached on what type of biosensor is the most suitable for the wider range of scenarios, and for now, different options for biosensing must be ponder for each case.

**Platforms for cell culture secretion monitoring**

In the recent years, the development of systems for the monitoring of cell cultures has increased exponentially. For example, more than half of the articles in this revision, which covers the most prominent systems that integrate sensoring of cell secretion in the last 5 years, were published from 2019 onwards. This could be attributed to a series of factors.

On the one hand, the exploration of microfluidics and lab-on-a-chip devices has allowed the generation of intricate systems with infinite possible configurations of cell culture devices. The capabilities to generate independent sections for cell culture and biosensing with their own required chemical and biochemical functionalizations, to generate elaborated fluidic structures that connect each section with high fluidic control and the reduced requirement in reagents and volumes are just a few of the advantages that these type of systems presents [50–53].

On the other hand, the advancement on the research of materials and biomaterials has enabled both the development of suitable substrates for the generation of complex microenvironments for cell cultures and the fabrication of novel biosensors. The surge of smart, functional and biocompatible

materials in the recent years has allowed to speed up the development of multifunctional platforms for cell culture [54–56].

However, everything is still on very early stages of development, as most of what has been achieved so far is barely more than proof-of-concept of what could be achieved in the near future.

*Defining integrated cell culture secretion monitoring platforms*

Ideally, a fully integrated platform should combine the culture of cells with high control of the microenvironment and the monitoring of cell secretion within the same system, independently of the biosensing method used.

However, a standard on what classifies as a true integrated cell culture secretion monitoring platform or what components should it have does not exist, due to the early phase in which this research area currently is. For that reason, what have been described as “integrated” so far present different degrees of implementation of the cell culture and monitoring within the same system.

Some platforms do not incorporate cell culture themselves but require loading the sensor into a conventional cell culture well. Others allow culturing the cells in the platform but require to collect the supernatant and to perform the entire analysis on an entire independent unit. Finally, others enable both the cell culture and the capture of cell secretion but require to do the analysis outside in an external unit.

For the most part, what has been developed so far has followed one of two design strategies. The first one takes advantage of microfluidics to generate intricate systems composed of independent cell culture and biosensing sections, incorporating a fluidic network that allows connecting both of them and associate the secretion from each cell culture section to a biosensing chamber [57–64]. The second one relies on detection of the secreted biomolecule in the direct vicinity of the cells, usually through the use of functionalized micro-beads or barcodes, in order to capture the secretion

directly and, usually, easily adapt the biosensing method to the cells microenvironment [60,63,65–79].

*Main biological models explored*

Most platforms developed so far have been limited to the exploration of greatly known secretion models in order to test and validate the method and technology. The models used in the monitoring of cell excretion and secretion of metabolism related products have been quite varied, including the detection of inorganic and organic analytes [80–82].

However, when it comes to models concerning cell secretion, especially of signaling molecules and regulatory factors, the variety of biomolecules researched is far narrower.

Cytokines are the most explored analyte model. Interleukins (IL) 2, 4, 6 and 8, Tumor Necrosis Factor (TNF) and Interferon-γ (IFN) are some of the secreted cytokines whose detection and quantification have been incorporated in the most recent cell culture platforms [58,60–63,65–67,69,70,73–79,83–86]. There are various reasons for this. Firstly, cytokine secretion models are well known and have been thoughtfully studied, presenting a broad window of well standardized detection methodologies that can be adapted into the desired platform, easing the process of development and validation of the biosensing technique. Secondly, cytokines are widely used as biomarkers and reporters to address pathological conditions, giving the resulting product excellent potential in clinical practice. Finally, the type of cell cultures used to generate these models so far have been mostly based on cells derived from the immune system, which are much easier to implement into a platform than other cell types. This is because of their non-adherent, transient nature, which comes hand-in-hand with the much simpler microenvironment required for their proper culture when compared to other cell types coming from more complex physiological microenvironments.

The second model most used is that of the monitoring of growth factors secretion, such as the Vascular Endothelial Growth Factor (VEGF) and the Hepatocyte Growth Factor (HGF) [57,59,68,71,73,74,79]. These are also well

established models that present a huge clinical potential because of their regulatory actions and relation with pathological conditions. In addition, insulin, prostate specific antigen (PSA) and β-2-microglobulin have also been used as detection models.

*Multiplexing: monitoring of several secreted biomolecules*

A big part of the research has focused on the development of multiplex cell culture secretion biosensors. The advantage of this is clear: cells produce from hundreds to thousands of signals, and a full profiling of cell secretion can give massive information about cell conditions and behaviors. The vast majority of the multiplex cell secretion monitoring platforms developed so far focus on the detection of cytokines. Apart from the reasons previously listed, when it comes to multiplex detection, the wide variety of well-known cytokines a cell can produce is vast, making it the excellent model for the initial testing of multiplex analysis. Once more, the second most used model is that of growth factors.

When it comes to the type of bioreceptors and signals used, specific antibodies against the different biomolecules and adapted fluorescence immunoassays have mostly been used, respectively [60,62,63,65,73,75]. Antibodies are the most logical option so far for multiplexing monitoring, as their high specificity for all the different biomolecules ensures the precise capture of each one. Fluorescence-based adapted immunoassays give both the sensitivity required and an easy way to label each biomolecule independently. Understandably, this means that most of the multiplex systems that have been developed do not allow label-free monitoring of cell secretion. Multiplex cell secretion detection based on Surface Plasmon Resonance and electrochemical sensors have been developed [76,79,83,86]. However, true integration of multiplex monitoring on novel cell culture platforms, barring a few exceptions [76], is yet to be achieved.

The work of Abdullah *et al.* should be remarked [65], where they developed a micro-bead based *in situ* tagging (MIST) array that enabled the capture of single, non-adherent cells in thousands of nanowells containing micro-beads as sensoring probes for the capture, and later recognition through

fluorescence secondary immunolabelling, of a wide variety of secreted cytokines including IL1, IL6, IL8, Migration Inhibitory Factor and Monocyte Chemoattractant Protein, making it one of the most complete multiplex sensoring systems to date.

*Label-free and real-time monitoring of secretion*

Developing label-free methods to monitor and quantify cell culture secretion within a platform is one, if not the most, desirable step forward in the current search for novel cell culture and cell analysis tools. This is mainly because of two reasons. Firstly, not requiring the addition of a secondary label implies a reduction on the invasive steps that needs to be done, which results in a less intrusive method in general. Secondly, label-free detection opens the door to real-time monitoring, making it possible to address secretion profiles throughout the entirety of an assay and not at the end-point.

Optical label-free monitoring methods based on Surface Plasmon Resonance rise as the most prominent method explored for this type of platforms [57,70,72,76,77,79,83]. The very specific changes in the resonant conditions that occur when biomolecules come closer to metallic plasmonic compounds allow to easily detect the presence of a desired analyte without the need of secondary labels. For the most part, the proposed platforms have used specific antibodies for the capture of the secreted biomolecules, mostly cytokines once again, bound to gold nanoparticles or gold layers. However, due to the intricacy of the instrumentation and the nature of the materials required both for the production of the plasmon phenomena and the detection of the plasmonic signal, only very few of the proposed platforms have fully implemented cell culture and optical label-free detection. Electrochemical detection has also been explored, even though it still showcase the same limitations [85,86]. Aptamer based detection methods, combined with chemiluminiscence, and Structure Switching Aptamer strategies are currently arising as promising methods for the detection of cell secretion. Their biochemical nature makes them, in principle, more suitable to be successfully adapted into a cell culture environment than most of the synthetic materials used in other label-free methodologies [59].

*Monitoring of secretion on complex cell culture microenvironments*

When talking about platforms aimed for the monitoring of cell secretion on complex microenvironments, like those composed of highly structured extracellular matrices and more than one cell type, true development is virtually non-existent. This lack of prominence can be attributed to two common themes present in the systems developed so far. Firstly, as previously explained, the use of non-adherent cells as models for secretion does not represent the most common type of cell microenvironment present in complex organism, as in the case of mammal and human models. Secondly, the development of single-cell monitoring methodologies has been a hot topic in the last decade. The isolation of cells is usually achieved through the encapsulation or trapping of single cells in droplets, carved holes or microfluidic chambers [62,65–70,75,77,79]. While it offers immense potential in a wide variety of areas, including the development of high-throughput analysis and the study of cells heterogeneity, cells are not commonly found in a isolated state in their physiological microenvironments, and, therefore, cell microenvironment has not been taken into account when developing novel platforms aimed for single cell analysis.

This lack of development for secretion monitoring is especially clear when looking at the platforms that replicate full physiological conditions, such as organ-on-chip [87–89]. The integration of sensors to monitor cells' physical, electrical and metabolic processes has been more developed than sensors for cell secretion, especially when it comes to signaling molecules. The monitoring of secreted signaling biomolecules in complex microenvironments has been limited, so far, to adipose tissue and pancreatic isles models combined with Surface Plasmon Resonance sensoring probes/barcodes [64,76].

Considering all this, there is a clear gap in exploring new platforms that truly integrate complex microenvironments and cell secretion monitoring.

**Table 1** summarizes the most prominent integrated platforms for monitoring of cell culture secretion developed in the last 5 years, used for the critical revision of the state of the art.

**Table 1.** Platforms for cell culture secretion monitoring developed in the last 5 years.

| Biomolecule | Measurement type | Bioreceptor | Author and year |
|---|---|---|---|
| PSA, β-2-microglobulin | SPR | Antibody | Berthuy *et al.* 2016 [72] |
| TNF-β, INF-γ, IL-1, IL-8 | Fluorescence | Antibody | Kongsuphol *et al.* 2016 [73] |
| IL-6, TNF-α | SPR | Antibody | Lau *et al.* 2016 [83] |
| VEGF | Nanoplasmonics | Antibody | Li *et al.* 2017 [57] |
| TNF | Fluorescence | Antibody | Kaestly *et al.* 2017 [58] |
| VEGF | Chemiluminiscence | Aptamer | Shan *et al.* 2017 [59] |
| HGF, TGF | Fluorescence | Antibody | Son *et al.* 2017 [74] |
| IL-6, IL-8, TNF-α | Fluorescence | Antibody | Cui *et al.* 2018 [60] |
| IL-6, IL-8, MCP-1 | Fluorescence | Antibody | Hsu *et al.* 2018 [75] |
| IL-6, IL-10, TNF-α | SPR | Antibody | Zhu *et al.* 2018 [76] |
| IL-2 | Nanoplasmonics | Antibody | Li *et al.* 2018 [77] |
| IL-8 | Fluorescence | Antibody | Zhang *et al.* 2018 [61] |
| IL-6 | Fluorescence | Antibody | Liu *et al.* 2019 [78] |
| IL-8, VEGF | SPR | Antibody | Wei *et al.* 2019 [79] |
| TNF, CCL2, CCL3, CCL5 | Fluorescence | Antibody | Ramji *et al.* 2019 [62] |
| TNF-α | Calorimetry | Antibody | Bari *et al.* 2019 [84] |
| IFN-γ | Electrochemical | SSA | Liu *et al.* 2019 [85] |
| IL-1, 6, 8, MIF, MCP-1, TNF | Fluorescence | Antibody | Abdullah *et al.* 2019 [65] |
| IFN-γ | Fluorescence | Antibody | Antona *et al.* 2020 [66] |
| IFN-γ | Fluorescence | Antibody | Zhou *et al.* 2020 [67] |
| G-CSF | Fluorescence | Antibody | Ambrecht *et al.* 2020 [68] |
| IFN-γ | Fluorescence | Antibody | Yuan *et al.* 2020 [69] |
| IL-6 | SPR | Antibody | Zhu *et al.* 2020 [70] |
| IL-8, TNF-α | Fluorescence | Antibody | R-Moncayo *et al.* 2020 [63] |
| HGF | Fluorescence | Antibody | Neel *et al.* 2020 [71] |
| IL-2, IL-4 | Electrochemical | Antibody | Rani *et al.* 2020 [86] |
| Insulin | SPR | Antibody | Ortega *et al.* 2021 [64] |

## Future perspectives

As every year the quantity and complexity of the platforms aimed for the monitoring of cell secretion increase over what came before, a big progress will be made in the foreseeable future. As no consensus has been reached on what the best approach to develop said technologies is, the individual advancements being made in biosensing, materials, microfluidics and biological sciences will all add something important in what there is to come. Standardizing what truly makes a cell culture platform integrated, and what individual components are realistically expected to be included in one is essential for future research.

Last decade, the predominating platforms for cell secretion monitoring were focused on single cell analysis. However, it is expected that the focus will now shift into true replication of complex microenvironments based on physiological and pathological conditions. While microfluidics itself has allowed huge progress in the development of these technologies, combining novel microfabrication techniques, smart biomaterials and microfluidics systems is, most probably, the best move forward for achieving complex controlled cell microenvironments with secretion biosensing.

Finally, most platforms developed so far have not presented a true advance on easing the monitoring to the users when compared to conventional methods, as they usually require laborious fluidic and analytical setups. It is more than probable that creating easy to use, versatile platforms adaptable to the users' requirements will become the key milestone to achieve in the near future.

# Objectives and hypothesis

## Hypothesis

This thesis is aligned with the growing interest in the development of new technologies for cell culture that enable the monitoring of the cell behavior subjected to complex microenvironments. The general goal in this research area is to develop systems that can provide different degrees of control in the interaction of cells with their microenvironment and that can integrate biosensors to monitor cell behavior in the most dynamic and precise way possible, including the detection and quantification of cell secretion.

Microfabrication, combined with molecular and biological sciences, would allow the creation of novel platforms to reach the aforementioned goal. In particular, fabrication of complex micropatterns of cells and microbeads on transparent substrates would enable:

*1.* To control cell distribution on a substrate, cell-cell contact and cell-substrate interaction, as well as to achieve efficient presentation of signaling molecules to the cells resembling physiological conditions.

*2.* To optical monitor cell proliferation, migration, viability, intracellular and membrane protein expression, as well as efficiently detect cell secreted molecules from a small number of cells.

## Objectives

The main objective of this thesis is the development of an analytical platform that allows analyzing the behavior of cells under controlled interactions with their microenvironment. For this, the creation of complex patterns that serve as models to evaluate the effect of the cell microenvironment and the development of new biosensors that can be integrated into these patterns will be studied. Substrates will be patterned with proteins, cells and microbeads. The protein patterns will enable the controlled distribution of the cells over the substrate in order to achieve control over cell-cell contact. The nanoparticles will act as carriers of molecules in adjacent positions to the cells. These molecules can be signaling molecules for localized stimulation of cells or sensing probes for the detection and monitoring of cell secretion.

To achieve the main objective, the following sub-objectives have been established in order to address the development of biosensors, cell patterns and complex patterns that will be finally integrated into a single platform:

*1.* To review the state of the art on the different cell interactions that can affect cell behavior as well as the methodologies and microtechnologies that have been developed in the quest to control and study cell cultures in complex microenvironments (Appendix 1).

*2.* To develop biosensors based on DNA probes for the direct detection of biomolecules on solid supports. The design, manufacture and evaluation of a DNAzyme for the colorimetric detection of single-stranded DNA (Appendix 2) and a Structure Switching Signaling Aptamer (SSSA) for the fluorescence-based detection of Vascular Endothelial Growth Factor (VEGF) will be carried out (Appendix 3). Likewise, the probes will be immobilized, both in paper devices and in microbeads, to evaluate their usefulness when immobilized on solid supports and the possibility of integrating them into cell analysis platforms.

*3.* To manufacture adherent cell patterns made up of multiple (dozens to thousands) cell colonies replicates, containing one or more cells each. The patterns will provide control over cell-cell and cell-material interactions. The impact of cell-cell contact in gene transfection efficiency on mesenchymal stromal cells (MSCs) will be studied (Appendix 4). The suitability of different substrates for cell patterning will be evaluated, and a methodology to convert cytophobic polymers like PMMA into a cytophilic substrate will be developed (Appendix 5).

*4.* To create complex patterns composed of small MSC-colonies surrounded by microbeads and to monitor cell behavior under specific conditions provided by the properties of the micropattern. The microbeads will serve as molecular carriers for cell signaling molecules or sensing probes. On the one hand, microbeads functionalized with Fibroblast Growth Factor type 2 (FGF-2) will be used for the solid-phase presentation of the growth factor to the cells, and the cell proliferation and expression of membrane receptors in the MSC-colonies will be evaluated (Appendix 6). On the other hand, the microbeads

will be functionalized with anti-VEGF antibodies or an SSSA probe for localized monitoring of VEGF secretion from each MSC-colony on the substrate with micropatterns (Appendix 7).

These objectives are graphically summarized in Figure 1.

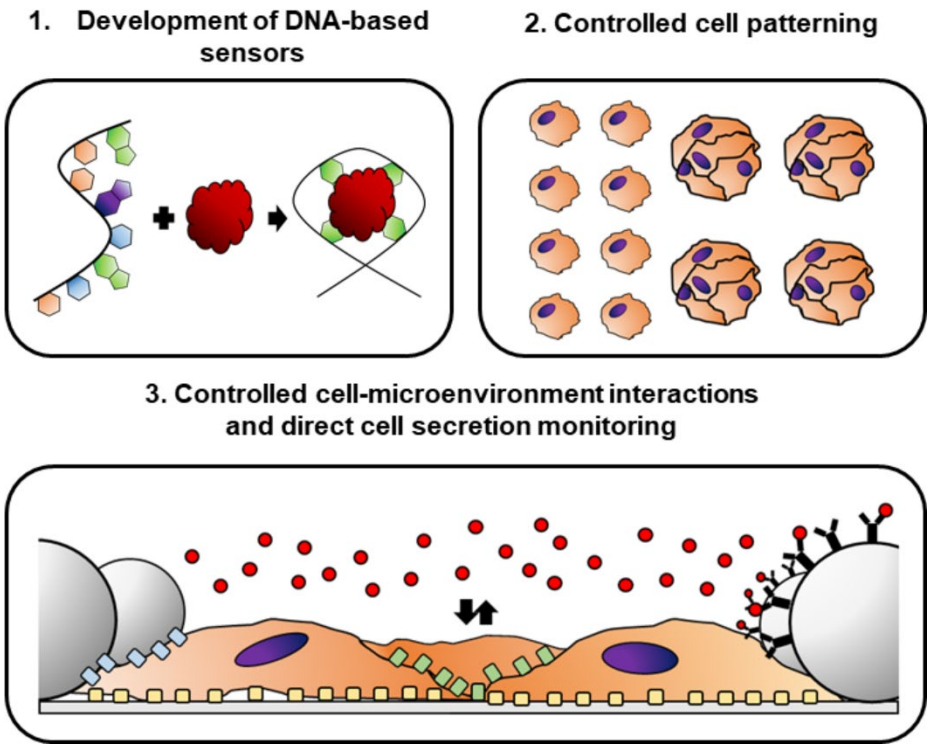


**Figure 1**. Strategy followed in the thesis. 1. To develop DNA-based biosensors for the label-free analysis of biomolecules. 2. To generate cell patterns with controlled cell confluence (from single cell to small cell colonies). 3. To control different types of cell interactions (cell-material, cell-cell and cell-carriers depicted in yellow, green and blue, respectively, as well as cell-soluble factors) and to directly monitor cell secretion through integrated sensor probes.

# General methods

Here, a summary of the main methods used throughout the thesis are briefly explained. Any possible variation required of a general method as explained here, as well as any methodology required exclusively in a single experimental procedure, are thoughtfully explained in their respective Annexes.

## Fabrication methods

### *Wax printing of paper substrates*

Wax printing of different features, including microfluidic channels, was performed by a Xerox ColorQube 8570 on Whatman filter paper 1 (Sigma Aldrich, Spain) and Hi-Flow Plus HFC 12004 nitrocellulose (EMD Millipore, Ireland). After printing, wax was melted on an oven at 125 ºC for 5 min to let the wax pass-through both sides of the substrates and generate the hydrophobic barriers.

### *Photolithography*

All designs were done in CleWin. Polyester PET photomask were purchased from JD Photodata, UK. SU-8 20005 and 2025 were purchased from ChimieTech, France. Master silicon wafers were fabricated on a SU-8 mold fabrication station (BlackHole-Lab, France), consisting of a spinner for homogeneous and controlled deposition of SU-8 on the silicon wafers, a UV irradiator for photopolymerization of the resin, and a hot plate for the controlled evaporation of the solvents and continuation of the polymerization of the resin.

### *Fabrication of PDMS stamps/slabs*

Polydimethylsiloxane (PDMS) SYLGARD 184, with a ratio 10:1 of silicone elastomer and curing agent (Ellsworth adhesives, Spain) was poured on top of silicon wafers. The mix was degassed for 30 min under vacuum and was polymerized inside of an oven at 80º for 90 min afterwards. Finally, the PDMS was detached from the silicon wafer and each individual PDMS stamp/slab was cut.

*Fabrication of multilayered PMMA wells and microfluidic device*

Polymethyl methacrylate (PMMA) homemade wells and microfluidic device were fabricated through multilayered fabrication. Layers consisted of either PMMA slides Plexiglas 4mm (Evonik Industries AG, Germany), glass covers 24 x 60 mm (Fisher Scientific, Spain) or PDMS. Layers were joint together by pressure sensitive adhesive (PSA) ARcare 8939 (Adhesive Research, Ireland). PMMA wells and slides were cut with a $CO_2$ VERSA VLS2.30 Desktop Universal Laser System (USA). PSA layers were cut with a Graphtec cutting Plotter CE6000-40 (CPS Cutter Printer Systems, Spain).

**Protein and cell patterning**

*Microcontact printing of fibronectin*

PDMS stamps, containing different carved features, were wetted with 50 µL of a 50 µg $mL^{-1}$ fibronectin solution in phosphate buffer solution (PBS) for 30 min. Subsequently, the ink was removed and the PDMS stamps were rinsed with distilled water and dried with compressed air. The carved side of the PDMS stamp was put in contact with either the bottom plate of the well in a 12-well microtiter plate (Fisher Scientific, Spain), PMMA or glass cover for another 30 min, in order to transfer the protein from the PDMS stamp replicating the features carved in the PDMS surface. Finally, PDMS stamps were removed and the wells were blocked with 1 mL of BSA solution 1% (w/v) in PBS.

*Printing and vacuum lithography*

PDMS slabs containing channel-like structures with pillars inside were punched twice in order to generate a 2 mm diameter inlet and a 1 mm outlet. Pillars inside of the channels were wetted with a solution of fibronectin 50 µg $mL^{-1}$ for 30 minutes. Afterwards, PDMS slabs were rinsed with distilled water, dried with compressed air and attached to the glass bottom PMMA wells. The resulted assembly PDMS slabs on glass were put under vacuum inside of a desiccator for 30 minutes. Afterwards, the outlets were closed with tape and 2 µL of micro-beads suspension were loaded on the inlets. Suspension was

let flow until it started filling the outlet. Tape was removed after 5 minutes and PDMS slabs-glass covers were left overnight for solvent evaporation at 4 ºC. Finally, PDMS slabs were removed afterwards.

*Adhesion of cells on fibronectin patterns*

Human hair follicle-derived mesenchymal stromal cells (hHF-MSCs) were obtained from human follicles. Prostate cancer cells (PC3) and colorectal cancer cells (HCT116) were purchased from ATCC, USA. Cells were suspended on serum-free conditions at a concentration of $10^5$ cells per mL. Cell suspensions were added to the fibronectin patterns and were left on constant oscillation in a Vari-Mix steep angle rocker (Thermo Fisher, Spain) inside an incubator at 37 ºC and 5 % $CO_2$ air atmosphere. The time required to achieve full adhesion depended on the assay and the cell type. Afterwards, the remaining suspension was removed and the patterns were rinsed 3 times with PBS.

**Cell and biochemical analysis**

*Solution assays*

Assays for the detection of biomolecules in solution were performed in either transparent (for colorimetric detection) or black (for fluorescence detection) 96-microtirer plates (Fisher Scientific, Spain) on a Beckman Coulter DTX 880 Multimode Detector (USA) or a Promega Globax Multi Detection fluorometer (USA).

*Microscopy imaging*

Brightfield and fluorescence images of paper substrates, cell cultures, cell patterns and micro-beads patterns were taken using a modified Nikon Eclipse TE2000-S inverted microscope (USA), with and adapted Andor Zyla sCMOS black and white camera (Oxford Instruments, UK). Lumencor laser 640 nm was used as light source for excitation and Quad EM filter: 446/523/600/677 with 4 TM bands: 446/34 + 523/42 + 600/36 + 677/28.

### Images, data and statistical analysis

Microscopy images were processed and analyzed either in FiJi/ImageJ software, NIS elements analysis software or in a combination of both. Data analysis, including curve fitting and statistical analysis, were performed either in Excel software, Origin Pro 2018 software or in a combination of both.

# Results and discussion

## Experimental results and discussions

*Biosensors based on DNA probes for the direct detection of biomolecules on solid supports*

A DNAzyme biosensor was developed for the colorimetric detection of single strand DNA (ssDNA) and immobilized on a paper support (Appendix 2).

The sensor in question followed a DNAzyme strategy. DNAzymes are three-dimensional DNA structures with catalytic abilities akin to that of enzymes [90]. The DNAzyme was designed for the specific detection of a synthetic sequence based on the human Y amelogenin gene ($Y_f$), highly used for sex identification in medical and forensic fields [91]. Two Specific DNA probes were designed with the ability to bind specifically to the $Y_f$ sequence. Only when all three sequences bind together, the three-dimensional conformation gains the capability to bind a hemin group and gain a peroxidase ability. This peroxidase ability was used to oxidate the uncolored ABTS [2,2'-azino-bis(3-ethylbenzothiazoline-6-sulfonic acid)] into the green-colored oxidized $ABTS^+$, enabling to correlate the presence of color to the presence of the $Y_f$ and the intensity of the color to the quantity of the analyte.

The detection of $Y_f$ was firstly tested and optimized in solution, allowing not only to discern specificly $Y_f$ from its X counterpart ($X_f$) but also to quantify different concentrations of the analyte, detecting as low as 655 ng. The reaction was then transported into a paper support, testing both cellulose paper and nitrocellulose paper. To localize the reaction, wax-circles were printed through wax printing. Cellulose paper was chosen out of the two. The reaction once again allowed to specifically detect different concentrations of $Y_f$ both qualitatively through naked eye observation (**Figure 2 A**) and quantitatively through mobile phone camera pictures analysis (**Figure 2 B**). For all concentrations studied, a clear coffee-ring effect was observed in the samples where $Y_f$, was loaded, where as low as 143 ng of the analyte could be detected. Through quantitative analysis of mobile phone camera images, as low as 45.7 ng of the analyte could be detected. Finally, the reaction was transported into a simple, proof-of-concept cellulose paper analytical

microfluidic device (μPAD), allowing to analyze $Y_f$ and $X_f$ in a single device. Once again, $Y_f$ was specifically detected (**Figure 2 C**).

In summary, a DNAzyme for the colorimetric detection of ssDNA was developed, tested and optimized. The sensor was successfully integrated into a paper microfluidic device made of cellulose, which not only improved the analysis sensitivity compared to the solution assay, but allowed the generation of a proof-of-concept, low-cost device with potential medical and forensic use.

Continuing in the line of developing DNA-based biosensors, a self-reporting synthetic DNA probe for the fluorescence-based detection of cell secreted proteins that could directly be applied for the monitoring of cell cultures was developed. Once more, the biosensor was transported into a paper microfluidic device (Appendix 3).

The strategy followed was that of Structure Switching Signaling Aptamer (SSSA). SSSAs are double-stranded DNAs composed of an aptamer sequence specific for the desired analyte, a fluorophore and a quencher [47]. In its native state, the proximity between the fluorophore and the quencher suppresses the fluorophore's emission. In the presence of the target analyte, the interaction between the aptamer and the analyte induces a conformational change on the SSSA and a displacement of the quenchers, enabling the production of a fluorescence signal that can be correlated with the presence and quantity of the analyte. In this case, the SSSA was developed for the detection of cell secreted Vascular Endothelial Growth Factor (VEGF), a regulatory biomolecule for which altered levels can be associated with several pathological conditions [92].

The VEGF-SSSA was initially tested on solution, being it an inadequate matrix for the detection of VEGF due to the formation of protein-aptamers agglomerates. The reaction was then transported into cellulose paper, using wax printing for the generation of wax-circles. The reaction on a solid support allowed the specific detection of VEGF with high sensitivity, enabling the quantification of VEGF concentration through fluorescence microscopy

imaging and analysis of the paper substrates (**Figure 3 A and B**). As low as 0.57 ng of VEGF could be detected with this biosensor.

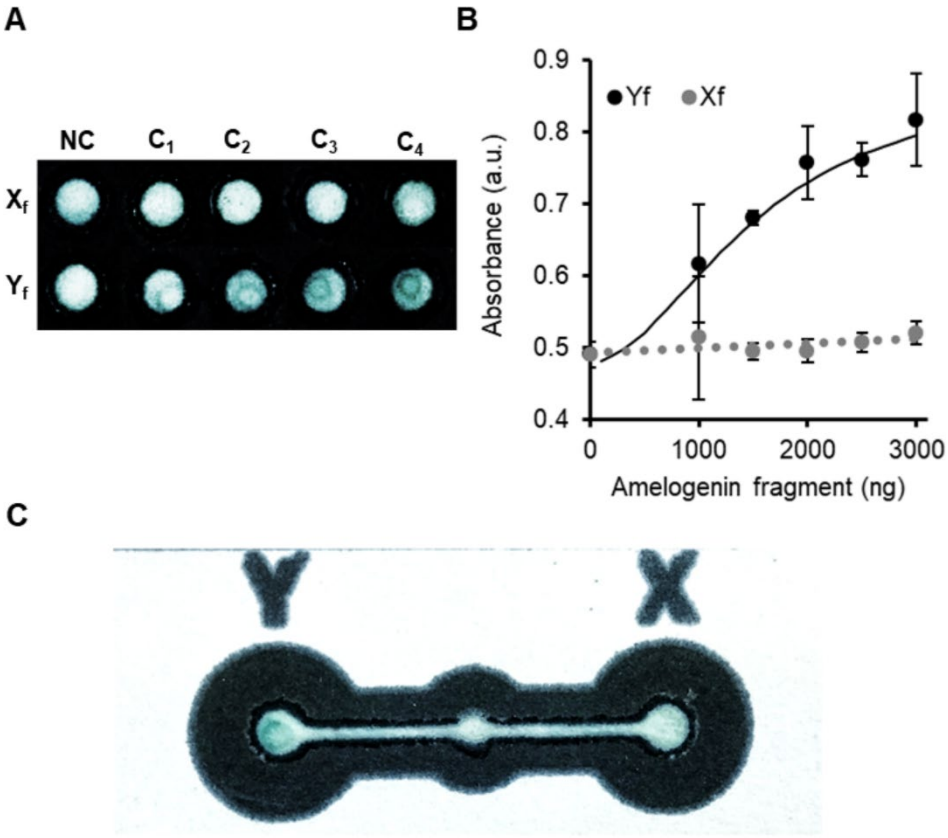


**Figure 2. Development of DNAzyme for naked eye, colorimetric detection of Y amelogenin fragment in a paper microfluidic device.** A) Picture of the 2 by 5 array of wax-circles printed in paper after 5 min DNAzyme reaction. $C_1$, $C_2$, $C_3$ and $C_4$ refers to the different concentrations of $Y_f$ or $X_f$ solutions added to the paper substrate [25 (143 ng), 50 (286 ng), 100 (572 ng) and 200 (1144 ng) μM, respectively] and NC is the negative control. B) Plot of the color intensity obtained from the picture taken by the mobile camera 5 min after reaction. Error bars mean ± SD (n = 3 samples per experimental condition). C). Pictures of the μPAD taken 5 min after the $H_2O_2$ solution reached the analysis zones. Detection circles correspond to sample loading of $Y_f$ (left) and $X_f$ (right). Increased green intensity relates to increasing presence of $ABTS^+$.

The reaction was then transported into simple, proof-of-concept microfluidic device that incorporated a detection zone for VEGF and a fluorescence control zone in the same device. Finally, the device was validated for real samples, being able to detect the VEGF secreted from a human Hair Follicle-derived Mesenchymal Stromal Cells (hHF-MSCs) culture, **Figure 3 C and D**.

Following a SSSA strategy allowed the development of a label-free biosensor for VEGF directly applicable to real cell culture scenarios with good specificity and sensitivity.

Once again, the incorporation of the sensing into a μPAD not only greatly improved the performance of the biosensor, but also allowed the production of an easy-to-use and user-friendly device for detection of cell culture secretion.

*Manufacture of adherent cell patterns*

Patterning of adherent cells was studied for the generation of discrete cell-colonies with high control over cell interactions. In this case, cell patterning was used in order to control cell-cell contact (presence or absence) and explore its effect on gene transfection efficiency of patterned hHF-MSCs (Appendix 4).

Gene transfection is a common procedure in which exogenous genetic material is incorporated into a cell for its expression using the cell's own gene expression process [93]. To evaluate the efficiency of the procedure, transfection of plasmids encoding Green Fluorescence Protein (GFP) are usually used.

The patterning of cells was obtained through microcontact printing (μCP), where fibronectin was printed on the surface of cell culture well plates. Polydimethylsiloxane (PDMS) stamps were fabricated containing array of pillars with a 100 or a 20 μm diameter, in order to generate arrays of fibronectin dots of 100 μm ($D_{100}$) and 20 μm ($D_{20}$), respectively. This enabled controlling cell-cell contact, generating scenarios of small cell-colonies or single cells, with or without cell-cell contact respectively.

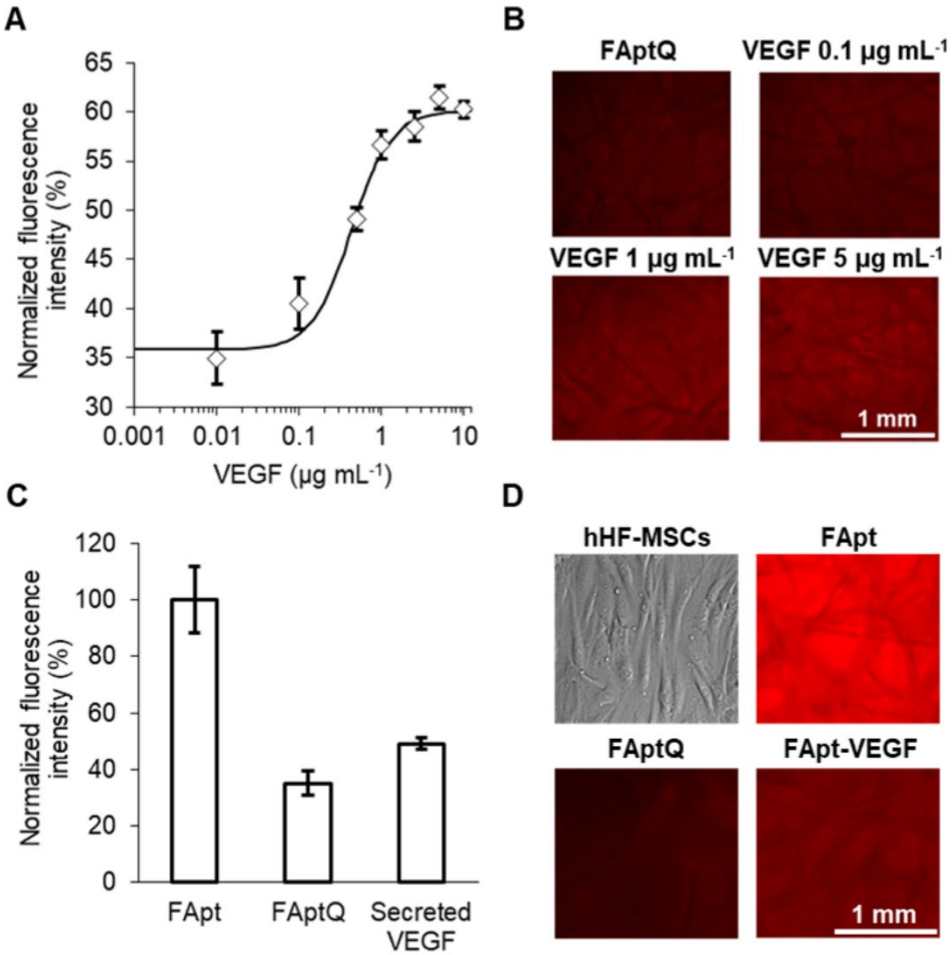


**Figure 3. Development of a SSSA for the label-free detection of cell secreted VEGF in a paper microfluidic device.** A) Plot of the fluorescence intensity obtained by the incubation with different concentrations of VEGF (0.01, 0.1, 0.5, 1, 2.5, 5 and 10 µg $mL^{-1}$), normalized to the fluorescence control intensity. Error bars correspond to mean values ± SD (n = 4). B) Microscope images of the fluorescence obtained in paper samples treated with different concentrations of VEGF. C) Plot of the normalized fluorescence intensity obtained in the fluorescence control (FApt), negative control (FAptQ) and in cell's secreted VEGF (FApt-VEGF), normalized to the fluorescence control (FApt) intensity. Error bars correspond to mean values ± SD (n = 3). D) Brightfield microscopy image of hHF-MSCs in high confluence (top left) and fluorescence microscope images of fluorescence control, negative control, and secreted VEGF incubated samples.

Both scenarios were transfected with GFP through lipofection, and GFP expression was monitored through fluorescence microscopy imaging. While small cell-colonies presented a similar transfection efficiency to that of conventional cultures (20% after 24 h), single cells presented a slight increase in the transfection efficiency and a displacement on the peak of maximum expression of GFP (from 24 h to 18 h), confirming that cell-cell contact affects gene transfection and expression of the transfected product, **Figure 4 A**.

Each individual cell of the single cell arrays was monitored over the course of 30 h, enabling to quantify the absolute transfection efficiency and to monitor each cell event more thoroughly, **Figure 4 B**.

This methodology allowed, for the first time, to address the effect of cell-cell contact on transfection efficiency, something conventional methodologies are not able to achieve due to the lack of control over cell-cell interactions. Furthermore, the generation of thousands of individual and localized cell events that can be continuously monitored is possible because of the use of patterns.

Manufacture and commercialization of microsystems often require the development of manufacturing protocols using off-the-shelf materials. For this reason, the possibility to create cell patterns on commonly used polymers such as polymethyl methacrylate (PMMA) was explored (Appendix 5).

PMMA is a polymer widely used in the generation of microfluidic devices due to its malleability and adaptability. However, it is a relatively hydrophobic and highly cytophobic material, which distances its use for cell culture [94,95].

A combined physicochemical and biochemical treatment was optimized to generate controlled adhesion of cell patterns on PMMA. Localized oxygen plasma treatment oxidized the surface of PMMA, improving its hydrophilicity [96]. μCP of different fibronectin features enabled the generation of discrete and controlled spots for cell adhesion on the hydrophilic zones generated.

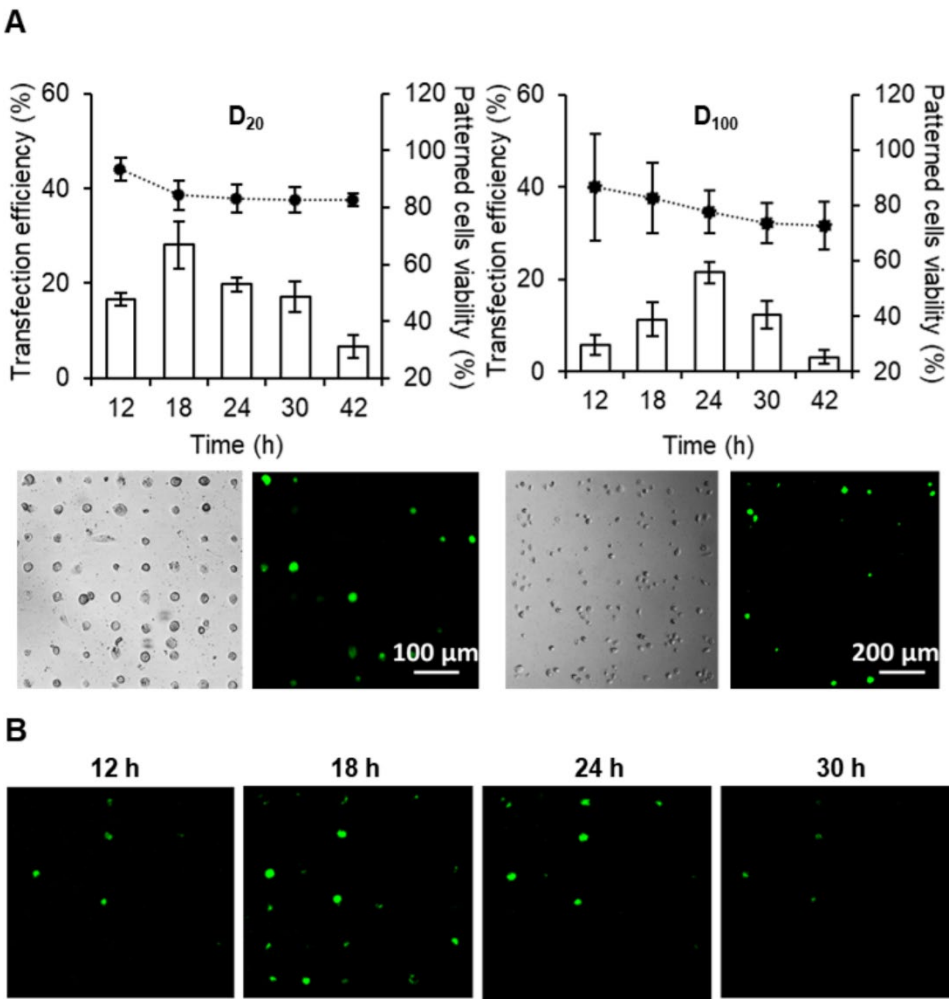


**Figure 4. Continuous monitoring of gene transfection efficiency with controlled cell-cell contact.** A) Top: plots of transfection efficiency (bar chart) and patterned cell viability (dotted line) *versus* time of $D_{20}$ (left) and $D_{100}$ (right). Error bars mean ± SD ($n$ = 3 patterns, with ~700 cells and ~4000 cells monitored for $D_{20}$ and $D_{100}$ respectively per sample and per time). Bottom: brightfield and fluorescence microscopy images of single cell (left) and small cell-colony (right) 18 and 24 h, respectively after transfection of GFP. B) Fluorescence microscopy images representing the time of apparition of the fluorescence on $D_{20}$ patterns.

patterns. Monitoring of protein expression of both intracellular proteins and cell membrane expressed receptors could be carried out through the fluorescence microscopy observation of the fluorescence labelled products. Finally, the microbeads could also serve as sensing probes for the detection and quantification of cell secreted signaling molecules in the surroundings of the cells, both through the adaptation of a conventional immunoassay and the incorporation of a novel self-reporting DNA probe biosensor.

The platform offers significant improvements for *in vitro* cell studies when compared with conventional cell culture methods. The enhanced control over cell interactions that can be achieved and the capability to monitor several cell processes *in situ* greatly differ from the uncontrollable batch cultures on well plates and the invasive, end-of-assay monitoring methods usually carried out. The platform presented in this thesis also demonstrated some advantages when compared to the most novel methodologies and systems for cell secretion monitoring developed so far. All of the studies were carried out and optimized using adherent cells, which differs from the common practice of using non-adherent cells, thus opening the door for the adaptation of the substrate to a much broader variety of cell microenvironments. This allows the combination of both control over cell interactions and monitoring of cell secretion, not only in the same platform but also by using the same functional element (microbeads as molecular carriers). The fact that the platform is based on simple and interchangeable components would give the methodology the capability to be easily adapted to any desired cell study. Furthermore, the localization of the sensing probes near the cells enabled the detection of cell secretion coming from a small number of cells without the need of complex microfluidics setups.

It should be noted that most of the capabilities demonstrated by the platform have been tested and optimized individually and that integration of full control over cell interactions and monitoring of all the different cell processes is yet to be achieved in a single assay. Furthermore, exploring the inclusion of biomaterials, as in example, the combination of gel-structures with the microbeads, would definitely improve the capabilities of the platform to better adapt cell contexts. Finally, while conventional culture and analysis methods

were carried out in all cases as a way to compare the outcomes of each experimental procedure, further experiments are required in order to address all the possible benefits and limitations this platform can offer, as in example, the maximum duration in which cells can be maintained in patterned conditions.

In general, this thesis presents the initial results and prospects into what can be achieved with these methodologies and the platform developed. While the assays have narrowed to the patterning of arrays of cell-colonies, the generation of more complex structures could certainly allow the formation of cellular scenarios more analogous to physiological conditions. Similarly, even though the different experimental procedures presented in this thesis are based on highly standardized models, the versatility of the platforms implies that they can be easily adapted to the requirements of each scenario. The microbeads can be easily functionalized to incorporate other signaling molecules or sensing probes, as in example the ssDNA sensor developed in this thesis. Furthermore, the material chosen as substrate, the arrays geometry, the protein printed, the cell type and the type of microbead could be modified depending on the necessity.

Therefore, after the results obtained during this thesis, the use of this methodology is envisioned to be able to recreate complex microenvironments in devices that allow real-time monitoring of cell behaviors. The methodology proposed for the fabrication of cell analysis platforms is readily accessible to any research laboratory. This can lead up to its extensive use and impact on the generation of novel knowledge on cellular biology, biomedicine, regenerative therapies and drug discovery, among others.

# References

(1) Aiyelabegan, H. T.; Sadroddiny, E. Fundamentals of Protein and Cell Interactions in Biomaterials. *Biomed. Pharmacother.* **2017**, *88*, 956–970.

(2) Baust, J. M.; Buehring, G. C.; Campbell, L.; Elmore, E.; Harbell, J. W.; Nims, R. W.; Price, P.; Reid, Y. A.; Simione, F. Best Practices in Cell Culture: An Overview. *Vitr. Cell. Dev. Biol. - Anim.* **2017**, *53* (8), 669–672.

(3) Zhang, W.; Zhuang, A.; Gu, P.; Zhou, H.; Fan, X. A Review of the Three-Dimensional Cell Culture Technique: Approaches, Advantages and Applications. *Curr. Stem Cell Res. Ther.* **2016**, *11* (4), 370–380.

(4) Caliari, S. R.; Burdick, J. A. A Practical Guide to Hydrogels for Cell Culture. *Nat. Methods* **2016**, *13* (5), 405–414.

(5) van Duinen, V.; Trietsch, S. J.; Joore, J.; Vulto, P.; Hankemeier, T. Microfluidic 3D Cell Culture: From Tools to Tissue Models. *Curr. Opin. Biotechnol.* **2015**, *35*, 118–126.

(6) Funano, S.; Tanaka, N.; Tanaka, Y. User-friendly Cell Patterning Methods Using a Polydimethylsiloxane Mold with Microchannels. *Dev. Growth Differ.* **2020**, *62* (3), 167–176.

(7) Verjans, E.-T.; Doijen, J.; Luyten, W.; Landuyt, B.; Schoofs, L. Three-Dimensional Cell Culture Models for Anticancer Drug Screening: Worth the Effort? *J. Cell. Physiol.* **2018**, *233* (4), 2993–3003.

(8) Cornel, A. M.; Szanto, C. L.; Til, N. P.; Velzen, J. F.; Boelens, J. J.; Nierkens, S. A "No-Touch" Antibody-Staining Method of Adherent Cells for High-Throughput Flow Cytometry in 384-Well Microplate Format for Cell-Based Drug Library Screening. *Cytom. Part A* **2020**, *97* (8), 845–851.

(9) Du, G.; Fang, Q.; den Toonder, J. M. J. Microfluidics for Cell-Based High Throughput Screening Platforms—A Review. *Anal. Chim. Acta* **2016**, *903*, 36–50.

(10) Zhao, Y.; Kankala, R.; Wang, S.-B.; Chen, A.-Z. Multi-Organs-on-Chips: Towards Long-Term Biomedical Investigations. *Molecules* **2019**, *24* (4), 675.

(11) Prot, J. M.; Leclerc, E. The Current Status of Alternatives to Animal Testing and Predictive Toxicology Methods Using Liver Microfluidic Biochips. *Ann. Biomed. Eng.* **2012**, *40* (6), 1228–1243.

(12) Bédard, P.; Gauvin, S.; Ferland, K.; Caneparo, C.; Pellerin, È.; Chabaud, S.; Bolduc, S. Innovative Human Three-Dimensional Tissue-Engineered Models as an Alternative to Animal Testing. *Bioengineering* **2020**, *7* (3), 115.

(13) Velasco, V.; Shariati, S. A.; Esfandyarpour, R. Microtechnology-Based Methods for Organoid Models. *Microsystems Nanoeng.* **2020**, *6* (1), 76.

(14) Gilazieva, Z.; Ponomarev, A.; Rutland, C.; Rizvanov, A.; Solovyeva, V. Promising Applications of Tumor Spheroids and Organoids for Personalized Medicine. *Cancers (Basel).* **2020**, *12* (10), 2727.

(15) Seo, J.; Shin, J.-Y.; Leijten, J.; Jeon, O.; Camci-Unal, G.; Dikina, A. D.; Brinegar, K.; Ghaemmaghami, A. M.; Alsberg, E.; Khademhosseini, A. High-Throughput Approaches for Screening and Analysis of Cell Behaviors. *Biomaterials* **2018**, *153*, 85–101.

(16) Knight, E.; Przyborski, S. Advances in 3D Cell Culture Technologies Enabling Tissue-like

Structures to Be Created in Vitro. *J. Anat.* **2015**, *227* (6), 746–756.

(17) Modena, M. M.; Chawla, K.; Misun, P. M.; Hierlemann, A. Smart Cell Culture Systems: Integration of Sensors and Actuators into Microphysiological Systems. *ACS Chem. Biol.* **2018**, *13* (7), 1767–1784.

(18) He, J.; Brimmo, A. T.; Qasaimeh, M. A.; Chen, P.; Chen, W. Recent Advances and Perspectives in Microfluidics-Based Single-Cell Biosensing Techniques. *Small Methods* **2017**, *1* (10), 1700192.

(19) Hillger, J. M.; Lieuw, W.-L.; Heitman, L. H.; IJzerman, A. P. Label-Free Technology and Patient Cells: From Early Drug Development to Precision Medicine. *Drug Discov. Today* **2017**, *22* (12), 1808–1815.

(20) Shih, H.-C.; Lee, T.-A.; Wu, H.-M.; Ko, P.-L.; Liao, W.-H.; Tung, Y.-C. Microfluidic Collective Cell Migration Assay for Study of Endothelial Cell Proliferation and Migration under Combinations of Oxygen Gradients, Tensions, and Drug Treatments. *Sci. Rep.* **2019**, *9* (1), 8234.

(21) Schwarz, J.; Bierbaum, V.; Merrin, J.; Frank, T.; Hauschild, R.; Bollenbach, T.; Tay, S.; Sixt, M.; Mehling, M. A Microfluidic Device for Measuring Cell Migration towards Substrate-Bound and Soluble Chemokine Gradients. *Sci. Rep.* **2016**, *6* (1), 36440.

(22) Rodriguez-Rodriguez, R.; Muñoz-Berbel, X.; Demming, S.; Büttgenbach, S.; Herrera, M. D.; Llobera, A. Cell-Based Microfluidic Device for Screening Anti-Proliferative Activity of Drugs in Vascular Smooth Muscle Cells. *Biomed. Microdevices* **2012**, *14* (6), 1129–1140.

(23) Lei, K. F.; Wu, M.-H.; Hsu, C.-W.; Chen, Y.-D. Real-Time and Non-Invasive Impedimetric Monitoring of Cell Proliferation and Chemosensitivity in a Perfusion 3D Cell Culture Microfluidic Chip. *Biosens. Bioelectron.* **2014**, *51*, 16–21.

(24) Qin, J.; Ye, N.; Liu, X.; Lin, B. Microfluidic Devices for the Analysis of Apoptosis. *Electrophoresis* **2005**, *26* (19), 3780–3788.

(25) Wlodkowic, D.; Khoshmanesh, K.; Sharpe, J. C.; Darzynkiewicz, Z.; Cooper, J. M. Apoptosis Goes on a Chip: Advances in the Microfluidic Analysis of Programmed Cell Death. *Anal. Chem.* **2011**, *83* (17), 6439–6446.

(26) Ohkubo, T.; Kinoshita, H.; Maekawa, T.; Kunida, K.; Kimura, H.; Kuroda, S.; Fujii, T. Development of a Microfluidic Cell Culture and Monitoring System for Intracellular Signaling Studies. *bioRxiv* **2018**.

(27) King, K. R.; Wang, S.; Irimia, D.; Jayaraman, A.; Toner, M.; Yarmush, M. L. A High-Throughput Microfluidic Real-Time Gene Expression Living Cell Array. *Lab Chip* **2007**, *7* (1), 77–85.

(28) Ullman, G.; Wallden, M.; Marklund, E. G.; Mahmutovic, A.; Razinkov, I.; Elf, J. High-Throughput Gene Expression Analysis at the Level of Single Proteins Using a Microfluidic Turbidostat and Automated Cell Tracking. *Philos. Trans. R. Soc. B Biol. Sci.* **2013**, *368* (1611), 20120025.

(29) Tam, J.; Cordier, G. A.; Bálint, Š.; Sandoval Álvarez, Á.; Borbely, J. S.; Lakadamyali, M. A Microfluidic Platform for Correlative Live-Cell and Super-Resolution Microscopy. *PLoS One* **2014**, *9* (12), e115512.

(30) Nair, A.; Chauhan, P.; Saha, B.; Kubatzky, K. F. Conceptual Evolution of Cell Signaling. *Int. J. Mol. Sci.* **2019**, *20* (13), 3292.

(31) Stastna, M.; Van Eyk, J. E. Secreted Proteins as a Fundamental Source for Biomarker Discovery. *Proteomics* **2012**, *12* (4–5), 722–735.

(32) Severino, V.; Farina, A.; Chambery, A. Analysis of Secreted Proteins. In *Methods in Molecular Biology*; 2013; pp 37–60.

(33) Shin, S. R.; Kilic, T.; Zhang, Y. S.; Avci, H.; Hu, N.; Kim, D.; Branco, C.; Aleman, J.; Massa, S.; Silvestri, A.; Kang, J.; Desalvo, A.; Hussaini, M. A.; Chae, S.-K.; Polini, A.; Bhise, N.; Hussain, M. A.; Lee, H.; Dokmeci, M. R.; Khademhosseini, A. Label-Free and Regenerative Electrochemical Microfluidic Biosensors for Continual Monitoring of Cell Secretomes. *Adv. Sci.* **2017**, *4* (5), 1600522.

(34) Bhalla, N.; Jolly, P.; Formisano, N.; Estrela, P. Introduction to Biosensors. *Essays Biochem.* **2016**, *60* (1), 1–8.

(35) Byrne, B.; Stack, E.; Gilmartin, N.; O'Kennedy, R. Antibody-Based Sensors: Principles, Problems and Potential for Detection of Pathogens and Associated Toxins. *Sensors* **2009**, *9* (6), 4407–4445.

(36) Morales, M. A.; Halpern, J. M. Guide to Selecting a Biorecognition Element for Biosensors. *Bioconjug. Chem.* **2018**, *29* (10), 3231–3239.

(37) Subramani, I. G.; Ayub, R. M.; Gopinath, S. C. B.; Perumal, V.; Fathil, M. F. M.; Md Arshad, M. K. Lectin Bioreceptor Approach in Capacitive Biosensor for Prostate-Specific Membrane Antigen Detection in Diagnosing Prostate Cancer. *J. Taiwan Inst. Chem. Eng.* **2021**, *120*, 9–16.

(38) Liu, Y.; Liu, Y.; Matharu, Z.; Rahimian, A.; Revzin, A. Detecting Multiple Cell-Secreted Cytokines from the Same Aptamer-Functionalized Electrode. *Biosens. Bioelectron.* **2015**, *64*, 43–50.

(39) Seo, H. Bin; Gu, M. B. Aptamer-Based Sandwich-Type Biosensors. *J. Biol. Eng.* **2017**, *11* (1), 11.

(40) Wang, G.; Liu, J.; Chen, K.; Xu, Y.; Liu, B.; Liao, J.; Zhu, L.; Hu, X.; Li, J.; Pu, Y.; Zhong, W.; Fu, T.; Liu, H.; Tan, W. Selection and Characterization of DNA Aptamer against Glucagon Receptor by Cell-SELEX. *Sci. Rep.* **2017**, *7* (1), 7179.

(41) Strianese, M.; Staiano, M.; Ruggiero, G.; Labella, T.; Pellecchia, C.; D'Auria, S. Fluorescence-Based Biosensors. *Methods Mol. Biol.* **2012**, 193–216.

(42) Senutovitch, N.; Vernetti, L.; Boltz, R.; DeBiasio, R.; Gough, A.; Taylor, D. L. Fluorescent Protein Biosensors Applied to Microphysiological Systems. *Exp. Biol. Med.* **2015**, *240* (6), 795–808.

(43) Nguyen, H.; Park, J.; Kang, S.; Kim, M. Surface Plasmon Resonance: A Versatile Technique for Biosensor Applications. *Sensors* **2015**, *15* (5), 10481–10510.

(44) Peltomaa, R.; Glahn-Martínez, B.; Benito-Peña, E.; Moreno-Bondi, M. Optical Biosensors for Label-Free Detection of Small Molecules. *Sensors* **2018**, *18* (12), 4126.

(45) Baraket, A.; Lee, M.; Zine, N.; Sigaud, M.; Bausells, J.; Errachid, A. A Fully Integrated

Electrochemical Biosensor Platform Fabrication Process for Cytokines Detection. *Biosens. Bioelectron.* **2017**, *93*, 170–175.

(46) Hasan, A.; Nurunnabi, M.; Morshed, M.; Paul, A.; Polini, A.; Kuila, T.; Al Hariri, M.; Lee, Y.; Jaffa, A. A. Recent Advances in Application of Biosensors in Tissue Engineering. *Biomed Res. Int.* **2014**, *2014*, 1–18.

(47) Nutiu, R.; Li, Y. Structure-Switching Signaling Aptamers: Transducing Molecular Recognition into Fluorescence Signaling. *Chem. - A Eur. J.* **2004**, *10* (8), 1868–1876.

(48) Ruttkay-Nedecky, B.; Kudr, J.; Nejdl, L.; Maskova, D.; Kizek, R.; Adam, V. G-Quadruplexes as Sensing Probes. *Molecules* **2013**, *18* (12), 14760–14779.

(49) Unser, S.; Bruzas, I.; He, J.; Sagle, L. Localized Surface Plasmon Resonance Biosensing: Current Challenges and Approaches. *Sensors* **2015**, *15* (7), 15684–15716.

(50) Vigneshvar, S.; Sudhakumari, C. C.; Senthilkumaran, B.; Prakash, H. Recent Advances in Biosensor Technology for Potential Applications – An Overview. *Front. Bioeng. Biotechnol.* **2016**, *4*.

(51) Lin, S.; Yu, Z.; Chen, D.; Wang, Z.; Miao, J.; Li, Q.; Zhang, D.; Song, J.; Cui, D. Progress in Microfluidics-Based Exosome Separation and Detection Technologies for Diagnostic Applications. *Small* **2020**, *16* (9), e1903916.

(52) Coluccio, M. L.; Perozziello, G.; Malara, N.; Parrotta, E.; Zhang, P.; Gentile, F.; Limongi, T.; Raj, P. M.; Cuda, G.; Candeloro, P.; Di Fabrizio, E. Microfluidic Platforms for Cell Cultures and Investigations. *Microelectron. Eng.* **2019**, *208*, 14–28.

(53) Luan, Q.; Macaraniag, C.; Zhou, J.; Papautsky, I. Microfluidic Systems for Hydrodynamic Trapping of Cells and Clusters. *Biomicrofluidics* **2020**, *14* (3), 031502.

(54) Park, Y.; Huh, K. M.; Kang, S.-W. Applications of Biomaterials in 3D Cell Culture and Contributions of 3D Cell Culture to Drug Development and Basic Biomedical Research. *Int. J. Mol. Sci.* **2021**, *22* (5), 2491.

(55) Hilderbrand, A. M.; Ovadia, E. M.; Rehmann, M. S.; Kharkar, P. M.; Guo, C.; Kloxin, A. M. Biomaterials for 4D Stem Cell Culture. *Curr. Opin. Solid State Mater. Sci.* **2016**, *20* (4), 212–224.

(56) Khan, F.; Tanaka, M. Designing Smart Biomaterials for Tissue Engineering. *Int. J. Mol. Sci.* **2017**, *19* (1), 17.

(57) Li, X.; Soler, M.; Özdemir, C. I.; Belushkin, A.; Yesilköy, F.; Altug, H. Plasmonic Nanohole Array Biosensor for Label-Free and Real-Time Analysis of Live Cell Secretion. *Lab Chip* **2017**, *17* (13), 2208–2217.

(58) Kaestli, A. J.; Junkin, M.; Tay, S. Integrated Platform for Cell Culture and Dynamic Quantification of Cell Secretion. *Lab Chip* **2017**, *17* (23), 4124–4133.

(59) Shan, S.; He, Z.; Mao, S.; Jie, M.; Yi, L.; Lin, J.-M. Quantitative Determination of VEGF165 in Cell Culture Medium by Aptamer Sandwich Based Chemiluminescence Assay. *Talanta* **2017**, *171*, 197–203.

(60) Cui, X.; Liu, Y.; Hu, D.; Qian, W.; Tin, C.; Sun, D.; Chen, W.; Lam, R. H. W. A Fluorescent Microbead-Based Microfluidic Immunoassay Chip for Immune Cell Cytokine Secretion

Quantification. *Lab Chip* **2018**, *18* (3), 522–531.

(61) Zhang, W.; He, Z.; Yi, L.; Mao, S.; Li, H.; Lin, J.-M. A Dual-Functional Microfluidic Chip for on-Line Detection of Interleukin-8 Based on Rolling Circle Amplification. *Biosens. Bioelectron.* **2018**, *102*, 652–660.

(62) Ramji, R.; Alexander, A. F.; Muñoz-Rojas, A. R.; Kellman, L. N.; Miller-Jensen, K. Microfluidic Platform Enables Live-Cell Imaging of Signaling and Transcription Combined with Multiplexed Secretion Measurements in the Same Single Cells. *Integr. Biol.* **2019**, *11* (4), 142–153.

(63) Rodriguez-Moncayo, R.; Jimenez-Valdes, R. J.; Gonzalez-Suarez, A. M.; Garcia-Cordero, J. L. Integrated Microfluidic Device for Functional Secretory Immunophenotyping of Immune Cells. *ACS Sensors* **2020**, *5* (2), 353–361.

(64) Ortega, M. A.; Rodríguez-Comas, J.; Yavas, O.; Velasco-Mallorquí, F.; Balaguer-Trias, J.; Parra, V.; Novials, A.; Servitja, J. M.; Quidant, R.; Ramón-Azcón, J. In Situ LSPR Sensing of Secreted Insulin in Organ-on-Chip. *Biosensors* **2021**, *11* (5), 138.

(65) Abdullah, M. A. A.; Wang, J. Ultrasimple Single-Cell Detection of Multiple Cytokines by a Nanowell Chip Integrated with Encoded Microarrays. *ACS Sensors* **2019**, *4* (9), 2296–2302.

(66) Antona, S.; Abele, T.; Jahnke, K.; Dreher, Y.; Göpfrich, K.; Platzman, I.; Spatz, J. P. Droplet-Based Combinatorial Assay for Cell Cytotoxicity and Cytokine Release Evaluation. *Adv. Funct. Mater.* **2020**, *30* (46), 2003479.

(67) Zhou, Y.; Shao, N.; Bessa de Castro, R.; Zhang, P.; Ma, Y.; Liu, X.; Huang, F.; Wang, R.-F.; Qin, L. Evaluation of Single-Cell Cytokine Secretion and Cell-Cell Interactions with a Hierarchical Loading Microwell Chip. *Cell Rep.* **2020**, *31* (4), 107574.

(68) Armbrecht, L.; Rutschmann, O.; Szczerba, B. M.; Nikoloff, J.; Aceto, N.; Dittrich, P. S. Quantification of Protein Secretion from Circulating Tumor Cells in Microfluidic Chambers. *Adv. Sci.* **2020**, *7* (11), 1903237.

(69) Yuan, Y.; Brouchon, J.; Calvo-Calle, J. M.; Xia, J.; Sun, L.; Zhang, X.; Clayton, K. L.; Ye, F.; Weitz, D. A.; Heyman, J. A. Droplet Encapsulation Improves Accuracy of Immune Cell Cytokine Capture Assays. *Lab Chip* **2020**, *20* (8), 1513–1520.

(70) Zhu, C.; Luo, X.; Espulgar, W. V.; Koyama, S.; Kumanogoh, A.; Saito, M.; Takamatsu, H.; Tamiya, E. Real-Time Monitoring and Detection of Single-Cell Level Cytokine Secretion Using LSPR Technology. *Micromachines* **2020**, *11* (1), 107.

(71) van Neel, T. L.; Berry, S. B.; Berthier, E.; Theberge, A. B. Localized Cell-Surface Sampling of a Secreted Factor Using Cell-Targeting Beads. *Anal. Chem.* **2020**, *92* (20), 13634–13640.

(72) Berthuy, O.; Blum, L.; Marquette, C. Cancer-Cells on Chip for Label-Free Detection of Secreted Molecules. *Biosensors* **2016**, *6* (1), 2.

(73) Kongsuphol, P.; Liu, Y.; Ramadan, Q. On-Chip Immune Cell Activation and Subsequent Time-Resolved Magnetic Bead-Based Cytokine Detection. *Biomed. Microdevices* **2016**, *18* (5), 93.

(74) Son, K. J.; Gheibi, P.; Stybayeva, G.; Rahimian, A.; Revzin, A. Detecting Cell-Secreted Growth Factors in Microfluidic Devices Using Bead-Based Biosensors. *Microsystems Nanoeng.* **2017**, *3* (1), 17025.

(75) Hsu, M. N.; Wei, S.-C.; Guo, S.; Phan, D.-T.; Zhang, Y.; Chen, C.-H. Smart Hydrogel Microfluidics for Single-Cell Multiplexed Secretomic Analysis with High Sensitivity. *Small* **2018**, *14* (49), 1802918.

(76) Zhu, J.; He, J.; Verano, M.; Brimmo, A. T.; Glia, A.; Qasaimeh, M. A.; Chen, P.; Aleman, J. O.; Chen, W. An Integrated Adipose-Tissue-on-Chip Nanoplasmonic Biosensing Platform for Investigating Obesity-Associated Inflammation. *Lab Chip* **2018**, *18* (23), 3550–3560.

(77) Li, X.; Soler, M.; Szydzik, C.; Khoshmanesh, K.; Schmidt, J.; Coukos, G.; Mitchell, A.; Altug, H. Label-Free Optofluidic Nanobiosensor Enables Real-Time Analysis of Single-Cell Cytokine Secretion. *Small* **2018**, *14* (26), 1800698.

(78) Liu, G.; Bursill, C.; Cartland, S. P.; Anwer, A. G.; Parker, L. M.; Zhang, K.; Feng, S.; He, M.; Inglis, D. W.; Kavurma, M. M.; Hutchinson, M. R.; Goldys, E. M. A Nanoparticle-Based Affinity Sensor That Identifies and Selects Highly Cytokine-Secreting Cells. *iScience* **2019**, *20*, 137–147.

(79) Wei, S.-C.; Hsu, M. N.; Chen, C.-H. Plasmonic Droplet Screen for Single-Cell Secretion Analysis. *Biosens. Bioelectron.* **2019**, *144*, 111639.

(80) Giménez-Gómez, P.; Rodríguez-Rodríguez, R.; Ríos, J. M.; Pérez-Montero, M.; González, E.; Gutiérrez-Capitán, M.; Plaza, J. A.; Muñoz-Berbel, X.; Jiménez-Jorquera, C. A Self-Calibrating and Multiplexed Electrochemical Lab-on-a-Chip for Cell Culture Analysis and High-Resolution Imaging. *Lab Chip* **2020**, *20* (4), 823–833.

(81) Zhu, Q.; Liang, B.; Liang, Y.; Ji, L.; Cai, Y.; Wu, K.; Tu, T.; Ren, H.; Huang, B.; Wei, J.; Fang, L.; Liang, X.; Ye, X. 3D Bimetallic Au/Pt Nanoflowers Decorated Needle-Type Microelectrode for Direct in Situ Monitoring of ATP Secreted from Living Cells. *Biosens. Bioelectron.* **2020**, *153*, 112019.

(82) Rivera, K. R.; Pozdin, V. A.; Young, A. T.; Erb, P. D.; Wisniewski, N. A.; Magness, S. T.; Daniele, M. Integrated Phosphorescence-Based Photonic Biosensor (IPOB) for Monitoring Oxygen Levels in 3D Cell Culture Systems. *Biosens. Bioelectron.* **2019**, *123*, 131–140.

(83) Lau, U. Y.; Saxer, S. S.; Lee, J.; Bat, E.; Maynard, H. D. Direct Write Protein Patterns for Multiplexed Cytokine Detection from Live Cells Using Electron Beam Lithography. *ACS Nano* **2016**, *10* (1), 723–729.

(84) Bari, S. M. I.; Reis, L. G.; Nestorova, G. G. Calorimetric Sandwich-Type Immunosensor for Quantification of TNF-α. *Biosens. Bioelectron.* **2019**, *126*, 82–87.

(85) Liu, G.; Cao, C.; Ni, S.; Feng, S.; Wei, H. On-Chip Structure-Switching Aptamer-Modified Magnetic Nanobeads for the Continuous Monitoring of Interferon-Gamma Ex Vivo. *Microsystems Nanoeng.* **2019**, *5* (1), 35.

(86) Rani, D.; Singh, Y.; Salker, M.; Vu, X. T.; Ingebrandt, S.; Pachauri, V. Point-of-Care-Ready Nanoscale ISFET Arrays for Sub-Picomolar Detection of Cytokines in Cell Cultures. *Anal. Bioanal. Chem.* **2020**, *412* (25), 6777–6788.

(87) Doherty, E. L.; Aw, W. Y.; Hickey, A. J.; Polacheck, W. J. Microfluidic and Organ-on-a-Chip Approaches to Investigate Cellular and Microenvironmental Contributions to Cardiovascular Function and Pathology. *Front. Bioeng. Biotechnol.* **2021**, *9*.

(88) Clarke, G. A.; Hartse, B. X.; Niaraki Asli, A. E.; Taghavimehr, M.; Hashemi, N.; Abbasi Shirsavar, M.; Montazami, R.; Alimoradi, N.; Nasirian, V.; Ouedraogo, L. J.; Hashemi, N. N.

Advancement of Sensor Integrated Organ-on-Chip Devices. *Sensors* **2021**, *21* (4), 1367.

(89) Zhang, Y. S.; Aleman, J.; Shin, S. R.; Kilic, T.; Kim, D.; Mousavi Shaegh, S. A.; Massa, S.; Riahi, R.; Chae, S.; Hu, N.; Avci, H.; Zhang, W.; Silvestri, A.; Sanati Nezhad, A.; Manbohi, A.; De Ferrari, F.; Polini, A.; Calzone, G.; Shaikh, N.; Alerasool, P.; Budina, E.; Kang, J.; Bhise, N.; Ribas, J.; Pourmand, A.; Skardal, A.; Shupe, T.; Bishop, C. E.; Dokmeci, M. R.; Atala, A.; Khademhosseini, A. Multisensor-Integrated Organs-on-Chips Platform for Automated and Continual in Situ Monitoring of Organoid Behaviors. *Proc. Natl. Acad. Sci.* **2017**, *114* (12), E2293–E2302.

(90) Silverman, S. K. Catalytic DNA: Scope, Applications, and Biochemistry of Deoxyribozymes. *Trends Biochem. Sci.* **2016**, *41* (7), 595–609.

(91) von Wurmb-Schwark, N.; Bosinski, H.; Ritz-Timme, S. What Do the X and Y Chromosomes Tell Us about Sex and Gender in Forensic Case Analysis? *J. Forensic Leg. Med.* **2007**, *14* (1), 27–30.

(92) Storkebaum, E.; Lambrechts, D.; Carmeliet, P. VEGF: Once Regarded as a Specific Angiogenic Factor, Now Implicated in Neuroprotection. *BioEssays* **2004**, *26* (9), 943–954.

(93) Rose, J. K. Optimization of Transfection. *Curr. Protoc. Cell Biol.* **2003**, *19* (1), 20.7.1-20.7.4.

(94) Matellan, C.; del Río Hernández, A. E. Cost-Effective Rapid Prototyping and Assembly of Poly(Methyl Methacrylate) Microfluidic Devices. *Sci. Rep.* **2018**, *8* (1), 6971.

(95) Rega, R.; Gennari, O.; Mecozzi, L.; Pagliarulo, V.; Mugnano, M.; Oleandro, E.; Nazzaro, F.; Ferraro, P.; Grilli, S. Pyro-Electrification of Freestanding Polymer Sheets: A New Tool for Cation-Free Manipulation of Cell Adhesion in Vitro. *Front. Chem.* **2019**, *7*, 429.

(96) Schmalenberg, K. E.; Buettner, H. M.; Uhrich, K. E. Microcontact Printing of Proteins on Oxygen Plasma-Activated Poly(Methyl Methacrylate). *Biomaterials* **2004**, *25* (10), 1851–1857.

(97) Hamon, C.; Henriksen-Lacey, M.; La Porta, A.; Rosique, M.; Langer, J.; Scarabelli, L.; Montes, A. B. S.; González-Rubio, G.; de Pancorbo, M. M.; Liz-Marzán, L. M.; Basabe-Desmonts, L. Tunable Nanoparticle and Cell Assembly Using Combined Self-Powered Microfluidics and Microcontact Printing. *Adv. Funct. Mater.* **2016**, *26* (44), 8053–8061.

(98) Hurley, M. M.; Gronowicz, G.; Zhu, L.; Kuhn, L. T.; Rodner, C.; Xiao, L. Age-Related Changes in FGF-2, Fibroblast Growth Factor Receptors and β-Catenin Expression in Human Mesenchyme-Derived Progenitor Cells. *J. Cell. Biochem.* **2016**, *117* (3), 721–729.

(99) Ng, F.; Boucher, S.; Koh, S.; Sastry, K. S. R.; Chase, L.; Lakshmipathy, U.; Choong, C.; Yang, Z.; Vemuri, M. C.; Rao, M. S.; Tanavde, V. PDGF, TGF-β, and FGF Signaling Is Important for Differentiation and Growth of Mesenchymal Stem Cells (MSCs): Transcriptional Profiling Can Identify Markers and Signaling Pathways Important in Differentiation of MSCs into Adipogenic, Chondrogenic, and Oste. *Blood* **2008**, *112* (2), 295–307.

# Section 2

## Conclusions

## Conclusions from this thesis

In view of the results obtained in this work, the following conclusions are drawn:

*1.* A colorimetric assay using a DNAzyme was developed for the specific, qualitative and quantitative detection of a fragment of the Y amelogenin gene. In solution, the limit of detection (LOD) of the assay was 655 ng. When the assay was integrated into cellulose paper, the LOD of the assay was 45.7 ng. In addition, the reaction was successfully carried out inside of a proof-of-concept paper microfluidic analytical device (μPAD).

*2.* A fluorescence-based assay using a Structure Switching Signaling Aptamer (SSSA) was developed for the specific and quantitative detection of cell secreted Vascular Endothelial Growth Factor (VEGF). When adapted to cellulose paper, the LOD of the assay was 0.57 ng. The reaction was successfully carried out inside of a proof-of-concept μPAD. The device was validated for its use on cell culture scenarios through the detection of human Hair Follicle-derived Mesenchymal Stromal Cells (hHF-MSCs) secreted VEGF.

*3.* Direct monitoring and quantification of the gene transfection efficiency on hHF-MSCs arrays was achieved with high control over cell-cell interactions through surface patterning. Single hHF-MSCs arrays presented an earlier peak of maximum expression of transfected green fluorescence protein (GFP, from 24 h to 18 h), and a slight increment on the maximum transfection efficiency (from 22 % to 28 %) when compared with hHF-MSCs conventionally cultured or patterned in small cell-colonies. The single cell arrays also enabled the continuous monitoring of GFP expression, allowing the quantification of the absolute transfection efficiency.

*4.* Polymethyl methacrylate (PMMA) surface was successfully converted from cytophobic to cytophilic through combined physicochemical and biochemical treatments. Patterns of hHF-MSCs, colorectal and prostate cancer cells were fabricated on cytophilic PMMA controlling cell-cell contact and cell confluence. The patterns were greatly stable due to the high contrast between the treated and the untreated zones of the PMMA surface. The cell patterns

could be directly integrated into a simple polydimethylsiloxane microfluidic device.

*5.* Combined patterns of small hHF-MSC-colonies and microbeads were obtained through Printing and Vacuum Lithography. The localization of the functionalized microbeads neighboring the cell-colonies enabled the solid-phase presentation of the Fibroblast Growth Factor type 2 (FGF-2) to the cells with controlled cell-cell contact and controlled dosage of FGF-2. The enhanced effect of the growth factor on cell survival and cell proliferation could be observed in all the arrays containing FGF-2. Furthermore, the effect on the expression of membrane receptors could also be quantified through the fluorescent labelling of Fibroblast Growth Factor Receptor 1 and fluorescence microscopy imaging of the arrays.

*6.* Direct detection of VEGF in the surroundings of small cell-colonies was carried out on combined patterns of hHF-MSCs and microbeads. The microbeads were functionalized either with a conventional sandwich immunoassay or with the SSSA previously developed, presenting a LOD of 0.75 ng $mL^{-1}$ and 8 ng $mL^{-1}$ for the immunoassay and the SSSA assay, respectively. The system enabled the detection of cell secreted VEGF coming from a small number of adherent cells (4 to 5 cells) in both scenarios.

**Final remarks**

In view of these conclusions, the following statements can be determined:

*1.* Advances in microfabrication, microfluidics and material sciences has allowed the foundation of a new generation of microtechnologies for in vitro cell studies with high control over cell interaction and the possibility of high-throughput analysis of cell processes. These technologies in combination with data-analysis strategies for image-based cell profiling are expected to facilitate novel biological discoveries.

*2.* DNA probes form a highly versatile toolbox with which a large number of biosensors can be designed for the direct detection of analytes. Immobilization of DNA probes on solid substrates such as paper or microbeads does not interfere with their efficiency in detecting target

analytes, but rather improves their performance. These paper-immobilized probes can provide low-cost, easy-to-use devices (μPADs) for rapid analysis of samples, such as cell culture supernatant or forensic traces. Furthermore, the combination of DNA probes with microbeads, which act as molecular carriers and can form patterns on cell culture substrates, allows real-time detection of analytes secreted by a small number of adherent cells.

*3.* The fabrication of protein micropatterns on flat transparent substrates is a very powerful technique in the development of cell analysis platforms. It not only enables optical analysis of proliferation, migration, viability, intracellular and membrane protein expression of adherent cells but also allows the simultaneous creation of thousands of replicates on the same substrate, which permits a robust statistical analysis of whole cell populations or even the identification of subpopulations. In addition, it serves to control the contact of a cell with other cells, as well as the interaction between the cells and the substrate. It can be performed on a wide variety of substrates, including glass, culture dishes, and other common polymers like PMMA, what will facilitate in the future the manufacturing of commercial devices based on this technology.

*4.* The formation of complex patterns composed of cell-colonies and microbeads constitutes in itself a modular toolbox for the fabrication of cell analysis platforms, increasing the degree of control over cell interactions. Functionalized microbeads precisely placed in the cellular environment can be used as solid supports for efficient presentation of molecules, such as growth factors, to cells, or as supports for sensing probes for the highly sensitive detection of proteins secreted by a small number of cells.

*5.* This thesis presents a versatile methodology that can be used to introduce different signals into the system and monitor various aspects of cell behavior with high sensitivity, temporal and spatial resolution, allowing many different models of cell colonies or even tissue to be recreated and studied. In summary, a modular methodology based on the use of micropatterning techniques and nanomaterials is proposed that would enable the production of novel platforms for multiparametric high throughput analysis of cellular systems, presenting high control over the cell microenvironment and integrated biosensors for the monitoring of cellular processes.

# Section 3

## Appendixes

Appendix 1

# Microtechnologies for cell microenvironment control and monitoring

## Microtechnologies for cell microenvironment control and monitoring

Enrique Azuaje-Hualde, Maite García-Hernando, Jaione Etxebarria-Elezgarai, Marian Martínez de Pancorbo, Fernando Benito-Lopez, Lourdes Basabe-Desmonts

*Published in: Micromachines (2017)* [1]

*Impact Factor: 2.222 (Q2)*

*Area: Instruments and instrumentations*

### Abstract

A great breadth of questions remains in cellular biology. Some questions cannot be answered using traditional analytical techniques and so demand the development of new tools for research. In the near future, the development of highly integrated microfluidic analytical platforms will enable the acquisition of unknown biological data. These microfluidic systems must allow cell culture under controlled microenvironment and high throughput analysis. For this purpose, the integration of a variable number of newly developed micro- and nano-technologies, which enable control of topography and surface chemistry, soluble factors, mechanical forces and cell–cell contacts, as well as technology for monitoring cell phenotype and genotype with high spatial and temporal resolution will be necessary. These multifunctional devices must be accompanied by appropriate data analysis and management of the expected large datasets generated. The knowledge gained with these platforms has the potential to improve predictive models of the behavior of cells, impacting directly in better therapies for disease treatment. In this review, we give an overview of the microtechnology toolbox available for the design of high throughput microfluidic platforms for cell analysis. We discuss current microtechnologies for cell microenvironment control, different methodologies to create large arrays of cellular systems and finally techniques for monitoring cells in microfluidic devices.

**Keywords**: Cell analysis; High-throughput; Microfluidics; Microtechnology

## 1. Introduction

Native cells are in a dynamic multifactorial environment, their own microenvironment. The cell microenvironment is constituted by: their extracellular matrix (ECM), the topography and physical properties of the ECM and by soluble factors on their fluidic environment. All of them strongly affect cell fate and cell behavior. Changes in the cell microenvironment are transduced into intracellular signaling pathways, which regulate cell fate and cell behavior. Conventional cell culture systems often rely on batch experiments with limited control of cell microenvironments. In order to obtain a comprehensive knowledge of cell function and behavior, it would be desirable to develop experimental methods that could explain the contribution of each of those environmental factors, as well as their synergetic effects on cell behavior, **Figure 1**.

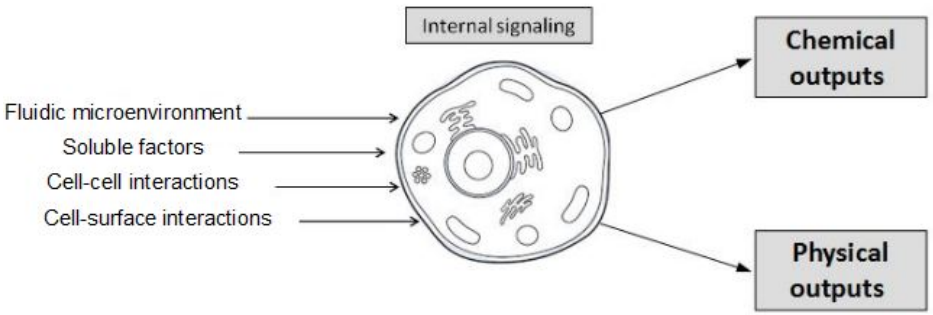


**Figure 1.** Input signals from cell microenvironment induce internal signaling of cells and modulate their outputs, affecting cell behavior.

During the last two decades, we have witnessed a number of key developments in the area of the microtechnologies, which allows introducing control and complexity over a full range of environmental factor at the microscale level. For example, technologies for the accurate structuration of surfaces for subsequent cell culture, microfluidic architectures, synthesis of novel biomaterials and nanomaterials with sensing and actuating capabilities have been developed and their potential for cell culture, stimulation and analysis has been proven. In particular, the miniaturized scale of

microchannels in microfluidic devices offers advantages such as low contamination risk, fast transfer of nutrients and heat, short equilibration times, parallelization of processes and automation, low reagent and power consumption, portability, etc. Moreover, since the dimensional environment is analogous to in vivo conditions, the small sizes of the channels permit medium and nutrients to diffuse to nutrient-poor areas. Currently, there is little development of microtechnologies that can successfully mimic the in vivo microenvironments, since any change in material, surface chemistry, cell number or flow conditions can affect the results of the assays [2]. Nowadays, there is an increasing use of microfluidic techniques on cell culture that have opened a broad range of possibilities for studying cells in a variety of contexts, allowing to understand the specific contribution of each different parameter to cellular behavior, such as shear forces, nutrient gradients, etc. [3]. An extra advantage of the use of microtechnologies is the scalability and the possibility of parallelization of cellular samples which allow high-throughput (HTP) measurements, essential for the statistical analysis of multi-parameter environments, and for the construction of predictive models.

The current trend is to develop HTP and multiplexed technologies, essentially those who also allow a real time or near-real time analysis for both single cell and multi cell platforms. The properties that can be quantified from analysis includes the study of the cells mechanics (deformation, migration and growth), the proteome, genome and secretome, and both their extracellular and intracellular interactions and their stimuli [4].

Integration of several microtechnologies to create controlled multi-parametric environments and monitoring is still a challenge. Microfluidics has emerged as a new way to fabricate large cellular arrays in defined patterns which allows the study of a large number of cells in a specific microenvironment as well as the observation and quantification of several outcomes from a single study. Looking for the best way to design novel platforms for cell analysis, in this manuscript, we review examples on how different parameters of cell microenvironment may be controlled through microtechnologies, as well as the techniques available for monitoring cells in microfluidic devices, centering

on the analysis of chemicals outcomes. Additionally, we give an overview of current microfluidic platforms already available for cell analysis.

## 2. Microtechnologies for cell microenvironment control

The term “cell microenvironment” involves those factors that directly or indirectly affect cell behavior, by biophysical, biochemical or other pathways. As previously stated, those factors can be classified in: ECM, cells surrounding a single cell, soluble factors, topography or physical properties of the ECM, and fluidic cues. All of them strongly affect cell proliferation and differentiation. However, despite this distinction, each factor cannot be considered independently, as all affect cell behavior in an orchestrated manner. During the past few years, the development of microfluidic platforms has been focused on the production of an optimal microenvironment that replicates cells natural conditions and allows their manipulation, **Figure 2**. The use of microfluidics brings many advantages in regulating cellular microenvironment, since microscale technologies make possible the control of soluble factors, cell adhesion to the surface, and also cell–cell contact [5].

To study cellular behavior in similar conditions to the in vivo responses, two approaches can be taken: study the interaction of each cell with their respective microenvironment or study the general interaction between the cell microenvironment and a cluster of cells. The isolation of cells as single cells allows the study of cell population heterogeneity, which enables analyzing the responses and behavior of a large number of individual cells and therefore distinguishing between cell subpopulation [6]. On the contrary, microfluidic multi-cell studies offer information about the entire cell population. These types of cultures have been largely used to try to understand the general responses of an entire cellular population to a specific reagent [7,8].

By housing a small number of cells in microwells or spots, both the cell–cell interactions and microenvironment changes can be observed and quantified, opposite to the single cell studies. In general, to carry out either of these studies, it is necessary to have under control the specific microenvironmental parameters.

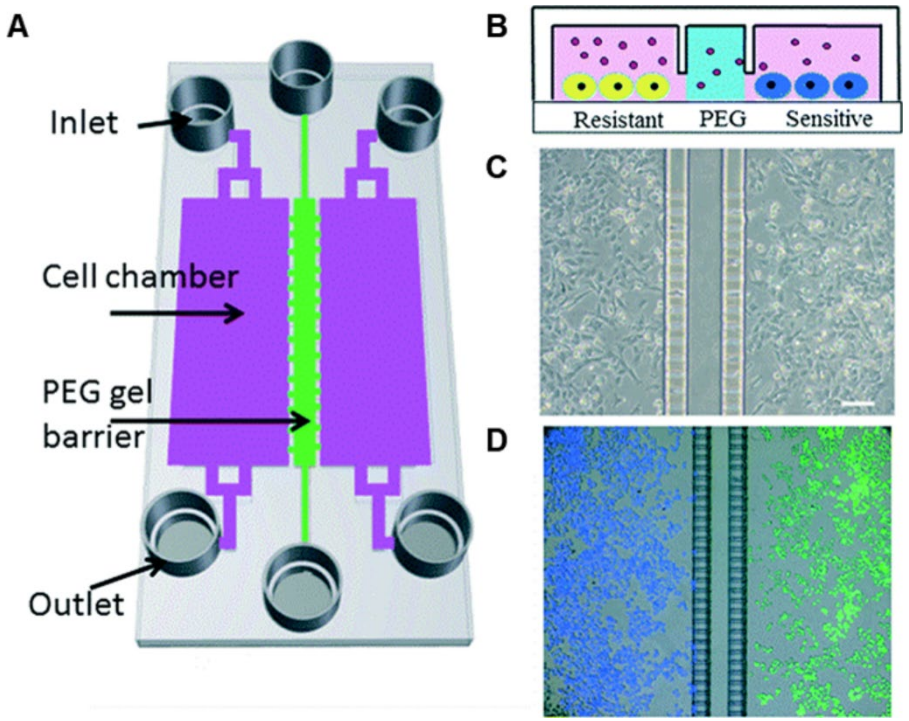


**Figure 2.** An example of a microfluidic co-culture device with semi-permeable PEG barrier to control soluble factors in small volumes. (A) Schematic of a device with two 1.8 mm-wide cell culture chambers in pink separated by a 100 μm PEG gel channel in green. (B) Cross-sectional view of two types of melanoma cells cultured in close proximity. (C) Brightfield image of A-375 cells cultured at Day 1. Scale bar represents 100 μm. (D) A-375 cells were labeled with either green or blue cell-tracker dyers before being seeded in alternate chambers. Migration was assessed after a 48 h culture period. Reproduced from [9] with permission of The Royal Society of Chemistry.

### *2.1. Topography*

Cells are capable of sensing and responding to different signals, including those provided by the ECM. In vivo, ECM has a specific physical structure and molecular composition; it presents a variety of geometrically-defined three-dimensional (3D) physical cues on the order of micron and sub-micron scale known as topographies. The interaction between cells and topography is driven by a phenomenon named “contact guide”, and it is related to cell

adhesion, morphology and differentiation [10]. Therefore, being capable of modifying surfaces at nano- and micro-scale emerges as crucial to study cell–surface interactions, as shown in **Figure 3**, where mesenchymal stem cells (MSCs) differentiation to bone tissue is affected by the topography of the substrate.

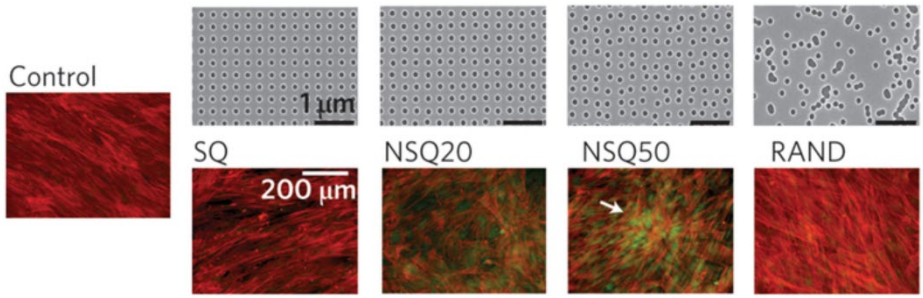


**Figure 3.** Topographical manipulation by electron-beam lithography. Osteoinduction (Generation of bone tissue) of MSCs was not obtained neither in square (SQ) nor random (RAND) patterns, while appearing on the controlled disorder patterns (NSQ20 and NSQ50 same as SQ but with ±20 nm and ±50 nm offset from the 300 nm center–center position) Adapted from [11] with the permission of Nature Publishing Group.

One of the main interests in topography in the last years lies on its effect on Mesenchymal Stem Cells (MSC), where changes on surface properties, proliferation and differentiation can be caused by cell–ECM or cell–surface interactions. Recently, it has been confirmed that, when mouse Embryonic Stem Cells (mESC) are cultured on poly(2-hydroxyethyl methacrylate-*co*-ethylene dimethacrylate) **(**HEMA-EDMA) surfaces with hierarchical micro to nano roughness, their long-term self renewal is promoted, while, when culturing them in contact with smooth or nanorough polymer surfaces, differentiation is induced [12]. As reported by Jaggy *et al.,* when cells were cultured on controlled topographies, hierarchical micro-nanoscale surface roughness favored the pluripotent character of mESCs when compared to a chemically identical nano rough or smooth surface. Because of the previous experiments, roughness was identified to maintain stem cell self-renewal capabilities, as long as the surface chemistry remained hydrophilic.

There is a wide spectrum of biocompatible techniques available to perform topographical features at microscale. It is worth mentioning that biocompatibility of the fabrication techniques and the materials used is a crucial factor in ensuring cell viability on those rough surfaces incorporating micro/nanofabricated structures [13,14].

Until now, photolithography is the most extended technique to make micro- and nanostructures in flat surfaces, while other biocompatible microfabrication techniques based on 3D printing, electrospinning and self-assembly are currently emerging [15]. Currently, soft lithography is the most used technique. However, other lithography methods are being developed in order to overcome the drawbacks this methodology presents, such as the need of knowledge on Microcontact Printing process (μCP) and its limitations on creating patterns of multiple proteins.

Actually, various researches focused on the studying of migration in different topographical microenvironments [16,17]. As an example, a promising method was developed by Kon and co-workers, based on a protein-friendly photoresist, combining Capillary Force Lithography (CFL) and Microscope Projection Photolithography (MPP), to study cellular dynamics under topographical microenvironments [18]. This lithography method was adequate to create multiscale multiple protein patterns, even though it did not reach good precision in the creation of submicrometer features. Nevertheless, this technique was meaningful to study the effect of topography on human colon cancer cells, demonstrating that hierarchically organized structures on the surface, modulates processes such as cell migration and adherence.

In contrast, when it comes to high precision, Nanoimprint Lithography (NIL) emerges as a technique capable of creating nanostructures with molecular resolution [19]. NIL and surface functionalization have been used to create RGD peptide functionalized nanodots on silicon surfaces. As cells tend to adhere to RGD peptide, the combination of these two techniques has been successfully used to study of the effect of surface nanostructures on MSC behavior.

Furthermore, a method based on “multiphoton ablation lithography” has been developed to create patterns of different pitches and constant nanocrater dimensions on a surface. Topographical structures were produced by “multiphoton ablation lithography”. It has been demonstrated that modifying surfaces with topographical structures at the nano-scale, cell behavior without any chemical treatment of the substrate can be modulated, showing a clear trend of the cells to certain features [17].

Nanoparticles have also been employed to modify the topography of cell culture substrates. Recently, a method called Printing and Vacuum Lithography *(*PnV lithography*)* has emerged from our laboratories*,* enabling multi-patterning of biomolecules and gold nanoparticles (GNPs) by combination of vacuum soft-lithography and microcontact printing. Control of the surface coatings of the nanoparticles enabled controlled NP assembly and therefore substrate topographies. This technique allowed the controlled assembly of cells in adjacent positions to multiple topographies [20].

Furthermore, a method for dynamic cell micropatterning on nanostructured surfaces was developed with a cell-friendly photoresist [21]. A device with different topographies was fabricated, and it showed how cells respond to distinct topographies during spreading. Moreover, with this device, it was possible to observe the dynamic behavior of ~30 cells simultaneously and, thus, systematically compare the influence of topography in their spreading. This technique looks promising due to its dynamic working, which proposes information read out in real time, giving a more realistic point of view of cell behavior.

*2.2. Biochemical factors: surface chemistry and soluble factors*

Cells not only interact with their bottom substrate, as they create 3D interactions with all surrounding elements. As previously stated, the cell microenvironment and its ECM composition heavily influence the cells growth, proliferation, orientation, organelles distribution and signal transduction. Thus, understanding the chemical composition of the microenvironment and the mechanism that affects the cell behavior both physically and chemically is essential to develop an artificial ECM for efficient

cell studies [22]. ECMs are made of different types of macromolecules, mainly collagens, elastin, fibronectin, glycoproteins, proteoglycans and glycosaminoglycans, whose composition and structure varies from tissue to tissue. These compounds reorder, forming three-dimensional matrices; interstitial matrices surrounding cells; and pericellular matrices in direct contact with the cells [23,24] (**Figure 4**).

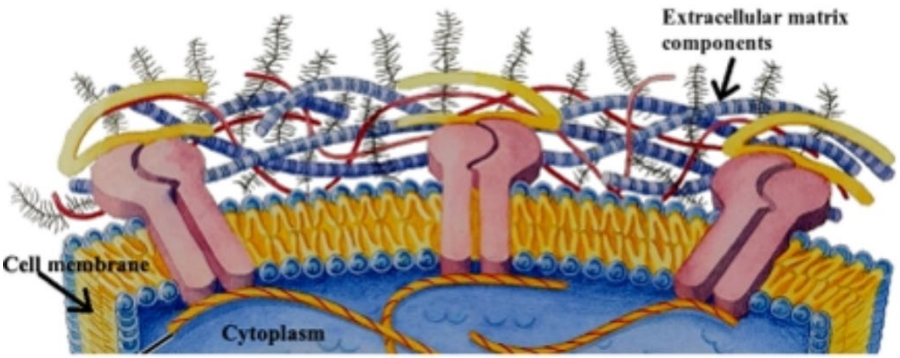


**Figure 4.** This figure shows the intimate contact between cellular membrane and the extracellular matrix (ECM, protein fibers embedded into a polysaccharide gel). Understanding the interaction between cells and ECM is essential for understanding cellular behavior. Adapted from [25] with permission from PLOS computational biology.

The formation and dynamics of cell adhesion mostly rely on the direct interactions made by focal adhesions (FAs). In the eukaryotic cells, integrin and integrin-like substances form transmembrane heterodimers in the cell membrane that join to the ECM, providing links between the ECM and both cytoplasmatic proteins and the actin cytoskeleton. This connection not only serves as a mechanical link, but also acts as a mechanoreceptor, regulating the cell phenotype [26–28].

Apart from direct interactions between the cells and the ECM, surrounding fluids play an important role in cell behavior. It is necessary for the surrounding fluids to have fluidic mechanics, which could provide a suitable chemical surrounding of nutrients and oxygen for cell growth. Soluble factor signaling is involved in regulating many biological events such as embryonic stem cell pluripotency, mammalian embryogenesis, tumor formation and

metastasis. They are especially important in Stem Cell cultures, since Stem cell fate in these niches is regulated by chemical and biological microenvironments [29,30].

Nowadays, the aim is to recreate and engineer nanoscaled ECMs for the design of cell culture platforms. In order to control cell cultures and regulate their signaling pathways, synthetic platforms made by either natural or artificial biomaterials that mimic the ECM are being developed. In the past few years, this has been mostly achieved by the use of micro- and nanopatterning, in which a desired pattern of 2D or 3D motifs with the ECM compounds is reproduced in a two-dimensional or three-dimensional substrate. Microscale technologies, in the form of microfluidic platforms appear as efficient techniques to achieve a precise control of soluble factors in small volumes, and so, modulation of signals between cells would be possible [9].

Two different approaches may be taken in order to recreate ECMs, a top down one in which the ECM are reproduced first from a macroscopic level to be later applied in its entirety on the substrate, and a bottom up approach in which the ECM is created by the assembly and gathering of smaller parts over the substrate [31,32].

Three major methods have been described for the patterning of ECM compounds. The first one was a direct method in which the final composition of the matrix is directly added to the substrate [33]. The second consists of a self-assembly method, in which small components interact with each other forming a larger structure with high hierarchy [34]. Deeg *et al*. obtained a simultaneous control of the ligand spacing and ligand density on a 2D cell culture by a self-assembly micropatterning [35]. The third is a replication method, in which a master, previously made by lithography methods such as nanoimprint lithography or soft lithography, is used several times in order to reproduce a specific pattern [19], enabling serial repetition of experiments using a previously designed and well organized patterns. Tan *et al*. used this replication method for the printing of a monolayer of initiator molecules to control the polymerization process, enabling controlled cell adhesion to the

designed pattern [36]. As opposed to the direct method, the self-assembly method and the replication method allows a proper reconstruction of the ECM by a nano- and micro-scaled fabrication of the ECM. The replication method also gives the opportunity of serialization of cell arrays as the master can be used multiple times.

### *2.3. Cell–cell contact*

Direct cell–cell contact is a type of communication between cells that relies on the interaction between cells themselves and their surrounding environment that acts as both physical anchor that constrain cells and plays as signaling interchange between cells. Together with cell shape, cell–cell contact is described as an influential factor affecting cell fate decisions, and, therefore, modulating cell behavior. Moreover it is an essential parameter to be regulated in order to achieve a successful cell culture. There is a huge range of methods which enable the precise control of the contact between cells. They can be divided into two main types: techniques involving cell adhesion to the surface, and techniques based on the confinement of cells in a definite space.

Microtechnologies are considered powerful tools to control cell–cell interactions, leading to a certain control of cell behavior could be possible. Direct contact between cells is known to induce cell differentiation in conventional cell cultures [37]. Tang *et al*. confirmed that the differentiation of mesenchymal stem cells to osteogenic and adipogenic cells was regulated by cell–cell contact by using a polyethylene glycol micropatterns for controlled cell adhesion [38] (**Figure 5**).

In contrast, methods lacking cell adhesion have also been proven to be useful to control cell–cell contact. Interactions between cells play an essential role in creating immunologic functional cells, and therefore, in immunological response. Juxtacrine interactions or interactions that require close contact are the most important ones mediating in immunological responses. Therefore, the study of the interactions between immune cells is a good proof of principle of the capability of the microtechnologies to control cell–cell interactions. In this regard, a method based on surface acoustic valves was reported, which

was capable to locate individual cells with micrometer precision, and thus enabling the control of cell–cell interactions in T-cell cultures [39]. In this work, Guo *et al*. demonstrated that the use of an acoustic well is useful for intercellular communication studies since the technique enables the control of the intercellular distance, the engineering of homotypic or heterotypic cell assemblies and monitoring the transformation of cellular aggregates from suspended to adherent states and the subsequent investigation of the assembly and the communication in those adherent cells.

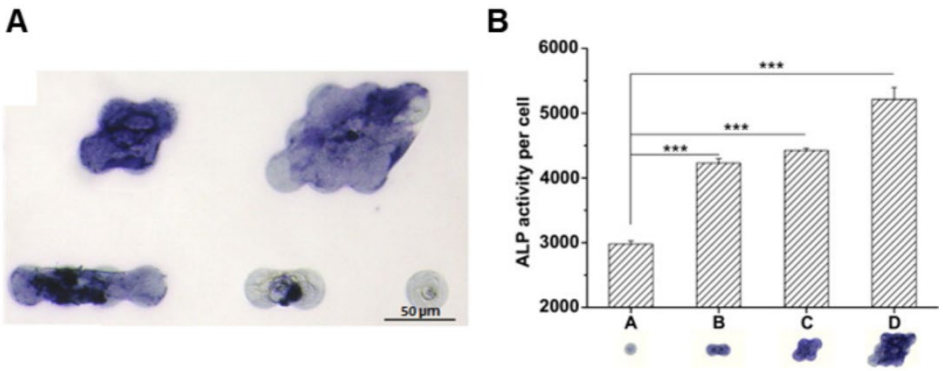


**Figure 5.** Cell–cell contacts enhance osteogenic differentiations of mesenchymal stem cells confirmed by the increased expression of alkaline phosphatase (ALP). (a) A brightfield images of MSCs on adhesive microdomains after six days in osteogenic differentiation medium. ALP was stained in blue by Fast Blue. Scale bar, 50 μm. (b) ALP activity per cell on indicated microdomains. Adapted from [38] with the permission of Elsevier.

Further, in terms of real time and high throughput analysis, a method based on ultrasonic waves was developed for time-controlled induction of cell–cell contact [40]. This method allowed simultaneous trapping and aggregation of cells using ultrasonic standing waves, without affecting cell viability. Ultrasound forces were proven useful for generating cell–cell contacts, inducing synchronized contacts between Natural Killer (NK) immunological cells and giving real time information of NK cell heterogeneity.

Going to 3D, direct contact between cells is also being studied. Microfabrication techniques such as bottom-up and directed assembly of

microscale hydrogels are becoming very popular, as they are considered powerful tools that enable the fabrication of 3D structures, replicating in vitro the microenvironment found in vivo. The engineering of tissues and organs, requires a scaffold which mimic cell ECM and enables cell adhesion to the surface and cell–cell contact, while it also allows the necessary soluble factors diffusion in order to get a functional organ or tissue. To mimic ECM, first, hydrogel stiffness can be controlled, in order to get the desired transport of solutes and gases through the scaffold. Moreover, hydrogel surface can be functionalized to promote cell adhesion. Finally, microtechnologies applied to produce microengineered hydrogels, allow the creation of 3D structures (scaffolds), where it is possible to precisely control the size of cell aggregates, and so, the interactions between cells [41], being capable to create a biomimetic microenvironment for cell growth. Due to the mimicking that can be achieved with microengineered hydrogels, multiple researches will be doing at this field in the near future, bringing us closer to personalized therapies.

As an example of hydrogel microfabrication, a laser printing of three-dimensional multicellular arrays method was developed to study of complex and dynamic relationships between cells and their local environment. The scaffold structure was built layer by layer, and thanks to the precise control of cell amount per spot, ratios between different cell types and the spot-to-spot spacing were evaluated by Gruene *et al.* [42]. This technology would provide the possibility to create precisely designed microenvironments for cell culture, and therefore, due to the mimicking reached with this technique, a more realistic study of cell behavior could be performed.

Cell–ECM interactions, chemical signaling between cells, and direct cell–cell interactions are cell stimuli sources that cannot be understood as independent factors. It is known that cell–ECM interactions affects cell–cell tension, and therefore, cell–cell contact, resulting in an interdependence of cell–cell and cell–ECM interactions [43]. Recently, a microdevice of capable identifying the optimal combination of topographical (physical) and biochemical cues has been developed [44]. It was found that cells respond to topography and physical cues and that different biochemical signals alter cell response to topography.

Furthermore, a microtechnology based on polyacrilamide gels, capable of describing the effects of the combination of topographical, mechanical, chemical and intracellular electrical stimuli on a co-culture of fibroblasts and skeletal muscle cells, was described by Ricotti and co-workers [45]. The work demonstrated that muscle cell differentiation was synergistically enhanced with the combination of intracellular stimulation produced by piezoelectric nanostructures activated by ultrasounds. Cytokines were over-expressed by fibroblasts in the co-culture in correspondence to surface microtopography stimuli.

*2.4. Fluidic microenvironment*

Fluidics and flow factors are vital for controlling the cellular microenvironment and cell behavior, as not only the diffusion and uptake of soluble factors depend on it, but it also affects physically the cells. Different microfluidic scenarios can be found in literature for cell analysis, that vary in configurations depending on the type of the studied cell or the application of the integrated assays. Moreover, specific shear and flow profiles are required in order to imitate in vivo conditions of cells, e.g., in blood vessels [46], and to be able to control those in microfluidics is very important. In certain cases, when properties of drugs are tested, the flows are driven by peristaltic pumps that work at back pressures and generate pulses inside the microfluidic bioreactors [47]. This could be a drawback in applications such as cell proliferation that require highly stable and continuous flow rates to generate constant shear stress on cells [48]. On the other hand, microfluidic devices can be used to manipulate the characteristics of cell matrixes. While some systems have been designed to simulate the mass transfer by convective transport of nutrients in capillary vessels in order to mimic the in vivo tissue environment, others use cell chambers that are isolated from the main fluid channel so that cells receive the nutrient via diffusive transfer [49].

Stefano et al. analyzed the effect of different flow conditions, from continuous to periodic perfusion, on long-term cell culture using microfluidic platforms for cell medium delivery [50]. The different perfusion conditions employed for C2C12 cell culture and the results obtained for each flow profiles are shown

in **Figure 6**. On the one hand, the experiments demonstrated that a periodic medium delivery with fast pulses (P2) resulted in a homogeneous cell culture in terms of cell viability, colony morphology and maintenance of pluripotency markers. On the contrary, a continuous flow (C1) resulted in cell heterogeneity, with abnormal morphology and vesiculation.

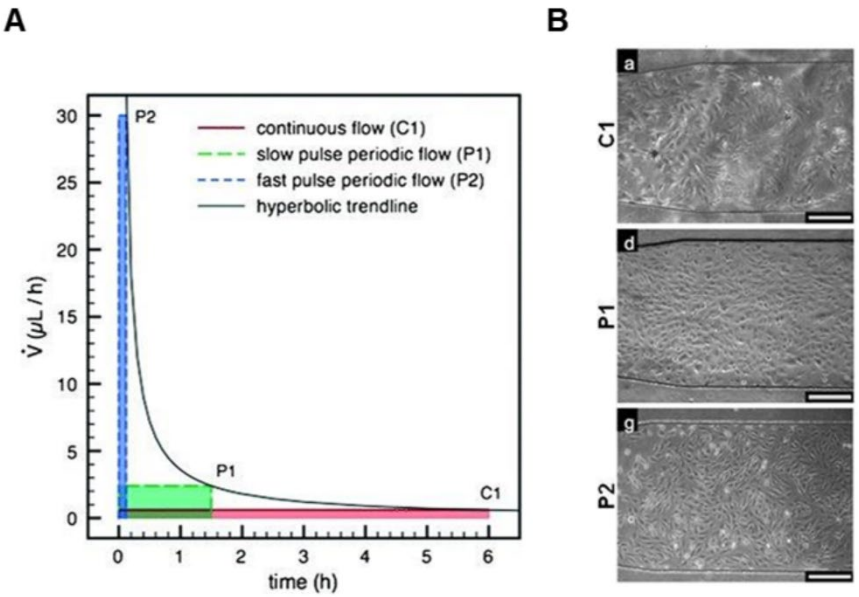


**Figure 6.** Study of different medium delivery strategies on long-term cell culture, varying the flow rate and the perfusion interval. (a) The same amount of medium was delivered using different perfusion conditions, assuming 6-h cycles. (b) The results for microfluidic C2C12 cell culture after four days show that a continuous perfusion with a stable flow condition leads to a heterogeneous growth (C1), while a fast pulse perfusion with periodic flow condition renders a uniform cell growth along the channel. White bars are 250 μm. Adapted from [50] with permission of The Royal Society of Chemistry.

Overall, continuous or pulsed medium delivery was used to maintain the cell microenvironments, but the optimal strategy for medium delivery is still an open issue. In this line, computational fluid dynamics is becoming a useful tool to try to understand the implications of fluid flow and nutrient transport on cell function and responses [49].

As mentioned above, flow control in microfluidics usually requires the use of external pumps or pneumatic fluid handling systems to generate continuous and stable or periodic and pulsed flows. Therefore, many investigations are being carried out to adequate fluid manipulation to the requirements of these novel microfluidic platforms. It is important to mention that many of these flow control components generate flow pneumatically by using air to pressurize the medium, therefore in case where the media which contains bicarbonate buffers, special attention must be paid to in the composition of the air used with correct percentage of $CO_2$ and $O_2$, to avoid pH changes in the medium. Therefore, it is recommendable to consider from the very beginning an adequate flow method [2].

Microfluidics also offers potential for tight medium composition control and devices that implement chemical gradients and droplet-based microfluidics are examples of widely used microfluidic systems that improve the sensitivity and complexity of experiments for studying cellular responses. Microfluidic devices involving gradient of soluble factors have been used to obtain a good differentiation of Stem Cells [51]. In order to avoid the exposure of cells to shear stress, a membrane-based microfluidic device has been developed by Kawada et al. to maintain, long term, an adequate delivery of soluble factors [52]. Chemical gradient devices can be driven under perfusion or statically: in continuous perfusion, the mixing of chemical species between two streams of fluid in laminar flow occurs due to diffusion, generating gradients of species at stream interfaces, and exposing the cells to these gradients across the microchannels. The perfusion also allows continuous nutrient supply and waste of removal, agreeing the in vivo microenvironment quality of most mammalian cell types. Limitations of perfusion include requirement of highly stable fluid flow and therefore fluid handling setups, relatively large volumes of reagents to maintain continuous and stable flowing gradients, and in situations where cell–cell communication is important perfusion is unsuitable for probing cellular responses. Instead, for the last case, static methods can be used, since static fluid preserves paracrine signaling. Static chemical gradients are formed between a source and a sink along a thin channel, and the gradient profile can be controlled by adjusting the input concentration, distance from source sink, or by changing the geometry of the channel.

However, for this kind of device, special attention must be taken to avoid evaporation of the liquids, which could impair appropriate performance of the device increasing the concentrations, and the time required to set up the gradients is often rather long [53].

## 3. Large arrays of individually addressable cellular systems under controlled microenvironment

To understand what is happening inside cells, it is necessary to perform biochemical analysis of cell components, and detect substances released by the cells. In general, for these type of analyses, it is necessary to create homogeneous populations of cells from a tissue, and to culture them to obtain enough material to be analyzed. Techniques like Fluorescently Activated Cell Sorting (FACS) enable the preparation of uniform populations of cells which can then be expanded in culture plates to produce large amounts of material to analyze.

Ideally, researchers would have some type of tool that would extract reliable information from small amount of cells, thus avoiding the need of cell culture. Such a tool could simultaneously also provide information about the nature of cells, avoiding in this case the need to separate different cell types within the tissue. The development of several microtechnologies enable the discrete manipulation and observation of small cellular systems, where each system may be comprised of a small number of cells, ranging from a single cell to several cells. Hence it is possible to observe and analyze a heterogeneous population of cells simultaneously, without the need of previous cell sorting or cell culture for expansion.

Currently, the most used cell culture methodologies rely on general protocols and large culture plates, only exceptionally taking into consideration substrate characteristic. As new discoveries have been made in how cells interact with their extracellular matrix and with each other, it has arisen the need to explore and study new ways to perfectly control and adapt the medium and the substrate to each type of cell [54]. For example, interesting cells such as stem cells or iPSCs usually requires specific characteristic for their culture, growth

and differentiation that can not always be achieved by conventional methods, thus requiring new techniques for cell culture [55]. In addition, creation of complex cultures such as body-on-a-chip requires new technologies that enable the recreation of physiological functions [56]. All this denotes the advantages and the need to control the cell microenvironment as much as possible to perform meaningful analytical measurements of the biology of cells.

Rapid screening methods and large samples have the potential to impact the development of predicting models for both conventional cell studies and the new models previously cited. The combination of high throughput methodologies with cell microenvironment control will pave the way to obtain high resolution information on dynamic cell behavior. Several methodological approaches and platforms have been developed to achieve large and dense arrays of individually addressable cellular systems to facilitate their study in a HTP manner. Those cellular systems, which can be fabricated in order to replicate the desired microenvironment, may vary in size ranging from individual single cells to groups of specific number of cells. The use of HTP methods enables parallelization and automation in both the creation of different microenvironments and the rapid screening of cellular outputs.

Microfluidic large-scale integration (mLSI) systems refer to microfluidic chips with large arrays of thousands of interconnected individually addressable microchambers [57], where individual cells can be independently isolated, assayed and recovered. mLSI, shown in **Figure 7**, are based on the integration of micromechanical elastomeric valves into multilayer polymeric microfluidic networks [58,59]. Recent applications of these type of platforms include single cell genome sequencing [60], single cell microRNA expression profiling [61], RT-qPCR, on more than 3000 cells [62], and HTP mammalian cell transfection and culturing [63].

Droplet microfluidics is a type of microfluidic platform amenable for HTP analysis. Unlike continuous flow systems, droplet-based systems focus on creating discrete volumes with the use of immiscible phases. Droplets are usually generated by pressure-driven flow and are surrounded by an

immiscible oil phase such that each droplet behaves as an individual microreactor or cell container [64] (**Figure 8**). Pressurized immiscible fluids are mixed at an orthogonal junction of two or more microchannels, combining cross-flow and viscous shear to generate monodisperse water-oil droplets with picolitre-scale volumes.

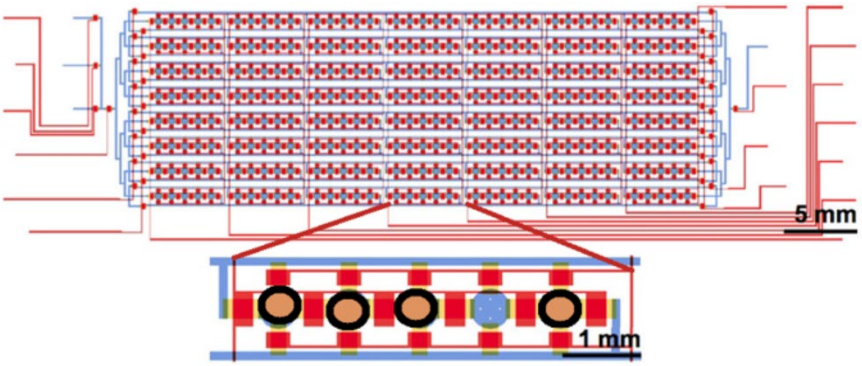


**Figure 7.** Schematic overview of a microfluidic large integration system where a great amount of single cells or cluster of cells can get entrapped simultaneously controlled by a valve system, adapted from [63] with the permission of Nature Publishing Group.

Cells can be entrapped inside the droplets and reagents can be administered using very low volumes, even 1000 times smaller than the ones used in conventional microplate assays [65,66], enabling the creation of thousands of microenvironments within the same assay. Biocompatible surfactants for the development of the droplets and storage systems made of polymers are needed for the maintenance of cells in a liquid microenvironment in which they can proliferate and be controlled and manipulated. An application of this technology is the compartmentalization of single cells in droplets to enable the analysis of molecules that have been secreted by cells, such as antibodies secreted from single mouse hybridoma cells [67]. This process overcomes one of the major limitations of traditional flow cytometry and fluorescence-activated cell sorting techniques: the detection of secreted molecules. Full droplet microfluidics systems based on continuous workflow have also been used for manipulating and monitor continuous growth of bacteria populations. Bacteria populations are encapsulated on hundreds of

microdroplets acting each as independent chemostats, microdroplets with specific chemical composition for continuous culture of microorganisms. The system allows studying the dynamics of bacterial populations in microdroplet chemostats as well as cellular responses to a range of stable or changing antibiotic concentrations [67,68]. DropSeq, is a recently developed HTP technology for single cell DNA sequencing based on droplet microfluidics. Individual cells are co-encapsulated with coded DNA-functionalized polymeric beads. It has been used for highly parallel genome-wide expression profiling of individual cells using nanoliter droplets [69]. Other droplet based methods have been developed, combining droplet microfluidics and reconfigurable flow-routing capabilities of integrated microvalve technology. It has been applied to multi-parameter analysis of single microbes and microbial communities [70].

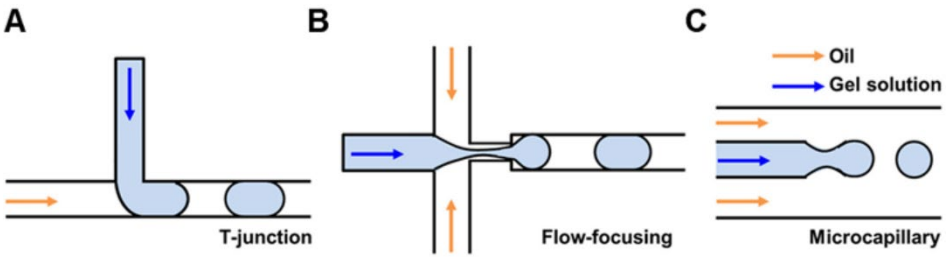


**Figure 8.** Three principle microfluidic geometries available for hydrogel droplet generation: (a) T-junction, (b) flow focusing, and (c) microcapillary. Reproduced from [71] with the permission of The Royal Society of Chemistry.

Droplet-based techniques can be used to encapsulate the cells with different mediums at different concentrations and an enhanced mixing can be achieved due to internal recirculation. Furthermore, it allows highly parallelized experiments for HTP as described above [72]. This has also gained importance in the co-culture of cells since utilizing a microfluidic device in which co-encapsulation of cells was performed resulted in a technology capable of modulating signaling of microenvironment [73]. It is important to assure a correct performance of the droplet-microfluidics device to generate highly stable flows, and thus the control and stability of the flow rate. This is extremely important in order to avoid oscillations of pressure inside the

system that could break its steady state and impede obtaining homogeneous and reproducible droplet size.

Other strategies for the fabrication of highly dense cell arrays for HTP analysis include the fabrication of three-dimensional cell microarrays (**Figure 9**), for example on glass slides using robotic spotters, capable of dispensing and immobilizing nanolitters of material [74–78]. Suspensions of cells in different solutions containing proteins and other biomaterials are spotted on top of solid glass slides to create arrays of thousands of spatially addressable spots, each spot containing tens of cells.

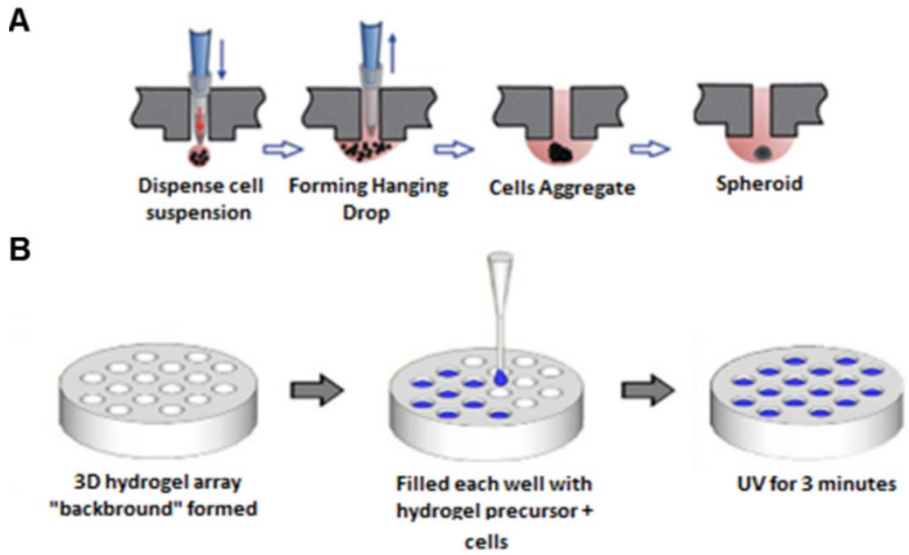


**Figure 9.** Fabrication of 3D cultures: (a) The suspension of cell in a hanging drop and the later formation of a spheroid containing all cells, adapted from [79] with permission of The Royal Society of Chemistry; and (b) the fabrication of a 3D cellular array by the filling of a hydrogel background with a solution of cells in a hydrogel precursor followed by a UV irradiation, adapted from [80] with permission of Elsevier.

These types of arrays have been used for example for HTP toxicology assays [81], containing array spots of an average of 60 cells in each spot. A limitation of the most extended spotting robots is that the minimum spot size or drop volume is much larger than a single cell. Additionally, Popova *et al.* described

a droplet-array (DA) sandwiching technology, a miniaturized platform for cell-based HTP assays, based on superhydrophobic–superhydrophilic micropatterns on nanoporous polymer films [76]. HTP 3D spheroid culture and drug testing using 384 hanging drops have also been reported [78,79].

When 3D culture is not required, other techniques enable cell adhesion to a substrate in a controlled manner (**Figure 10**). Those strategies include the fabrication of patterned substrates with thousands of individually addressable adhesive areas where individual cells or groups of cells may be immobilized. Adhesive patterned substrates may be done using low volume spotters such as Nanoenabler® [82] and Nanoink® (based on spotting and dip-pen nanolithography, respectively), or by microcontact printing [83].

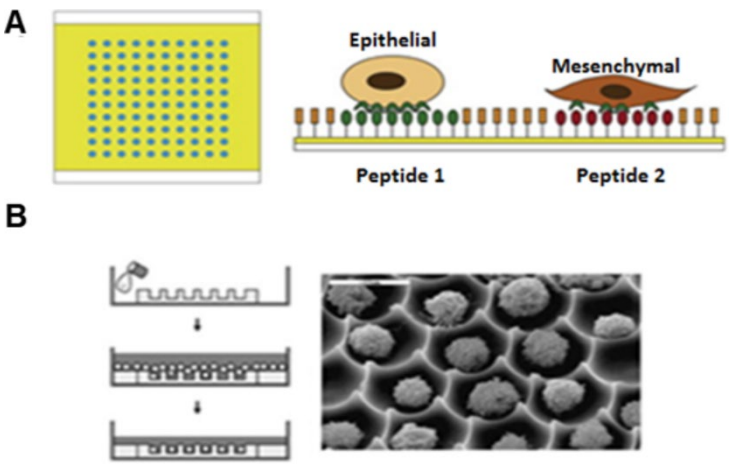


**Figure 10.** Non 3D cell patterning platforms: (a) The fabrication of cellular arrays in protein patterned substrate, where single cell or cluster of cells from different types can be isolated on top of the substrate specifically depending on their affinity to the patterned proteins, adapted from [84] with permission of Elsevier; and (b) the fabrication of cell arrays using craved microwells in a polymeric substrate where single cell or cluster of cells can be isolated in each well, adapted from [85] with permission of Elsevier.

Microcontact printing is a faster process for the creation of thousand of adhesive areas, because it only requires placing the substrate to pattern in contact with an inked stamp, for several minutes. Spotting instruments such

as Nanoenabler or Nanoink, have the advantage of offering the possibility of creating multicomponent patterns. However, the time required for creating large arrays of adhesive areas is much higher than by microcontact printing because they rely on spotting on each of the areas to functionalize. Lin *et al.* reported the fabrication of printed arrays using spotting of multiple specific peptide ligands. They used a DNA microarrayers to demonstrate their utility in monitoring the induction of epithelial to mesenchymal transition (EMT) in murine mammary epithelial cells [84]. Recently, recombinant antibodies have been used as specific ligands for the formation of cell microarrays [86].Finally, photolithography, and the fabrication of arrays of microwells or microsieves by die-cast molding of microstructures also enable the creation of highly dense cell arrays containing thousands of cellular systems, each of them trapped in microsieves or microwells [87]. Cellular systems created with these methods are comprised of one or several cells [18,88]. Techniques to create large density arrays of cellular systems are summarized in Table 1.

## 4. Monitoring

Besides high parallelization and microenvironment control, the other essential tool to progress on HTP cell studies is data acquisition and analysis. Important aspects related to different methods for data acquisition are: (1) provide real time measurements; (2) the need of stopping the cell culture media flow before measuring; (3) the use of label free method; or (4) the need to add extra reagents to obtain the data. All those aspects will influence the quality and frequency of data acquired. Higher frequency data production means more complex data analysis, but, at the same time, also provides a more accurate picture of the real situation.

Conventional methods such as immunofluorescence and immunohistochemistry using commercial fluorescence kits and microscopy observation are the leading technique for cell monitoring. While these techniques have been extremely useful for data acquisition from cellular behavior, most methods rely on costly-labeled substances that in some cases do not offer the required sensibility for cellular study. Apart from that, most of

**Table 1.** Comparison of the different novel techniques for creation of cellular cultures.

| Technique | Definition | Cell Isolation Capacity | 2D/3D Culture | Other Characteristics |
|---|---|---|---|---|
| **Microfluidic large-scale integration systems (mLSI)** | Interconnected addressable microchambers for isolation and recovering of cells | Multiple and single cell | Two-dimensional cultures | Thousands of addressable events |
| **Droplet microfluidic platforms** | Droplet-based systems for cell entrapping in discrete volumes of immiscible phases | Multiple and single cell | Two- and three-dimensional cultures | Thousands of addressable events<br>Low volume requirement |
| **3D microfluidic platforms** | Spotting of biological suspension on addressable spots | Multiple cells | Three-dimensional cultures | Low volume requirement |
| **Hanging drops platforms** | Entrapping of spheroid cultures inside a hanging drop | Multiple cells | Three-dimensional cultures | Hundreds of addressable events |
| **Patterned substrates** | Patterning of chemical adhesive areas for cell immobilization | Multiple and single cell | Two-dimensional cultures | Thousands of addressable events<br>Low volume requirement<br>Fast processes |
| **Microwell structures** | Molding of microsieves or microwells for cellular trapping | Multiple and single cell | Two-dimensional cultures | Thousands of addressable events |

the current cell observation methods can only be used at the end of the assay, disabling the possibility of a real time observation.

Nowadays, the development of new techniques for cell monitoring and observation is focused on label-free methodologies, which consist in the direct observation and characterization of cells without the need of secondary markers. The absence of secondary substances for the cell characterization allows lower cost and more efficient cellular studies. These techniques not only retain the integrity of the cell culture and their biomolecules, but also allow to some extent the observation and monitoring of real-time events (**Figure 11**). These techniques also provide a higher sensibility up to a certain degree, allowing the monitoring of several individual events in a HTP manner [89–91].

Following the route of label-free techniques, new integrated sensors have been applied within microfluidic devices for biological applications and therefore increase the existing tool box of monitoring methods. Conventionally, light sources use laser or lamps; several alternatives were developed, such as the incorporation of light self-emitting diodes (LEDs) and organic photodiodes. Other researchers integrated optical sensors into the microfluidics devices, using light scattering, absorption, transmission and fluorescence [75,92]. For a more real-time like cell analysis, high-speed cameras have also been applied in order to obtain as much information from the sources and the sensors in the lowest time lapse [93].

A new approach was investigated by Casterllanau *et al.*, which involved the integration of particles working as sensors into the device. These fluorescent particles were used for the identification of both single-cells and small collection of cells [94]. Newer nanorobotic manipulation inside electron scanning based microscopes has also been postulated as new ways to characterize cell cultures [95].

Physicochemical factors and biophysicials processes have also been used as novel techniques for the cellular characterization and monitoring of cells. Electro-analytical methods such as voltammetry, potentiometry and impedance spectroscopy were also employed.

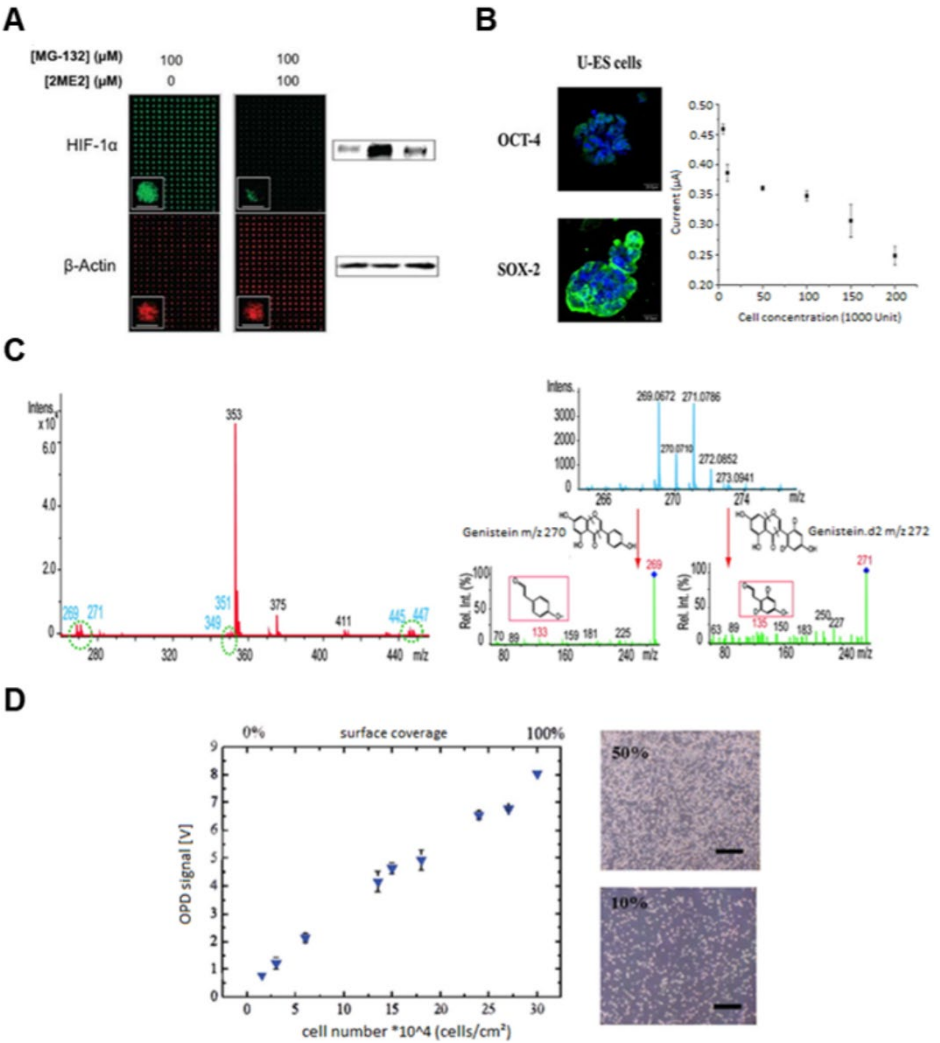


**Figure 11.** Monitoring of cell events. A) Immunofluorescence imaging and Western blotting of proteins for cell characterization on cellular arrays, adapted with the permission of [74], copyright 2008 American Chemical Society. B) Identification of undifferentiated cells by the fluorescent marking of undifferentiated mouse stem cells compounds, adapted from [96] with permission from Elsevier. C) Mass spectra of extracts from MCF-7 cells on a microfluidic chip, adapted with the permission of [97], copyright 2012 American Chemical Society. D) Light scattering signals measured in organic photodiodes following injection of increasing concentrations of cell suspension, adapted from [75] with permission of The Royal Society of Chemistry.

They were used to study the electrical properties of cell cultures, as well as electrical-dependable cell processes, such as viability, proliferation and motility changes. Impedance spectroscopy was used along with light scattering for cell analysis. In addition, an electro-analytical method based on trans-epithelial electrical resistance was used for the analysis of physiological barriers [96,98].

Novel magnetic based monitoring techniques were developed considering the magnetic properties of cells, especially during the up-take and transfer. In particular, magnetic nanoparticles were proposed as excellent tools for both cell separation and detection techniques. Integrated magnetic biosensors with superparamagnetic nanoparticles were functionalized to identify biological species and to quantify the released products [99,100].

Finally, mass spectroscopy was postulated as a powerful tool for qualitative and quantitative analysis of metabolites of cells. Mass spectroscopy has been widely used for the detection of secreted substances by cells in batch experiments. Nowadays, new microchips have been created for the simultaneous culture of cells and the detection in situ of some of the secreted substances by mass spectroscopy [97].

## 5. Conclusions

There is a high demand and a constant increase in the development of microtechnologies for cell analysis. During the last two decades, we have witnessed a number of key developments in the area of microtechnology and their applications in cell culture and analysis. For example, the manipulation of the topography of substrates creating micro- and nano-patterns has allowed evaluating the effect of topography in cell culture and differentiation; the creation of chemical patterns with precision in the microscale has enabled to look at the importance of cell adhesion, cell shape and cell–cell contact in their behavior; controlling the composition of cell culture medium, through microfluidics networks helped understanding the effect of the nutrients concentration on cell growth; and novel printing and dispensing techniques, in combination with biomaterials, enabled to create micro-scaled 3D cell

cultures allowing to look at cellular systems that resemble tissue architectures. All these recently developed tools enable performing experiments with a higher level of control in the cellular microenvironment than those classically conducted on flat cell culture plates.

Additionally, a number of strategies have been developed for the fabrication of dense arrays of cellular systems, where a large number of systems are created for subsequent stimulation, observation and monitoring. Depending on the methodology, the cellular systems can be comprised of a single cell or few cells; each of those system may be anchored to a surface or suspended in a fluid, and they may be distributed in a plane or in a 3D distribution, for example embedded into a gel structure. The possibility of creating a collection of individually addressable cellular systems improves both, the statistical analysis of the properties of cells, and the possibility to observe heterogeneous behavior on a cell population.

Finally, there is also an increasing interest in monitoring methods for cell characterization. Newcomers in the area of monitoring cells include integrated optical and electrical sensors and label-free characterization techniques.

The usages of microtechnologies in cell biology will not only provide the possibility of acquiring new data, but it will also allow to perform analysis using small amount of biological material. Microtechnologies, such as microfluidics, is opening the possibility of undergoing subsequent analysis on the same cellular system, reducing in this way the operation time, the need of cell separation, and the need of cell expansion. Depending on the aim of the study, each different methodology offers a set of benefits and disadvantages that could influence the election of one technique over another.

The transition from macroscale to microscale in cell analysis is still developing, and it will be only through the integration of several microtechnologies that we will obtain a new generation of cell analysis microsystems able to provide information on those still undiscovered steps of cell function and differentiation. In the future, highly integrated microfluidic analytical devices will find applications in different areas, such as drug

discovery and cell studies for regenerative medicine. These microfluidic platforms must enable cell culture under controlled microenvironment and lead to a possible HTP and real time analysis. For this purpose, it will be necessary the integration of a variable number of newly developed micro- and nano-technologies, that will allow controlling the topography, the surface chemistry, soluble factors, mechanical forces and cell–cell contacts; and technology for monitoring cell phenotype and genotype with high spatial and temporal resolution on a HTP

## 6. References

(1) Azuaje-Hualde, E.; García-Hernando, M.; Etxebarria-Elezgarai, J.; De Pancorbo, M.; Benito-Lopez, F.; Basabe-Desmonts, L. Microtechnologies for Cell Microenvironment Control and Monitoring. *Micromachines* **2017**, *8* (6), 166.

(2) Halldorsson, S.; Lucumi, E.; Gómez-Sjöberg, R.; Fleming, R. M. T. Advantages and Challenges of Microfluidic Cell Culture in Polydimethylsiloxane Devices. *Biosens. Bioelectron.* **2015**, *63*, 218–231.

(3) Lautenschläger, F.; Piel, M. Microfabricated Devices for Cell Biology: All for One and One for All. *Curr. Opin. Cell Biol.* **2013**, *25* (1), 116–124.

(4) Weaver, W. M.; Tseng, P.; Kunze, A.; Masaeli, M.; Chung, A. J.; Dudani, J. S.; Kittur, H.; Kulkarni, R. P.; Di Carlo, D. Advances in High-Throughput Single-Cell Microtechnologies. *Curr. Opin. Biotechnol.* **2014**, *25*, 114–123.

(5) Bloemen, V.; Schoenmaker, T.; de Vries, T. J.; Everts, V. Direct Cell-Cell Contact between Periodontal Ligament Fibroblasts and Osteoclast Precursors Synergistically Increases the Expression of Genes Related to Osteoclastogenesis. *J. Cell. Physiol.* **2010**, *222* (3), 565–573.

(6) Karabacak, N. M.; Spuhler, P. S.; Fachin, F.; Lim, E. J.; Pai, V.; Ozkumur, E.; Martel, J. M.; Kojic, N.; Smith, K.; Chen, P.; Yang, J.; Hwang, H.; Morgan, B.; Trautwein, J.; Barber, T. A.; Stott, S. L.; Maheswaran, S.; Kapur, R.; Haber, D. A.; Toner, M. Microfluidic, Marker-Free Isolation of Circulating Tumor Cells from Blood Samples. *Nat. Protoc.* **2014**, *9* (3), 694–710.

(7) Kim, J.; Taylor, D.; Agrawal, N.; Wang, H.; Kim, H.; Han, A.; Rege, K.; Jayaraman, A. A Programmable Microfluidic Cell Array for Combinatorial Drug Screening. *Lab Chip* **2012**, *12* (10), 1813.

(8) Song, H.; Chen, T.; Zhang, B.; Ma, Y.; Wang, Z. An Integrated Microfluidic Cell Array for Apoptosis and Proliferation Analysis Induction of Breast Cancer Cells. *Biomicrofluidics* **2010**, *4* (4), 044104.

(9) Patel, D.; Gao, Y.; Son, K.; Siltanen, C.; Neve, R. M.; Ferrara, K.; Revzin, A. Microfluidic Co-Cultures with Hydrogel-Based Ligand Trap to Study Paracrine Signals Giving Rise to Cancer Drug Resistance. *Lab Chip* **2015**, *15* (24), 4614–4624.

(10) Wolf, K.; Müller, R.; Borgmann, S.; Bröcker, E.-B.; Friedl, P. Amoeboid Shape Change and Contact Guidance: T-Lymphocyte Crawling through Fibrillar Collagen Is Independent of Matrix Remodeling by MMPs and Other Proteases. *Blood* **2003**, *102* (9), 3262–3269.

(11) Dalby, M. J.; Gadegaard, N.; Oreffo, R. O. C. Harnessing Nanotopography and Integrin–Matrix Interactions to Influence Stem Cell Fate. *Nat. Mater.* **2014**, *13* (6), 558–569.

(12) Jaggy, M.; Zhang, P.; Greiner, A. M.; Autenrieth, T. J.; Nedashkivska, V.; Efremov, A. N.; Blattner, C.; Bastmeyer, M.; Levkin, P. A. Hierarchical Micro-Nano Surface Topography Promotes Long-Term Maintenance of Undifferentiated Mouse Embryonic Stem Cells. *Nano Lett.* **2015**, *15* (10), 7146–7154.

(13) van Midwoud, P. M.; Janse, A.; Merema, M. T.; Groothuis, G. M. M.; Verpoorte, E. Comparison of Biocompatibility and Adsorption Properties of Different Plastics for Advanced Microfluidic Cell and Tissue Culture Models. *Anal. Chem.* **2012**, *84* (9), 3938–3944.

(14) Ren, K.; Chen, Y.; Wu, H. New Materials for Microfluidics in Biology. *Curr. Opin. Biotechnol.* **2014**, *25*, 78–85.

(15) Zhu, W.; O'Brien, C.; O'Brien, J. R.; Zhang, L. G. 3D Nano/Microfabrication Techniques and Nanobiomaterials for Neural Tissue Regeneration. *Nanomedicine* **2014**, *9* (6), 859–875.

(16) Suri, S.; Singh, A.; Nguyen, A. H.; Bratt-Leal, A. M.; McDevitt, T. C.; Lu, H. Microfluidic-Based Patterning of Embryonic Stem Cells for in Vitro Development Studies. *Lab Chip* **2013**, *13* (23), 4617.

(17) Jeon, H.; Koo, S.; Reese, W. M.; Loskill, P.; Grigoropoulos, C. P.; Healy, K. E. Directing Cell Migration and Organization via Nanocrater-Patterned Cell-Repellent Interfaces. *Nat. Mater.* **2015**, *14* (9), 918–923.

(18) Kwon, K. W.; Choi, J.-C.; Suh, K.-Y.; Doh, J. Multiscale Fabrication of Multiple Proteins and Topographical Structures by Combining Capillary Force Lithography and Microscope Projection Photolithography. *Langmuir* **2011**, *27* (7), 3238–3243.

(19) Cheng, Z. A.; Zouani, O. F.; Glinel, K.; Jonas, A. M.; Durrieu, M.-C. Bioactive Chemical Nanopatterns Impact Human Mesenchymal Stem Cell Fate. *Nano Lett.* **2013**, *13* (8), 3923–3929.

(20) Hamon, C.; Henriksen-Lacey, M.; La Porta, A.; Rosique, M.; Langer, J.; Scarabelli, L.; Montes, A. B. S.; González-Rubio, G.; de Pancorbo, M. M.; Liz-Marzán, L. M.; Basabe-Desmonts, L. Tunable Nanoparticle and Cell Assembly Using Combined Self-Powered Microfluidics and Microcontact Printing. *Adv. Funct. Mater.* **2016**, *26* (44), 8053–8061.

(21) Kweon, S.; Song, K. H.; Park, H.; Choi, J.-C.; Doh, J. Dynamic Micropatterning of Cells on Nanostructured Surfaces Using a Cell-Friendly Photoresist. *ACS Appl. Mater. Interfaces* **2016**, *8* (6), 4266–4274.

(22) Geiger, B.; Spatz, J. P.; Bershadsky, A. D. Environmental Sensing through Focal Adhesions. *Nat. Rev. Mol. Cell Biol.* **2009**, *10* (1), 21–33.

(23) Clause, K. C.; Barker, T. H. Extracellular Matrix Signaling in Morphogenesis and Repair. *Curr. Opin. Biotechnol.* **2013**, *24* (5), 830–833.

(24) Frantz, C.; Stewart, K. M.; Weaver, V. M. The Extracellular Matrix at a Glance. *J. Cell Sci.* **2010**, *123* (24), 4195–4200.

(25) Gevertz, J. L.; Torquato, S. A Novel Three-Phase Model of Brain Tissue Microstructure. *PLoS Comput. Biol.* **2008**, *4* (8), e1000152.

(26) Petit, V.; Thiery, J.-P. Focal Adhesions: Structure and Dynamics. *Biol. Cell* **2000**, *92* (7), 477–494.

(27) Roca-Cusachs, P.; del Rio, A.; Puklin-Faucher, E.; Gauthier, N. C.; Biais, N.; Sheetz, M. P. Integrin-Dependent Force Transmission to the Extracellular Matrix by -Actinin Triggers Adhesion Maturation. *Proc. Natl. Acad. Sci.* **2013**, *110* (15), E1361–E1370.

(28) Malmström, J.; Christensen, B.; Jakobsen, H. P.; Lovmand, J.; Foldbjerg, R.; Sørensen, E. S.; Sutherland, D. S. Large Area Protein Patterning Reveals Nanoscale Control of Focal Adhesion Development. *Nano Lett.* **2010**, *10* (2), 686–694.

(29) Peerani, R.; Zandstra, P. W. Enabling Stem Cell Therapies through Synthetic Stem Cell–

Niche Engineering. *J. Clin. Invest.* **2010**, *120* (1), 60–70.

(30) Ngangan, A. V; Waring, J. C.; Cooke, M. T.; Mandrycky, C. J.; McDevitt, T. C. Soluble Factors Secreted by Differentiating Embryonic Stem Cells Stimulate Exogenous Cell Proliferation and Migration. *Stem Cell Res. Ther.* **2014**, *5* (1), 26.

(31) Nie, Z.; Kumacheva, E. Patterning Surfaces with Functional Polymers. *Nat. Mater.* **2008**, *7* (4), 277–290.

(32) Wen, J. H.; Vincent, L. G.; Fuhrmann, A.; Choi, Y. S.; Hribar, K. C.; Taylor-Weiner, H.; Chen, S.; Engler, A. J. Interplay of Matrix Stiffness and Protein Tethering in Stem Cell Differentiation. *Nat. Mater.* **2014**, *13* (10), 979–987.

(33) Ginger, D. S.; Zhang, H.; Mirkin, C. A. The Evolution of Dip-Pen Nanolithography. *Angew. Chemie Int. Ed.* **2004**, *43* (1), 30–45.

(34) Mai, Y.; Eisenberg, A. Self-Assembly of Block Copolymers. *Chem. Soc. Rev.* **2012**, *41* (18), 5969.

(35) Deeg, J. A.; Louban, I.; Aydin, D.; Selhuber-Unkel, C.; Kessler, H.; Spatz, J. P. Impact of Local versus Global Ligand Density on Cellular Adhesion. *Nano Lett.* **2011**, *11* (4), 1469–1476.

(36) Tan, K. Y.; Lin, H.; Ramstedt, M.; Watt, F. M.; Huck, W. T. S.; Gautrot, J. E. Decoupling Geometrical and Chemical Cues Directing Epidermal Stem Cell Fate on Polymer Brush-Based Cell Micro-Patterns. *Integr. Biol.* **2013**, *5* (6), 899–910.

(37) Nelson, C. M.; Chen, C. S. Cell-Cell Signaling by Direct Contact Increases Cell Proliferation via a PI3K-Dependent Signal. *FEBS Lett.* **2002**, *514* (2–3), 238–242.

(38) Tang, J.; Peng, R.; Ding, J. The Regulation of Stem Cell Differentiation by Cell-Cell Contact on Micropatterned Material Surfaces. *Biomaterials* **2010**, *31* (9), 2470–2476.

(39) Guo, F.; Li, P.; French, J. B.; Mao, Z.; Zhao, H.; Li, S.; Nama, N.; Fick, J. R.; Benkovic, S. J.; Huang, T. J. Controlling Cell–Cell Interactions Using Surface Acoustic Waves. *Proc. Natl. Acad. Sci.* **2015**, *112* (1), 43–48.

(40) Christakou, A. E.; Ohlin, M.; Vanherberghen, B.; Khorshidi, M. A.; Kadri, N.; Frisk, T.; Wiklund, M.; Önfelt, B. Live Cell Imaging in a Micro-Array of Acoustic Traps Facilitates Quantification of Natural Killer Cell Heterogeneity. *Integr. Biol.* **2013**, *5* (4), 712–719.

(41) Gauvin, R.; Parenteau-Bareil, R.; Dokmeci, M. R.; Merryman, W. D.; Khademhosseini, A. Hydrogels and Microtechnologies for Engineering the Cellular Microenvironment. *Wiley Interdiscip. Rev. Nanomedicine Nanobiotechnology* **2012**, *4* (3), 235–246.

(42) Gruene, M.; Pflaum, M.; Hess, C.; Diamantouros, S.; Schlie, S.; Deiwick, A.; Koch, L.; Wilhelmi, M.; Jockenhoevel, S.; Haverich, A.; Chichkov, B. Laser Printing of Three-Dimensional Multicellular Arrays for Studies of Cell–Cell and Cell–Environment Interactions. *Tissue Eng. Part C Methods* **2011**, *17* (10), 973–982.

(43) Maruthamuthu, V.; Sabass, B.; Schwarz, U. S.; Gardel, M. L. Cell-ECM Traction Force Modulates Endogenous Tension at Cell-Cell Contacts. *Proc. Natl. Acad. Sci.* **2011**, *108* (12), 4708–4713.

(44) Moe, A. A. K.; Suryana, M.; Marcy, G.; Lim, S. K.; Ankam, S.; Goh, J. Z. W.; Jin, J.; Teo, B.

K. K.; Law, J. B. K.; Low, H. Y.; Goh, E. L. K.; Sheetz, M. P.; Yim, E. K. F. Microarray with Micro- and Nano-Topographies Enables Identification of the Optimal Topography for Directing the Differentiation of Primary Murine Neural Progenitor Cells. *Small* **2012**, *8* (19), 3050–3061.

(45) Ricotti, L.; Fujie, T.; Vazão, H.; Ciofani, G.; Marotta, R.; Brescia, R.; Filippeschi, C.; Corradini, I.; Matteoli, M.; Mattoli, V.; Ferreira, L.; Menciassi, A. Boron Nitride Nanotube-Mediated Stimulation of Cell Co-Culture on Micro-Engineered Hydrogels. *PLoS One* **2013**, *8* (8), e71707.

(46) Tsai, M.; Kita, A.; Leach, J.; Rounsevell, R.; Huang, J. N.; Moake, J.; Ware, R. E.; Fletcher, D. A.; Lam, W. A. In Vitro Modeling of the Microvascular Occlusion and Thrombosis That Occur in Hematologic Diseases Using Microfluidic Technology. *J. Clin. Invest.* **2012**, *122* (1), 408–418.

(47) Schober, A.; Augspurger, C.; Fernekorn, U.; Weibezahn, K.-F.; Schlingloff, G.; Gebinoga, M.; Worgull, M.; Schneider, M.; Hildmann, C.; Weise, F.; Hampl, J.; Silveira, L.; Cimalla, I.; Lübbers, B. Microfluidics and Biosensors as Tools for NanoBioSystems Research with Applications in the “Life Science.” *Mater. Sci. Eng. B* **2010**, *169* (1–3), 174–181.

(48) Etxebarria, J.; Berganzo, J.; Elizalde, J.; Fernández, L. J.; Ezkerra, A. Highly Integrated COP Monolithic Membrane Microvalves by Robust Hot Embossing. *Sensors Actuators B Chem.* **2014**, *190*, 451–458.

(49) Huang, M.; Fan, S.; Xing, W.; Liu, C. Microfluidic Cell Culture System Studies and Computational Fluid Dynamics. *Math. Comput. Model.* **2010**, *52* (11–12), 2036–2042.

(50) Giulitti, S.; Magrofuoco, E.; Prevedello, L.; Elvassore, N. Optimal Periodic Perfusion Strategy for Robust Long-Term Microfluidic Cell Culture. *Lab Chip* **2013**, *13* (22), 4430.

(51) Chung, B. G.; Flanagan, L. A.; Rhee, S. W.; Schwartz, P. H.; Lee, A. P.; Monuki, E. S.; Jeon, N. L. Human Neural Stem Cell Growth and Differentiation in a Gradient-Generating Microfluidic Device. *Lab Chip* **2005**, *5* (4), 401.

(52) Kawada, J.; Kimura, H.; Akutsu, H.; Sakai, Y.; Fujii, T. Spatiotemporally Controlled Delivery of Soluble Factors for Stem Cell Differentiation. *Lab Chip* **2012**, *12* (21), 4508.

(53) Paguirigan, A. L.; Beebe, D. J. Microfluidics Meet Cell Biology: Bridging the Gap by Validation and Application of Microscale Techniques for Cell Biological Assays. *BioEssays* **2008**, *30* (9), 811–821.

(54) Ekerdt, B. L.; Segalman, R. A.; Schaffer, D. V. Spatial Organization of Cell-adhesive Ligands for Advanced Cell Culture. *Biotechnol. J.* **2013**, *8* (12), 1411–1423.

(55) Chen, K. G.; Mallon, B. S.; McKay, R. D. G.; Robey, P. G. Human Pluripotent Stem Cell Culture: Considerations for Maintenance, Expansion, and Therapeutics. *Cell Stem Cell* **2014**, *14* (1), 13–26.

(56) Williamson, A.; Singh, S.; Fernekorn, U.; Schober, A. The Future of the Patient-Specific Body-on-a-Chip. *Lab Chip* **2013**, *13* (18), 3471.

(57) Araci, I. E.; Quake, S. R. Microfluidic Very Large Scale Integration (MVLSI) with Integrated Micromechanical Valves. *Lab Chip* **2012**, *12* (16), 2803.

(58) Unger, M. A.; Chou, H. P.; Thorsen, T.; Scherer, A.; Quake, S. R. Monolithic Microfabricated

Valves and Pumps by Multilayer Soft Lithography. *Science* **2000**, *288* (5463), 113–116.

(59) Park, E. S.; Brown, A. C.; DiFeo, M. A.; Barker, T. H.; Lu, H. Continuously Perfused, Non-Cross-Contaminating Microfluidic Chamber Array for Studying Cellular Responses to Orthogonal Combinations of Matrix and Soluble Signals. *Lab Chip* **2010**, *10* (5), 571–580.

(60) Gawad, C.; Koh, W.; Quake, S. R. Single-Cell Genome Sequencing: Current State of the Science. *Nat. Rev. Genet.* **2016**, *17* (3), 175–188.

(61) Petriv, O. I.; Kuchenbauer, F.; Delaney, A. D.; Lecault, V.; White, A.; Kent, D.; Marmolejo, L.; Heuser, M.; Berg, T.; Copley, M.; Ruschmann, J.; Sekulovic, S.; Benz, C.; Kuroda, E.; Ho, V.; Antignano, F.; Halim, T.; Giambra, V.; Krystal, G.; Takei, C. J. F.; Weng, A. P.; Piret, J.; Eaves, C.; Marra, M. A.; Humphries, R. K.; Hansen, C. L. Comprehensive MicroRNA Expression Profiling of the Hematopoietic Hierarchy. *Proc. Natl. Acad. Sci.* **2010**, *107* (35), 15443–15448.

(62) White, A. K.; VanInsberghe, M.; Petriv, O. I.; Hamidi, M.; Sikorski, D.; Marra, M. A.; Piret, J.; Aparicio, S.; Hansen, C. L. High-Throughput Microfluidic Single-Cell RT-QPCR. *Proc. Natl. Acad. Sci.* **2011**, *108* (34), 13999–14004.

(63) Woodruff, K.; Maerkl, S. J. A High-Throughput Microfluidic Platform for Mammalian Cell Transfection and Culturing. *Sci. Rep.* **2016**, *6* (1), 23937.

(64) Teh, S.-Y.; Lin, R.; Hung, L.-H.; Lee, A. P. Droplet Microfluidics. *Lab Chip* **2008**, *8* (2), 198.

(65) Shembekar, N.; Chaipan, C.; Utharala, R.; Merten, C. A. Droplet-Based Microfluidics in Drug Discovery, Transcriptomics and High-Throughput Molecular Genetics. *Lab Chip* **2016**, *16* (8), 1314–1331.

(66) Yu, L.; Chen, M. C. W.; Cheung, K. C. Droplet-Based Microfluidic System for Multicellular Tumor Spheroid Formation and Anticancer Drug Testing. *Lab Chip* **2010**, *10* (18), 2424.

(67) Mazutis, L.; Gilbert, J.; Ung, W. L.; Weitz, D. A.; Griffiths, A. D.; Heyman, J. A. Single-Cell Analysis and Sorting Using Droplet-Based Microfluidics. *Nat. Protoc.* **2013**, *8* (5), 870–891.

(68) Jakiela, S.; Kaminski, T. S.; Cybulski, O.; Weibel, D. B.; Garstecki, P. Bacterial Growth and Adaptation in Microdroplet Chemostats. *Angew. Chemie Int. Ed.* **2013**, *52* (34), 8908–8911.

(69) Macosko, E. Z.; Basu, A.; Satija, R.; Nemesh, J.; Shekhar, K.; Goldman, M.; Tirosh, I.; Bialas, A. R.; Kamitaki, N.; Martersteck, E. M.; Trombetta, J. J.; Weitz, D. A.; Sanes, J. R.; Shalek, A. K.; Regev, A.; McCarroll, S. A. Highly Parallel Genome-Wide Expression Profiling of Individual Cells Using Nanoliter Droplets. *Cell* **2015**, *161* (5), 1202–1214.

(70) Leung, K.; Zahn, H.; Leaver, T.; Konwar, K. M.; Hanson, N. W.; Page, A. P.; Lo, C.-C.; Chain, P. S.; Hallam, S. J.; Hansen, C. L. A Programmable Droplet-Based Microfluidic Device Applied to Multiparameter Analysis of Single Microbes and Microbial Communities. *Proc. Natl. Acad. Sci.* **2012**, *109* (20), 7665–7670.

(71) Collins, D. J.; Neild, A.; DeMello, A.; Liu, A.-Q.; Ai, Y. The Poisson Distribution and beyond: Methods for Microfluidic Droplet Production and Single Cell Encapsulation. *Lab Chip* **2015**, *15* (17), 3439–3459.

(72) Choi, J.-W.; Kang, D.-K.; Park, H.; DeMello, A. J.; Chang, S.-I. High-Throughput Analysis of Protein–Protein Interactions in Picoliter-Volume Droplets Using Fluorescence Polarization. *Anal. Chem.* **2012**, *84* (8), 3849–3854.

(73) Tumarkin, E.; Tzadu, L.; Csaszar, E.; Seo, M.; Zhang, H.; Lee, A.; Peerani, R.; Purpura, K.; Zandstra, P. W.; Kumacheva, E. High-Throughput Combinatorial Cell Co-Culture Using Microfluidics. *Integr. Biol.* **2011**, *3* (6), 653.

(74) Fernandes, T. G.; Kwon, S.-J.; Lee, M.-Y.; Clark, D. S.; Cabral, J. M. S.; Dordick, J. S. On-Chip, Cell-Based Microarray Immunofluorescence Assay for High-Throughput Analysis of Target Proteins. *Anal. Chem.* **2008**, *80* (17), 6633–6639.

(75) Charwat, V.; Purtscher, M.; Tedde, S. F.; Hayden, O.; Ertl, P. Standardization of Microfluidic Cell Cultures Using Integrated Organic Photodiodes and Electrode Arrays. *Lab Chip* **2013**, *13* (5), 785–797.

(76) Coyle, R.; Jia, J.; Mei, Y. Polymer Microarray Technology for Stem Cell Engineering. *Acta Biomater.* **2016**, *34*, 60–72.

(77) Jose, B.; McCluskey, P.; Gilmartin, N.; Somers, M.; Kenny, D.; Ricco, A. J.; Kent, N. J.; Basabe-Desmonts, L. Self-Powered Microfluidic Device for Rapid Assay of Antiplatelet Drugs. *Langmuir* **2016**, *32* (11), 2820–2828.

(78) Lovchik, R.; von Arx, C.; Viviani, A.; Delamarche, E. Cellular Microarrays for Use with Capillary-Driven Microfluidics. *Anal. Bioanal. Chem.* **2008**, *390* (3), 801–808.

(79) Tung, Y.-C.; Hsiao, A. Y.; Allen, S. G.; Torisawa, Y.; Ho, M.; Takayama, S. High-Throughput 3D Spheroid Culture and Drug Testing Using a 384 Hanging Drop Array. *Analyst* **2011**, *136* (3), 473–478.

(80) Jongpaiboonkit, L.; King, W. J.; Lyons, G. E.; Paguirigan, A. L.; Warrick, J. W.; Beebe, D. J.; Murphy, W. L. An Adaptable Hydrogel Array Format for 3-Dimensional Cell Culture and Analysis. *Biomaterials* **2008**, *29* (23), 3346–3356.

(81) Lee, M.-Y.; Kumar, R. A.; Sukumaran, S. M.; Hogg, M. G.; Clark, D. S.; Dordick, J. S. Three-Dimensional Cellular Microarray for High-Throughput Toxicology Assays. *Proc. Natl. Acad. Sci.* **2008**, *105* (1), 59–63.

(82) Arshak, K.; Korostynska, O.; Cunniffe, C. Nanopatterning Using the Bioforce Nanoenabler. *NATO Sci. Peace Secur. Ser. B Phys. Biophys.* **2008**, 299–304.

(83) Basabe-Desmonts, L.; Ramstrom, S.; Meade, G.; O'Neill, S.; Riaz, A.; Lee, L. P.; Ricco, A. J.; Kenny, D. Single-Step Separation of Platelets from Whole Blood Coupled with Digital Quantification by Interfacial Platelet Cytometry (IPC). *Langmuir* **2010**, *26* (18), 14700–14706.

(84) Lin, E.; Sikand, A.; Wickware, J.; Hao, Y.; Derda, R. Peptide Microarray Patterning for Controlling and Monitoring Cell Growth. *Acta Biomater.* **2016**, *34*, 53–59.

(85) Vasdekis, A. E.; Stephanopoulos, G. Review of Methods to Probe Single Cell Metabolism and Bioenergetics. *Metab. Eng.* **2015**, *27*, 115–135.

(86) Helma, J.; Cardoso, M. C.; Muyldermans, S.; Leonhardt, H. Nanobodies and Recombinant Binders in Cell Biology. *J. Cell Biol.* **2015**, *209* (5), 633–644.

(87) Jen, C.-P.; Hsiao, J.-H.; Maslov, N. A. Single-Cell Chemical Lysis on Microfluidic Chips with Arrays of Microwells. *Sensors* **2011**, *12* (1), 347–358.

(88) Chen, S.; Bremer, A. W.; Scheideler, O. J.; Na, Y. S.; Todhunter, M. E.; Hsiao, S.; Bomdica,

P. R.; Maharbiz, M. M.; Gartner, Z. J.; Schaffer, D. V. Interrogating Cellular Fate Decisions with High-Throughput Arrays of Multiplexed Cellular Communities. *Nat. Commun.* **2016**, *7* (1), 10309.

(89) Sun, Y.-S. Label-Free Sensing on Microarrays. *Small Mol. Microarrays* **2013**, 515–517.

(90) Sun, Y.-S. Use of Microarrays as a High-Throughput Platform for Label-Free Biosensing. *J. Lab. Autom.* **2015**, *20* (4), 334–353.

(91) Chen, J.-K.; Zhou, G.-Y.; Chang, C.-J.; Lee, A.-W.; Chang, F.-C. Label-Free DNA Detection Using Two-Dimensional Periodic Relief Grating as a Visualized Platform for Diagnosis of Breast Cancer Recurrence after Surgery. *Biosens. Bioelectron.* **2014**, *54*, 35–41.

(92) Rothbauer, M.; Wartmann, D.; Charwat, V.; Ertl, P. Recent Advances and Future Applications of Microfluidic Live-Cell Microarrays. *Biotechnol. Adv.* **2015**, *33* (6), 948–961.

(93) Zhang, Q.; Li, Z.; Zhao, S.; Wen, W.; Chang, L.; Yu, H.; Jiang, T. Analysis of Red Blood Cells' Dynamic Status in a Simulated Blood Circulation System Using an Ultrahigh-Speed Simultaneous Framing Optical Electronic Camera. *Cytom. Part A* **2017**, *91* (2), 126–132.

(94) Rothbauer, M.; Zirath, H.; Ertl, P. Recent Advances in Microfluidic Technologies for Cell-to-Cell Interaction Studies. *Lab Chip* **2018**, *18* (2), 249–270.

(95) Shi, C.; Luu, D. K.; Yang, Q.; Liu, J.; Chen, J.; Ru, C.; Xie, S.; Luo, J.; Ge, J.; Sun, Y. Recent Advances in Nanorobotic Manipulation inside Scanning Electron Microscopes. *Microsystems Nanoeng.* **2016**, *2* (1), 16024.

(96) Yea, C.-H.; An, J. H.; Kim, J.; Choi, J.-W. In Situ Electrochemical Detection of Embryonic Stem Cell Differentiation. *J. Biotechnol.* **2013**, *166* (1–2), 1–5.

(97) Chen, Q.; Wu, J.; Zhang, Y.; Lin, J.-M. Qualitative and Quantitative Analysis of Tumor Cell Metabolism via Stable Isotope Labeling Assisted Microfluidic Chip Electrospray Ionization Mass Spectrometry. *Anal. Chem.* **2012**, *84* (3), 1695–1701.

(98) Booth, R.; Kim, H. Characterization of a Microfluidic in Vitro Model of the Blood-Brain Barrier (MBBB). *Lab Chip* **2012**, *12* (10), 1784.

(99) Gijs, M. A. M.; Lacharme, F.; Lehmann, U. Microfluidic Applications of Magnetic Particles for Biological Analysis and Catalysis. *Chem. Rev.* **2010**, *110* (3), 1518–1563.

(100) Shoshi, A.; Schotter, J.; Schroeder, P.; Milnera, M.; Ertl, P.; Charwat, V.; Purtscher, M.; Heer, R.; Eggeling, M.; Reiss, G.; Brueckl, H. Magnetoresistive-Based Real-Time Cell Phagocytosis Monitoring. *Biosens. Bioelectron.* **2012**, *36* (1), 116–122.

Appendix 2

# Naked eye Y amelogenin gene fragment detection using DNAzymes on a paper-based device

## Naked eye Y amelogenin gene fragment detection using DNAzymes on a paper-based device

Enrique Azuaje-Hualde, Susana Arroyo-Jimenez, Gaizka Garai-Ibabe, Marian Martinez de Pancorbo, Fernando Benito-Lopez, Lourdes Basabe-Desmonts

*Published in: Analytica Chimica Acta (2020)* [1]

*Impact Factor: 5.977 (Q1)*

*Area: Analytical Chemistry*

**Abstract**

Nowadays, there is an increasing interest in developing new technology for rapid detection of specific DNA sequences for environmental monitoring, forensic analysis and rapid biomedical diagnosis applications. That is where microfluidic paper-based analytical devices are positioned as suitable platforms for the development of point of care analytical devices, due to their simple fabrication protocols, ease of use and low cost. Herein, a methodology was developed for the *in situ* colorimetric detection of single strand DNA based on the formation of a DNAzyme within a paper substrate. A DNAzyme that could only be formed in the presence of a specific sequence of the Y human amelogenin gene was designed. The performance of the DNAzyme was followed colorimetrically first in solution and then in paper substrates. The reaction was found to be specific to the Y fragment selected as analyte. The DNAzyme reaction on paper enabled the unequivocal colorimetric identification of the Y single strand DNA fragment both qualitatively, with the naked eye (143 ng), and quantitatively by image analysis (45.7 ng). As a proof of concept, a microfluidic paper-based device, pre-loaded with all DNAzyme reagents, was characterized and implemented for the simultaneous detection of X and Y single strand DNA fragments.

**Keywords**: DNAzyme; Amelogenin; Paper substrate; Gene detection; Colorimetric; Paper based microfluidics.

## 1. Introduction

There is an increasing interest in producing new technology for fast detection of specific DNA sequences at the point of need for forensic analysis, environmental monitoring and rapid biomedical diagnosis applications. Widely known methodologies such as qPCR or PCR-capillary electrophoresis are mainly based on the amplification of DNA samples to achieve enough quantity of DNA to be analyzed [2]. These methods require specialized procedures, equipment and personnel to carry out the analysis.

On the other hand, point of care tests (POC) [3] refer to devices that analyze, with minimum intervention of the user, small volume of samples at the point of necessity in short times. Moreover, they are usually designed to be mass-fabricated at low costs [4]. Microfluidic paper-based analytical devices (μPADs) constitute suitable platforms for the development of POC systems since they fulfil all the previously described characteristics [5,6]. Several paper-based types of materials, such as cellulose and nitrocellulose, can be easily adapted to serve as μPADs [7–9]. Due to their fibers distribution, liquid can flow inside of the material by imbibition, enabling the movement of liquids through its matrix without the requirement of external pumps [10]. Wax-printing, which involves the generation of hydrophobic walls within the paper matrix by printing and melting of wax, is proposed as the best methodology for the fabrication of μPADs due to the easiness of the procedure and the capacity to be escalated to mass-production [9,11]. Furthermore, μPADs are disposable, becoming a more environmentally friendly option than other microfluidic devices [12]. A number of μPADs including, HIV Tests (Home Access, USA), paper ELISA, and low-cost colorimetric diagnostic assays have been already described [13,14] and commercialized.

Traditionally, available paper-based devices are centered on the detection of big molecules such as proteins. Nevertheless, the development of novel μPADs for nucleic acid detection, such as nucleic acids capture on cellulose filter paper with *in situ* PCR [15], loop-mediated isothermal amplification of several DNA targets on paper device[16] and colorimetric DNA detection

through gold nanoparticles capture and agglomeration in paper device[17], among others, is a hot topic at the moment.

DNAzyme is composed of a DNA oligonucleotide, capable of performing a chemical reaction, often a catalytic reaction. In particular, DNAzymes sensing probes based on G-rich sequences, known as G-quadruplex, are gathering special attention due to their simplicity, high sensitivity and selectivity for the recognition of small molecules [18,19]. The G-quadruplex creates a special hairpin on the DNA sequences forming a complex with peroxidase activity, enabling the oxidation of substrates like 2,2'-azino-bis(3-ethylbenzothiazoline-6-sulphonic acid) (ABTS) in the presence of hydrogen peroxide ($H_2O_2$), producing an appreciable color change of the solution where dissolved [20–22]. By controlling the design of the DNAzyme sequence, it is possible to specifically detect ribonucleic acid (RNA), DNA, proteins and metal ions [23,24]. In this regards, designing a DNAzyme able to hybridize to a single strand DNA (ssDNA) sequence allows for the specific detection of the sequence of interest [25–27].

The use of DNAzymes in paper substrates was recently presented for the design of novel analytical devices. Zhang Y. *et al.* [28] demonstrated that hemin/G-quadruplex DNAzymes can be used on a paper support for the detection of potassium cations. Monsur Ali M. *et al* [29] achieved the genetic detection of *Escherichia coli* RNA on a paper-based filter support using DNAzyme catalytic reactions. However, their detection method was based on fluorescence, which required of specific instrumentation, thus increasing the complexity and cost of the methodology, whereas a colorimetric detection could be a better choice to make [30].

Here, a colorimetric methodology for the detection of ssDNA sequences by specific DNAzymes in solution, a Whatman filter paper 1 support and a paper-based device is presented, Figure 1. The formation of the DNAzyme in the presence of the analyte allows the oxidation of ABTS producing a green color, $ABTS^+$, which is detected with the naked eye and can be quantified, by colorimetric analysis of images from a mobile camera. As a proof of concept, a synthetic fragment corresponding to Y amelogenin gene, which differs from

its X counterpart by 6 base pairs, was designed as a model to test ssDNA detection [31–33].

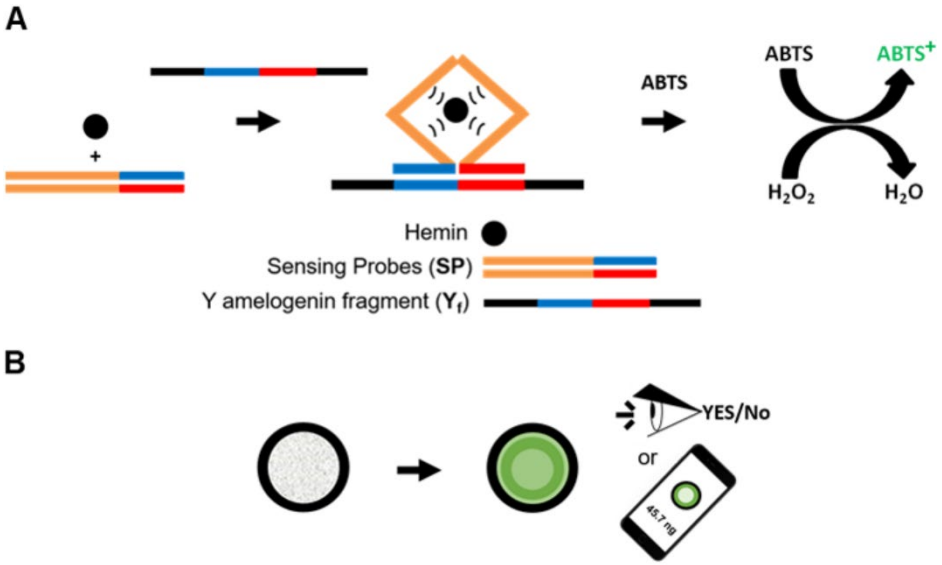


**Figure 1.** Schematic representation of the DNAzyme formation and specific Y amelogenin fragment ($Y_f$) identification of paper support. A) DNA sensing probes and hemin specifically bind to $Y_f$ to form a three dimensional structure with catalytic activity able to oxidize ABTS in the presence of $H_2O_2$, producing green colored $ABTS^+$. B) DNAzyme reaction on paper support produces an appreciable green color in the presence of the $Y_f$ thanks to the oxidation of ABTS. The reaction can be monitored colorimetrically.

## 2. Materials and methods

### *2.1. Materials*

DNA sequences (DNA-active, DNA-sensing probes and Y and X amelogenin fragments) were synthesized by Integrated DNA Technologies (IDT, Belgium). Hemin, ABTS, dimethyl sulfoxide (DMSO), HEPES buffer, sodium chloride, Triton X-100 and dimethylsulfoxide were purchased from Sigma-Aldrich (Spain). $H_2O_2$ was obtained from E. Merck (Germany). Potassium chloride was purchased from Panreac (Spain).

Buffer solution: HEPES 2.5 $10^{-2}$ M (Sigma-Aldrich, Spain), Potassium Chloride 2 $10^{-2}$ M (Panreac, Spain), sodium chloride 0.2 M (Sigma-Aldrich, Spain), Triton X-100 0.05 % and dimethylsufoxide 1 % (Sigma-Aldrich, Spain), at pH 7.4 with sodium hidroxide (Sigma-Aldrich, Spain) in water, was freshly prepared in the laboratory.

Solution assays were performed in a microtiter plate CORNING 96 wells and colorimetric values were recorded with a Beckman Coulter DTX 880 Multimode Detector. Paper assays were performed on Whatman filter paper 1(Sigma Aldrich, Spain) and Hi-Flow Plus HFC 12004 nitrocellulose (EMD Millipore, Ireland). The paper assays and the paper-based device were printed by a Xerox ColorQube 8570 wax printer and the wax barriers were generated by heating in an oven, set at 125 ºC for 5 min.

*2.2. DNAzyme performance in solution*

For specific $Y_f$ detection, 1 µL of a mix of DNA-sensing probes 1 and 2 (SP1 and SP2, Supporting Information 1) (100 µM each probe) and 47 µL of buffer solution were pipetted in the microtiter plate and incubated for 1 h. Then, 1 µL of hemin solution (100 µM) was added and incubated for 1 h. After that, 1 µL of either $Y_f$ or X amelogenin fragment ($X_f$) solutions ranging from 50 to 150 µM were added and incubated for 30 min (n = 3). Finally, 25 µL ABTS solution (28.8 mM) and 25 µL $H_2O_2$ solution (1.76 mM) were pipetted. The concentrations were previously optimized for this reaction, see Supporting Information 2, as well as the type of probe used for the assay, see Supporting information 3. The absorbance was measured at 415 nm every 5 min for 30 min using a Beckman Coulter DTX 880 Multimode Detector.

*2.3. Y amelogenin fragment discrimination and analysis in paper substrate*

The $Y_f$ detection through DNAzyme was carried out in a paper substrate. Therefore, circle-shaped structures (1 cm, inner diameter after heating) were wax-printed to set the sensing areas in the two paper supports. After printing, the circles were heated in the oven for 5 min at 125 °C. The heating step is necessary in order to melt the wax trough the paper and generate the hydrophobic barriers [9,11].

In order to test the most suitable type of paper for $Y_f$ detection, the oxidation of ABTS with a DNAzyme-active solution, serving as a control, was carried out in Whatman filter paper 1 and nitrocellulose membrane. First, 1 cm wax-circles were printed on both type of substrates. Then, 0.5 µL of DNA-active (100 µM), 0.5 µL of hemin (100 µM) and 24 µL of buffer solutions were pipetted and incubated for 1 h, at room temperature (RT). The concentrations of DNA-active and hemin were previously optimized for this reaction in solution, see Supporting Information 2. Finally, 12.5 µL of ABTS solution (28.8 mM) and 12.5 µL of $H_2O_2$ solution (1.76 mM) were added in order to initiate the color formation. The concentrations of ABTS/$H_2O_2$ were previously optimized for this reaction in solution, see Supporting Information 2. Photos were taken with a mobile phone camera before the addition of ABTS and $H_2O_2$ solutions and 5 and 60 min after addition.

For the detection and quantification of $Y_f$ on cellulose Whatman filter paper, 0.5 cm diameter wax circles (inner circle, after melting) were wax-printed. 0.25 µL of a 1:1 mix of SP1 and SP2 (100 µM each), 0.25 µL of hemin-stock solution (100 µM), 6 µL of ABTS-stock solution (40 mM) and 7 µL of buffer solution were mixed in an Eppendorf. The resulting mixture was pipetted on the paper wax-circle. After overnight storage at 4 ºC, either 0.25 µL of $Y_f$ (25, 50, 100 or 200 µM), $X_f$ (25, 50, 100 or 200 µM) or buffer solution were pipetted in the wax-circles (n = 3) and 30 min incubated at RT. Then, 6 µL of $H_2O_2$ (2.4 mM) were pipetted in all wax-circles. Images were taken by a mobile phone camera after 5 min incubation.

For the specific detection of $Y_f$ fragment in the paper-based device (for device specifications, see Supporting Information 4). An optimized mixture of the reagents, ABTS and $H_2O_2$ were used for these experiments, see Supporting Information 2 and 3. 0.25 µL of a 1:1 mix of SP1 and SP2 (100 µM), 0.25 µL of hemin-stock solution (100 µM), 6 µL of ABTS-stock solution (21.6 mM) and 7 µL of buffer solution were pipetted in the device reservoirs (Y and X wax-circles,), in three different devices. The mix of this reagents forms the $Y_f$-DNAzyme cocktail. After overnight storage at 4 ºC, 0.25 µL of $Y_f$ and 0.25 µL of $X_f$ (100 µM) were pipetted on their respective detection zones and incubated for 3 min at RT. Finally, 12 µL of $H_2O_2$ solution (1.32 mM) was

pipetted on the inlet (center of the device) and the solution was left to run until it reached both detection zones. Photographs were taken by the mobile phone camera 5 min after $H_2O_2$ solution reached the detection zones.

### *2.4. Image and data analysis*

Photographs were taken by a Sony Xperia Z3 D6603 mobile phone camera (20.7 MP, f/2.0, 25 mm (wide), 1/2.3", 1.12 µm, AF) or a LaserJet Pro 400 MFP scanner (Scanning Method: Flatbed; Scanner Type Flatbed: DF; Bit Depth: 30-bit).

All images were transformed to 8-bit and grey intensities (corresponding to the total color intensity [13,34]). They were analyzed using Image-J software. Paper background intensity was subtracted from all data. Data plotting and statistical analysis were carried out in Excel and Origin Pro 2018.

## 3. Results and discussion

In order to investigate the use of DNAzymes on paper substrates for the naked eye detection of ssDNA fragments and the quantification by image analysis of mobile phone camera pictures, a DNAzyme for the detection of a specific fragment of the Y amelogenin gene ($Y_f$) was designed. Then, a reaction cocktail comprised of hemin, ABTS and two sensing probes (SP1 and SP2, which bind specifically to $Y_f$ was developed; see Supporting Information 2 and 3 for detailed information of the characterization of the different components of the cocktail.

To evaluate the sensitivity and selectivity of the designed DNAzyme assay for the detection of $Y_f$ *versus* $X_f$, the DNAzyme cocktail was incubated with different concentrations of $Y_f$ and $X_f$ ranging from 0.5 to 1.5 µM (corresponding to a range between 1000 and 3000 ng of ssDNA per sample), and the absorbance of the final solutions were measured in a conventional microtiter plate reader after 5 min of incubation.

An increase in absorbance was appreciated over time and when increasing the concentration of $Y_f$. On the other hand, the absorbance values for the

reaction performed with the $X_f$ remained constant over time and for all concentrations investigated, **Figure 2**. These results demonstrate the specific recognition of $Y_f$ and formation of the DNAzyme through the oxidation of ABTS, while the same DNAzyme compounds were unable to detect the $X_f$ fragment in solution.

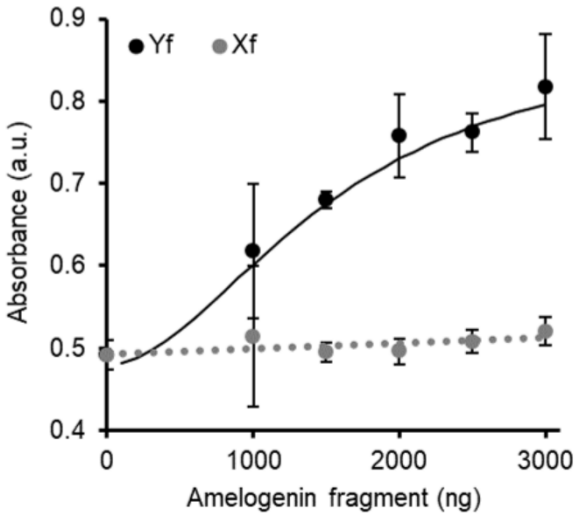


**Figure 2.** Graphical representation of $Y_f$ detection in solution. Y axis indicates the absorbance obtained from the oxidation of ABTS with different amounts of $Y_f$ and $X_f$ after 5 min of incubation. Fitting curve of $Y_f$ was done through the equation $y = 0.89-(0.41/(1+(x/1.58)^{1.89}))$, $R^2 = 0.9909$. Error bars mean ± SD (n = 3 samples per experimental condition).

$Y_f$ absorbance values were fitted to a 4 parametric logistic (4PL) curve, which was used before in immunoassays and binding ligand assays [35]. A limit of detection (LoD) of 655 ng of $Y_f$ was calculated following the equation 1, where $mean_{blank}$ is the absorbance value of the reaction mix without $Y_f$ and $X_f$ , and *SD* is the standard deviation (n = 3) of the mean value of the blank.

$$LoD = mean_{blank} + 3\,SD_{blank}$$

(eq. 1)

A limit of quantification (LoQ) of 1462 ng of $Y_f$ was calculated following the equation 2, where $mean_{blank}$ is the absorbance value of the reaction mix without $Y_f$ and $X_f$ , and *SD* is the standard deviation (n = 3) of the mean value of the blank.

$$LoQ = mean_{blank} + 10\, SD_{blank}$$

(eq. 2)

High *SD* values were observed at low amounts of $Y_f$ and $X_f$, (1000 ng). This higher *SD* corresponds to the experimental error, which comes from the number of dilutions needed to reach this 1000 ng solution from the $X_f$ and $X_f$ main stock solution. This error could be reduced by increasing the number of experiments per concentration. Therefore, the calculated LoQ value was taken as more certain value in the analysis of the dynamic range of the reaction. The dynamic detection range (1462 – 3000 ng) is limited by the increasing signal of the background over time, provided by the spontaneous ABTS oxidation in the reaction mix, as previously described in literature [36,37].

### *3.1. Selectivity and Sensitivity of the assay in the Whatman filter paper substrate*

In order to get an assay that is suitable for a paper-based device configuration, it is necessary that all the reagents of the assay are compatible with paper, can be preloaded and, if possible, stored for long periods of time and at different ambient conditions (*e.g.* light and temperature). Therefore, the stability of the assay over time was investigated for two light conditions (daylight and dark at RT) as well as at 4 ºC in the dark for 24 h storage; see Supporting Information 5. The absorbance values of the assay in solution were lower than those carried out without the 24 h storage, but clearly allowed the detection of the $Y_f$ in the same range of concentrations and times than when no storage was carried out. Therefore, these protocols can be implemented during the fabrication of a µPAD, with all the reagents preloaded and stored in paper. The assay kept at 4 ºC in the dark presented higher absorbance values than those stored at RT due to a better preservation of

the reagents at low temperature, see Figure SI-4 D, being this protocol (4 ºC in the dark) the one used in experiments hereafter.

After confirming the possibility to detect $Y_f$ using the designed DNAzyme in solution, the materials to perform the detection of the assay on a paper substrate were investigated. Two different papers, nitrocellulose membrane and Whatman filter paper 1, which are commonly used for the fabrication of lateral flow assays and µPADs, were investigated. Using a wax printer, 1 cm diameter wax-circles were printed on both types of substrates. Initial experiments on paper were performed using a positive control mix comprised of DNA-active sequence and hemin group to form a DNAzyme without the presence of the target analyte (DNAzyme-control mix). First, 0.5 µL of DNAzyme-control mix and 24 µL of buffer solution were pipetted and incubated for 1 h at RT in the paper substrates. Then, 12.5 µL of ABTS solution (28.8 mM) and 12.5 µL $H_2O_2$ (1.76 mM) solution were added. Photos of the substrates were taken with a mobile phone camera 0, 5 and 60 min after addition of ABTS and $H_2O_2$ (**Figure 3**).

The Whatman filter paper 1 presented a better performance than the nitrocellulose. The Whatman paper 1 had high ability to absorb the reagents and integrate them within the paper fibers, with the reaction taking place in the paper substrate. After the assay was carried out (addition of ABTS/ $H_2O_2$ solutions), the paper substrate kept the green color even after 60 min in the dry paper. Considering this result, it can be speculated that the fibers of the Whatman paper 1 were able to stabilize the $ABTS^+$ over time up to 60 min.

On the other hand, the nitrocellulose paper substrate did not absorb the reagents, which remained in solution in the drop held by the wax-printed-circle. After the assay was carried out (addition of ABTS/ $H_2O_2$ solutions), the oxidation reaction took place in solution and not in the fibers of the nitrocellulose paper. The oxidized $ABTS^+$ molecules (green color) were not stabilized by the paper substrate and continued the oxidation process. Under prolonged oxidative conditions, $ABTS^+$ suffers over-oxidation into $ABTS^{2+}$, which is not stable in aqueous solution and decompose into several uncolored by-products, losing its characteristic green color [38–40]. In view of

these results, the Whatman filter paper was selected as the right support for the DNAzyme reaction.

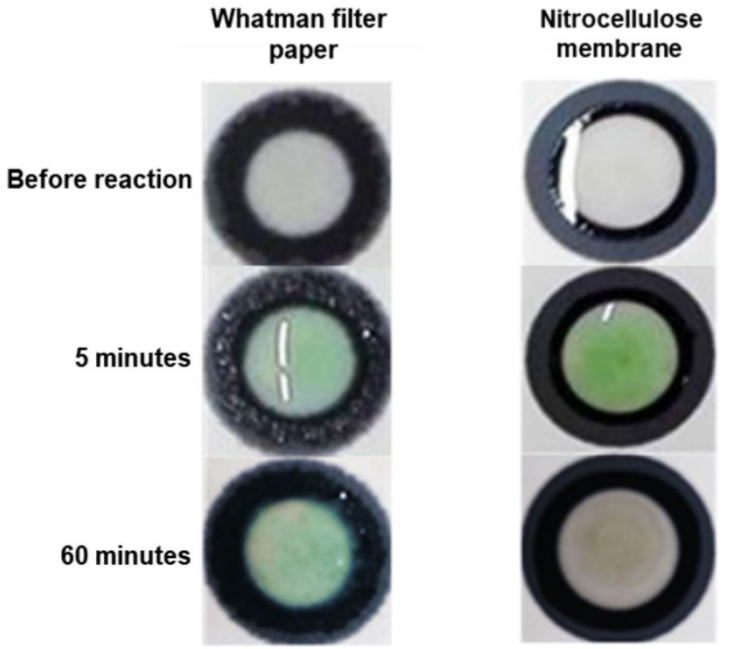


**Figure 3.** Pictures of DNAzyme control mix in Whatman filter paper 1 and nitrocellulose membrane. Photographs were taken at times 0, 5 and 60 min after ABTS/$H_2O_2$ solutions addition. Green color indicates the presence of $ABTS^+$.

The detection of $Y_f$ on Whatman paper 1 was then evaluated. For that, a 2 by 5 array of 0.5 cm diameter (internal diameter, after heating) wax-printed circles were fabricated. 12 µL of a solution containing 0.25 µL of the sequences SP1 and SP2 (1 µM) with 0.25 µL of hemin solution (1 µM), 6 µL of ABTS (40 mM) and 7 µL of buffer were pipetted and subsequently dry over night at 4 $^oC$ in the dark in each circle. Then, 0.25 µL of solutions with increasing concentrations of $Y_f$ or $X_f$ ranging from 0 (negative control) to 200 µM were loaded in each reaction circle and let dry for 30 min at RT. Finally, 6 µL of $H_2O_2$ (2.4 mM) were added to each reaction circle. After 5 min a green color was appreciated in all the reaction circles, by naked eye. A pronounced “coffee ring” effect was identified in all the circles containing $Y_f$, while this

coffee ring was not appreciated in the circles containing $X_f$. The shape of the coffee ring corresponded with the shape of the drop of $X_f$ previously loaded on the substrate. The reason for the formation of this ring can be explained by the concentration of the reagents during the drying process of the sample drop pipetted in the paper support [41]. Additionally, a darker green color intensity was appreciated in those circles containing higher concentrations of $Y_f$. Differently, the negative control and the circles containing $X_f$ exhibited the same light green color coming from the uncontrolled residual oxidation of ABTS, **Figure 4 A**.

Mixtures of $Y_f$ and $X_f$ were also investigated in the 2 by 5 array of wax-printed circles. The same green color intensity than samples containing only $Y_f$ were obtained, indicating that the presence of the $X_f$ does not inhibit the formation of the $Y_f$ - DNAzyme (Supporting Information Figure SI-6).

The quantification of the DNAzyme reaction was done analyzing the color intensity of the circles (green color intensity) by just taking pictures of the array with a mobile phone color camera. The whole area of the reaction circle was selected, without differentiating the presence or absence of the coffee ring. **Figure 4 B** shows the plot of the color intensity *versus* $Y_f$ and $X_f$ concentrations. As qualitatively observed by eye before, the green color intensity increased with the concentration of $Y_f$, while it remained constant for the assay containing $X_f$. There was a significant difference in the signal obtained with and without $Y_f$ in all the cases, indicating that this assay could be used in paper for quantification of specific fragments of ssDNA. $Y_f$ values were fitted to a 4PL curve. A LoD of 45.7 ng and a LoQ of 172 ng of $Y_f$ were calculated using eq. 1 and eq. 2, respectively, obtaining a dynamic range of 172 - 1200 ng, which is much lower than in solution. Therefore, transfer the reaction to a paper support greatly improved the LoD, reducing 14 times the minimum amount of $Y_f$ that can be detected. This improvement can be attributed to the higher concentrations of reagents in respect to the detection zone available in the paper substrate. Moreover, after quantification it can be concluded that at least 143 ng of Y amelogenin fragment could be detected by naked eye.

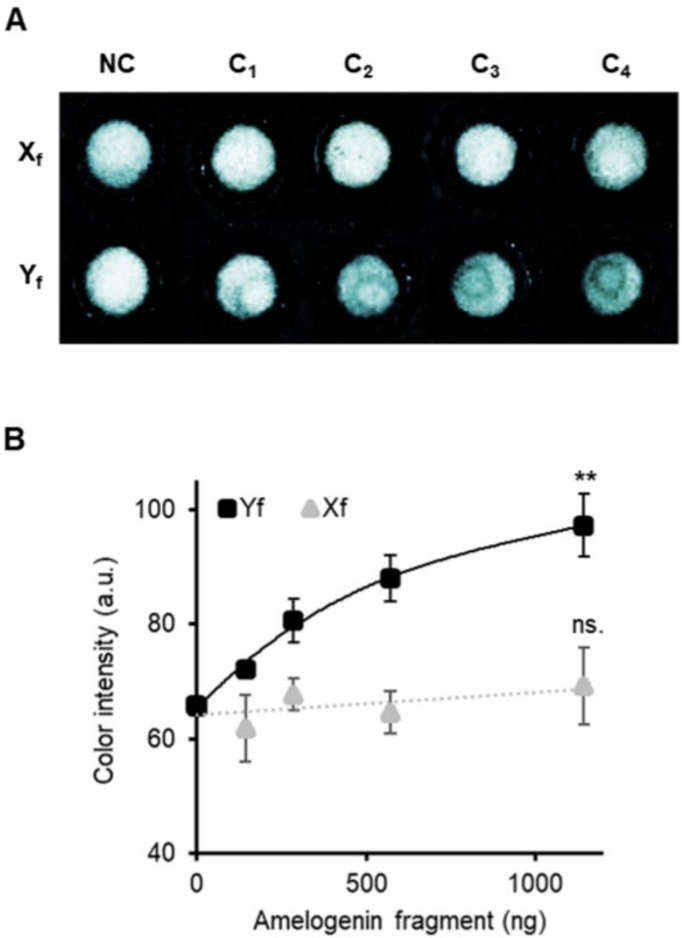


**Figure 4.** Pictures and graphical representation of $Y_f$ detection on Whatman filter paper 1. A) Picture of the 2 by 6 array printed in paper after 5 min DNAzyme reaction. $C_1$, $C_2$, $C_3$ and $C_4$ refers to the different concentrations of $Y_f$ or $X_f$ solutions added to the paper substrate (25 (143 ng), 50 (286 ng), 100 (572 ng) and 200 (1144 ng) μM, respectively) and NC is the negative control. B) Graphical representation of the color intensity obtained from the picture taken by the mobile camera 5 min after reaction. Fitting curve of $Y_f$ was done through the equation $y = 97-(31.44/(1+(x/51.7)^{1.23}))$, $R^2 = 0.9917$. Error bars mean ± SD (n = 3 samples per experimental condition). Statistical significance; paired two-tailed t-test (** $p < 0.01$, ns. $p \geq 0.5$).

In order to fabricate a paper-based device useful in real applications, it is desirable that the reagents are stable for long period of time embedded in the device, preferably in a controlled environment. Therefore, the stability of the reagents (SP1, SP2, hemin and ABTS) forming the assay was tested by storing them at 4 ºC from 24 h to 48 h and 7 days, see Supporting Information Figure SI-7. For the three times investigated, the "coffee ring" was clearly visible in all samples containing $Y_f$ while the green color remained imperceptible with the naked eye for the $X_f$ samples, See Figure SI-6 A. Pictures of the wax-circles were taken and analyzed, see Figure SI-6 B, allowing for the quantification of the ABTS oxidation process.

The values obtained for each experiment are comparable within the error (n=3), indicating that the reagents are well preserved in the paper substrate maintaining their chemical properties at least for one week, under refrigeration.

*3.3 DNA samples analysis on a paper-based device.*

A final test was performed to evaluate the applicability of $Y_f$ detection on a paper –based device for the simultaneous analysis of $Y_f$ and $X_f$ samples. As a proof of concept a microfluidic paper-based device was designed and wax-printed. It has a channel with two analysis zones, one at each edge of the channel and an inlet for reagent loading in the middle of the channel (**Figure 5**).

The $Y_f$ - DNAzyme cocktail was pre-loaded in both analysis zones at kept for 24 h at 4 ºC (dark conditions). Then, two samples containing 570 ng of $Y_f$ or $X_f$ were loaded in each analysis zone and let dry for 30 min. Finally, 12 µL of $H_2O_2$ (1.32 mM) were pipetted in the inlet of the device.

The $H_2O_2$ flowed equally in both detections reaching the analysis zones in less than 10 s. The ABTS oxidation reaction took place and a clear green coffee ring appeared only in the analysis zone containing $Y_f$ after 5 min while the intensity of the green color in the analysis zone containing the $X_f$ sample was very low.

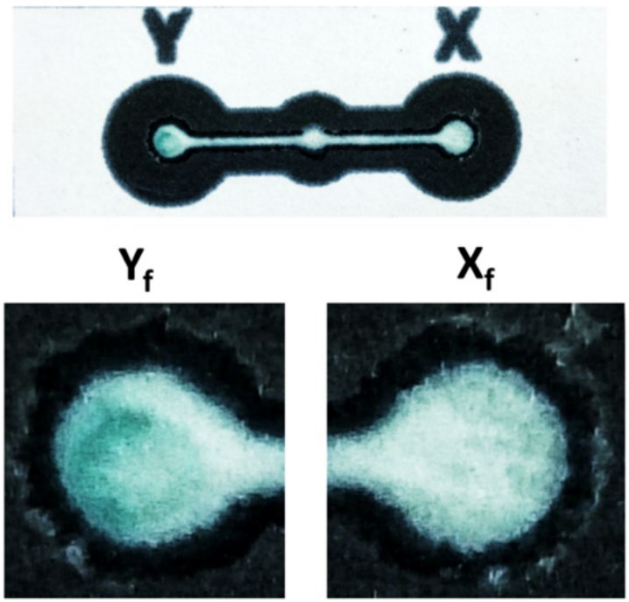


**Figure 5.** μPAD for $Y_f$ detection. Pictures were taken 5 min after the $H_2O_2$ solution reached the analysis zones. Detection circles correspond to sample loading of $Y_f$ (left) and $X_f$ (right). Increased green intensity relates to increasing presence of $ABTS^+$.

## 4. Conclusions

Rapid tests for DNA detection have application in forensic practice, biomedical diagnostics, and environmental monitoring among others. Current ways to analyze DNA sequences often require long procedures at centralized labs, and there is a need to developed technologies that enable in-field and rapid sample analysis and detection of the DNA of interest.

An optimized methodology for easy and in-field ssDNA detection in a paper-based device was presented. By using a DNAzyme specific to the desired DNA sequence, a label-free, easy to use and colorimetric based detection method for ssDNA was developed. This reaction was optimized in solution in

order to obtain a distinguishable specific and positive signal in a short time with a LOD of 655 ng.

The assay developed in solution was then transferred to a paper support and to a paper-based device. Two types of paper were tested, Whatman filter paper 1 and nitrocellulose membrane, both highly used in paper microfluidics and/or DNA research [7–9]. It was found out that Whatman filter paper 1 was more adequate for the DNAzyme reaction and thus was chosen as the desired substrate. The DNAzyme reaction on paper enabled the unequivocal colorimetric identification of the $Y_f$ ssDNA fragment by qualitative detection, with the naked eye, and quantitative determination by image analysis. At least 143 ng of Y amelogenin fragment could be detected by naked eye, while 45.7 ng could be detected by the quantification of the color intensity values from a picture of the paper substrate. The transfer of the reaction to a paper support significantly reduced the LoD, improving the sensitivity of the reaction.

Multisampling analysis on a paper-based device pre-loaded with the DNAzyme cocktail was carried out. Although the configuration of the device is not optimized, two analytes, $Y_f$ and $X_f$, were analyzed. The analysis of different genes from a single individual would need of further validation and optimization of the process, including device flow control and prevention of cross-contamination of samples. Furthermore, the devices were stored for up to 7 days at 4 ºC before use, indicating that they could be stored and used at the point of care

This work constitutes the first steps into what could become an in-field paper-based device for several applications. In the case of fast typifying of human samples for forensic analysis it should be noted that human samples are more complex than the proposed 74 bases synthetic sequence, usually presenting the genome in a double strand structure with high packing, safeguarded inside the cell's nucleus. Also, while the detection limits achieved are optimal for our synthetic sequence, the total genetic material found per human cell can be very low (between 3 and 6 picograms per cell) and the amount of cells that can be found in human samples can vary significantly, depending on the sample origins[42], being this scenario a limitation of this technology in its

current configuration. Therefore, for the incorporation of real human samples, research on the integration and the optimization of extraction methods (Chelex 100 [43]) and DNA denaturalization methods (chemical denaturalization [44]) inside the paper supports would be necessary. Conventional techniques for human genome analysis, such as qPCR, only require nanograms of whole genomes to produce data with high specificity. Our proposed methodology would extremely benefits from complementary amplification methods of the genetic material, such as isothermal amplification, that can be incorporated in the future to an in-field device for the successful detection of human DNA[45,46]. The technology presented in this manuscript could also be applied in the field of biomedicine for the detection and diagnosis of bacterial and viral infections, which present shorter genomes and more variety of DNA structures, including ssDNA[47,48].

## 5. Supporting information

### *SI-1: DNA probes*

**Scheme SI-1.** DNA probes. Colors red and green underlined indicated complementary sequence to $Y_f$. Colors blue and yellow indicate same sequence to the DNA-active sequence.

| |
|---|
| **Y amelogenin fragment ($Y_f$)** |
| CCCTGGGCTCTGTAAAGAATAGTGGGTGGATTCTTCATCCCAAATAAAGTGGTTTCTCAAGTGGTCCCAATTTT |
| **X amelogenin fragment ($X_f$)** |
| CCCTGGGCTCTGTAAAGAATAGTGTGTTGATTCTTTATCCCAGATGTTTCTCAAGTGGTCCTGATTTTACAGTTCC |
| **DNA-active** |
| TTTGGGTAGGGCGGGTAGGG |
| **DNA sensing probe 1 (SP1)** |
| CGGGATGGGTTTTTGGGATGAAGAATCCA |
| **DNA sensing probe 2 (SP2)** |
| GAAACCACTTTATAAAGGGTAGGG |
| **DNA sensing probe 3** |
| GGGCGGGTGGGTTTGGGATGAAGAATCCA |
| **DNA sensing probe 4** |
| GAAACCACTTTATTGGGT |
| **DNA sensing probe 5** |
| CGGGATGGGTGATGAAGAATCCACC |
| **DNA sensing probe 6** |
| CACTTTATTTGTGGGTAGGG |
| **DNA sensing probe 7** |
| TGGGTGATGAAGAATCCACC |
| **DNA sensing probe 8** |
| CACTTTATTTGTGGGTAGGGCGGG |

*SI-2: DNA-active assay characterization in solution*

All stock solutions were diluted in buffer solution. DNA-active stock solutions 1, 2 and 3 (50, 100 and 200 μM , respectively); Hemin stock solutions 1, 2 and 3 (50, 100 and 200 μM, respectively); DNA-sensing probes sequences mix stock solutions 1, 2, 3 and 4 (100 μM each); Y amelogenin fragment stock solutions 1, 2, 3, 4, 5, 6 and 7 (25, 50, 75, 100, 125, 150 and 200 μM, respectively); X amelogenin fragment stock solutions 1, 2, 3, 4, 5, 6 and 7 (25, 50, 75, 100, 125, 150 and 200 μM, respectively); ABTS stock solutions 1, 2, 3 and 4 (2.88, 21.6, 28.8 and 40 mM, respectively); $H_2O_2$ stock solutions 1, 2, 3 and 4 (0.176, 1.32, 1.76 and 2.4 mM, respectively).

Reactions were performed by triplicate in a 96 wells microtiter plate. 1 μL of DNA-active stock solutions, for a final concentration of either 0.5, 1 or 1.5 μM inside the microtiter plate ($V_f$ = 100 μL), were mixed with 1 μL of hemin-stock solution of the same concentrations and with 48 μL of buffer solution in each well and incubated for 1 h. Afterwards, 50 μL of one of four 1:1 mixture of ABTS and $H_2O_2$ solutions (for a final concentration inside the microtiter plate of: 7.2 mM ABTS, 440 μM $H_2O_2$ for ABTS/ $H_2O_2$ mix 1; 7.2 mM ABTS, 44 μM $H_2O_2$ for ABTS/ $H_2O_2$ mix 2; 720 μM ABTS, 440 μM $H_2O_2$ for ABTS/$H_2O_2$ mix 3 or 720 μM ABTS, 44 μM $H_2O_2$ for ABTS/$H_2O_2$ mix 4, ($V_f$ = 100 μL)) were added. Absorbance at 415 nm was measured every 5 min for 30 min using a Beckman Coulter DTX 880 Multimode Detector, **Figure SI-2**.

For all the DNA-active/hemin concentrations (A, B, C), the same trend was observed when the different mixtures of ABTS/$H_2O_2$ were added (mix 1 to 4). In order to get a higher absorbance signal, higher concentrations of $H_2O_2$ (mix 1 and mix 3) are necessary, as the reaction depends on the hydrogen peroxide availability in the solution, independently of the ABTS concentration[49].

At lower concentrations of $H_2O_2$ the absorbance was very similar (mix 2 and 4) regardless the concentration of DNA-active and hemin. Finally, the reactions with the higher DNA-active/hemin mixtures presented the higher absorbance values, following the trend: A < B < C.

Considering these results, the ABTS/ $H_2O_2$ mix 1 was selected as the best candidate for the assay due to the high absorbance signal obtained over time. In real scenarios, the amount of available sample and DNA for analysis is very low; therefore, we chose the 1 μM concentration for the DNA sequences as a good starting method for further characterization, despite the fact 1.5 μM DNA-active/hemin concentrations, C samples, performed better.

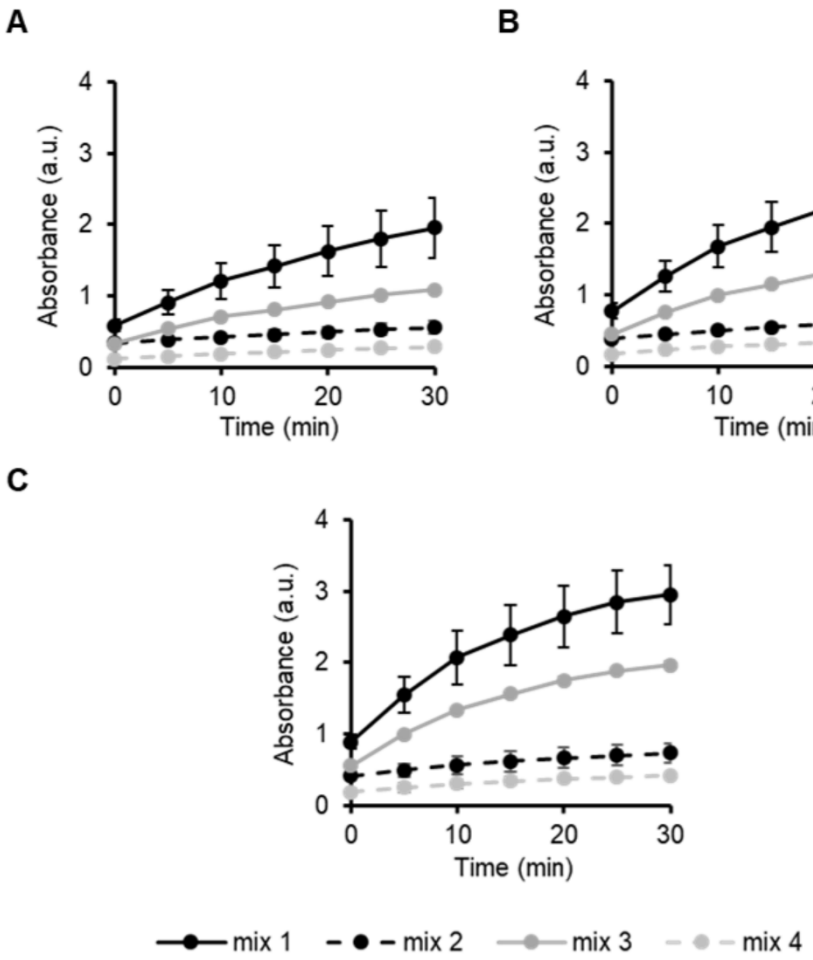


**Figure SI-2.** Plot of UV-vis absorbance intensity at 450 nm versus time during the oxidation of ABTS catalyzed by DNA-active at different concentrations. DNA-active and hemin compounds were used at 0.5, 1 and 1.5 μM, in A, B and C respectively, in the presence of different concentrations of ABTS and $H_2O_2$ (mix 1, 2, 3, 4). Error bars represent the standard deviation of three values. For each value, the absorbance of ABTS solution without DNA-active was subtracted.

*SI-3. DNA-sensing probes assays characterization in solution*

Once optimized the concentration of the reagents needed in the colorimetric DNAzyme assay, this assay was tested for the detection of Y amelogenin fragment. Each of the DNA-sensing probes mixture solutions contains a sequence complementary to different specific regions of the Y amelogenin gene and a part of the DNA-active sequence. The DNA used here is a synthetic ssDNA sequence based on the Y chromosome amelogenin gene, greatly used for gender discrimination especially in forensic science, that differs from its homologous X chromosome amelogenin gene by six pair of bases [31–33]. To verify the specificity to the Y amelogenin gene, an oligonucleotide consisting 74 nucleotides, reproducing a small fragment of the Y human chromosome amelogenin gene, was designed. As a negative control, another oligonucleotide based on the X chromosome amelogenin gene was designed too. Differences between the sequences were either the change of the sequence of nucleotides that hybridize with Y amelogenin fragment or the distribution of the guanine triplets. Half of the DNA-sensing probes pairs had a symmetric (2:2) split of the GGG groups between the two sequences of the pair, and half with a asymmetric (3:1) of the guanine triplets between the sequences of the pair; the latter was reported to work better for specific DNAzyme reactions [50,51].

Experimental protocol: 1 µL of a mixture of DNA-sensing probes 1 and 2 (mix 1, Figure SI-2 A); 3 and 4 (mix 2, Figure SI-2 B); 5 and 6 (mix 3, Figure SI-2 C) and 7 and 8 (mix 4, Figure SI-2 D) were pipetted with 47 µL of buffer solution in the microtiter plate and incubated for 1 h. Then, 1 µL of hemin-stock solution 2 was added and incubated for another 1 h. After that, 1 µL of either Y- or X-stock solutions 2, 3, 4, 5 and 6 were added at different concentrations (for a concentration of 0.5, 0.75, 1, 1.25 and 1.5 µM inside the microtiter plate ($V_f$ = 100 µL), respectively) and incubated for 30 min. Finally, 25 µL ABTS-stock solution 3 and 25 µL $H_2O_2$-stock solution 3 were added ($V_f$ = 100 µL). Absorbance was measured at 415 nm every 5 min for 30 min using a Beckman Coulter DTX 880 Multimode Detector.

In the case of the DNA-sensing probes, mix 1, the hybridization with the Y amelogenin fragment and the formation of the DNAzyme is possible (**Figure SI-3 A**). Therefore, when increasing the concentration of the Y amelogenin fragment the values of absorbance at 450 nm increased, and this behavior was observed over time, for an experimental period of 30 min. This clear effect was not observed so significantly for the rest of the DNA-sensing mixture solutions (mix 2, 3 and 4) investigated. See **Figures SI-3 B, C and D**, where the increment on the analyte concentration did not result in a specific response.

It was observed that the obtained absorbance values were, in general, lower than those performed with the DNA-active at the same experimental conditions and reagent concentrations. This is explained since there is loss of efficiency in the reaction during the hybridization of these DNA-sensing probes sequences, mainly due to the increased complexity of the process of the DNAzyme formation.

It is important to mention here that negative controls, where no Y amelogenin fragment was added, present an increment in the absorbance value at 450 nm over time, see green dotted line in all Figures of the SI-2, indicating that a low non-controllable oxidation reaction of ABTS was taking place. This side reaction has been previously described by others in literature [36], and needs to be considered for the colorimetric quantification of the assay both qualitatively and quantitatively speaking.

Our results showed that the combination of the DNA-sensing probes 1 and DNA-sensing probes 2 fragments gives both good sensitivity, with high absorbance values for the oxidation of ABTS, and similar reaction kinetics than the model DNA-active. Among the four mixture solutions of DNA-sensing probes sequences, mix 1 had good merge of all its components, as demonstrated by its capability to produce an active DNAzyme with reasonable ABTS oxidation reaction color values over time, *e.g.* $\Delta A = 0.95 \pm 0.05$ at 30 min, with respect to the “no analyte” colorimetric reaction. The rest of the mixture solutions showed little or no DNAzyme capacity, most likely

due to the lack of interaction between the sequences and the rest of components.

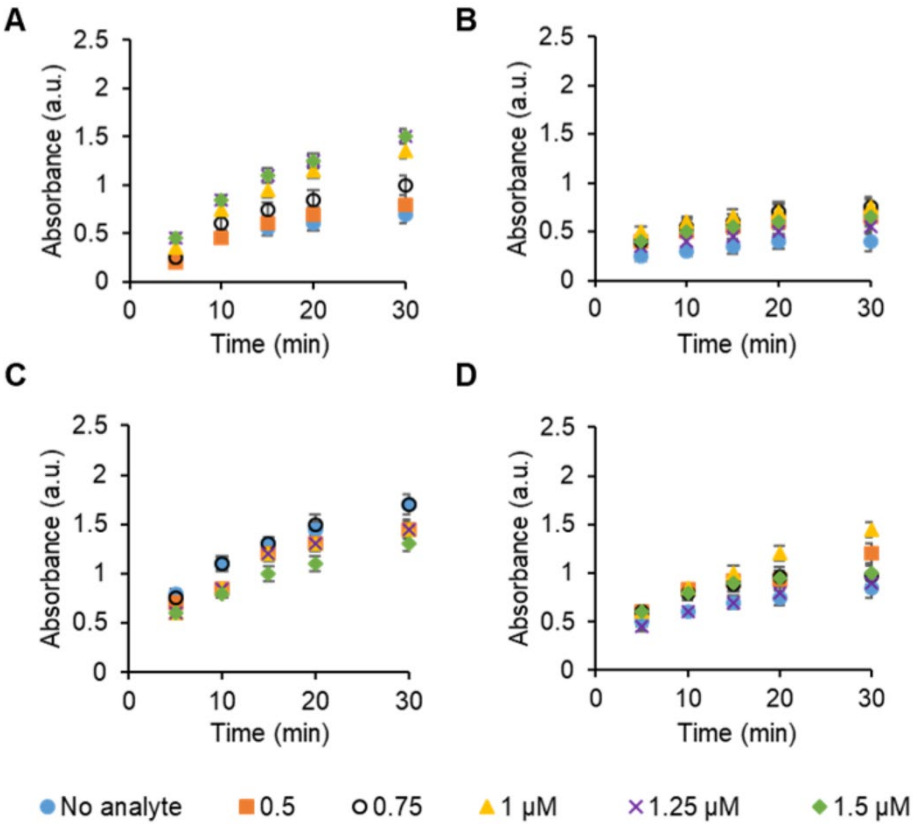


**Figure SI-3.** Absorbance values obtained from the DNAzyme catalyzed oxidation reaction of ABTS. Reactions were performed with four pairs of DNA-sensing: DNA-sensing 1 and 2 (A), DNA sensing 3 and 4 (B), DNA-sensing 5 and 6 (C) and DNA-sensing 7 and 8 (D) with increasing concentrations of the Y amelogenin fragment, ranging from 0 to 1.5 µM (final concentration in the well of the microtiter plate). DNA-sensing, hemin, ABTS and $H_2O_2$ solutions concentration in the well were 1 µM, 1 µM, 7.2 mM and 440 µM respectively. Error bars represent the standard deviation of three values. For each value, the absorbance of ABTS solution without DNA-sensing sequences was subtracted (0.24 a.u.).

## SI-4. Device specifications

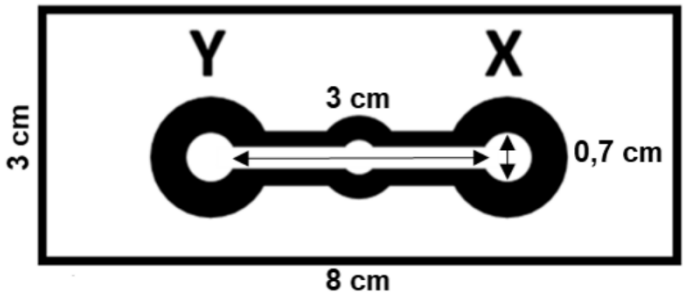


**Figure SI-4.** Design of the paper-based device (3 x 8 cm). The channel length is 3 cm and the channel width is 4 mm.

*SI-5. Characterization of the assay in solution at different conditions*

After adding 1 µL of the 1:1 SP1 and SP2 mix (100 µM), 1 µL of hemin solution (100 µM), 25 µL of ABTS solution (28.8 mM) and 47 µL of buffer in a microtiter plate, three assays were stored for 24 h, at RT daylight, at RT in the dark and at 4 ºC in the dark. After that, 1 µL of either $Y_f$ (100 µM), $X_f$ (100 µM) or buffer were added and incubated for 30 min. Finally, 25 µL of $H_2O_2$ solution (1.76 mM) was added to generate the assay. Absorbance was measured at 415 nm every 5 min for 30 min using a Beckman Coulter DTX 880 Multimode Detector. The performance of the assay (ABTS oxidation over time), when all the reagents were mixed together at the different conditions of light and ambient temperature, were compared with the results of the assay in solution performed before (**Figure SI-5 A**) and are shown in the **Figure SI-5 B-D**, over time.

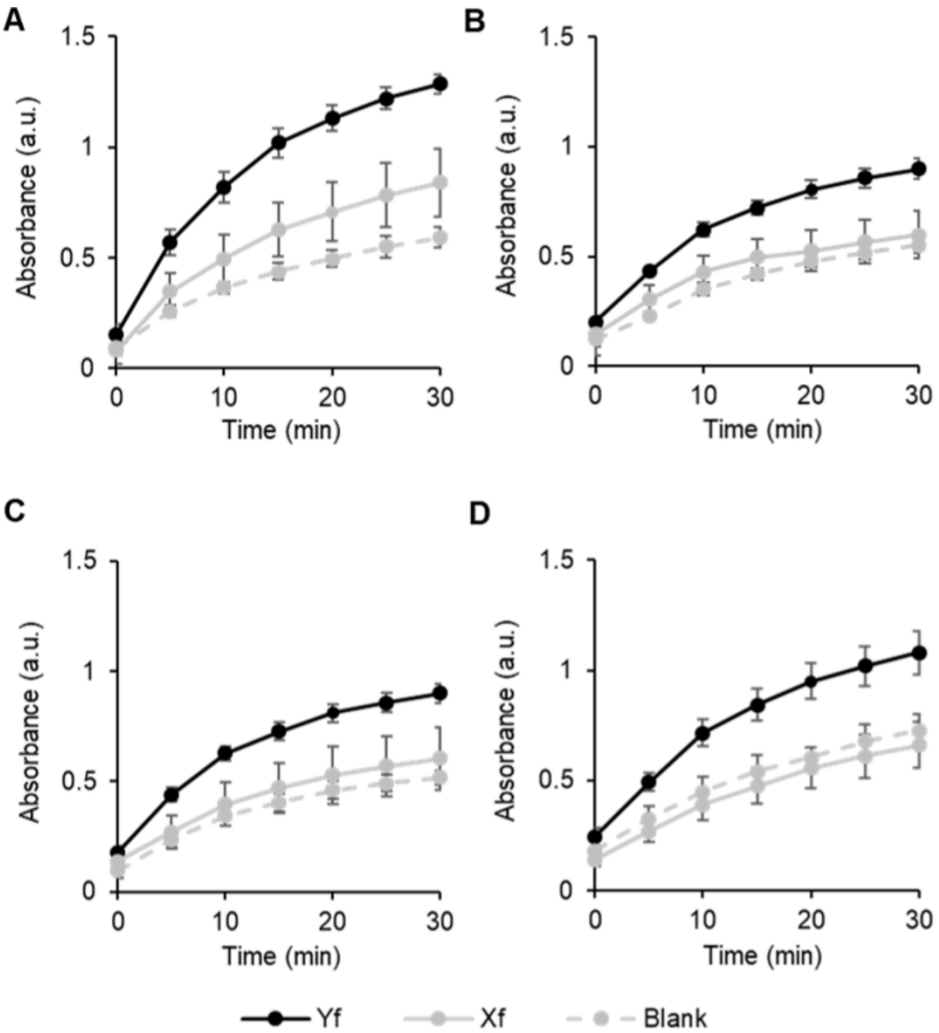


**Figure SI-5. Plot representation of the absorbance obtained during ABTS oxidation under different light and temperature and light conditions**. A) Daylight at RT assay without 24 h storage. B) 24 h storage at room temperature and ambient light conditions; C) 24 h storage at room temperature and protected from ambient light. D) 24 h storage at 4 °C, protected from ambient light. Error bars represent the standard deviation of three values. All absorbance values had the ABTS own absorbance (0.24 a.u.) subtracted.

*SI-6: $Y_f$ DNAzyme reaction in the presence of $X_f$*

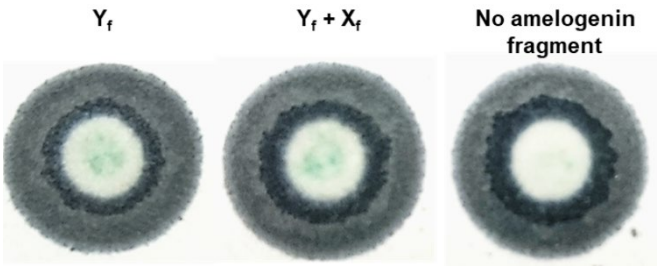


**Figure SI-6.** $Y_f$ detection on wax-circles using only $Y_f$ or a mixture of $Y_f$ and $X_f$. Photographs were taken 5 min after ABTS oxidation reaction.

*SI-7: Stability of the assay in the Whatman Filter paper 1 substrate*

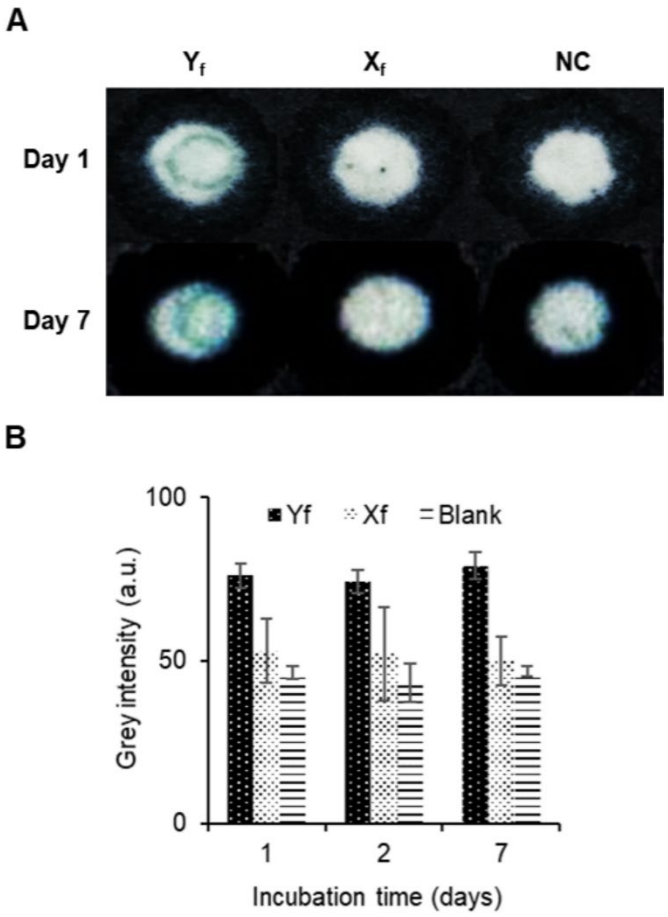


**Figure SI-7.** Pictures and graphical representation of $Y_f$ detection at different shelf-life times**.** A) Pictures of wax-circles taken 5 min after reaction for the first and seventh day of storage at 4 ºC in the dark. NC refers to negative control. B) Plot of the color intensity 5 min after reaction for $Y_f$, $X_f$ and NC for the three times studied (1, 2 and 7 days). Error bars mean ± SD (n = 3 samples per experimental condition).

## 6. References


(1) Azuaje-Hualde, E.; Arroyo-Jimenez, S.; Garai-Ibabe, G.; de Pancorbo, M. M.; Benito-Lopez, F.; Basabe-Desmonts, L. Naked Eye Y Amelogenin Gene Fragment Detection Using DNAzymes on a Paper-Based Device. *Anal. Chim. Acta* **2020**, *1123*, 1–8.

(2) Garai-Ibabe, G.; Möller, M.; Saa, L.; Grinyte, R.; Pavlov, V. Peroxidase-Mimicking DNAzyme Modulated Growth of CdS Nanocrystalline Structures in Situ through Redox Reaction: Application to Development of Genosensors and Aptasensors. *Anal. Chem.* **2014**, *86* (20), 10059–10064.

(3) Abel, G. Current Status and Future Prospects of Point-of-Care Testing around the Globe. *Expert Rev. Mol. Diagn.* **2015**, *15* (7), 853–855.

(4) Claret, P.-G.; Bobbia, X.; Roger, C.; Sebbane, M.; de La Coussaye, J.-E. Review of Point-of-Care Testing and Biomarkers of Cardiovascular Diseases in Emergency and Prehospital Medicine. *Acta Cardiol.* **2015**, *70* (5), 510–515.

(5) Ren, K.; Chen, Y.; Wu, H. New Materials for Microfluidics in Biology. *Curr. Opin. Biotechnol.* **2014**, *25*, 78–85.

(6) Akyazi, T.; Saez, J.; Elizalde, J.; Benito-Lopez, F. Fluidic Flow Delay by Ionogel Passive Pumps in Microfluidic Paper-Based Analytical Devices. *Sensors Actuators B Chem.* **2016**, *233*, 402–408.

(7) Sher, M.; Zhuang, R.; Demirci, U.; Asghar, W. Paper-Based Analytical Devices for Clinical Diagnosis: Recent Advances in the Fabrication Techniques and Sensing Mechanisms. *Expert Rev. Mol. Diagn.* **2017**, *17* (4), 351–366.

(8) Zou, Y.; Mason, M. G.; Wang, Y.; Wee, E.; Turni, C.; Blackall, P. J.; Trau, M.; Botella, J. R. Nucleic Acid Purification from Plants, Animals and Microbes in under 30 Seconds. *PLOS Biol.* **2017**, *15* (11), e2003916.

(9) Lu, Y.; Shi, W.; Qin, J.; Lin, B. Fabrication and Characterization of Paper-Based Microfluidics Prepared in Nitrocellulose Membrane By Wax Printing. *Anal. Chem.* **2010**, *82* (1), 329–335.

(10) Castro, C.; Rosillo, C.; Tsutsui, H. Characterizing Effects of Humidity and Channel Size on Imbibition in Paper-Based Microfluidic Channels. *Microfluid. Nanofluidics* **2017**, *21* (2), 21.

(11) Carrilho, E.; Martinez, A. W.; Whitesides, G. M. Understanding Wax Printing: A Simple Micropatterning Process for Paper-Based Microfluidics. *Anal. Chem.* **2009**, *81* (16), 7091–7095.

(12) Ma, J.; Yan, S.; Miao, C.; Li, L.; Shi, W.; Liu, X.; Luo, Y.; Liu, T.; Lin, B.; Wu, W.; Lu, Y. Paper Microfluidics for Cell Analysis. *Adv. Healthc. Mater.* **2019**, *8* (1), 1801084.

(13) Shen, L.; Hagen, J. A.; Papautsky, I. Point-of-Care Colorimetric Detection with a Smartphone. *Lab Chip* **2012**, *12* (21), 4240.

(14) Katis, I. N.; Holloway, J. A.; Madsen, J.; Faust, S. N.; Garbis, S. D.; Smith, P. J. S.; Voegeli, D.; Bader, D. L.; Eason, R. W.; Sones, C. L. Paper-Based Colorimetric Enzyme Linked Immunosorbent Assay Fabricated by Laser Induced Forward Transfer. *Biomicrofluidics* **2014**, *8* (3), 036502.

(15) Qiu, X.; Mauk, M. G. An Integrated, Cellulose Membrane-Based PCR Chamber. *Microsyst.*

*Technol.* **2015**, *21* (4), 841–850.

(16) Seok, Y.; Joung, H.-A.; Byun, J.-Y.; Jeon, H.-S.; Shin, S. J.; Kim, S.; Shin, Y.-B.; Han, H. S.; Kim, M.-G. A Paper-Based Device for Performing Loop-Mediated Isothermal Amplification with Real-Time Simultaneous Detection of Multiple DNA Targets. *Theranostics* **2017**, *7* (8), 2220–2230.

(17) Teengam, P.; Siangproh, W.; Tuantranont, A.; Vilaivan, T.; Chailapakul, O.; Henry, C. S. Multiplex Paper-Based Colorimetric DNA Sensor Using Pyrrolidinyl Peptide Nucleic Acid-Induced AgNPs Aggregation for Detecting MERS-CoV, MTB, and HPV Oligonucleotides. *Anal. Chem.* **2017**, *89* (10), 5428–5435.

(18) Platella, C.; Riccardi, C.; Montesarchio, D.; Roviello, G. N.; Musumeci, D. G-Quadruplex-Based Aptamers against Protein Targets in Therapy and Diagnostics. *Biochim. Biophys. Acta - Gen. Subj.* **2017**, *1861* (5), 1429–1447.

(19) Zhang, S.; Wu, Y.; Zhang, W. G-Quadruplex Structures and Their Interaction Diversity with Ligands. *ChemMedChem* **2014**, *9* (5), 899–911.

(20) Navarro, E.; Serrano-Heras, G.; Castaño, M. J.; Solera, J. Real-Time PCR Detection Chemistry. *Clin. Chim. Acta* **2015**, *439*, 231–250.

(21) Roembke, B. T.; Nakayama, S.; Sintim, H. O. Nucleic Acid Detection Using G-Quadruplex Amplification Methodologies. *Methods* **2013**, *64* (3), 185–198.

(22) Ruttkay-Nedecky, B.; Kudr, J.; Nejdl, L.; Maskova, D.; Kizek, R.; Adam, V. G-Quadruplexes as Sensing Probes. *Molecules* **2013**, *18* (12), 14760–14779.

(23) Silverman, S. K. Catalytic DNA: Scope, Applications, and Biochemistry of Deoxyribozymes. *Trends Biochem. Sci.* **2016**, *41* (7), 595–609.

(24) Zhou, W.; Saran, R.; Liu, J. Metal Sensing by DNA. *Chem. Rev.* **2017**, *117* (12), 8272–8325.

(25) Xiao, Y.; Pavlov, V.; Niazov, T.; Dishon, A.; Kotler, M.; Willner, I. Catalytic Beacons for the Detection of DNA and Telomerase Activity. *J. Am. Chem. Soc.* **2004**, *126* (24), 7430–7431.

(26) Fu, R.; Li, T.; Lee, S. S.; Park, H. G. DNAzyme Molecular Beacon Probes for Target-Induced Signal-Amplifying Colorimetric Detection of Nucleic Acids. *Anal. Chem.* **2011**, *83* (2), 494–500.

(27) Li, W.; Li, Y.; Liu, Z.; Lin, B.; Yi, H.; Xu, F.; Nie, Z.; Yao, S. Insight into G-Quadruplex-Hemin DNAzyme/RNAzyme: Adjacent Adenine as the Intramolecular Species for Remarkable Enhancement of Enzymatic Activity. *Nucleic Acids Res.* **2016**, *44* (15), 7373–7384.

(28) Zhang, Y.; Fan, J.; Nie, J.; Le, S.; Zhu, W.; Gao, D.; Yang, J.; Zhang, S.; Li, J. Timing Readout in Paper Device for Quantitative Point-of-Use Hemin/G-Quadruplex DNAzyme-Based Bioassays. *Biosens. Bioelectron.* **2015**, *73*, 13–18.

(29) Ali, M. M.; Brown, C. L.; Jahanshahi-Anbuhi, S.; Kannan, B.; Li, Y.; Filipe, C. D. M.; Brennan, J. D. A Printed Multicomponent Paper Sensor for Bacterial Detection. *Sci. Rep.* **2017**, *7* (1), 12335.

(30) Kehoe, E.; Penn, R. L. Introducing Colorimetric Analysis with Camera Phones and Digital Cameras: An Activity for High School or General Chemistry. *J. Chem. Educ.* **2013**, *90* (9), 1191–1195.

(31) von Wurmb-Schwark, N.; Bosinski, H.; Ritz-Timme, S. What Do the X and Y Chromosomes Tell Us about Sex and Gender in Forensic Case Analysis? *J. Forensic Leg. Med.* **2007**, *14* (1), 27–30.

(32) Iwase, M.; Satta, Y.; Takahata, N. Sex-Chromosomal Differentiation and Amelogenin Genes in Mammals. *Mol. Biol. Evol.* **2001**, *18* (8), 1601–1603.

(33) Tozzo, P.; Giuliodori, A.; Corato, S.; Ponzano, E.; Rodriguez, D.; Caenazzo, L. Deletion of Amelogenin Y-Locus in Forensics: Literature Revision and Description of a Novel Method for Sex Confirmation. *J. Forensic Leg. Med.* **2013**, *20* (5), 387–391.

(34) Dutta, S.; Nath, P. A Fully Automated Colorimetric Sensing Device Using Smartphone for Biomolecular Quantification. *Opt. Biophotonics Low-Resource Settings III* **2017**, 1005512.

(35) Findlay, J. W. A.; Dillard, R. F. Appropriate Calibration Curve Fitting in Ligand Binding Assays. *AAPS J.* **2007**, *9* (2), 260–267.

(36) Cui, X.; Li, R.; Liu, X.; Wang, J.; Leng, X.; Song, X.; Pei, Q.; Wang, Y.; Liu, S.; Huang, J. Low-Background and Visual Detection of Antibiotic Based on Target-Activated Colorimetric Split Peroxidase DNAzyme Coupled with Dual Nicking Enzyme Signal Amplification. *Anal. Chim. Acta* **2018**, *997*, 1–8.

(37) Zhang, Y.; Li, B. Reducing Background Signal of G-Quadruplex–Hemin DNAzyme Sensing Platform by Single-Walled Carbon Nanotubes. *Biosens. Bioelectron.* **2011**, *27* (1), 137–140.

(38) Kadnikova, E. N.; Kostić, N. M. Oxidation of ABTS by Hydrogen Peroxide Catalyzed by Horseradish Peroxidase Encapsulated into Sol–Gel Glass. *J. Mol. Catal. B Enzym.* **2002**, *18* (1–3), 39–48.

(39) Konan, K. V.; Le Tien, C.; Mateescu, M. A. Electrolysis-Induced Fast Activation of the ABTS Reagent for an Antioxidant Capacity Assay. *Anal. Methods* **2016**, *8* (28), 5638–5644.

(40) Venkatasubramanian, L.; Maruthamuthu, P. Kinetics and Mechanism of Formation and Decay of 2,2-Azinobis-(3-Ethylbenzothiazole-6-Sulphonate) Radical Cation in Aqueous Solution by Inorganic Peroxides. *Int. J. Chem. Kinet.* **1989**, *21* (6), 399–421.

(41) Ghosh, R.; Vaishampayan, V.; Mahapatra, A.; Malhotra, R.; Balasubramanian, S.; Kapoor, A. Enhancement of Limit of Detection by Inducing Coffee-Ring Effect in Water Quality Monitoring Microfluidic Paper-Based Devices. *Desalin. WATER Treat.* **2019**, *156*, 316–322.

(42) Rethmeyer, J. A.; Tan, X.; Manzardo, A.; Schroeder, S. R.; Butler, M. G. Comparison of Biological Specimens and DNA Collection Methods for PCR Amplification and Microarray Analysis. *Clin. Chem. Lab. Med.* **2013**, *51* (5).

(43) Walsh, P. S.; Metzger, D. A.; Higuchi, R. Chelex 100 as a Medium for Simple Extraction of DNA for PCR-Based Typing from Forensic Material. *Biotechniques* **2013**, *54* (3).

(44) Wang, X.; Lim, H. J.; Son, A. Characterization of Denaturation and Renaturation of DNA for DNA Hybridization. *Environ. Health Toxicol.* **2014**, *29*, e2014007.

(45) Reboud, J.; Xu, G.; Garrett, A.; Adriko, M.; Yang, Z.; Tukahebwa, E. M.; Rowell, C.; Cooper, J. M. Paper-Based Microfluidics for DNA Diagnostics of Malaria in Low Resource Underserved Rural Communities. *Proc. Natl. Acad. Sci.* **2019**, *116* (11), 4834–4842.

(46) Notomi, T.; Okayama, H.; Masubuchi, H.; Yonekawa, T.; Watanabe, K.; Amino, N.; Hase, T.

Loop-Mediated Isothermal Amplification of DNA. *Nucleic Acids Res.* **2000**, *28* (12), E63.

(47) Krupovic, M.; Forterre, P. Single-Stranded DNA Viruses Employ a Variety of Mechanisms for Integration into Host Genomes. *Ann. N. Y. Acad. Sci.* **2015**, *1341* (1), 41–53.

(48) Labonté, J. M.; Suttle, C. A. Previously Unknown and Highly Divergent SsDNA Viruses Populate the Oceans. *ISME J.* **2013**, *7* (11), 2169–2177.

(49) Kosman, J.; Juskowiak, B. Peroxidase-Mimicking DNAzymes for Biosensing Applications: A Review. *Anal. Chim. Acta* **2011**, *707* (1–2), 7–17.

(50) Deng, M.; Feng, S.; Luo, F.; Wang, S.; Sun, X.; Zhou, X.; Zhang, X.-L. Visual Detection of RpoB Mutations in Rifampin-Resistant Mycobacterium Tuberculosis Strains by Use of an Asymmetrically Split Peroxidase DNAzyme. *J. Clin. Microbiol.* **2012**, *50* (11), 3443–3450.

(51) Lu, X.; Shi, X.; Wu, G.; Wu, T.; Qin, R.; Wang, Y. Visual Detection and Differentiation of Classic Swine Fever Virus Strains Using Nucleic Acid Sequence-Based Amplification (NASBA) and G-Quadruplex DNAzyme Assay. *Sci. Rep.* **2017**, *7* (1), 44211.

# Appendix 3

# Paper based microfluidic analytical device for single-step detection of mesenchymal stromal cells secreted VEGF

## Paper based microfluidic analytical device for single-step detection of mesenchymal stromal cells secreted VEGF

Enrique Azuaje-Hualde, Marian Martínez de Pancorbo, Fernando Benito-Lopez, Lourdes Basabe-Desmonts

*Manuscript submitted to: Analytical Chemistry*

*Impact Factor: 6.785 (Q1)*

*Area: Analytical Chemistry*

**Abstract**

There is an increased interest in developing sensing platforms to automate the monitoring of cell culture secretion. Paper microfluidics are low cost and user-friendly platforms widely used for the integration of biosensors. On the other hand, DNA-based sensing probes with binding capacities for specific molecules have been proposed for the formulation of new biosensors. In this work, the first cellulose microfluidic paper-based analytical device is presented for the single-step detection of cell secreted vascular endothelial growth factor, a growth factor with clinical potential in regenerative medicine and cancer research. The detection mechanism is based on a self-reporting Structure Switching Signaling Aptamer. A three-part Structure Switching Signaling Aptamer was designed with an aptameric sequence based on the VEGF aptamer 3R02, which provides a fluorescent signal upon VEGF recognition. First, the VEGF biosensor was integrated in a paper substrate, allowing the detection of a VEGF, up to 0.57 ng, through fluorescence intensity analysis. Then, as a proof-of-concept, the biosensor was incorporated in a microfluidic paper-based analytical device format and applied for the detection of VEGF in the supernatant of mesenchymal stem cells culture plates.

## 1. Introduction

The vascular endothelial growth factor (VEGF) is a cell-secreted regulator of endothelial cells expression by inducing angiogenesis and vasculogenesis. Deregulations of the expression levels of VEGF are associated with several diseases, such as tumor growth, metastasis, Parkinson, Alzheimer and macular degeneration, among others, becoming both a potential therapeutic target and a disease indicator in diagnosis [1,2]. The VEGF family covers several type of monomers, distinguished by the number of amino acids, being the subtypes $VEGF_{121}$, $VEGF_{145}$ and $VEGF_{165}$ secreted proteins. In the majority of biological systems, $VEGF_{121}$ and $VEGF_{165}$ are the most abundant and important isoforms [3]. Conventional immunodetection techniques such as ELISA are often used for the detection and quantification of secreted VEGF, mainly in *in vitro* studies which involve several sequential manual steps [4]. However, there is an increasing interest in the development of microtechnologies and microfluidics platforms able to improve the automation on the process of cell culture and secretion monitoring. Research mainly focus on the generation of label-free and/or real-time systems for the continuous monitoring of large number of events. In particular, the recent advances in microfluidics and microtechnology have made possible investigations on new techniques and systems for VEGF detection [5].

Aptamers, which are nucleic acid sequences able to specifically bind to target molecules, have been proposed as novel sensing probes for the development of a new generation of biosensors [6]. These sequences are able to form various types of interactions with the target, *e.g.* electrostatic interactions and hydrogen bonds, and normally adopt specific three-dimensional configurations upon contact with the molecules. The G-quadruplex structure, formed by the interaction of internal loops and G-rich sequences, is the most common conformation observed in single strand DNA aptamers [7]. Usually designed and selected by SELEX (Systematic Evolution of Ligands by Exponential enrichment), the ideal aptamers present enhanced affinity and specificity for the desired target [8].

Several aptamers have been successfully designed for the detection and analysis of VEGF-isoforms [9]. Among them, the dimeric V7t1 and the 3R02 aptamers have shown remarkable results in research, with high affinities for VEGF with dissociation constants ($K_d$) down to picomolar levels [10,11]. Several strategies have been followed for the conversion of bare aptamers into a functional biosensor by a wide range of detection methods, including chemiluminiscence, optical and electrochemical detection of VEGF [12–14].

Structure switching aptamers are a special type of three-dimensional conformation aptamers in which a double stranded sequence goes into a strand displacement upon recognition of the target molecule [15]. These aptamers can have a single, dual or three-part strand designs depending on the number of independent DNA probes that forms the complex. When the conformation change allows the production or disruption of a signal, usually a fluorescence signal, becoming structure switching signaling aptamers (SSSA). The strategy to design SSSAs usually requires short displacement strands to partially block the recognition sequence. Upon interaction with the target molecule, the release of the displacement strand allows the production of the signal by the displacing of a quencher from a fluorophore, which is bounded to the SSSA [16]. The detection and the analysis of several molecules have been demonstrated using SSSAs, including physiological molecules like thrombin and ATP or drugs like chloramphenicol [17,18]. In line with the SSSA design, several biosensors for VEGF are present in recent literature. For instance, Freeman *et al*. designed a series of optical aptasensors, specific for VEGF, based on both fluorescence and bioluminescence signals [19]. More recently, Li *et al.* developed a fluorescence VEGF biosensor incorporating a structure switching strand for the detection of low concentrations of the growth factor [20].

Regarding the fabrication of novel microfluidics devices for biosensing, paper substrates are widely used due to their low cost, easy to use and environmental friendly qualities. Microfluidic paper-based analytical devices (μPADs) have been extensively used in the development of protein biosensors, including commercialized HIV chips and paper ELISA tests [21]. μPADs allow to produce whole quantification assays with low volume of

samples, ranging from micro- to nanoliters, using a simple fabrication procedure when compared to other microfluidics devices [22]. In particular, cellulose and nitrocellulose substrates have been widely used for DNA purification, adsorption and analysis [23,24]. Recently, paper materials have been investigated for the development of new analytical devices based on RNA and DNA sensors [25]. We previously reported the development of a paper microfluidic device using DNA-based sensors as DNAzymes for the colorimetric detection of ssDNA, which not only allowed to simplify the process but increased the sensitivity of the analysis when compared to the same assay in solution [26].

Aptamer-based μPADs have been developed for a wide range of detection systems, including virus, bacteria, ions and for drug analysis [27,28]. Therefore, it is ambitioned that new designed SSSA and μPADs could generate an unconventional set of technologies that get us closer to devices for multiplex detection of secreted substances from cells. While microfluidics devices have been proposed for the aptamer-based, single-step, detection of VEGF, even achieving a portable detection system that could be applied for the analysis of cell secretion [29], SSSAs have not been explored for the detection of VEGF on a paper microfluidic device. Furthermore, no analytical system has been proposed so far to unify the advantages of SSSA single-step and real time detection capabilities, the simplicity and cost-effectiveness of μPADs, and the enhanced sensitivity that can be achieved in the combination of DNA sensors and μPADs. Hence, we present here a designed and fabricated μPAD for the single-step detection of secreted VEGF using a novel SSSA design (VEGF-SSSA), based on the aptamer 3R02. This approach allows both, to improve the detection limits of the sensing assay thanks to the SSSA and to simplify the analytical method, reducing cost of the assay thanks to the advantages brought by the μPAD. The VEGF-SSSA biosensor performance was investigated in terms of the sequences hybridization, specificity and sensitivity during VEGF detection both, in solution and over cellulose paper substrates. Upon optimization of the process, as a proof-of-concept, the biosensor was integrated in a μPAD. Finally, the performance of the device was verified by the detection of secreted VEGF in the supernatant of mesenchymal stromal cells culture, **Figure 1.**

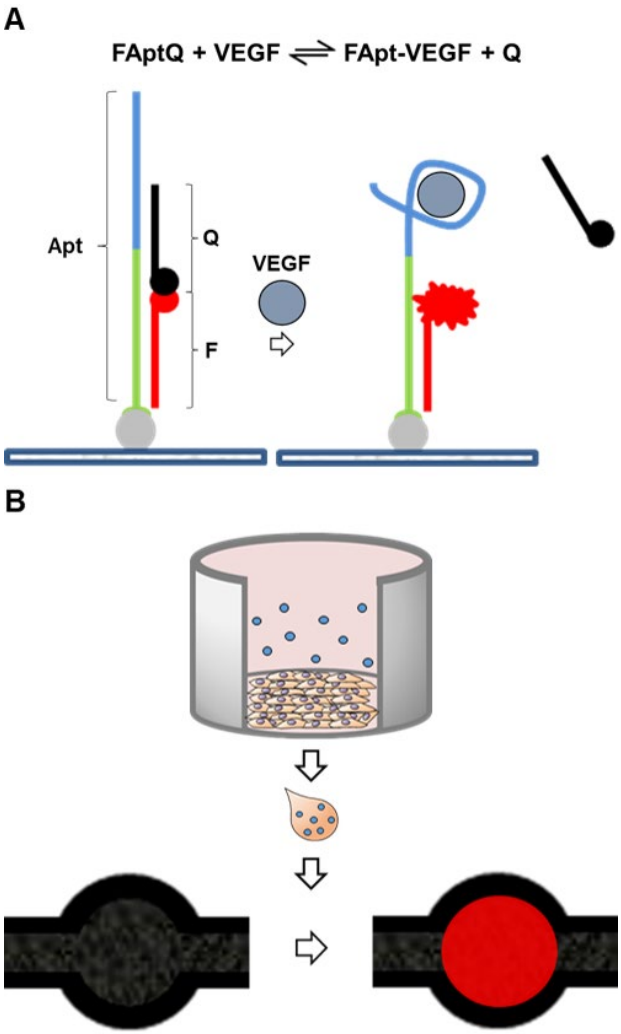


**Figure 1. Schematic representation of the VEGF detection by immobilized VEGF-SSSA.** A) The binding between the aptamer probe (Apt) the fluorescence probe (F) and the quencher probe (Q) produces the quenching of the fluorophore. In the presence of VEGF, the aptamer binds to it and displaces the quencher probe, allowing the excitation and emission of the fluorophore. B) Cell supernatant can be directly loaded on a μPAD with VEGF-SSSA. Through fluorescence microscopy imaging, the concentration of VEGF can be analyzed by the quantification of the fluorescence intensity recovery produced by the interaction of VEGF with the VEGF-SSSA.

## 2. Materials and methods

### *2.1. Materials*

All oligonucleotides were synthesized by Integrated DNA Technologies (IDT, Belgium). Three oligonucleotides sequences were purchased: 5'-TGTGGGGGTGGACTGGGTGGGTACCGTCACTCGCCTCGCACCGTCC – Biotin - 3' (Aptamer DNA probe, **Apt**), 5'- GGACGGTGCGAGGCG - Cy5Sp - 3' (Fluorophore DNA probe, **F**) and 5 – IabRQ - GTGACGGTACCC - 3' (Quencher DNA probe, **Q**). The fluorophore (Cy5) had an excitation wavelength of 648 nm and an emission wavelength of 668 nm. The quencher (Iowa Black RQ) had an absorbance between 500 and 700 nm. Vascular Endothelial Growth Factor 165 (referred as VEGF onwards) was purchased from Fisher Scientific (Spain). Sodium chloride was purchased from Sigma-Aldrich (Spain).Potassium chloride and TRIS were purchased from Panreac (Spain). Streptavidin, Bovine Serum Albumin (BSA) and Whatman filter paper #1 and glass covers were purchased from Sigma Aldrich (Spain). Polymethyl methacrylate (PMMA) Plexiglas 4 mm, was purchased from Evonik Industries AG (Germany). Pressure Sensitive Adhesive (PSA) ARcare 8939 was purchased from Adhesive Research (Ireland). Human adult Mesenchymal Stromal Cells were obtained from donated human hair follicles (hHF-MCSs, p6). Complete cell culture medium consisted of Dulbecco's Modified Eagle's Medium (DMEM), Fisher Scientific (Spain), supplemented with 30 % Fetal Bovine Serum (FBS), Fisher Scientific (Spain), and 10 % Penicillin/Streptomycin (P/S), Fisher Scientific (Spain).

### *2.2 Solutions*

Buffer solution consisted of sodium chloride 100 mM, potassium chloride 5 mM and TRIS 2 mM in distilled water, regulated to pH 7. All DNA probes were dissolved and then diluted in buffer solution. Three different VEGF-SSSA solutions were prepared. VEGF-SSSA solution 1 (FAptQ 1) consisted of F (1 μM), Apt (2 μM) and Q (3 μM), following a ratio 1:2:3. VEGF-SSSA solution 2 (FAptQ 2) consisted of F (200 nM), Apt (600 nM) and Q (600 nM) following a ratio 1:3:3. VEGF-SSSA solution 3 (FAptQ 3) consisted of F (200 nM), Apt (600 nM) and Q (1 μM), following a ratio 1:3:5. Two different fluorescence

control solutions were prepared. Fluorescence control solution 1 (FApt 1) consisted of F (1 μM) and Apt (2 μM) and fluorescence control solution 2 (FApt 2) consisted of F (200 nM) and Apt (600 nM). Additionally, three F:Q solutions were prepared. F:Q solution 1 (FQ 1) consisted of F (1 μM) and Q (3 μM), F:Q solution 2 (FQ 2) consisted of F (200 nM) and Q (600 nM) and F:Q solution 3 (FQ 3) consisted of F (200 nM) and Q (1 μM). Finally, two solutions of F were prepared: F 1 (1 μM) and F 2 (200 nM). VEGF was dissolved and diluted in PBS in all cases. VEGF solutions 1, 2, 3, 4, 5, 6 and 7 had a concentration of 0.01, 0.1, 0.5, 1, 2.5, 5 and 10 μg $mL^{-1}$, respectively.

### *2.3 Fluorescence measurements*

For solution assays: fluorescence measurements were done on a Promega Globax Multi Detection fluorometer (USA) at an excitation wavelength of 620 nm. Data were normalized to the fluorescence control intensity (F), taking the fluorescence control as the maximum possible fluorescence (100 %) and calculating the percentage for each sample and the negative controls, see equation 1.

$$Normalized\ Fluorescence\ Intensity = \frac{Fluorescence\ Intensity\ Sample}{Maximum\ Fluorescence\ Intensity\ Control}\ x\ 100$$

(eq. 1)

For paper assays: fluorescence microscopy images were acquired with a modified Nikon Eclipse TE2000-S inverted microscope (USA), with and adapted Andor Zyla sCMOS black and white camera (Oxford Instruments, UK). Lumencor laser 640 nm was used as light source for excitation and Quad EM filter: 446/523/600/677 with 4 TM bands: 446/34 + 523/42 + 600/36 + 677/28 4. Four different areas of each paper samples were imaged with a 20x objective, the fluorescence intensity was obtained from the NIS elements analysis software and then, the mean value of the four images was calculated. Data were normalized to the fluorescence control (F or FApt) intensity.

## 3. Results and discussion

The three-parts VEGF-SSSA developed in this work (see Figure 1 A), which is similar to the one described by R. Nutiu *et al*. [16], is composed of the following sequences: a lead probe containing an elongation sequence followed by the VEGF aptamer sequence bound to a biotin protein at its 3' end (aptamer probe, Apt); a probe containing the complementary sequence to the first 15 nucleotides of the elongation sequence bound to a Cy5 fluorophore at its 3' end (fluorescence probe, F); and a probe containing the complementary sequence to the last 5 nucleotides of the elongation sequence and the first 7 nucleotides of the VEGF aptamer sequence bound to a Iowa Black RQ quencher at its 5' end (quencher probe, Q). On its native form, the VEGF-SSSA is formed by the bonding of F and Q to Apt (FAptQ). In presence of VEGF, Q is displaced and Apt joins VEGF to form FApt - VEGF.

A biotinylated three parts design was chosen as the best option for immobilization on substrates. While DNA has been easily immobilized in some substrates (*i.e.* cellulose or nitrocellulose), the addition of a biotin residue at the 3' end of the aptamer enables the immobilization on other streptavidin functionalized substrates. As the biotin is bound to a lead probe where the other two probes bind to, and not to the Q itself, the immobilization should not affect the performance of the SSSA as the Q can detach from the FAptQ structure, releasing the fluorophore. The Q was designed to be complementary to both part of the elongation sequence and part of the Apt sequence. This configuration permits to anchor the Q to the Apt, to maintain the capture capabilities of the Apt and to disable any possible VEGF recognition without Q displacement.

The design of the VEGF-SSSA aimed to accomplish the following objectives; 1) to be able to detect, in a single step, low concentrations of VEGF with great specificity, 2) to enable immobilization on substrates for further implementation on microfluidics. The aptamer probe was an adaptation of the VEGF aptamer 3R02. The 3R02 was reported by Nonaka *et al*. [10] as mutation of the VEap121 aptamer made by *in silico* maturation, with improved

sensitivity. Authors reported that the 3R02 has a good specificity for the growth factor with the lowest dissociation constants ($K_d$) for VEGF among all the aptamers found in literature at 300 pM so far.

### *3.1. VEGF-SSSA performance and VEGF detection in solution*

For a correct VEGF-SSSA design, the DNA probes must form a three-dimensional structure in which only the proximity obtained between the fluorescence probe and the quencher probe, when both F and Q are assembled to the aptamer strand, results in an efficient fluorescence quenching.

First, we evaluated the quenching performance of the Q in our VEGF-SSSA. Solutions of F, FApt, FQ and FAptQ, in a ratio of 1:2:3, respectively (solution FAptQ 1, see experimental section), were analyzed in solution. The detailed experimental procedure can be found in Supporting Information 1.

The fluorescence signal obtained from F, FQ or FApt solutions were similar, while the signal from the FAptQ solution was 80 % lower. These results indicated an efficient formation of the FAptQ duplex and quenching of the fluorescence signal (**Figure 2 A**).

However, contrary to our expectations, the incubation of FAptQ with the target VEGF (10 µg $mL^{-1}$), did not cause a change in the fluorescent signal.

Looking for the explanation of this negative result, the whole assay was carried out in the homemade PMMA well array in order to reduce the sample volume from 100 µL to 7.5 µL and so, to improve microscopy observation. Bright fluorescent aggregates were observed in the solutions containing VEGF (**Figure 2 B**).

Those aggregates were considered the come from the agglomeration of a FApt - VEGF complex formed after the displacement of the Q, which would explain the low fluorescence signal obtained from the FAptQ after the addition of VEGF [30].

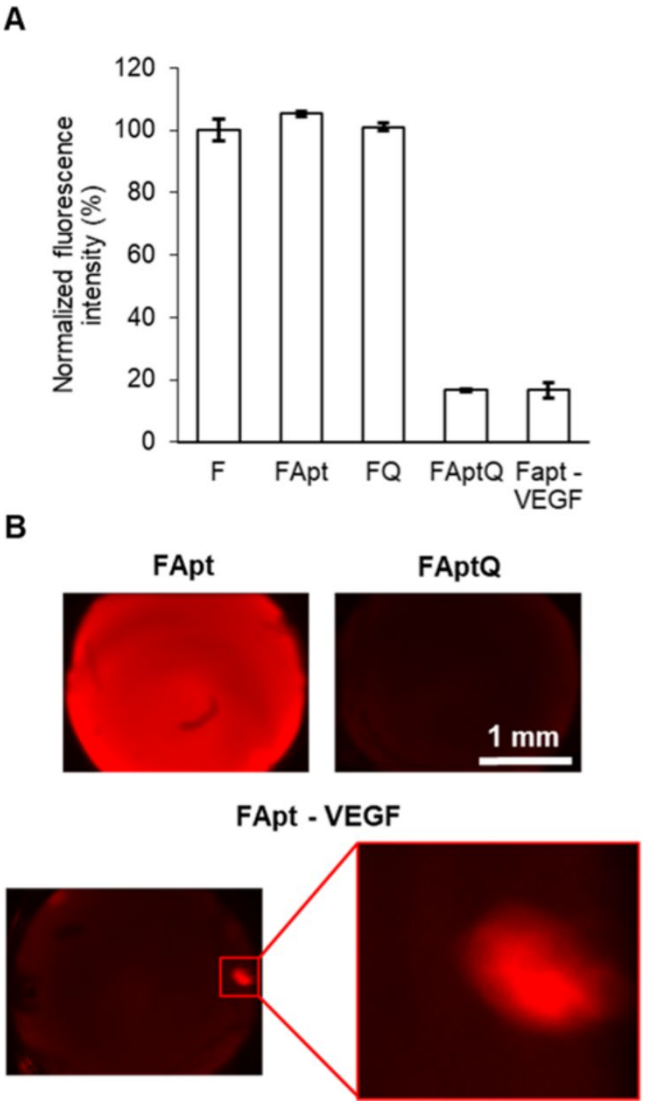


**Figure 2.** Characterization of VEGF-SSSA performance and VEGF detection in solution. A) Plot of the fluorescence intensity for different combinations of Fluorescence probe (F), Aptamer probe (Apt) and Quencher probe (Q) solutions, as well as the formed VEGF-SSSA (FAptQ) before and after the addition of 10 μg $mL^{-1}$ of VEGF, all normalized to F intensity. Error bars correspond to mean values ± SD (n = 3). B) Fluorescence microscopy images of the solutions containing FApt, FAptQ and FAptQ after the addition of a 10 μg $mL^{-1}$ VEGF solution (FApt - VEGF).

### *3.2. VEGF-SSSA performance and VEGF detection on printed wax-circles*

To characterize the quenching performance of Q in our VEGF-SSSA assay on cellulose paper wax-circles were printed, see **Figure 3 A**. The detailed experimental procedure for the paper devices fabrication can be found in Supporting Information 2. The detailed experimental procedure for the VEGF detection assays on cellulose paper can be found in Supporting Information 3.

Solutions of FApt, FQ and FAptQ in ratios of 1:3:3 (solution FAptQ 2) and 1:3:5 (solution FAptQ 3) for F, Apt and Q, respectively, were loaded onto the cellulose paper and analyzed using fluorescence microscopy. In the case of the solutions following a 1:3:3 ratio, the FAptQ solution presented 65 % lower fluorescence signal than the one obtained for the FApt solution, indicating proper assembly of the VEGF-SSSA. FQ solution presented a similar fluorescence intensity to that of FApt, indicating that without the presence of the Apt, the Q was not able to quench the fluorophore from F. In the case of the 1:3:5 ratio solutions, the sole combination of free Q with free F in the FQ solution induced a reduction of the fluorescence signal by 15 %, indicating that a higher concentration of Q could quench the fluorophore even in the absence of the Apt. For that reason, the rest of the experiments were performed with the 1:3:3 ratio solutions (solution FAptQ 3) (**Figure 3 B**).

For the detection of VEGF in paper, either 1µL of 10 µg $mL^{-1}$ VEGF solution or PBS (negative control) were incubated on the wax-circles treated with FAptQ, see experimental section, and imaged by fluorescence microscopy. The fluorescence signal increased by a 17 % in the presence of the VEGF (53 ± 2 %) when compared to the fluorescence signal of the negative control (36 ± 3 %), indicating binding of VEGF to FApt and the formation of FApt - VEGF.

To evaluate the specificity of the assay, other proteins were tested. Either 1 µL of BSA or a streptavidin solution (100 µg $mL^{-1}$) were loaded into the wax-circles with VEGF-SSSA. In both cases, the fluorescence signal remained similar to the signal of the negative controls (36 ± 2 % and 36 ± 6 %, respectively) (**Figure 3 C**).

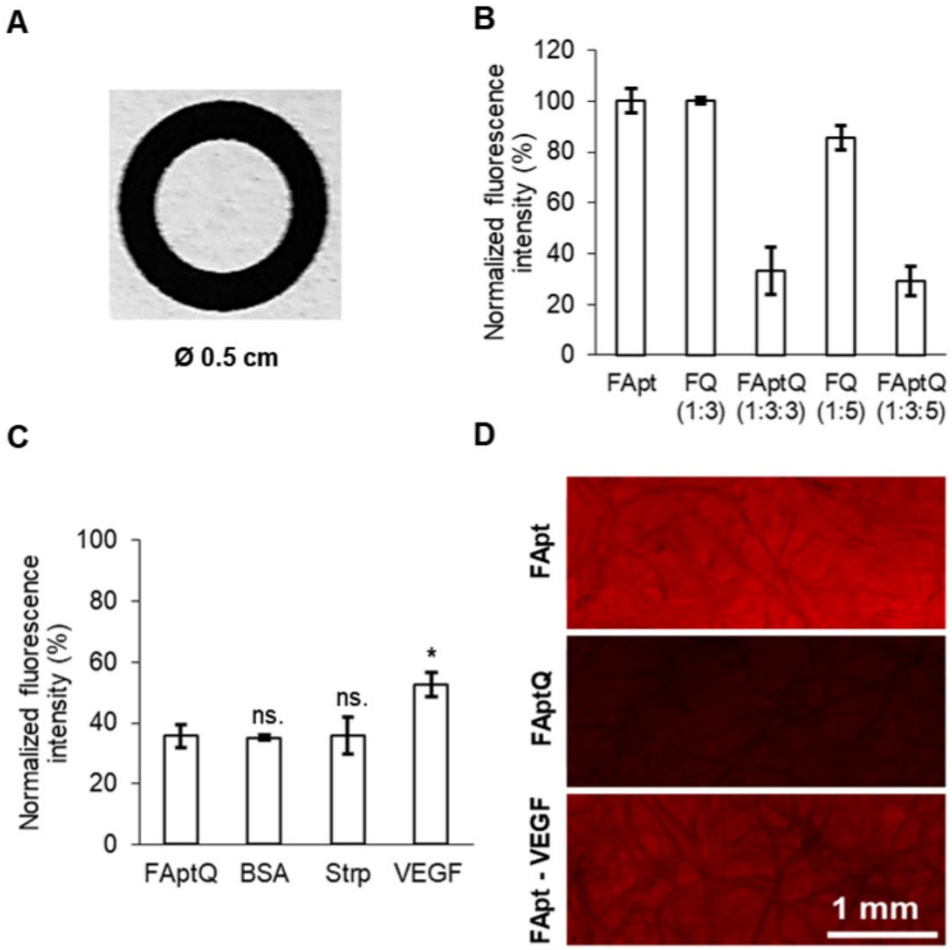


**Figure 3.** VEGF-SSSA binding performance and VEGF detection on cellulose paper. A) Photographs and specifications for printed wax-circles (internal diameter 0.75 cm). B) Plot of the normalized fluorescence intensity in samples containing different combinations of Fluorescence probe (F), Aptamer probe (Apt) and Quencher probe (Q) at different ratios, normalized to the fluorescence control (FApt) intensity. Error bars correspond to mean values ± SD (n = 3). C) Plot of the fluorescence intensity observed in the negative control (FAptQ) and in samples incubated with streptavidin (Strp, 100 µg $mL^{-1}$), BSA (100 µg $mL^{-1}$) and VEGF (FApt - VEGF, 10 µg $mL^{-1}$), normalized to the fluorescence control (FApt) intensity. Error bars mean ± SD (n = 3). Statistical significance: One-Way ANOVA, where ns. means $p > 0.05$ and ** means $p \leq 0.01$ D) Microscope images of the wax circles, showing the fluorescence obtained in the fluorescence control (FApt), the negative control (FAptQ) and the VEGF treated (FApt - VEGF) samples.

These results confirmed, the affinity of the FApt probe for VEGF, an efficient displacement of the Q producing the release of the fluorophore, and the specificity of the FApt probe for VEGF over other proteins such as BSA and streptavidin.

Contrary to the results obtained in the solution assays, fluorescence intensity in paper was more homogenous through the entire sample surface, since no agglomerates were observed. This behavior can be attributed to the spreading and deposition of the VEGF-SSSA among the cellulose surface. The higher fluorescence intensity values can also be associated with the evaporation of the reagents, as evaporation itself has been previously described to improve sensing on surfaces due to enrichment of the reagents found in the droplet increasing molecular interaction frequency and reaction rates [31]. Finally, the fact of having obtained better results in the detection of VEGF with the paper SSSA assay than with the solution assay could be explained by the fact that aptasensors often improve their functionality when they are immobilized on solid supports [32].

To evaluate the sensitivity of our VEGF-SSSA for VEGF, different concentrations of VEGF solution (ranging from 0.01 to 10 μg $mL^{-1}$) were loaded on the printed wax-circles.

As seen in **Figure 4**, VEGF was detected on the paper substrate starting from the 0.1 μg $mL^{-1}$ VEGF solution onwards. Higher fluorescence intensity, increasing from 5 % to 27 % from the quenched FAptQ, was observed with increasing concentrations of VEGF (40 ± 3 % for the concentration of 0.1 μg $mL^{-1}$ to 61 ± 1 % for the concentration of 10 μg $mL^{-1}$, total normalized fluorescence intensity). A plateau was reached at the concentration of 5 μg $mL^{-1}$, as higher concentrations produced similar fluorescence intensities. This demonstrated the sensitivity of our VEGF-SSSA to different VEGF concentrations.

A calibration curve was fitted in a logistic regression curve and both, VEGF limit of detection (LOD, 3 x Blank values) and limit of quantification (LOQ, 3.3 x LOD) were calculated to be 229.24 and 756.49 ng $mL^{-1}$ respectively,

corresponding to 0.57 ng and 1.89 ng respectively of VEGF in our assay. The $K_d$ calculated from the curve [33] was 436.14 ng mL$^{-1}$ (19 nM).

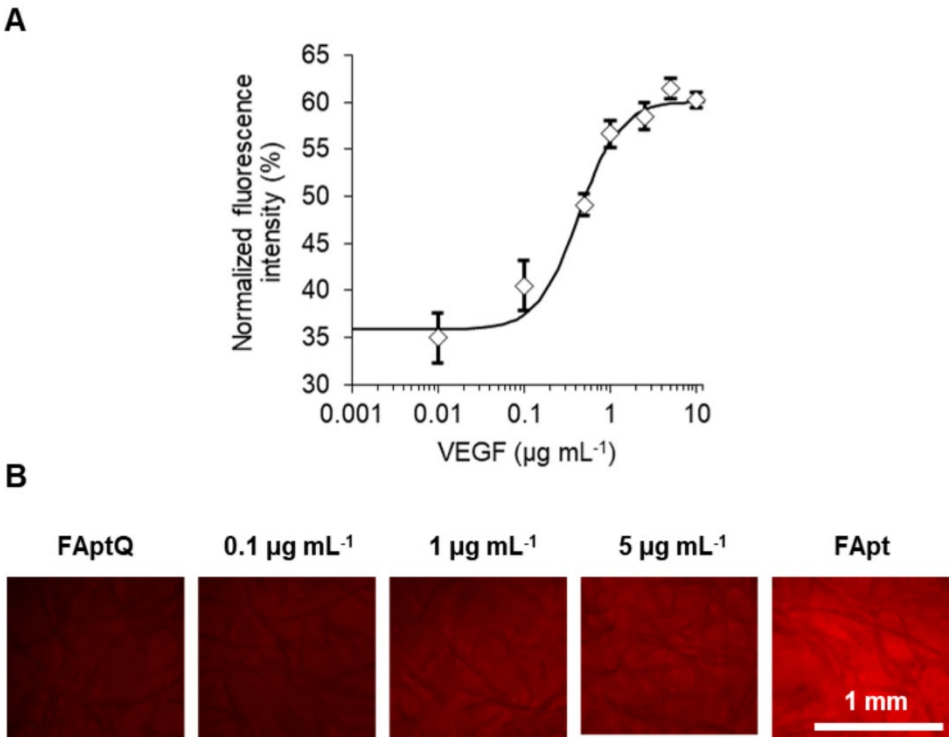


**Figure 4.** Detection of different concentrations of VEGF on the VEGF-SSSA treated Whatman filter paper. A) Plot of the fluorescence intensity obtained by the incubation with different concentrations of VEGF (0.01, 0.1, 0.5, 1, 2.5, 5 and 10 µg mL$^{-1}$), normalized to the fluorescence control intensity. Error bars correspond to mean values ± SD (n = 4). B) Microscope images of the fluorescence obtained in paper samples treated with different concentrations of VEGF.

The range of VEGF concentrations that can be detected with our VEGF-SSSA treated paper support was between 200 and 5000 ng mL$^{-1}$. While the LOD of this technique was higher than those found in the literature, where detection of concentrations as small as picograms and fentograms per liter have been achieved [14,34,35], thanks to the reduced volume of sample required by the paper substrate (1 - 2.5 µL), the minimum amount of VEGF that can be detected was calculated to be as low as 500 pg. While the $K_d$ obtained

was higher than the $K_d$ reported for the 3R02 aptameric sequence, it lied within the values obtained by other authors (between 0.3 to 20 nM) [11,36]. Cells have a wide range of secretion profiles of VEGF, for instance in the case of MSCs it ranges from 30 to 200 ng per $10^6$ cells per day depending on the stimuli [37,38]. Therefore, our technique could be useful for the monitoring of medium during long-term MSCs cultures.

### *3.3. VEGF detection in µPAD*

In order to integrate controls and samples analysis in the same analytical platform, the VEGF-SSSA detection assay was further developed on a µPAD format. The µPAD contained four interconnected zones: a sampling zone, a VEGF detection zone, a fluorescence control zone and an endpoint, **Figure 5 A**. As seen in **Figure 5 B**, loading of VEGF 10 µg $mL^{-1}$ sample produced a fluorescence recovery of 25 % (60 ± 1 %, total normalized fluorescence intensity) when compared with the negative controls (32.0 ± 0.9 %, total normalized fluorescence intensity), which remained in their native quenched state.

The performance of the VEGF-SSSA was similar to the previous assay performed in the Whatman filter paper substrate. Furthermore, all VEGF concentrations tested produced similar intensities to those obtained in the previous assays. This demonstrated that both, flow or static modes achieved to the same results (see Figure SI-3.3.). The same maximum intensity could be observed for the fluorescence controls in both samples where VEGF or buffer were loaded, indicating that the inclusion of both reservoirs did not affect the detection but simplified the methodology as the device includes a reference signal that could be analyzed alongside the sample.

### *3.4. Cell secreted VEGF detection in µPAD*

The VEGF-SSSA treated µPAD was applied for the determination of VEGF in the supernatant of hHF-MSCs culture. MSCs have interest in many biomedical applications due to their capacity of differentiation, reprogramming. MSCs have been reported to be VEGF secretors [39], which further validates their applicability.

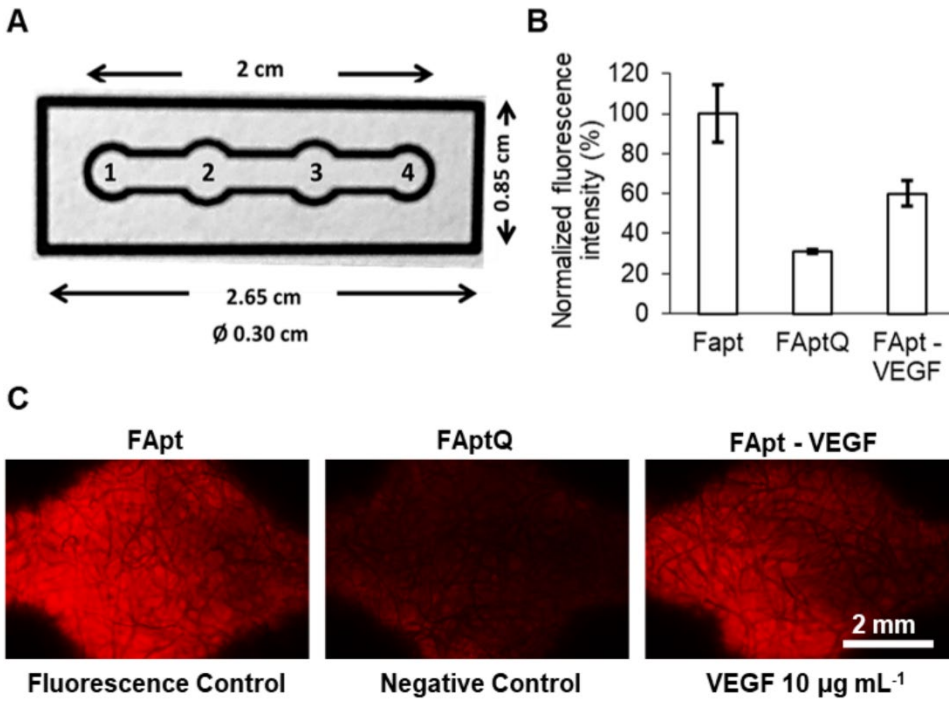


**Figure 5.** Detection of VEGF in µPAD. A) Photographs and specifications for the µPAD. Numbers refer to the different zones in the µPAD: (1) sampling zone, (2) VEGF detection zone, (3) fluorescence control zone and (4) endpoint, where flow stops. B) Plot of the normalized fluorescence intensity obtained by the fluorescence control (FApt), negative control (FAptQ) and samples incubated with VEGF 5 and 10 µg $mL^{-1}$ (FApt - VEGF), normalized to the fluorescence control (FApt) intensity. Error bars correspond to mean values ± SD (n = 3). C) Microscope images of fluorescence in the fluorescence control zone and detection zone incubated with and without VEGF.

hHF-MSCs (5 $10^6$ cells $mL^{-1}$) were cultured for 7 days on low volume of culture medium in order to promote cell secretion. After that, supernatant was loaded on the VEGF-SSSA treated µPAD and the fluorescence intensity was measured. The detailed experimental procedure can be found in Supporting Information 4. The normalized fluorescence intensity obtained in the µPADs, incubated with cell supernatant, was 49 ± 2 %, indicating that around 14 % of the fluorescence was recovered from its quenched state, which correlates with a VEGF secretion between 109-163 ng per $10^6$ cells per day, **Figure 6**.

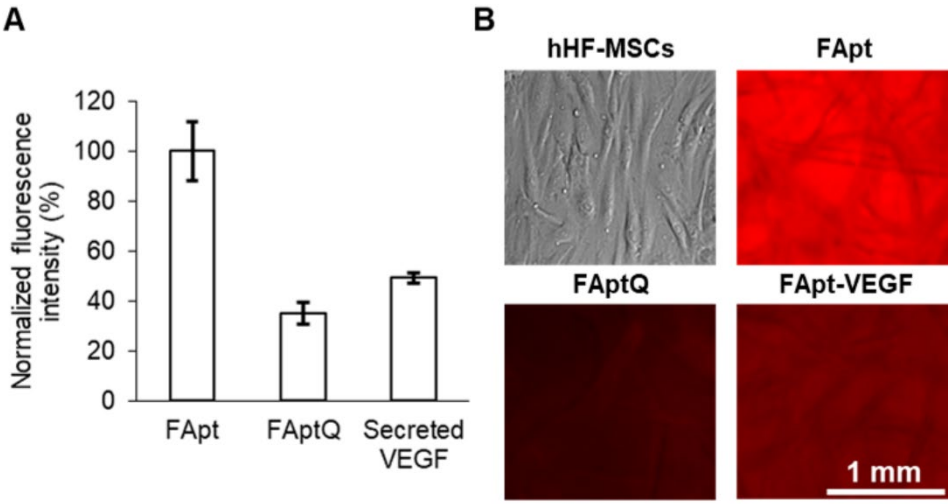


**Figure 6.** Detection of secreted VEGF in hHF-MSCs supernatant. A) Plot of the normalized fluorescence intensity obtained in the fluorescence control (FApt), negative control (FAptQ) and in cell's secreted VEGF (FApt - VEGF), normalized to the fluorescence control (FApt) intensity. Error bars correspond to mean values ± SD (n = 3, samples per experimental condition). B) Brightfield microscopy image of hHF-MSCs in high confluence (top left) and fluorescence microscope images of fluorescence control, negative control, and secreted VEGF incubated samples.

Our results showcased that the VEGF secretion in a cultured hHF-MSCs can be detected with the VEGF-SSSA μPAD. While promising, the data obtained from this analysis must be taken as indicative, as other secreted proteins by the cells such as less common VEGF subtypes might be interfering in the detection. However, both the previous work on the 3R02 aptamer [10,40] and this work have demonstrated specificity and sensitivity to the target protein, as materials coming from the μPAD fabrication process nor chemical from the DMEM medium have shown to interfere with the proposed assay.

While further work is required to establish the VEGF-SSSA μPAD as a fully validated VEGF biosensor device, these results give powerful insights in the capabilities of our aptasensor, demonstrating its function on real cell culture scenarios.

## 4. Conclusions

We developed a simple to use μPAD treated with a novel VEGF-SSSA for the single-step detection and quantification of VEGF with good sensitivity to different concentrations of the growth factor, being able to detect and quantify 0.57 and 1.89 ng of VEGF respectively. The immobilization of the self-reporting VEGF-SSSA on the cellulose paper improved the performance of the VEGF-SSSA and the homogeneity of the fluorescence signal, allowing a fast, single-step quantification of the VEGF concentration by fluorescence imaging of the substrates in a simple, low-cost material.

To the best of our knowledge, this is the first time a SSSA has been integrated into a paper microfluidics device. The μPAD was used, as a proof of concept, for the detection of VEGF in the supernatant from hHF-MSCs cell culture. In general, our approach is in concordance with previous reports, which demonstrated that DNA-based biosensors and μPADs are powerful combinations for the generation of simpler analytical tools to study biological samples.

## 5. Supporting information

### *SI-1. VEGF-SSSA assay in solution*

In order to test the quenching performance of the VEGF-SSSA, the fluorescence intensity obtained from solutions F 1, FApt 1, FQ 1 and FAptQ 1 was measured. Additionally, 1 µL of VEGF solution 7 was added to 99 µL of FAptQ 1 to address VEGF detection. After 30 min incubation at room temperature, all solutions were loaded in a 96-well black microtiter plate (100 µL per well, n = 3 per experimental condition) and fluorescence intensity was measured. Three wells were loaded with buffer solution to measure the background signal.

For the microscopy observation of the VEGF-SSSA + VEGF solutions a customized well array (16 wells of 2 mm diameter) was fabricated on a 4 mm thick PMMA with a glass cover at the bottom assembled with a double side pressure sensitive adhesive layer, see **Figure SI-1** for specifications. FApt 1 and FAptQ 1 solutions were incubated at room temperature for 10 min. Afterwards 5 µL of each solution were loaded in the wells and incubated at room temperature for another 5 min (n = 3 per experimental condition). Afterwards, wells containing FAptQ 1 were loaded with 2.5 µL of either VEGF solution 1 or PBS (negative control). Wells containing FApt 1 were loaded with 2.5 µL of PBS. All samples were protected from light during the performance of the assays.

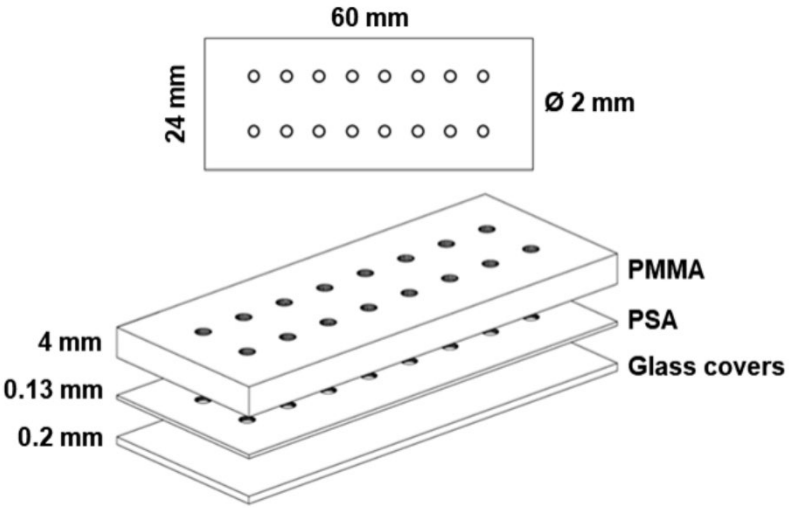


**Figure SI-1.** PMMA well array specifications.

The reservoirs were pretreated with streptavidin to ensure the stable immobilization of the biotinylated VEGF-SSSA. In addition, the whole µPAD was blocked with BSA as a way to avoid unspecific attachment of the VEGF to the cellulose paper.

### *SI-2. VEGF-SSSA µPAD fabrication*

The protocol for wax printing and µPAD fabrication is described in detail in previous publications [26,41]. Briefly, features were wax-printed on Whatman filter paper. Wax was melted for 5 min at 125 ºC on a hot plate. Two types of features were wax-printed. First, small wax-circles were printed for the characterization of the VEGF-SSSA performance and the detection of VEGF. Second, a proof-of-concept linear µPAD, containing four interconnected zones: a sampling zone, a VEGF detection zone, a fluorescence control zone and an endpoint, was used for the detection of secreted VEGF.

*SI-3. VEGF-SSSA assay on cellulose paper*

The quenching performance of the VEGF-SSSA was tested on the Whatman filter paper using the printed and melted wax-circles. FApt 2, FQ 2, FQ 3, FAptQ 2 and FAptQ 3 solutions were prepared and incubated at room temperature for 10 min. Afterwards, 5 µL of each solution were loaded on the printed wax-circles and were left for incubation and evaporation for another 10 min at 37 ºC on top of a hot plate. All samples were done by triplicate and were protected from light during the assay. Fluorescence intensity was measured using fluorescence microscopy.

For the experiments of the direct detection of VEGF on wax-circles the FAptQ 2 solution was incubated for 10 min. Afterwards, 5 µL of the solution was loaded in each wax-circle and incubated for another 10 min at 37 ºC. After the evaporation of the solution, 1 µL of either VEGF solution 7 or PBS (negative control) was loaded on the wax-circle and was incubated again for 20 min at room temperature until solvent evaporation.

In order to check the specificity to the growth factor and the possible interactions with other proteins, several wax-circles containing FAptQ 2 were also loaded with 1 µL of either BSA or streptavidin solution. BSA was added as a blocking agent to prevent nonspecific interaction of the DNA probes with the µPAD. On the other hand, streptavidin would allow a robust and specific binding of biotinylated DNA probes to the µPAD. In addition, several wax circles were prepared with FApt 2 as a positive fluorescence control. All samples were analyzed in triplicate and protected from light during the test.

The detection of different concentrations of VEGF was studied using printed wax-circles. Using the same procedure presented above. FAptQ 2 wax-circles were loaded with 2.5 µL VEGF solutions 1, 2, 3, 4, 5, 6 and 7. Fluorescence and negative controls were carried out, as previously explained. All samples were done by triplicate and were protected from light during assay performance.

The detection of VEGF was tested on the printed µPAD. After printing and heating the µPAD, 1 µL of streptavidin solution was loaded in both the VEGF

detection zone and the fluorescence control zone and were incubated for 5 min at 37 ºC. The streptavidin was added to anchor the biotinylated DNA probes to the detection and control zones. Afterwards, FApt 2 and FAptQ 2 solutions were prepared and incubated for 10 min at 37 ºC and let to dry. Then, 1 µL of FAptQ 2 solution was loaded on reservoir 1, whereas 1 µL of the FApt 2 solution was loaded on reservoir 2 and incubated at 37 ºC for 10 min, and let to dry. After this, 5 µL of BSA solution, serving as blocking agent to avoid unspecific deposition of the VEGF, were loaded on the sampling zone and let to flow through the channel. Finally, after 10 min incubation at 37 ºC, 4 µL of either VEGF solutions 2, 4, 6 and 7 or PBS (negative control) were loaded at the sampling zone and let to flow through the channel. The µPADs were left 20 min at room temperature and finally, their detection zones were analyzed by fluorescence microscopy. All samples were done by triplicate and were protected from light during assay performance.

The fluorescence intensities obtained for the different VEGF concentrations were similar to the assays on wax-printed circles, **Figure SI-3**.

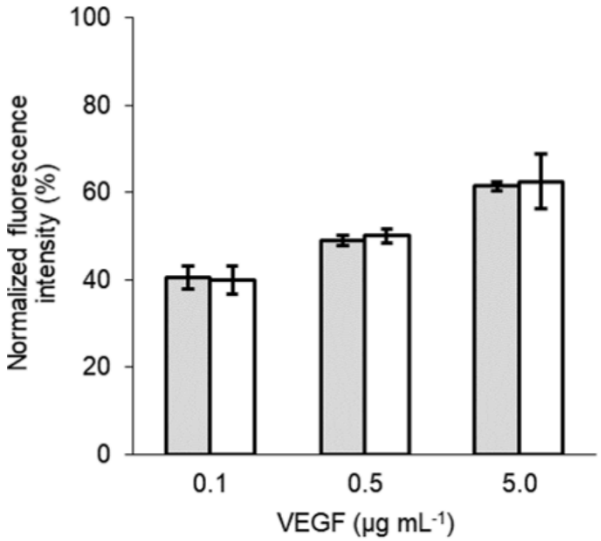


**Figure SI-3.** VEGF detection in µPAD. Graphical representation of the comparison between the fluorescence intensities observed in samples incubated with VEGF (0.1, 0.5 and 5 µg $mL^{-1}$) inside wax-printed circles (grey) and µPADs, normalized to their corresponding fluorescence control intensity. Error bars correspond to mean values ± SD (n = 3).

### *SI-4. Secreted VEGF detection in cell culture supernatant in µPAD*

For the detection of secreted VEGF with the VEGF-SSSA µPAD, hHF-MSCs at passage 6 were cultured in p75 flasks with 15 mL of complete DMEM medium (30 % FBS, 10 % penicillin-streptomycin). Cells were maintained in confluence for 5 days. Afterwards, to promote further VEGF secretion [42–44], 8 mL of medium was retrieved and cells were left secreting for another 48 h. At the end of day 7, supernatant was retrieved. Cells were detached and counted at the end of the experiment, presenting a concentration of 5 $10^6$ cells $mL^{-1}$.

During the fluorescence and negative controls, the addition of PBS solution was replaced by complete DMEM medium, which did not produce any significant difference in fluorescence intensity, see **Figure SI-4**.

VEGF-SSSA µPADs were fabricated and treated as previously explained (section 2.4 and 2.6). After the blocking step, 4 µL of either the subtracted cell's supernatant or DMEM medium (negative control) were loaded at the sampling zone and let flow through the channel. The channels were left incubating for 20 min at room temperature. Samples were analyzed by fluorescence microscopy. All samples were done by triplicate and were protected from light during the assay.

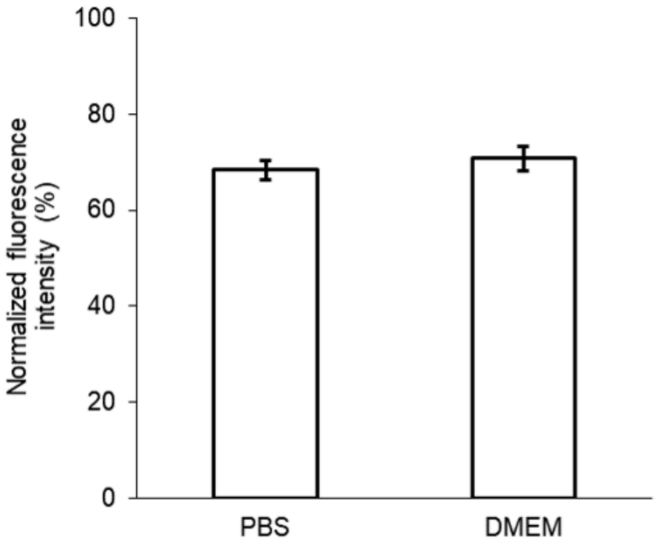


**Figure SI-4.** VEGF detection in PBS or DMEM dilution**.** Plot of the fluorescence intensity observed in samples incubated with VEGF (10 µg $mL^{-1}$) in either PBS or DMEM medium, normalized to the fluorescence control intensity. Error bars correspond to mean values ± SD (n = 3).

## 3.6. References

(1) Hicklin, D. J.; Ellis, L. M. Role of the Vascular Endothelial Growth Factor Pathway in Tumor Growth and Angiogenesis. *J. Clin. Oncol.* **2005**, *23* (5), 1011–1027.

(2) Storkebaum, E.; Lambrechts, D.; Carmeliet, P. VEGF: Once Regarded as a Specific Angiogenic Factor, Now Implicated in Neuroprotection. *BioEssays* **2004**, *26* (9), 943–954.

(3) Nakamura, M.; Abe, Y.; Tokunaga, T. Pathological Significance of Vascular Endothelial Growth Factor A Isoform Expression in Human Cancer. *Pathol. Int.* **2002**, *52* (5–6), 331–339.

(4) Sumner, G.; Georgaros, C.; Rafique, A.; DiCioccio, T.; Martin, J.; Papadopoulos, N.; Daly, T.; Torri, A. Anti-VEGF Drug Interference with VEGF Quantitation in the R&D Systems Human Quantikine VEGF ELISA Kit. *Bioanalysis* **2019**, *11* (5), 381–392.

(5) Rothbauer, M.; Zirath, H.; Ertl, P. Recent Advances in Microfluidic Technologies for Cell-to-Cell Interaction Studies. *Lab Chip* **2018**, *18* (2), 249–270.

(6) Kim, Y. S.; Raston, N. H. A.; Gu, M. B. Aptamer-Based Nanobiosensors. *Biosens. Bioelectron.* **2016**, *76*, 2–19.

(7) Tsukakoshi, K.; Ikuta, Y.; Abe, K.; Yoshida, W.; Iida, K.; Ma, Y.; Nagasawa, K.; Sode, K.; Ikebukuro, K. Structural Regulation by a G-Quadruplex Ligand Increases Binding Abilities of G-Quadruplex-Forming Aptamers. *Chem. Commun.* **2016**, *52* (85), 12646–12649.

(8) Kalra, P.; Dhiman, A.; Cho, W. C.; Bruno, J. G.; Sharma, T. K. Simple Methods and Rational Design for Enhancing Aptamer Sensitivity and Specificity. *Front. Mol. Biosci.* **2018**, *5*.

(9) Kaur, H.; Yung, L.-Y. L. Probing High Affinity Sequences of DNA Aptamer against VEGF165. *PLoS One* **2012**, *7* (2), e31196.

(10) Nonaka, Y.; Yoshida, W.; Abe, K.; Ferri, S.; Schulze, H.; Bachmann, T. T.; Ikebukuro, K. Affinity Improvement of a VEGF Aptamer by in Silico Maturation for a Sensitive VEGF-Detection System. *Anal. Chem.* **2013**, *85* (2), 1132–1137.

(11) Moccia, F.; Riccardi, C.; Musumeci, D.; Leone, S.; Oliva, R.; Petraccone, L.; Montesarchio, D. Insights into the G-Rich VEGF-Binding Aptamer V7t1: When Two G-Quadruplexes Are Better than One! *Nucleic Acids Res.* **2019**, *47* (15), 8318–8331.

(12) Li, W.; Zhang, Q.; Zhou, H.; Chen, J.; Li, Y.; Zhang, C.; Yu, C. Chemiluminescence Detection of a Protein through the Aptamer-Controlled Catalysis of a Porphyrin Probe. *Anal. Chem.* **2015**, *87* (16), 8336–8341.

(13) Hsu, C.-L.; Lien, C.-W.; Wang, C.-W.; Harroun, S. G.; Huang, C.-C.; Chang, H.-T. Immobilization of Aptamer-Modified Gold Nanoparticles on BiOCl Nanosheets: Tunable Peroxidase-like Activity by Protein Recognition. *Biosens. Bioelectron.* **2016**, *75*, 181–187.

(14) Kwon, O. S.; Park, S. J.; Jang, J. A High-Performance VEGF Aptamer Functionalized Polypyrrole Nanotube Biosensor. *Biomaterials* **2010**, *31* (17), 4740–4747.

(15) Feagin, T. A.; Maganzini, N.; Soh, H. T. Strategies for Creating Structure-Switching Aptamers. *ACS Sensors* **2018**, *3* (9), 1611–1615.

(16) Nutiu, R.; Li, Y. Structure-Switching Signaling Aptamers: Transducing Molecular Recognition into Fluorescence Signaling. *Chem. - A Eur. J.* **2004**, *10* (8), 1868–1876.

(17) Wu, Z.-S.; Guo, M.-M.; Zhang, S.-B.; Chen; Jiang, J.-H.; Shen, G.-L.; Yu, R.-Q. Reusable Electrochemical Sensing Platform for Highly Sensitive Detection of Small Molecules Based on Structure-Switching Signaling Aptamers. *Anal. Chem.* **2007**, *79* (7), 2933–2939.

(18) Ma, X.; Li, H.; Qiao, S.; Huang, C.; Liu, Q.; Shen, X.; Geng, Y.; Xu, W.; Sun, C. A Simple and Rapid Sensing Strategy Based on Structure-Switching Signaling Aptamers for the Sensitive Detection of Chloramphenicol. *Food Chem.* **2020**, *302*, 125359.

(19) Freeman, R.; Girsh, J.; Fang-ju Jou, A.; Ho, J. A.; Hug, T.; Dernedde, J.; Willner, I. Optical Aptasensors for the Analysis of the Vascular Endothelial Growth Factor (VEGF). *Anal. Chem.* **2012**, *84* (14), 6192–6198.

(20) Li, J.; Sun, K.; Chen, Z.; Shi, J.; Zhou, D.; Xie, G. A Fluorescence Biosensor for VEGF Detection Based on DNA Assembly Structure Switching and Isothermal Amplification. *Biosens. Bioelectron.* **2017**, *89*, 964–969.

(21) Hsu, M.-Y.; Hung, Y.-C.; Hwang, D.-K.; Lin, S.-C.; Lin, K.-H.; Wang, C.-Y.; Choi, H.-Y.; Wang, Y.-P.; Cheng, C.-M. Detection of Aqueous VEGF Concentrations before and after Intravitreal Injection of Anti-VEGF Antibody Using Low-Volume Sampling Paper-Based ELISA. *Sci. Rep.* **2016**, *6* (1), 34631.

(22) Akyazi, T.; Saez, J.; Elizalde, J.; Benito-Lopez, F. Fluidic Flow Delay by Ionogel Passive Pumps in Microfluidic Paper-Based Analytical Devices. *Sensors Actuators B Chem.* **2016**, *233*, 402–408.

(23) Zou, Y.; Mason, M. G.; Wang, Y.; Wee, E.; Turni, C.; Blackall, P. J.; Trau, M.; Botella, J. R. Nucleic Acid Purification from Plants, Animals and Microbes in under 30 Seconds. *PLOS Biol.* **2017**, *15* (11), e2003916.

(24) Shi, R.; Lewis, R. S.; Panthee, D. R. Filter Paper-Based Spin Column Method for Cost-Efficient DNA or RNA Purification. *PLoS One* **2018**, *13* (12), e0203011.

(25) Dutta, G.; Rainbow, J.; Zupancic, U.; Papamatthaiou, S.; Estrela, P.; Moschou, D. Microfluidic Devices for Label-Free DNA Detection. *Chemosensors* **2018**, *6* (4), 43.

(26) Azuaje-Hualde, E.; Arroyo-Jimenez, S.; Garai-Ibabe, G.; de Pancorbo, M. M.; Benito-Lopez, F.; Basabe-Desmonts, L. Naked Eye Y Amelogenin Gene Fragment Detection Using DNAzymes on a Paper-Based Device. *Anal. Chim. Acta* **2020**, *1123*, 1–8.

(27) Weng, X.; Neethirajan, S. Aptamer-Based Fluorometric Determination of Norovirus Using a Paper-Based Microfluidic Device. *Microchim. Acta* **2017**, *184* (11), 4545–4552.

(28) Cui, X.; Li, R.; Liu, X.; Wang, J.; Leng, X.; Song, X.; Pei, Q.; Wang, Y.; Liu, S.; Huang, J. Low-Background and Visual Detection of Antibiotic Based on Target-Activated Colorimetric Split Peroxidase DNAzyme Coupled with Dual Nicking Enzyme Signal Amplification. *Anal. Chim. Acta* **2018**, *997*, 1–8.

(29) Lin, X.; Leung, K.-H.; Lin, L.; Lin, L.; Lin, S.; Leung, C.-H.; Ma, D.-L.; Lin, J.-M. Determination of Cell Metabolite VEGF165 and Dynamic Analysis of Protein–DNA Interactions by Combination of Microfluidic Technique and Luminescent Switch-on Probe. *Biosens. Bioelectron.* **2016**, *79*, 41–47.

(30) Vega-Figueroa, K.; Santillán, J.; Ortiz-Gómez, V.; Ortiz-Quiles, E. O.; Quiñones-Colón, B. A.; Castilla-Casadiego, D. A.; Almodóvar, J.; Bayro, M. J.; Rodríguez-Martínez, J. A.; Nicolau, E. Aptamer-Based Impedimetric Assay of Arsenite in Water: Interfacial Properties and Performance. *ACS Omega* **2018**, *3* (2), 1437–1444.

(31) Beyazkilic, P.; Saateh, A.; Bayindir, M.; Elbuken, C. Evaporation-Induced Biomolecule Detection on Versatile Superhydrophilic Patterned Surfaces: Glucose and DNA Assay. *ACS Omega* **2018**, *3* (10), 13503–13509.

(32) Urmann, K.; Modrejewski, J.; Scheper, T.; Walter, J.-G. Aptamer-Modified Nanomaterials: Principles and Applications. *BioNanoMaterials* **2017**, *18* (1–2).

(33) Jarmoskaite, I.; AlSadhan, I.; Vaidyanathan, P. P.; Herschlag, D. How to Measure and Evaluate Binding Affinities. *Elife* **2020**, *9*, e57264.

(34) Zhang, H.; Li, M.; Li, C.; Guo, Z.; Dong, H.; Wu, P.; Cai, C. G-Quadruplex DNAzyme-Based Electrochemiluminescence Biosensing Strategy for VEGF165 Detection: Combination of Aptamer–Target Recognition and T7 Exonuclease-Assisted Cycling Signal Amplification. *Biosens. Bioelectron.* **2015**, *74*, 98–103.

(35) Fu, X.-M.; Liu, Z.-J.; Cai, S.-X.; Zhao, Y.-P.; Wu, D.-Z.; Li, C.-Y.; Chen, J.-H. Electrochemical Aptasensor for the Detection of Vascular Endothelial Growth Factor (VEGF) Based on DNA-Templated Ag/Pt Bimetallic Nanoclusters. *Chinese Chem. Lett.* **2016**, *27* (6), 920–926.

(36) Nonaka, Y.; Abe, K.; Ikebukuro, K. Electrochemical Detection of Vascular Endothelial Growth Factor with Aptamer Sandwich. *Electrochemistry* **2012**, *80* (5), 363–366.

(37) Cho, H.-M.; Kim, P.-H.; Chang, H.-K.; Shen, Y.; Bonsra, K.; Kang, B.-J.; Yum, S.-Y.; Kim, J.-H.; Lee, S.-Y.; Choi, M.; Kim, H. H.; Jang, G.; Cho, J.-Y. Targeted Genome Engineering to Control VEGF Expression in Human Umbilical Cord Blood-Derived Mesenchymal Stem Cells: Potential Implications for the Treatment of Myocardial Infarction. *Stem Cells Transl. Med.* **2017**, *6* (3), 1040–1051.

(38) Ozawa, C. R.; Banfi, A.; Glazer, N. L.; Thurston, G.; Springer, M. L.; Kraft, P. E.; McDonald, D. M.; Blau, H. M. Microenvironmental VEGF Concentration, Not Total Dose, Determines a Threshold between Normal and Aberrant Angiogenesis. *J. Clin. Invest.* **2004**, *113* (4), 516–527.

(39) Makridakis, M.; Roubelakis, M. G.; Vlahou, A. Stem Cells: Insights into the Secretome. *Biochim. Biophys. Acta - Proteins Proteomics* **2013**, *1834* (11), 2380–2384.

(40) Nonaka, Y.; Sode, K.; Ikebukuro, K. Screening and Improvement of an Anti-VEGF DNA Aptamer. *Molecules* **2010**, *15* (1), 215–225.

(41) Carrilho, E.; Martinez, A. W.; Whitesides, G. M. Understanding Wax Printing: A Simple Micropatterning Process for Paper-Based Microfluidics. *Anal. Chem.* **2009**, *81* (16), 7091–7095.

(42) Abcouwer, S. F.; Marjon, P. L.; Loper, R. K.; Vander Jagt, D. L. Response of VEGF Expression to Amino Acid Deprivation and Inducers of Endoplasmic Reticulum Stress. *Invest. Ophthalmol. Vis. Sci.* **2002**, *43* (8), 2791–2798.

(43) Lee, E. Y.; Xia, Y.; Kim, W.-S.; Kim, M. H.; Kim, T. H.; Kim, K. J.; Park, B.-S.; Sung, J.-H. Hypoxia-Enhanced Wound-Healing Function of Adipose-Derived Stem Cells: Increase in Stem Cell Proliferation and up-Regulation of VEGF and BFGF. *Wound Repair Regen.* **2009**,

*17* (4), 540–547.

(44) Baek, J. H.; Jang, J.-E.; Kang, C.-M.; Chung, H.-Y.; Kim, N. D.; Kim, K.-W. Hypoxia-Induced VEGF Enhances Tumor Survivability via Suppression of Serum Deprivation-Induced Apoptosis. *Oncogene* **2000**, *19* (40), 4621–4631.

Appendix 4

# Continuous monitoring of cell transfection efficiency with micropatterned substrates

## Continuous monitoring of cell transfection efficiency with micropatterned substrates

Enrique Azuaje-Hualde, Melania Rosique, Alba Calatayud-Sanchez, Fernando Benito-Lopez, Marian Martínez de Pancorbo, Lourdes Basabe-Desmonts

*Published in: Biotechnology and Bioengineering (2021)* [1]

*Impact Factor: 4.002 (Q1)*

*Area: Biotechnology and applied microbiology*

**Abstract**

The effect of cell-cell contact on gene transfection is mainly unknown. Usually, transfection is carried out in batch cell cultures without control over cellular interactions, and efficiency analysis relies on complex and expensive protocols commonly involving flow cytometry as the final analytical step. Novel platforms and cell patterning are being studied in order to control cellular interactions and improve quantification methods. In this work, we report the use of surface patterning of fibronectin for the generation of two types of mesenchymal stromal cells patterns: single cell patterns without cell-to-cell contact, and small cell-colony patterns. Both scenarios allowed the integration of the full transfection process and the continuous monitoring of thousands of individualized events by fluorescence microscopy. Our results showed that cell-to-cell contact clearly affected the transfection, as single cells presented a maximum transfection peak 6 hours earlier and had a 10 % higher transfection efficiency than cells with cell-to-cell contact.

**Keywords**: Surface Patterning; Cell Patterning; Gene Transfection: Cell-cell Contact; Continuous Monitoring; GFP; Mesenchymal Stromal Cell.

## 1. Introduction

The process of gene transfection refers to the manipulation of eukaryotic cell's genome. Most commonly, gene transfection is based on the insertion of exogenous genetic material into a cell for its expression using the cell's own gene expression process. In some cases, the exogenous gene is completely integrated into the genome of the cell. More recently, gene transfection has also been centered in the incorporation of editing tools for cell's genome through the generation of sequence-specific strand breaks and the synthetically guided modification of a desired gene [2,3]. It constitutes the base of gene therapy, which aims to cure and treat genetic-related diseases and disorders through the insertion of specific genes or the manipulation and editing of existing, pathological genes [4]. Cell cultures are commonly used to carry out the transfection of cells and test, quantify and optimize transfection protocols that could lead to the development of efficient gene therapies [5,6].

One major parameter studied to address the potential of a transfection protocol is the gene transfection efficiency, defined as the proportion of cells that, after exposure to transfection reagents, incorporate the genetic material inside their genome and express the desirable product. The efficiency of a transfection is directly related to the delivery system used, the design of the nucleic acid sequence, the target cell type and the cell cycle [7,8]. Usually, analysis of the gene transfection efficiency consists on the transfection of a gene that encodes the expression of a fluorescent protein reporter, such as green fluorescence protein (GFP), to cells seeded in conventional cell culture plates. Quantification of the efficiency is most commonly carried out by analysis of detached cells or non-adherent cells using flow cytometry, which allows the accurate quantification of the total number of cells as well as the quantification of the number of cells expressing the fluorescent protein. Microscopy imaging of attached cells is also widely used, where the images are compared to address the ratio of transfected cells over the total number of cells, usually relying on complex imaging processes or secondary dies for quantification [9–11].

While conventional analysis of the transfection efficiency is undeniably optimal in many cases, it also presents two major limitations that could affect the analysis. The first one is the lack of control over cell-cell interactions. Conventional cell culture lack control over the many cell-cell interactions and therefore, may not represent the best conditions for gene transfection. Moreover, it has been demonstrated that cell-substrate and cell-matrix interactions as well as cell architecture can affect cells behavior and in turn affect cell transfection [5,12]. Over the past decade, several studies helped to better understand and control the interactions that may affect gene transfection. For example, Dhaliwal *et al*. demonstrated that the interaction with the extracellular matrix heavily influences the process of transfection, since different mechanisms of gene transfection could be observed in regular seeded cells compared to cells cultured in a three-dimensional hydrogel scaffold [13]. Modaresi *et al.* demonstrated that the stiffness of the substrate influenced plasmid internalization due to the role of stress fibers associated with the endocytosis of the carriers [14]. Shui et *al.* showed that surface patterning on superhydrophobic areas improved cell adhesion, separation of cell colonies and transfection efficiency in comparison to flat poly-D-lysine substrates [15]. The effect of the substrate hydrophobicity of patterned cells and the chemical interactions of high density cell-clusters on the transfection efficiency were also studied [16,17]. Combined pattern of transfection reagents and extracellular matrix proteins into the surface, commonly known as reverse transfection, were employed. Recently, Yang *et al*. demonstrated that cell spreading affects and enhances gene transfection on patterned single cells [18].

Besides the lack of control over cell-cell interactions, the second main limitation found in conventional transfection efficiency studies is related to the methods of analysis. Flow cytometry, the most commonly used analytical methodology, has a relative high cost of materials and equipment, while requires trained personnel. On top of that, the different steps required during the analytical process, like detachment of cells or incorporation of secondary dyes, may affect cell state in a way that can affect the analysis of gene transfection. Furthermore, any process that requires cell fixation or detachment functions as end-of-assay analysis, disables the possibility for

real-time and continuous monitoring of gene transfection [9,19–22]. The current trend to facilitate and speed up data collection, as well as to incorporate non-invasive analytical measurements, is the design of platforms that provide high throughput real time screening capabilities. Microfabrication has enabled the development of miniaturized platforms with multiple interrogation sites that allow high throughput screening of transfection conditions. For example, microfluidics platforms such as droplet microfluidic systems enabled single cell transfection of hard-to-transfect cell lines with improved transfection efficiency [23]. Woodruff *et al*. developed a microfluidic device based on individual cell culture chambers that allowed the simultaneous monitoring of 280 independent transfections, achieving 99 % transfection efficiency [24]. Later, Guiponni *et al*. also developed an easy to use lab-on-a-chip device with cylindrical culture chambers that allowed the high-throughput analysis of transfection to compare vector efficiencies [25].

Overall, there is an increasing interest in developing new platforms for the analysis of gene transfection efficiency in order to improve the control over cell interactions, facilitate the method of analysis, or a combination of both. In particular, surface micropatterning is a methodology to produce localized deposition of adhesion proteins on a surface and to enable the formation of cell patterns with controlled cell-cell contact. These cell arrays have been proven to be suitable for gene transfection, having the potential to overcome the limitations of conventional cell cultures [26]. Thanks to the versatility of the technique, great control over cell interactions can be achieved, including cell-material and cell-cell interactions, while also enabling the easy generation of high number of data points in a small substrate area [27–31]. Cells patterns can be directly transfected and monitored, without the need of detaching and transporting the cells to a different setup, as the pattern itself simplifies quantification due to the highly controlled localization of the cells.

While previous studies have addressed how various types of cell interactions affect gene transfection, the degree in which cell-cell interaction and physical contact between cells affect the transfection processes is still mostly unknown. As cell-cell contact is a major factor in several transcriptional and translation pathways, it is expected to influence gene transfection. Regular

cell cultures hinders the control over cell-cell interaction, which in turn prevents a controlled analysis of its effect on gene transfection. Therefore, cell patterning arises as a promising methodology for this type of analysis. While surface micropatterning has been widely used for the monitoring of cultured cells, the use of this methodology for the study of gene transfection with controlled cell-cell contact has not been reported.

In this paper, we report on the use of surface micropatterns to create cell arrays and assess the effect of cell-cell contact on the efficiency of gene transfection, as well as to monitor the progress of the transfection process over time. Primary human Hair Follicles Mesenchymal Stromal Cells (hHF-MSCs) were chosen due to their potential use in regenerative medicine and their hard-to-transfect nature [23].

## 2. Materials and methods

### *2.1. Materials*

Primary human Hair Follicles Mesenchymal Stromal Cells (hHF-MSCs) were obtained from human follicles (passages 6 to 9). Bovine plasma fibronectin, Dulbecco's modified eagle's medium (DMEM), fetal bovine serum (FBS), penicillin/streptomycin (P/S), Gibco trypan blue solution (0.4 %), 4',6-diamino-2-phenylin (DAPI) dye, phalloidin dye, lipofectamine stem transfection reagent and opti-MEM I reduced serum medium were purchased from Fisher Scientific, Spain. Green Fluorescence Protein (GFP) encoding plasmid pCXLE-EGFP was purchased from Addgene, USA. Bovine serum albumin and propidium iodide were purchased from Sigma Aldrich, Spain. Polydimethylsiloxane silicone (PDMS) elastomer and curing agent were purchased from Ellsworth adhesives, Spain. Paraformaldehyde 4 % for fixation was purchased from Panreac Quimica, Spain.

Brightfield and fluorescence images were taken with a modified Nikon Eclipse TE2000-S (USA) microscope with a LUMENCOR laser light source (USA) and Zylar sCMOS camera (Oxford Instruments, UK). Flow cytometry analysis were carried out with a FACS Calibur system from Becton Dickinson.

Microsocopy images were processed by FiJi/ImageJ software. Flow cytometry data was analyzed by Summit Software v4.3 (Dako) and Gallios software v1.2 (Beckman Coulter). Rocker Vari-Mix steep angle rocker (Thermo Fisher) was used for cell patterning.

*2.2. Patterning of single hHF-MSCs and small hHF-MSC-colonies*

Patterning of hHF-MSCs was obtained by incubation of a cell suspension inside a cell culture-well containing a pattern of fibronectin dots created by microcontact printing. Microcontact printing of fibronectin was performed as described elsewhere [28,32]. Briefly, PDMS (ratio 10:1 of silicone and curing agent) was polymerized on top of silicon wafers containing holes of 20 µm or 100 µm diameter holes with 50 µm of separation between two holes, creating stamps with either 20 µm or 100 µm diameter pillars. PDMS stamps were wetted with 50 µL of a 50 $\mu g \cdot mL^{-1}$ fibronectin solution in PBS for 30 min. Afterwards, the ink was removed and the PDMS stamps were rinsed with distilled water and dried with compressed air. Each PDMS stamp was put in contact with the bottom plate of the well in a 12-well microtiter plate for another 30 min, in order to transfer the protein from the PDMS stamp to the substrate and create small dots of fibronectin. Finally, PDMS stamps were removed and the wells were blocked with 1 mL of BSA solution 1% (w/v). The total area of the printed pattern in each well was 1 $cm^2$. 20 µm ($D_{20}$) patterns were comprised of 20000 fibronectin dots with a 20 µm diameter and a 50 µm separation between dots. 100 µm ($D_{100}$) patterns were comprised of 4500 fibronectin dots with a 100 µm diameter and a 50 µm separation between dots. $D_{20}$ patterns were used to create single cell patterns. $D_{100}$ patterns were used to create small cell-colony patterns.

To attach the cells to the printed fibronectin $D_{20}$ and $D_{100}$ patterns, hHF-MSCs were incubated with complete medium (CM) in cell culture flasks until reaching 80 % confluence. CM consisted of DMEM supplemented with 30 % FBS and 10 % P/S. hHF-MSCs were detached from the flask, centrifuged and resuspended in serum-free medium (0% FBS) for a concentration of 100000 cells $mL^{-1}$. Serum-free medium for incubation on patterning and maintenance consisted in DMEM with 10 % P/S. 1 mL of the cell suspension was added to

each printed well and were left for 2 h on constant oscillation in a rocker inside an incubator at 37 ºC and 5 % $CO_2$ air atmosphere. Afterwards, the remaining suspension was removed and the wells were rinsed 3 times with PBS, **Figure 1 A**.

For the quantification of the number of cells per dot (dot occupancy), cell area and cell aspect ratio, cells were fixated with formaldehyde and then dyed with phalloidin for 30 min and with DAPI for 5 min. Images were taken by brightfield and fluorescence microscopy and were analyzed using ImageJ.

Stability of the $D_{100}$ hHF-MSCs patterns on different maintenance mediums varying the FBS concentration. After adhesion of the cells to the fibronectin pattern, the culture medium was changed to maintenance medium, containing different concentrations of FBS (0 %, 5 %, 10 % and 20 %), and samples were left inside of the incubator for 24 h. Afterwards, images were taken by brightfield microscopy to check the conservation of the cell pattern.

For the study of the viability of the patterned hHF-MSCs on serum free medium, substrates containing $D_{20}$ and $D_{100}$ cell patterns were kept for 72 h in maintenance medium 0 % FBS with daily medium changes. Every 24 h, brightfield microscopy images were taken. On the last day, cells were dyed with trypan blue to verify the survival of the remaining cells. Cell viability was calculated following equation 1. Images were analyzed using ImageJ.

$$Patterned\ cells\ viability = \frac{Patterned\ cells\ (tx)}{Patterned\ cells\ (t0)}\ x\ 100$$

(eq. 1)

### *2.3. Transfection of hHF-MSCs*

The transfection protocol was adapted from the commercial lipofectamine protocol. Both, the lipofectamine Stem Reagent and the pCXLE-EGFP were diluted in the serum free Opti-MEM medium at different concentrations, to generate four different transfection mixtures, the Transfection mix-1 containing, 0.80 % (v/v) lipofectamine and 0.40 % (v/v) GFP plasmid in Opti-

MEM medium; the transfection mix-2 containing 0.80 % (v/v) lipofectamine and 0.80 % (v/v) GFP plasmid in Opti-MEM; the transfection mix-3 containing 1.60 % (v/v) lipofectamine and 0.40 % (v/v) GFP plasmid in Opti-MEM; and transfection mix-4 containing 1.60 % (v/v) lipofectamine and 0.80 % (v/v) GFP plasmid in Opti-MEM. Transfection mixtures were incubated at room temperature for 10 min to form the DNA-lipid complexes.

To study the transfection efficiency of mix-1, 2, 3 and 4 in hHF-MSCs cultured in conventional cell culture well plates, hHF-MSCs were cultured in 24-well plates at 20000 cells per well and incubated to reach a confluence of about 70 % or 90 %. Before transfection, the culture medium was replaced by one of the previously listed lipofectamine/GFP plasmid mixtures. 4 h after transfection, the medium containing the mixtures was replaced by DMEM culturing medium and cells were cultured for another 24 h. GFP expression was quantified using flow cytometry. Cytotoxicity and cell viability was evaluated with propidium iodide using flow cytometry. Two tailed t-student statistical analysis was carried out using Excel software.

The same transfection methodology was followed for patterned hHF-MSCs in all assays. To test the transfection of patterned cells, cell-$D_{100}$ patterns were incubated after adhesion with 600 µL of either transfection mix-3 or transfection mix-4 for 4 h. Afterwards, patterned cells were put in maintenance medium 0 % FBS. Brightfield and fluorescence images were taken after 24 h, **Figure 1 B**.

For the analysis of the effect of cell-cell contact on the gene transfection efficiency, cell-$D_{20}$ and cell-$D_{100}$ patterns were transfected with mix-4 as previously indicated. Brightfield and fluorescence images were taken at 0, 12, 18, 24, 30 and 42 h after transfection. For the quantification of the absolute transfection efficiency on patterned single cells, $D_{20}$ cell patterns were transfected with mix-4. A grid was marked on the bottom of the 12-well microtiter plates dividing the cell pattern in 16 areas to facilitate continuous monitoring over the same area and the same cells over time. Brightfield and fluorescence images were taken at 0, 12, 18, 24, 30 and 42 h after transfection.

### *2.4. Quantification of transfection efficiency on patterned hHF-MSCs by microscopy images analysis*

For the quantification of transfection efficiency on patterned cells, two microscopy images of the patterns were taken after transfection: a brightfield image, to count the total number of patterned cells at a specific time, and a fluorescence microscopy image to count the number of cells expressing GFP, **Figure 1 C**. Total number of cells and transfected cells were counted using Image J. Images of non-transfected cells patterned and cultured under similar conditions were taken as negative controls. Fluorescence images were taken using an inverted Nikon microscope, equipped with a LUMENCOR laser light source with 4 emission filters (446, 523, 561 and 677 nm) and Zylar sCMOS camera. DAPI images were taken at an excitation wavelength of 395 nm. GFP images were taken at an excitation wavelength of 480 nm. Phalloidin images were taken at an excitation wavelength of 640 nm.

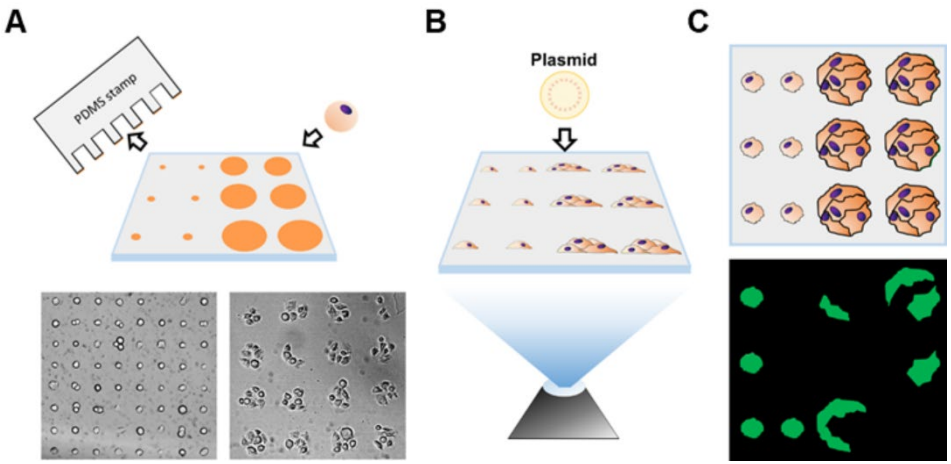


**Figure 1.** Graphical scheme of cell patterning, transfection and continuous evaluation of cell transfection efficiency with micropatterned substrates. A) Surface patterning of fibronectin features through microcontact printing and specific cell adhesion with controlled cell-cell contact to the fibronectin pattern. B) Direct transfection of patterned cells with GFP plasmid and liposome vector. Continuous observation of GFP expression is done through fluorescence microscopy. C) Transfection efficiency quantification through image analysis of total patterned cells and GFP expressing cells.

In all cases, higher fluorescence intensity was observed in the transfected samples when compared with the negative controls. Background signal, mainly coming from cells autofluorescence, was normalized from all images before the transfection evaluation by adjusting each transfected sample which its respective negative control, Supporting Information 1. Two tailed t-student statistical analysis was carried out in Excel.

In the case of the absolute transfection efficiency quantification, images were taken for each sample in the exact same position of the cell pattern on all times studied.

*2.5. Proliferation of patterned and transfected hHF-MSCs*

In order to check the capability of patterned and transfected hHF-MSCs to form a new culture after transfection, a proliferation assay was carried out. 48 h after transfection with mix-4. Cells patterns were kept in a complete medium (30 % FBS), in the incubator for another 48 h. Brightfield images were taken to check cell spreading and proliferation.

## 3. Results and discussion

hHF-MSC primary cells, which have enormous clinical potential for regenerative therapies, were used in this study. In general, these cells are difficult to transfect thus the development of new methods to improve its transfectability could have a big clinical impact [19]. Our hypothesis was that cell-cell contact might affect the efficiency of transfection in adherent cells. The quantification of the transfection efficiency of a green fluorescence protein encoding a DNA plasmid in hHF-MSCs was used as a model to study the feasibility of the method. The presence of fluorescence inside of a cell indicates that the transfection of the GFP plasmid was successfully carried out. This could be easily monitored by flow cytometry, or in the case of the patterned cells, by fluorescence microscopy. Lipofectamine, a cationic liposome previously reported for MSCs [33], was chosen as the carrier for the incorporation of the plasmid inside of the cell.

The formation of protein patterns using microcontact printing allows the generation of cell arrays with different interactions between cells. This procedure facilitates the comparison of the transfection efficiency between scenarios with no cell-cell contact (in arrays of single cells) and scenarios resembling conventional cultures (in arrays of small cell-colonies). This control over the absence or presence of cell-cell contact cannot be achieved in conventional cell culture, where factors such as cell confluence do not ensure the generation of a homogenous cell-cell contact scenario. Fibronectin was chosen as the adhesion protein as established in previous works [27,28].

*3.1. Cells seeding on custom protein pattern to control cell-cell contact.*

First, we evaluated the formation of cell patterns with controlled cell-cell contact. Two types of fibronectin patterns were produced on the bottom plates of 12-well microtiter plates. $D_{20}$ patterns with single cells and $D_{100}$ patterns with small cell-colonies. The images showed that cells adhered specifically to the fibronectin adhesion dots. In both types of patterns, 99 % of the dots were filled by cells. In $D_{20}$ substrates, more than 85 % of the dots contained only one cell per dot (the calculated mean occupancy value was 1.1 ± 0.1 cells per dot), while in the $D_{100}$ substrates more than 50 % of the dots contained 4 or 5 cells (the calculated mean occupancy value was 4.6 ± 0.8 cells per dot) with a range of 2 to 8 cells per dot, Figure SI-4.1. The cells adhered to the fibronectin dots did not contact to each other; since the distance between dots was 50 µm. The size of the fibronectin dots affected the spreading of the cells. Single cells in the $D_{20}$ substrates had a more rounded shape and filled a smaller area compared to the cells on $D_{100}$ substrates (see Figure SI-2).

Cells in culture media containing serum migrated out of the pattern in less than 24 h because it contained growth, migration and proliferation factors that directly affected the attachment of cells to the protein patterns (see Figure SI-3 B). For this reason, next experiments were performed in serum-free culture conditions in order to keep the cells in the protein pattern. Although the lack of serum may not be optimal for mesenchymal stromal cells maintenance, it synchronizes the cell culture, and equalizes the cell phase of all cells [32]. This

aspect may be important because cell transfection could be affected by the cell cycle [34].

The stability and viability of hHF-MSCs on both $D_{20}$ and $D_{100}$ cell patterns was evaluated during 72 h. Viable cells were defined as alive cells that remain adhered to the substrate. Trypan blue stained less than 5 % of the cells, indicating than most of the cell in the pattern were alive. Our results showed that the 60 % and 53 %, after 48 h, and the 44 % and 41 %, after 72 h, of the patterned cells in the $D_{20}$ and $D_{100}$, respectively, remained alive on the pattern, Figure SI-4.3. C.

*3.2. Optimization of GFP plasmid/lipofectamine transfection on hHF-MSCs*

For the optimization of the transfection with lipofectamine and the GFP plasmid, we evaluated the transfection of hHF-MSCs cultured on conventional well plates using flow cytometry for the analysis as explained in experimental section 2.3. Cultures of hHF-MSCs with two confluences (70 % and 90 %) were transfected with four transfection mixtures containing different concentrations of GFP plasmid and lipofectamine. GFP expression was evaluated and analyzed by flow cytometry 24 h after cell transfection [33,35]. In summary, the highest transfection efficiency (20 %) was observed in cell cultures at 70% confluence with transfection mix-3 and 4, which falls within the expected range for mesenchymal stromal cells [19,35]. For such reason, transfection mix-3 and mix-4 were used for the following transfection assay on patterned cells. The detailed results obtained from this assay are discussed on Supplementary Information 4.

The same transfection protocol was carried out on cell-$D_{100}$ patterns. Brightfield and fluorescence images were taken 24 h after transfection, in order to count the total number of attached cells and the GFP expressing cells, respectively. The efficiency of transfection using mix-3 and mix-4 on $D_{100}$ was 22 ± 4 % and 22 ± 2 % respectively, **Figure 2 A**. These results were similar to those obtained for the conventional culture analyzed trough flow cytometry, confirming that the transfection process could be done on patterned cells. As seen in **Figure 2 B**, when analyzing the small cell-colonies independently based on the number of cells per dot, similar transfection

efficiency where observed in all cases (21 ± 2 %, 22 ± 1 % and 22 ± 1 % for the small cell-colonies with 3, 4 and 5 cells per spot, respectively).

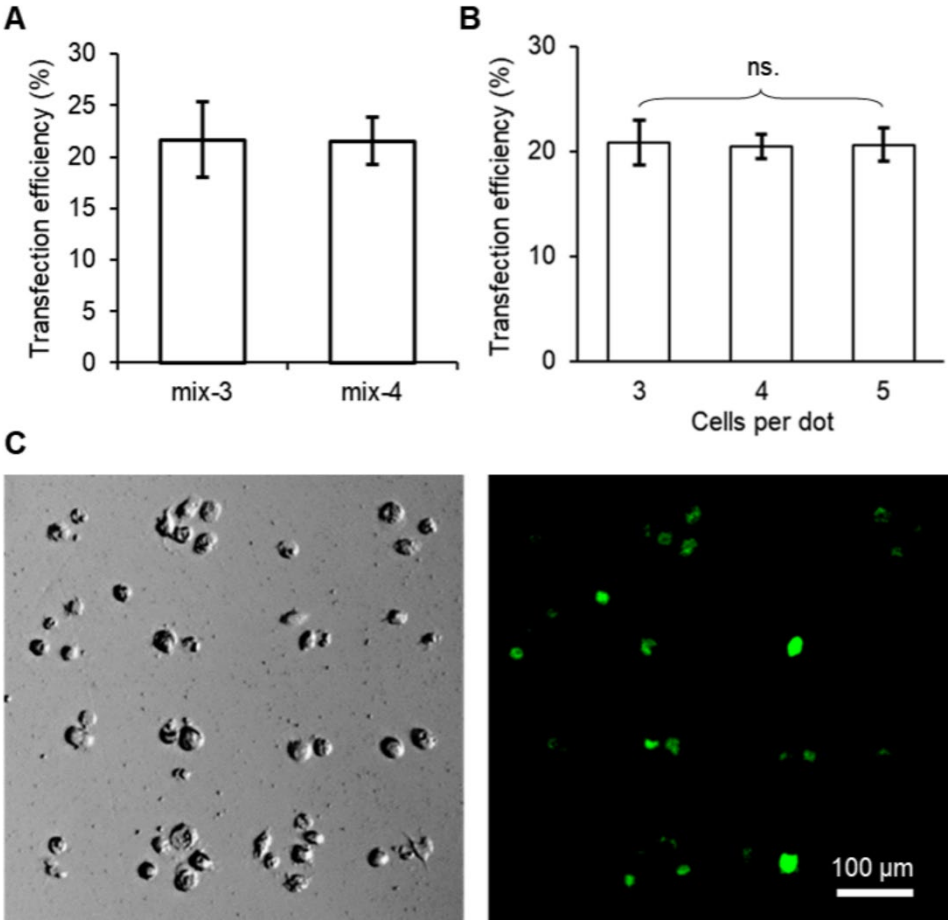


**Figure 2.** Transfection in hHF-MSCs. A) Graph representing the transfection efficiency of $D_{100}$ patterns transfected using mix-3 and 4. Error bars mean ± SD (n = 3, with ~4000 cells analyzed per sample). B) Graph representing the transfection efficiency of $D_{100}$ patterns transfected using mix-4 separated based on the number of cells per dot. Error bars mean ± SD (n = 3). Statistical significance; One-way ANOVA (ns means no significant statistical differences of $p \geq 0.05$). C) Brightfield and fluorescence images of a $D_{100}$ pattern.

This indicates that, in principle, the presence of cell-cell contact may be affecting the transfection efficiency, but the number of cells per dot do not affect transfection efficiency. Mix-4 was chosen as the optimum concentration for further experiments, as it presented a high transfection and low deviation between samples.

*4.3.3. Transfection efficiency quantification on patterned single hHF-MSCs and small hHF-MSCs-colonies*

In order to evaluate the effect of cell-to-cell contact in the transfection process of hHF-MSCs, cells from $D_{20}$ and $D_{100}$ patterns were treated with the transfection mix-4 and monitored over time, taking brightfield and fluorescence images at 0, 12, 24, 30 and 42 h, after transfection.

Cells within the small cell-colonies in $D_{100}$ patterns presented clear and intimate cell-cell contact with other cells in the same colony after patterning and during transfection, showcasing an initial spreading similar to those found in conventional cultures (**Figure 3 A**). Meanwhile, single cells in the $D_{20}$ patterns were completely isolated from others and presented a rounded architecture without spreading (**Figure 3 B**).

The transfection efficiency was calculated for each time, observing a Gaussian distribution of the transfection efficiency. Transfection efficiency was calculated using equation 2. GFP expressing cells were calculated using the number of cells presenting fluorescence after image processing at each specific time. Total number of alive cells for our patterns equals the number of cells that remain in the pattern at each specific time [27], SI-4.3.

$$Transfection\ Efficiency = \frac{GPF\ expressing\ cells\ (tx)}{Total\ number\ of\ alive\ cells\ (tx)}\ x\ 100$$

(eq. 2)

The maximum transfection efficiency was found to be 28 ± 4 % at 18 h from $D_{20}$ and 22 ± 2 % at 24 h for $D_{100}$, **Figure 3 B and C**. These measurements indicate a faster expression of GFP when cells are isolated and suggest that cell-cell contact may participate in the regulation of the uptake, the

transcription or the transduction of the plasmid, affecting the transfection process.

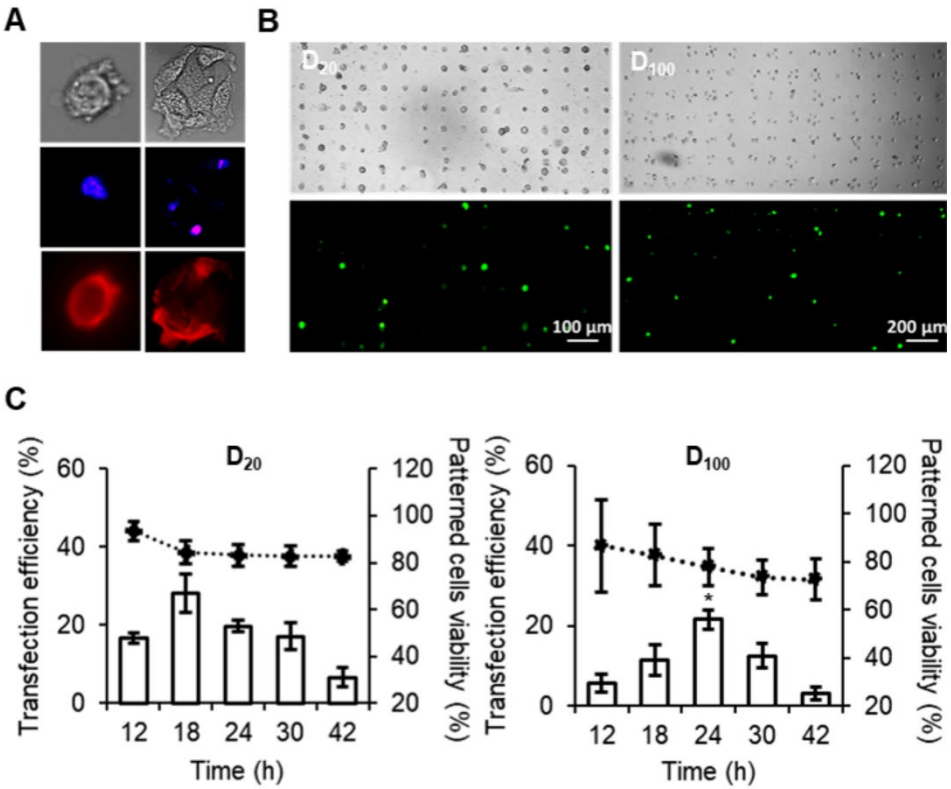


**Figure 3.** Transfection efficiency quantification on patterned single hHF-MSCs and small hHF-MSCs-colony patterns. A) Microscopy images of $D_{20}$ (left) and $D_{100}$ (right) patterns. Top: Brightfield images; middle: fluorescence images showing DAPI staining of cell nucleus; bottom: fluorescence images of phalloidin dyed cell cytoskeletons. B) Brightfield and fluorescence microscopy images of single cell (left) and small cell-colony (right) after 18 and 24 h, respectively after transfection of GFP. C) Plots of transfection efficiency (bar chart) and patterned cell viability (dotted line) *versus* time of $D_{20}$ (left) and $D_{100}$ (right). Error bars mean ± SD ($n$ = 3 patterns, with ~700 cells and ~4000 cells monitored for $D_{20}$ and $D_{100}$ respectively per sample and per time). Statistical significance; paired two-tailed t-test (* means significant statistical difference of $p < 0.05$ compared to $D_{100}$, 24 h).

This would be in agreement with current publications showing that reduction of cell spreading may induce cellular stress [36,37] and therefore affect DNA uptake, transcription and transduction processes [38,39], especially in regards of the secondary metabolism. Recently, Chang et al. reported that cell cytoskeleton is a fundamental factor on gene transfection, where nucleus reshaping and shorter actin microfilaments induces an increased transport of the plasmid inside the cells with smaller spreading [40]. Furthermore, it has been reported that cell-cell contact affects different transcription and transduction pathways and therefore influence nuclear and genetic regulation and cell growth and survival [32,41,42]. We hypothesize that the enhanced cell stress and the lack of direct cell signals may increase the velocity of the incorporation of the plasmid and the expression of the protein.

Regarding the viability of the patterned cells, both scenarios showcased low cell detachment, as 82 % and 72 % of cells remained at the $D_{20}$ and $D_{100}$ patterns respectively after 42 h.

### *3.4. Absolute transfection efficiency quantification on patterned single hHF-MSCs*

The patterning of single cells also gives the opportunity to monitor particular cells over a lapse of time, allowing the constant observation of all individual cells during the full course of the assay. As the expression time of GFP may vary between cells due to their heterogeneity, it is of interest to monitor when and for how long each cells appear fluorescent. Contrary to conventional transfection efficiency assays, which only take into account GFP expressing cells on the peak transfection time, the patterning of cells allowed to count cells that express the fluorescence protein at a different time than the usual peak time.

Unlike the previous transfection assays on patterned cells, which were done similar to the conventional assays only taking into account the GFP expressing cells at each individual time, in this case, cell transfection on each individual single cell was monitored over the course of 42 h, all GFP expressing cells were summed up and the absolute transfection efficiency was obtained. Absolute transfection efficiency was calculated following the

equation 3, where “New GFP Expressing Cells” means fluorescent cells not appreciable at previous time.

$$Absolute\ Transfection\ Efficiency = \frac{\sum New\ GFP\ expressing\ cells\ (t0, t1, t2 \dots tx)}{Total\ number\ of\ cells\ (t0)}\ x\ 100$$

(eq. 3)

**Figure 4** shows a section of a single cell pattern, at different times, after transfection. GFP expression was observed up to 30 h after transfection.

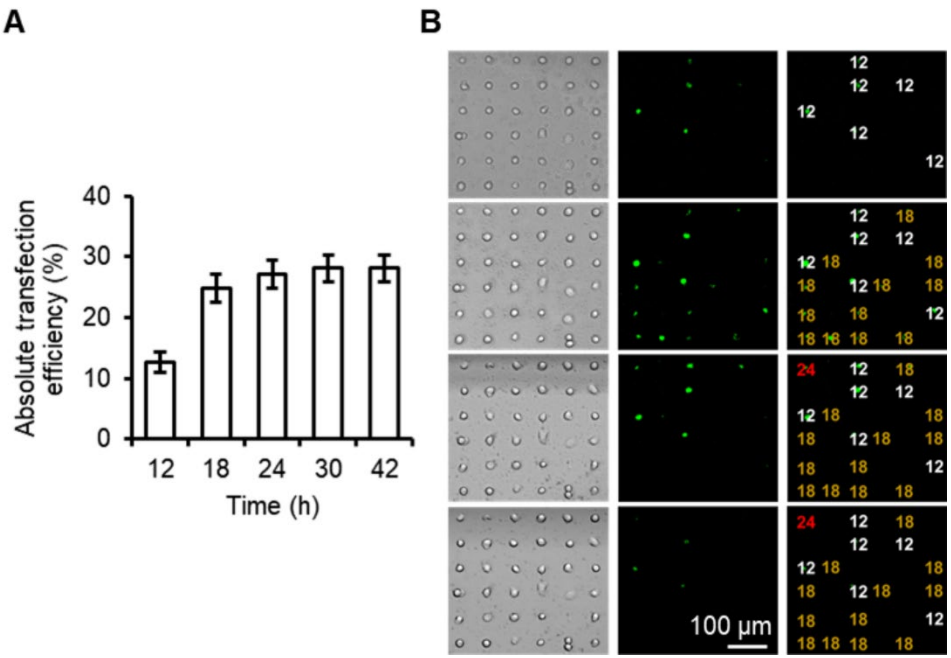


**Figure 4.** Absolute transfection efficiency quantification on single hHF-MSCs $D_{20}$ patterns. A) Graphical representation of the absolute transfection efficiency over time for 42 h. Error bars mean ± SD (n = 3 patterns with ~700 cells monitored per sample). B) Brightfield (left) and fluorescence (center) images of GFP expressing cells. Right: same fluorescence microscopy image than in center with colored numbers representing the time of apparition of the fluroescence in white (12 h), yellow (18h) or red (24h) on the transfected cells to calculate the absolute transfection efficiency following equation 2.

The majority of the cells expressing GFP were appreciable within the first 18 h, obtaining the highest number of cells expressing GFP (25 ± 2 % in transfection efficiency). From 18 h onwards, the expression of GFP decreased rapidly. The absolute transfection efficiency was calculated to be 28 ± 2 %.

This results showcased that analysis of cell transfection at only one specific time, as done in conventional flow cytometry assays, does not represent the totality of cells successfully transfected. Around 3% of the cells cannot be appreciated when only taking into account the peak transfection time (from 25 % to 28 %). Our methodology not only allows the continuous monitoring of each cell or cell colony, but also allows a more accurate analysis of transfection efficiency. For instance, our results showcase that cells where GFP was appreciable at early times (12 hours) usually maintained their fluorescence for a long period of time, indicating a high production and expression of GFP. Contrary to that, most cells expressing GFP in the peak transfection time (18 h) could only be appreciable for a few hours and usually presented smaller intensity than the others, indicating a lower expression of the gene. This also allowed to differentiate between cells that never expressed the gene and which cells were successfully transfected but detached at some point from the substrate.

*4.3.5 Proliferation of the hHF-MSCs from the transfected patterns*

In order to study the ability of patterned and transfected hHF-MSCs to produce a full cell culture, the maintenance cell medium of the transfected hHF-MSCs $D_{20}$ and $D_{100}$ patterns (0 % FBS) was changed to a complete DMEM medium 42 h after transfection. After another 48 h, cells replication, migration and expansion outside their pattern were observed, **Figure 5** In general, higher proliferation was observed for cells patterned on $D_{20}$ substrates than on $D_{100}$ substrates.

This indicates that patterned cells can be fully cultured after transfection, a desirable outcome that allows the growth and expansion of a culture of transfected cells. This can be achieved by the simply change in the serum concentration of the medium.

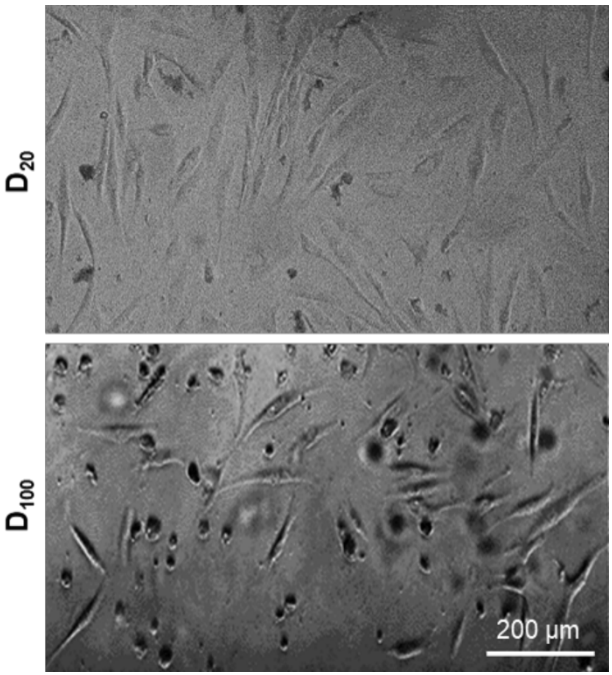


**Figure 5.** Cell proliferation after patterning and transfection. Brightfield microscopy images of substrates containing patterned and transfected $D_{20}$ (top) and $D_{100}$ (bottom) hHF-MSCs, 48 h after change from serum-free medium to complete medium, showing expansion and proliferation.

## 4. Conclusions

In this work, we demonstrated the use microcontact printing, a well-known and easy to use methodology aimed for generation of protein and cell patterns, for the quick, easy and dynamic analysis of the transfection efficiency. This opened the possibility to evaluate the effect of cell-cell contact during the cell transfection process, which is mostly unknown and cannot be studied with conventional cell culture methodologies.

In terms of transfection efficiency, the results obtained using patterned substrates were comparable to those obtained in regular cell culture by flow cytometry. The transfection process was monitored for single cell $D_{20}$ and

small cell-colony $D_{100}$ patterns up to 42 h. The time to reach a maximum transfection efficiency was 6 h earlier for single cells than for small cell-colonies. Additionally, the transfection efficiency on $D_{20}$ patterns was 10 % higher than on $D_{100}$ and conventional cultures. This confirms our hypothesis that cell-cell contact has an important effect during the transfection process.

Besides enabling the comparison of the transfection efficiency in isolated or non-isolated cells, the use of patterned substrates for transfection studies presented a series of additional advantages. The use of cell arrays makes it possible to assess the status of the cells and obtain continuous transfection data for several days. Unlike conventional techniques, it allows the quantification of the absolute transfection efficiency, counting the transfected cells on by one, at a desired time. Cell patterning allows the generation of a large number of independent events, be single cells or small cell-colonies, in a tiny substrate. The high density of the array provides to the platform with a high analytical capacity, allowing statistical studies or even the possibility of analysis cell subpopulations. All steps, cell adhesion, transfection and analysis can be done on the same substrate without manipulation, allowing the analysis of adherent cells without the need of detachment and enabling real time monitoring. The cell arrays containing more than 4000 and 20000 independent elements ($D_{20}$ single cells or $D_{100}$ small cell-colonies, respectively) were generated in just 2 h, being ready for transfection and analysis. This significantly reduces the number of cells needed to perform the assay. In addition, the assay time is drastically reduced compared to methods based on conventional cultures and flow cytometry, where cells must be cultured for at least 24 h and detached from the culture dish to be analyzed. Furthermore, our results show that the cells transfected in the patterns proliferate, allowing to culture them for subsequent studies and applications.

In its present form, our methodology present a limitation for cell sorting and cloning in contrast to the flow cytometry analysis. So far, our methodology enables the proliferation of both transfected and non-transfected cells, producing a mixture culture, disabling the possibility to isolate and clone exclusively the transfected cells. Stable transfection with antibiotic selection

[43] could serve to improve our methodology as a way to specifically isolate a culture made of transfected cells.

Further investigation will allow integrating these substrates into microfluidic platforms to leverage the use of flow for controlled delivery and removal of reagents and waste products in an automated manner. Novel studies could be directed to different applications such as, to discern the efficacy of different transfection vectors in different cell-cell contact scenarios, to study cell subpopulations, to understand which processes may cause the transfection efficiency variations, to evaluate toxicity for each transfection vector.

## 5. Supporting information

*SI-1. Image processing and analysis.*

All treated samples and negative controls were monitored and photographed under the same light intensity and exposure conditions. Due to the autofluorescence present in the cells and in the polystyrene well, the microscope images from each sample were normalized to their respective negative control of non-transfected cells using ImageJ.

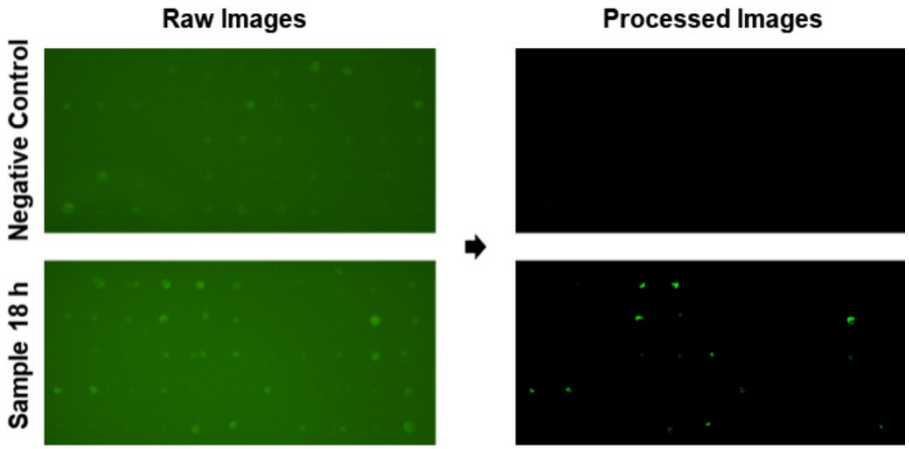


**Figure SI-1.** Image processing. Raw images (left) were processed equally (contrast and brightness) in both negative controls (up) and samples (down) in order to eliminate autofluorescence coming from the non-transfected cells and the polystyrene well (right). The remaining green cells after processing in the sample images were used for the analysis.

*SI-2. Cells per dot, cell area and cell ratio of patterned single hHF MSCs and small-hHF MSC colonies.*

Number of cells per dot (dot occupancy), cell area and cell aspect ratio were studied for cells patterned in dots of 20 and 100 μm ($D_{20}$ and $D_{100}$), **Figure SI-2.**

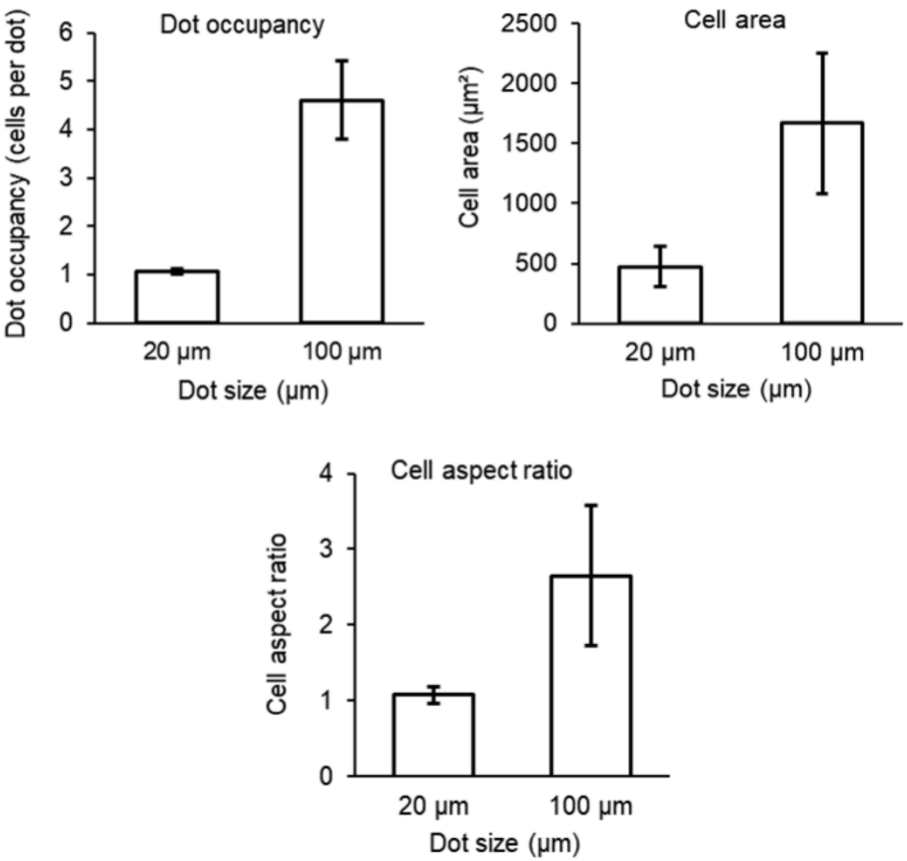


**Figure SI-2. Cell morphology and dot occupation.** Graphical representation of dot occupancy (number of cells per dot), cell area and cell aspect ratio for $D_{20}$ (20 μm, for single cell patterning) and $D_{100}$ (100 μm, for small cell-colony patterning). The spreading of the cells in the colony pattern is higher than in the single cells pattern, presenting a larger cell area (1668 ± 583 $\mu m^2$ compared to 472 ± 168 $\mu m^2$, mean values) and a higher cell aspect ratio (2.6 ± 0.9 compared to 1.1 ± 0.1 length/width, mean values), n = 3.

*SI-3. Stability and viability of patterned hHF-MSCs.*

We studied the stability and viability of the patterned cells over the course of several days, and were analyzed following three requirements. First, cells need to be adhered to the substrate. Second, the cells must remain in the pattern and third, the patterned cells need to be alive.

FBS contains growth, migration and proliferation factors that directly affect the attachment of cells to the patterns. Usually, FBS is required for the proper growth and sustainability of the cells, as the absence of serum does generate the optimal conditions for cell proliferation (**Figure SI-3 A**). Therefore, we studied the effect on patterned small hHF-MSCs-colonies on maintenance media containing different percentages of FBS (0 %, 5 %, 10 % and 20 %) for 24 h (n = 3 per maintenance medium type). Other supplements, such as milk serum, resulted inappropriate for the cells. In all cases containing FBS, cells migrated and spread outside of patterned dots, (**Figure SI-3 B**). In the 0 % of FBS the cells remained inside of their dots.

Stability and viability of single hHF MSCs and small hHF-MSCs-colony on $D_{20}$ and $D_{100}$ patterns respectively were investigated in 0 % FBS media (n = 3). It was found out that cells do not migrate to blocked zones and only detach from the substrate to the medium, **Figure SI-3 C**.

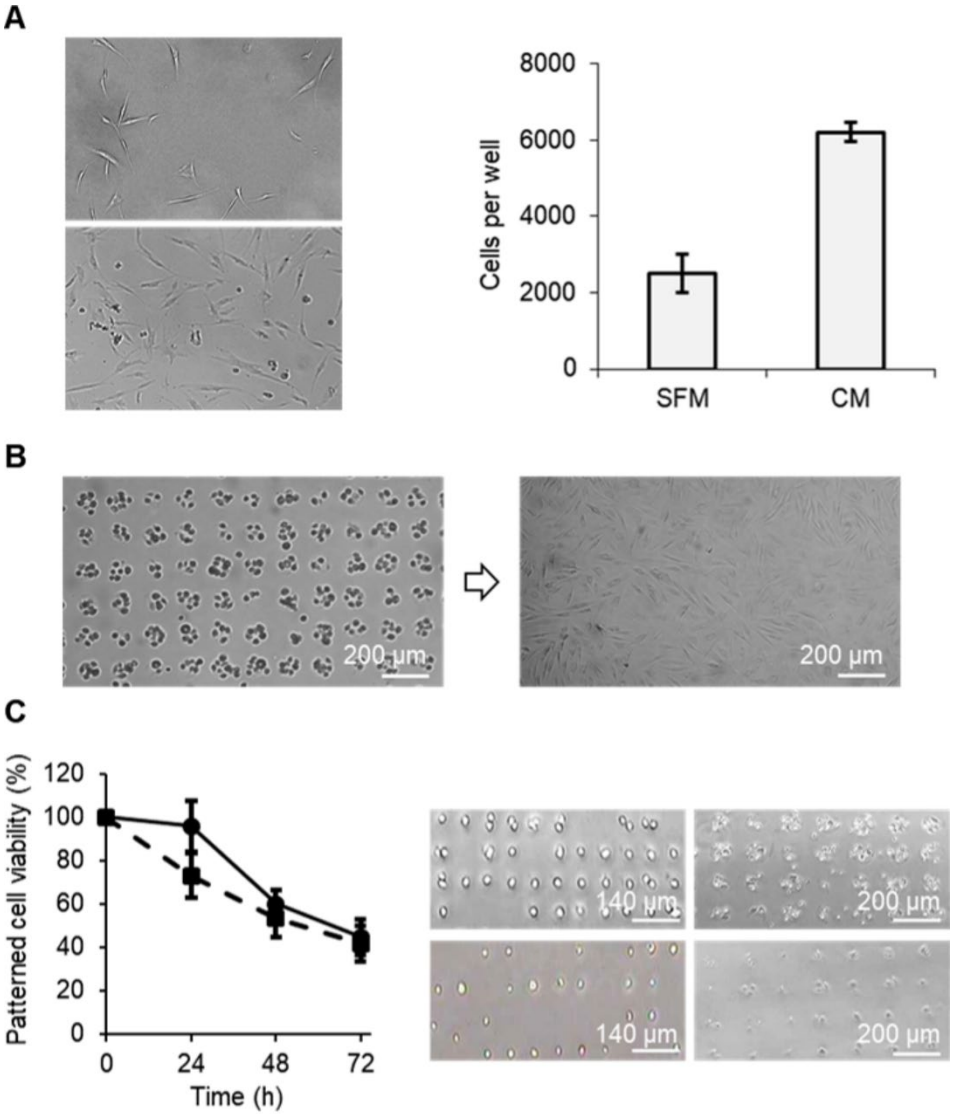


**Figure SI-3.** A) (right) Brightfield images of hHF-MSCs cultured without FBS (SFM, top) or with FBS 30% (CM, bottom) after 48 hours of culture. (left) Plot of the number of cell per well for the cultures in serum free medium (SFM) and complete medium (CM) after 48 hours. B) Brightfield images of the spreading of the cells after 24 h incubation with medium containing FBS. C) (left) Plot of the patterned cell viability (number of living cells in the pattern) for single cells (full line) and small cell-colonies (dotted line) for 72 h. (right) Images of the patterns at 0 and 72 h, same spots.

*SI-4. Optimization of GFP plasmid/lipofectamine transfection on hHF-MSCs.*

Four different mixes with different concentration of lipofectamine and GFP plasmid were prepared for the optimization of the transfection protocol of the hHF-MSCs. Transfection mix-1 containing, 0.80 % (v/v) lipofectamine and 0.40 % (v/v) GFP plasmid in Opti-MEM medium; the transfection mix-2 containing 0.80 % (v/v) lipofectamine and 0.80 % (v/v) GFP plasmid in Opti-MEM; the transfection mix-3 containing 1.60 % (v/v) lipofectamine and 0.40 % (v/v) GFP plasmid in Opti-MEM; and transfection mix-4 containing 1.60 % (v/v) lipofectamine and 0.80 % (v/v) GFP plasmid in Opti-MEM. hHF-MSCs cultured on conventional cell culture well plates at two different confluences (70% and 90%) were transfected with all 4 mixes and GFP expression was analyzed trough flow cytometry after 24 hours. Lower confluences were found inadequate for the analysis due to the high mortality rates or the low binding of the cells. Furthermore, a true single cell state could not be produced in regular cultures of our cell type as it always presented some kind of cell-cell interaction.

The highest transfection efficiency was observed for the 70% confluence cultures transfected with mix-3 and 4. The samples treated with mix-3 and 4 resulted in similar transfection efficiency, 19 ± 1 and 20 ± 1 %, respectively, On the other hand, an increase on cell´s mortality was observed when the plasmid and lipofectamine concentrations were high, as in the case of mix-4, with a 17 ± 1 % of death, **Figure SI-4.** Cells at 90% confluence presented lower transfection efficiency, most probably caused by the higher contact inhibition effect.

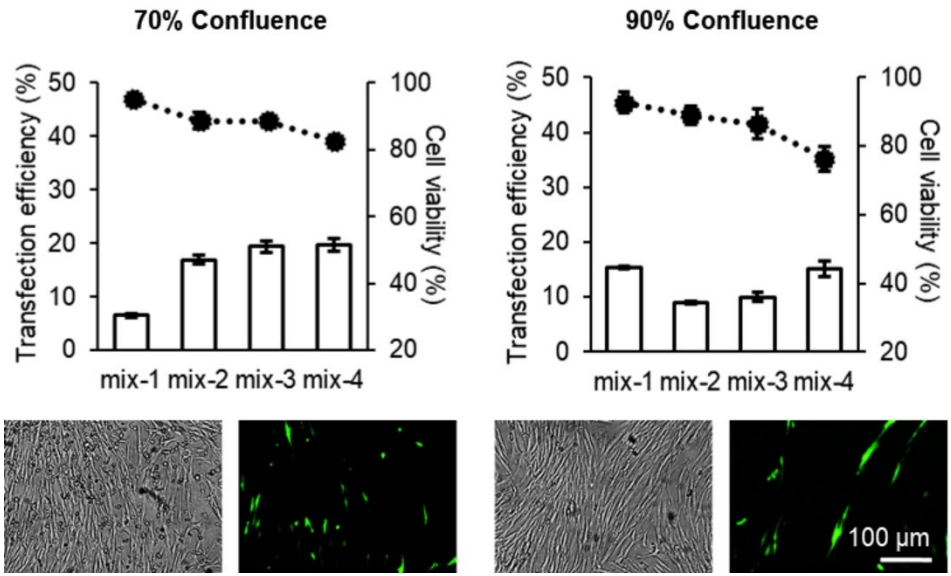


**Figure SI-4.** Top; graphics of the transfection efficiency (bars) and cell viability (lines) of conventional hHF-MSCs cultures with 70 % (left) or 90 % (right) confluence, transfected using four different mixtures (mix-1, 2, 3 and 4) of lipofectamine and GFP plasmid. The analysis was carried out trough flow cytometry. Error bars represent mean ± SD (n = 3). Bottom; brightfield and fluorescence images of transfected cultured cells at 70% (left) and 90% (right) confluence with mix 4.

## 4.6. References


(1) Azuaje-Hualde, E.; Rosique, M.; Calatayud-Sanchez, A.; Benito-Lopez, F.; M de Pancorbo, M.; Basabe-Desmonts, L. Continuous Monitoring of Cell Transfection Efficiency with Micropatterned Substrates. *Biotechnol. Bioeng.* **2021**, bit.27783.

(2) Rose, J. K. Optimization of Transfection. *Curr. Protoc. Cell Biol.* **2003**, *19* (1), 20.7.1-20.7.4.

(3) Yang, L.; Yang, J. L.; Byrne, S.; Pan, J.; Church, G. M. CRISPR/Cas9-Directed Genome Editing of Cultured Cells. *Curr. Protoc. Mol. Biol.* **2014**, *107* (1).

(4) Kaufmann, K. B.; Büning, H.; Galy, A.; Schambach, A.; Grez, M. Gene Therapy on the Move. *EMBO Mol. Med.* **2013**, *5* (11), 1642–1661.

(5) Azuaje-Hualde, E.; García-Hernando, M.; Etxebarria-Elezgarai, J.; De Pancorbo, M.; Benito-Lopez, F.; Basabe-Desmonts, L. Microtechnologies for Cell Microenvironment Control and Monitoring. *Micromachines* **2017**, *8* (6), 166.

(6) Hamann, A.; Nguyen, A.; Pannier, A. K. Nucleic Acid Delivery to Mesenchymal Stem Cells: A Review of Nonviral Methods and Applications. *J. Biol. Eng.* **2019**, *13* (1), 7.

(7) Yin, H.; Kanasty, R. L.; Eltoukhy, A. A.; Vegas, A. J.; Dorkin, J. R.; Anderson, D. G. Non-Viral Vectors for Gene-Based Therapy. *Nat. Rev. Genet.* **2014**, *15* (8), 541–555.

(8) Kim, B.-K.; Hwang, G.-B.; Seu, Y.-B.; Choi, J.-S.; Jin, K. S.; Doh, K.-O. DOTAP/DOPE Ratio and Cell Type Determine Transfection Efficiency with DOTAP-Liposomes. *Biochim. Biophys. Acta - Biomembr.* **2015**, *1848* (10), 1996–2001.

(9) Marjanovič, I.; Kandušer, M.; Miklavčič, D.; Keber, M. M.; Pavlin, M. Comparison of Flow Cytometry, Fluorescence Microscopy and Spectrofluorometry for Analysis of Gene Electrotransfer Efficiency. *J. Membr. Biol.* **2014**, *247* (12), 1259–1267.

(10) Usaj, M.; Torkar, D.; Kanduser, M.; Miklavcic, D. Cell Counting Tool Parameters Optimization Approach for Electroporation Efficiency Determination of Attached Cells in Phase Contrast Images. *J. Microsc.* **2011**, *241* (3), 303–314.

(11) Peng, L.; Xiong, W.; Cai, Y.; Chen, Y.; He, Y.; Yang, J.; Jin, J.; Li, H. A Simple, Rapid Method for Evaluation of Transfection Efficiency Based on Fluorescent Dye. *Bioengineered* **2017**, *8* (3), 225–231.

(12) Mantz, A.; Pannier, A. K. Biomaterial Substrate Modifications That Influence Cell-Material Interactions to Prime Cellular Responses to Nonviral Gene Delivery. *Exp. Biol. Med.* **2019**, *244* (2), 100–113.

(13) Dhaliwal, A.; Oshita, V.; Segura, T. Transfection in the Third Dimension. *Integr. Biol.* **2013**, *5* (10), 1206.

(14) Modaresi, S.; Pacelli, S.; Whitlow, J.; Paul, A. Deciphering the Role of Substrate Stiffness in Enhancing the Internalization Efficiency of Plasmid DNA in Stem Cells Using Lipid-Based Nanocarriers. *Nanoscale* **2018**, *10* (19), 8947–8952.

(15) Shiu, J.-Y.; Kuo, C.-W.; Whang, W.-T.; Chen, P. Observation of Enhanced Cell Adhesion and Transfection Efficiency on Superhydrophobic Surfaces. *Lab Chip* **2010**, *10* (5), 556.

(16) Ueda, E.; Feng, W.; Levkin, P. A. Superhydrophilic-Superhydrophobic Patterned Surfaces as High-Density Cell Microarrays: Optimization of Reverse Transfection. *Adv. Healthc. Mater.* **2016**, *5* (20), 2646–2654.

(17) Fujita, S.; Onuki-Nagasaki, R.; Fukuda, J.; Enomoto, J.; Yamaguchi, S.; Miyake, M. Development of Super-Dense Transfected Cell Microarrays Generated by Piezoelectric Inkjet Printing. *Lab Chip* **2013**, *13* (1), 77–80.

(18) Yang, Y.; Wang, X.; Hu, X.; Kawazoe, N.; Yang, Y.; Chen, G. Influence of Cell Morphology on Mesenchymal Stem Cell Transfection. *ACS Appl. Mater. Interfaces* **2019**, *11* (2), 1932–1941.

(19) de Carvalho, T. G.; Pellenz, F. M.; Laureano, A.; da Rocha Silla, L. M.; Giugliani, R.; Baldo, G.; Matte, U. A Simple Protocol for Transfecting Human Mesenchymal Stem Cells. *Biotechnol. Lett.* **2018**, *40* (3), 617–622.

(20) Hahnenberger, K.; Chan, S. Monitoring Transfection Efficiency by Green Fluorescent Protein (GFP) Detec-Tion with the Agilent 2100 Bioanalyzer. *Agil. App Note* **2001**.

(21) Cho, S. H.; Godin, J. M.; Chen, C.-H.; Qiao, W.; Lee, H.; Lo, Y.-H. Review Article: Recent Advancements in Optofluidic Flow Cytometer. *Biomicrofluidics* **2010**, *4* (4), 043001.

(22) Han, Y.; Gu, Y.; Zhang, A. C.; Lo, Y.-H. Review: Imaging Technologies for Flow Cytometry. *Lab Chip* **2016**, *16* (24), 4639–4647.

(23) Li, X.; Aghaamoo, M.; Liu, S.; Lee, D.-H.; Lee, A. P. Lipoplex-Mediated Single-Cell Transfection via Droplet Microfluidics. *Small* **2018**, *14* (40), 1802055.

(24) Woodruff, K.; Maerkl, S. J. A High-Throughput Microfluidic Platform for Mammalian Cell Transfection and Culturing. *Sci. Rep.* **2016**, *6* (1), 23937.

(25) Giupponi, E.; Visone, R.; Occhetta, P.; Colombo, F.; Rasponi, M.; Candiani, G. Development of a Microfluidic Platform for High-Throughput Screening of Non-Viral Gene Delivery Vectors. *Biotechnol. Bioeng.* **2018**, *115* (3), 775–784.

(26) McConnell, K. I.; Slater, J. H.; Han, A.; West, J. L.; Suh, J. Microcontact Printing for Co-Patterning Cells and Viruses for Spatially Controlled Substrate-Mediated Gene Delivery. *Soft Matter* **2011**, *7* (10), 4993.

(27) Garcia-Hernando, M.; Calatayud-Sanchez, A.; Etxebarria-Elezgarai, J.; de Pancorbo, M. M.; Benito-Lopez, F.; Basabe-Desmonts, L. Optical Single Cell Resolution Cytotoxicity Biosensor Based on Single Cell Adhesion Dot Arrays. *Anal. Chem.* **2020**, *92* (14), 9658–9665.

(28) Gonzalez-Pujana, A.; Santos-Vizcaino, E.; García-Hernando, M.; Hernaez-Estrada, B.; M. de Pancorbo, M.; Benito-Lopez, F.; Igartua, M.; Basabe-Desmonts, L.; Hernandez, R. M. Extracellular Matrix Protein Microarray-Based Biosensor with Single Cell Resolution: Integrin Profiling and Characterization of Cell-Biomaterial Interactions. *Sensors Actuators B Chem.* **2019**, *299*, 126954.

(29) Hamon, C.; Henriksen-Lacey, M.; La Porta, A.; Rosique, M.; Langer, J.; Scarabelli, L.; Montes, A. B. S.; González-Rubio, G.; de Pancorbo, M. M.; Liz-Marzán, L. M.; Basabe-Desmonts, L. Tunable Nanoparticle and Cell Assembly Using Combined Self-Powered Microfluidics and Microcontact Printing. *Adv. Funct. Mater.* **2016**, *26* (44), 8053–8061.

(30) Hu, S.; Chen, T.-H.; Zhao, Y.; Wang, Z.; Lam, R. H. W. Protein–Substrate Adhesion in Microcontact Printing Regulates Cell Behavior. *Langmuir* **2018**, *34* (4), 1750–1759.

(31) Kobel, S.; Lutolf, M. High-Throughput Methods to Define Complex Stem Cell Niches. *Biotechniques* **2010**, *48* (4), ix–xxii.

(32) Langan, T. J.; Chou, R. C. Synchronization of Mammalian Cell Cultures by Serum Deprivation. *J. Cell Sci.* **2011**, 75–83.

(33) Madeira, C.; Mendes, R. D.; Ribeiro, S. C.; Boura, J. S.; Aires-Barros, M. R.; da Silva, C. L.; Cabral, J. M. S. Nonviral Gene Delivery to Mesenchymal Stem Cells Using Cationic Liposomes for Gene and Cell Therapy. *J. Biomed. Biotechnol.* **2010**, *2010*, 1–12.

(34) Brunner, S.; Sauer, T.; Carotta, S.; Cotten, M.; Saltik, M.; Wagner, E. Cell Cycle Dependence of Gene Transfer by Lipoplex, Polyplex and Recombinant Adenovirus. *Gene Ther.* **2000**, *7* (5), 401–407.

(35) Cheung, W. Y.; Hovey, O.; Gobin, J. M.; Muradia, G.; Mehic, J.; Westwood, C.; Lavoie, J. R. Efficient Nonviral Transfection of Human Bone Marrow Mesenchymal Stromal Cells Shown Using Placental Growth Factor Overexpression. *Stem Cells Int.* **2018**, *2018*, 1–10.

(36) Quan, C.; Cho, M. K.; Perry, D.; Quan, T. Age-Associated Reduction of Cell Spreading Induces Mitochondrial DNA Common Deletion by Oxidative Stress in Human Skin Dermal Fibroblasts: Implication for Human Skin Connective Tissue Aging. *J. Biomed. Sci.* **2015**, *22* (1), 62.

(37) Koopman, W. J. H.; Verkaart, S.; van Emst-de Vries, S. E.; Grefte, S.; Smeitink, J. A. M.; Willems, P. H. G. M. Simultaneous Quantification of Oxidative Stress and Cell Spreading Using 5-(and-6)-Chloromethyl-2′,7′-Dichlorofluorescein. *Cytom. Part A* **2006**, *69A* (12), 1184–1192.

(38) Natkańska, U.; Skoneczna, A.; Skoneczny, M. Oxidative Stress Triggers Aggregation of GFP-Tagged Hsp31p, the Budding Yeast Environmental Stress Response Chaperone, and Glyoxalase III. *Cell Stress Chaperones* **2018**, *23* (4), 595–607.

(39) Hong, S.-Y.; Roze, L.; Linz, J. Oxidative Stress-Related Transcription Factors in the Regulation of Secondary Metabolism. *Toxins (Basel).* **2013**, *5* (4), 683–702.

(40) Chang, R.; Yan, Q.; Kingshott, P.; Tsai, W.-B.; Wang, P.-Y. Harnessing the Perinuclear Actin Cap (PnAC) to Influence Nanocarrier Trafficking and Gene Transfection Efficiency in Skeletal Myoblasts Using Nanopillars. *Acta Biomater.* **2020**, *111*, 221–231.

(41) Jamora, C.; DasGupta, R.; Kocieniewski, P.; Fuchs, E. Links between Signal Transduction, Transcription and Adhesion in Epithelial Bud Development. *Nature* **2003**, *422* (6929), 317–322.

(42) Cho, Y. Disruption of Cell-Cell Contact Maximally but Transiently Activates AhR-Mediated Transcription in 10T1/2 Fibroblasts. *Toxicol. Appl. Pharmacol.* **2004**, *199* (3), 220–238.

(43) Moore, J. C.; Atze, K.; Yeung, P. L.; Toro-Ramos, A. J.; Camarillo, C.; Thompson, K.; Ricupero, C. L.; Brenneman, M. A.; Cohen, R. I.; Hart, R. P. Efficient, High-Throughput Transfection of Human Embryonic Stem Cells. *Stem Cell Res. Ther.* **2010**, *1* (3), 23.

Appendix 5

# Cell patterning on polymethyl methacrylate through controlled physicochemical and biochemical functionalization

## Cell patterning on polymethyl methacrylate through controlled physicochemical and biochemical functionalization

Enrique Azuaje-Hualde, Job Komen, Albert van den Berg, Marian Martínez de Pancorbo, Fernando Benito-Lopez, Andries D. van der Meer, Lourdes Basabe-Desmonts

*Manuscript in preparation*

### Abstract

Microfluidic devices have emerged as powerful analytical technologies for cell monitoring. This often required the incorporation of cell patterning, which allows the monitoring from dozens to thousands of individual cell culture analytical replicas in a single device with high control over cell adhesion and cell-cell contact. Polymethyl methacrylate is a widely use polymer in the fabrication of microfluidic devices due to its durability, easy manipulation and transparency. However, like other hydrophobic materials, polymethyl methacrylate is cytophobic and present low cell adhesion, which distance its use in cell culture analytical devices. In this work, a strategy was explored and optimized to enable cell patterning on polymethyl methacrylate surfaces, combining localized oxidation through air plasma treatment and microcontact printing of fibronectin. This allowed the pattern of different adherent cell types (mesenchymal stromal, prostate cancer and colorectal cancer cells) in dozens of individual cell colonies with different spatial distribution and confluences. Furthermore, this methodology allowed cell patterning without requiring any blocking agent to the non-printed areas of the surface, speeding up the microcontact printing process. Finally, the cell patterns were incorporated in a polydimethylsiloxane channel to generate a proof-of-concept, simple to use microfluidic device that allowed the maintenance of the cell patterns up to at least 20 hours under constant flow conditions.

**Keywords:** Polymethyl methacrylate; Cell patterning; Microcontact printing; Air plasma; Microfluidic device

## 1. Introduction

In the recent years, many microfluidic devices have emerge for a wide variety of research areas. This trend can be attributed to the reduced cost of production and use of reagents, the simplification of the methodology in order to make it portable and user friendly and the enhanced performance of the device in comparison with conventional methodologies [1]. In the case of microtechnologies aimed for cell culture, microfluidic devices aim to increase the control over the different cell interactions or directly replicate full tissues or organs inside of a chip, allowing a more optimal analysis simulating physiological conditions. Another potential advantage is the generation of high-throughput, non-invasive and real-time analysis for cell culture monitoring that permit the continuous observation of cell behaviour [2,3].

Polymethyl methacrylate (PMMA) is a widely used material in the fabrication of microfluidic devices due to its durability, easy manipulation and capacity to be incorporated in many fabrication processes. Taken all into account, PMMA offers a very versatile option for a wide variety of device designs [4,5]. However, while PMMA presents moderate to good biocompatibility, it has low cell adhesion properties and has been described as cytophobic [6,7]. This is partially caused by its lack of hydrophilicity, which hinders the deposition and formation of cells microenvironments required for proper cell adhesion and maintenance [8,9]. This shortcoming disables, in principle, its potential use for the generation of cell culture microfluidic devices. For such reason, both chemical and light-based treatments of PMMA have been widely explored in order to increase the hydrophilicity of its surface and enhance its properties for cell adhesion and culture [10–13].

One of the easiest and quickest methods to improve a surface hydrophilicity is through air or oxygen plasma treatment. In short, the free radicals generated inside of a plasma chamber can oxidize the surface of a material, exposing polar functional groups that improves the hydrophilicity of the surface. Plasma treatment have been demonstrated to improve PMMA surface hydrophilicity, which in turn improves cell and protein interactions with

the material. This allows the adhesion of extracellular matrix proteins, permitting to control and study cell adhesion to PMMA[11,14,15].

In order to further control cell adhesion, surface micropatterning arises as a powerful method as it permits the deposition of adhesion proteins with a specific pattern, allowing to control localization, distribution and cell-cell contact of adherent cells. In particular, microcontact printing (μCP) allows the dry transfer of cell adhesion proteins from a polydimethylsiloxane (PDMS) stamp to a substrate, replicating the features carved on it. This methodology enables the easy and fast generation of several individual cell events on a single sample, relying on the contrast between adherent and non-adherent areas to isolate each cell event.

There are a few examples in the literature that combine surface oxidation of PMMA through plasma treatment and μCP in order to convert PMMA from cytophobic to cytophilic and achieved controlled cell adhesion. Schmalenberg et al. and  combined plasma treatment of PMMA surfaces and μCP of laminin for the adhesion and growth of Schwann and nerve cells with high potential to function as nerve guides [16,17]. However, this combination of physicochemical and biochemical modifications of PMMA surfaces for the control of cell adhesion on the usual cytophobic PMMA has not been extensively explored.

In this work, a hybrid physicochemical-biochemical functionalization of PMMA surfaces was evaluated for the controlled patterning of cells. Air plasma treatment was employed in order to improve hydrophilicity on the PMMA surfaces, using PDMS slabs as protectors for the generation of hydrophilic zones with high contrast with their hydrophobic surroundings. Direct functionalization and μCP of cell adhesion proteins was applied not only for the conversion of the material from cytophobic to cytophilic, but also for the generation of cell patterns with controlled cell-cell and cell-material interactions. Finally, the cell patterns were easily adapted into a simple, proof-of-concept PDMS microfluidic device bonded by pressure sensitive adhesive, which demonstrated the direct applicability of this methodology for the

maintenance and monitoring of the patterned cells inside this microfluidic device, **Figure 1**.

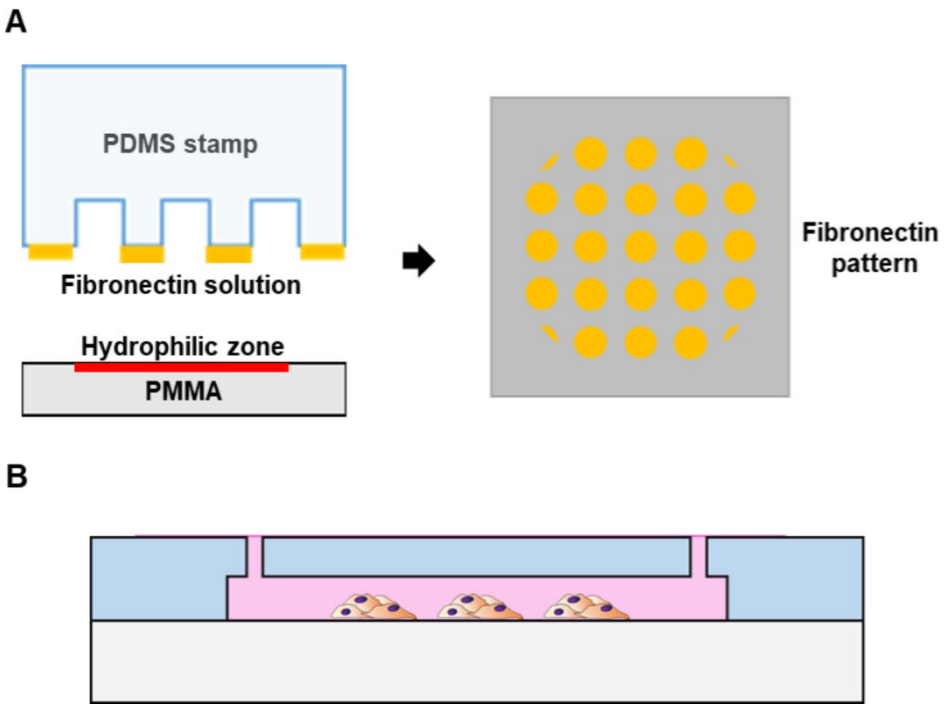


**Figure 1.** Drawing of cell patterning on PMMA. A) Microcontact printing of fibronectin dots is carried out on top of the hydrophilic zone of PMMA. B) Cell patterns composed of dozen individual cell events can be directly integrated in a PDMS microfluidic device.

## 2. Materials and methods

### *2.1. Materials*

Primary human Hair Follicle-derived Mesenchymal Stromal Cells (hHF-MSCs) were obtained from human follicles (passages 6 to 9). Prostate cancer cells PC3 and colorectal cancer cells HCT116 were purchased from ATCC, USA. Bovine plasma fibronectin, Dulbecco's modified eagle's medium

(DMEM), F-12 Medium, fetal bovine serum (FBS) and penicillin/streptomycin (P/S) were purchased from Fisher Scientific, Spain. Bovine serum albumin was purchased from Sigma Aldrich, Spain. Polydimethylsiloxane silicone (PDMS) elastomer and curing agent SYLGARD 184 were purchased from Ellsworth adhesives, Spain. Polymethyl methacrylate (PMMA) Plexiglas 4 mm, was purchased from Evonik Industries AG, Germany. Pressure Sensitive Adhesive (PSA) ARcare 8939 was purchased from Adhesive Research, Ireland. Luers and reservoirs (male 1/16 in barb and female luer lok compatible connectors white base) were purchased from Microfluidics ChipShop, Germany. Tubing was purchased from Altmann Analytik GmbH & Co, Germany.

### *2.2. Selective oxidation of PMMA surface*

In order to generate controlled hydrophilic zones within PMMA surface, air plasma treatment was used for the oxidation of the surface. PDMS slabs were used as protector for non-treated areas. In summary, 3 mm holes were punched on flat PDMS slabs (elastomer and curing agent proportion 10:1, 0.8 cm height). After carefully washed with ethanol, PDMS slabs were put on intimate contact with PMMA slides (3 x 5 x 0.4 cm, length x width x height). The other side of the PMMA slides were marked at the position of the hole for localization of the hydrophilic zone. The PDMS protected PMMA were oxidized using air plasma inside of a plasma cleaner with a power of 29.6 W for 150 seconds.

To verify the generation of controlled hydrophilic zones, spreading of distilled water (DI water) drop was analyzed. 1 µL of DI water was put on top of untreated PMMA, plasma treated PMMA and PDMS protected PMMA surface after PDMS retrieval. Contact angle was measured using an OCA 15EC Drop Shape Analyser-Goniometer (MRG Ibérica, Spain).

### *2.3. Biochemical functionalization of hydrophilic PMMA surfaces*

Biochemical functionalization of PMMA with cell adhesion proteins was obtained by incubation of fibronectin or collagen solution with the hydrophilic zone of the PMMA surface. Briefly, either 1 µL of fibronectin solution (40 µg

$mL^{-1}$) or collagen solution (1 mg $mL^{-1}$) were put on top of the hydrophilic zones and incubated for 1 hour. Incubation was carried out in a high humidity environment to avoid drop evaporation. Afterwards, drops were retrieved and the PMMA surface was carefully rinsed with PBS.

For cell adhesion on biochemical functionalized PMMA surfaces, colorectal cancer cells HCT116 were cultured until reaching 80% confluence, detached and re-suspended in culture medium (10% serum) for a final concentration of 2.5 $10^6$ cells $mL^{-1}$. Drops of 1 µL of cell suspension were put on top of the hydrophilic zones of the PMMA with fibronectin or collagen functionalization. Drops of 1 µL of cell suspension were also put on top of hydrophilic zones without biochemical functionalization.

Simultaneously, PDMS channels (see Supporting Information 1 for specifications) were rinsed with ethanol and adhered to the corresponding PSA film, covering all PDMS area except the channel itself.

After removal of the PSA protector, the PDMS channel was aligned and adhered to the PMMA, localizing the cell suspension drop on the middle of the channel. All samples were incubated at 37º C and 5% $CO_2$ inside a cell culture incubator for 1 hour with high humidity environment. Afterwards, 200 µL of cell culture medium were flowed three times trough hydrostatic pressure to rinse any non-adhered cell. Samples were imaged trough brightfield microscopy before rinse, right after rinse and 24 hours afterwards.

*2.4. Patterning of cells in functionalized PMMA surfaces*

For the patterning of cell adhesion proteins in the hydrophilic surface of PMMA, microcontact printing of fibronectin was carried out. PDMS stamps containing pillars with different features (lollipop-like, 50 and 100 µm dots) were wetted with 50 µL of a solution of fibronectin 50 µg $mL^{-1}$, BSA-TAMRA 6.25 µg $mL^{-1}$, for 30 minutes. Afterwards, the ink was removed and the PDMS stamps were rinsed with DI water and dried with compressed air. Each PDMS stamp was put in contact on top of the hydrophilic zones in the PMMA surface, in order to transfer the protein from the PDMS stamp to the substrate and

create small dots of fibronectin. Finally, PDMS stamps were retrieved after 30 min.

Patterning of HCT116, prostate cancer cells PC3 and hHF-MSCs was carried out through this procedure. Briefly, cells were cultured until reaching 80% confluence, detached and re-suspended in their respective culture mediums (10% FBS) for a final concentration of $10^6$ cells $mL^{-1}$. Drops of 1 µL of cell suspension were put on top of the hydrophilic zones with the fibronectin patterns and incubated at 37º and 5% $CO_2$ inside a cell culture incubator for 1 hour with high humidity environment. Afterwards, 200 µL of their corresponding cell culture medium were flown three times through hydrostatic pressure in order to rinse non-adhere cells. Brightfield microscopy images were taken after rinsing. The same patterning procedure was carried out in non-treated PMMA surfaces as control of protein deposition.

The same oxidation and patterning procedure was carried out in conventional cell culture 12-well plates and glass slides (60 x 24 x 0.2 mm, length · width · height) as control experiments. PDMS channels were adhered and aligned to all substrates.

PC3 cells patterned on 50 µm dots were maintained under constant flow (10 µL $min^{-1}$) of medium using a Pump 11 Elite Programmable Syringe Pump (Harvard apparatus, Spain) for 20 hours. Brightfield microscopy images were taken afterwards.

For single cell patterning, PMMA wells were fabricated, see Supporting Information 2 for specifications. PDMS stamps containing arrays of 20 µm dots separated by 50 µm were wetted with 50 µL of a fibronectin solution 50 µg $mL^{-1}$. Afterwards, the ink was removed and the PDMS stamps were rinsed with DI water and dried with compressed air. Each PDMS stamp was put in contact with the PMMA wells for 30 min. PMMA wells were previously oxidized using air plasma inside of a plasma cleaner with a power of 29.6 W for 150 seconds. PDMS stamps were retrieved, and wells were directly loaded with 750 mL of PC3 suspension $10^5$ cells $mL^{-1}$. Samples were left for 2 h on constant oscillation in a rocker inside an incubator at 37 ºC and 5 % $CO_2$ air atmosphere. Afterwards, samples were rinsed three times with PBS.

*2.5. Imaging and data analysis*

Brightfield and fluorescence images were taken with a modified Nikon Eclipse TE2000-S (USA) microscope with a LUMENCOR laser light source (USA) and Zylar sCMOS camera (Oxford Instruments, UK). Microscopy images were processed by FiJi/ImageJ software.

## 3. Results and Discussion

*3.1. Cell adhesion on biochemical functionalized PMMA surface*

Polymethyl methacrylate (PMMA) is a widely polymer used in the fabrication of microfluidic devices due to its versatility and easy manipulation. While PMMA has moderate biocompatibility, it does not present good properties for cell adhesion. In general, moderate to highly hydrophobic surfaces do not allow the generation of optimal cell-surface interactions, which leads to a lack of important signals required for cell adhesion, proliferation and survival. For such reason, in order to obtain cell patterning on PMMA, a combined physicochemical and biochemical functionalization of the surface was carried out. Firstly, PMMA was selectively oxidized to improve its hydrophilicity. Secondly, PMMA surfaces were homogeneously coated with cell adhesion proteins to test the best conditions for cell adhesion. Finally, cell patterning was studied.

It is known that plasma treatment to PMMA surfaces increase the hydrophilicity of the material and improves cell adhesion [14,15]. By using a PDMS slab with holes as stencil for the PMMA surface, it is possible to control the plasma exposure to specific parts of the PMMA surface. This allows the generation of discrete hydrophilic zones in the surface, which not only can improve cell adhesion and protein interaction with the substrate, but also allow to control the distribution of cell adhesion zones within the PMMA surface. Here, a 3 mm zone of the PMMA surface was treated with air plasma as a way to generate one unique small zone for cell adhesion in a PMMA slide, which would later serve as the cell adhesion zone in a microfluidic device. To generate the 3 mm zone, a PDMS slab with a 3 mm hole was

used, **Figure 2 A**. The contact angles of untreated PMMA, plasma treated PMMA and PDMS protected PMMA surface were measured.

As expected, differences could be observed between untreated and fully plasma treated PMMA, as the drop highly spread and the contact angle decreased in the later (from 62º to 40º), **Figure 2 B**. This confirmed that plasma treatment increased the hydrophilicity and wettability of the PMMA surface. Regarding the protected surface, the contact angle increased when compared to the untreated surface, which implies that PDMS protection not only shields the surface from oxidation, but also enhances its hydrophobicity due to the contact and interaction with the PDMS.

For the deposition of fibronectin microcontact printing (μCP) was tested on the hydrophilic zone of PMMA and compared with non-treated PMMA surfaces. Fluorescent BSA-TAMRA was used as reporter of the deposition of the protein. As seen in **Figure 2 C**, higher and more homogeneous deposition of the protein could be observed in the oxidized zone when compared with non-treated PMMA. Furthermore, deposition of fibronectin was higher on the hydrophilic zone than in the surface that was protected with the PDMS. This confirmed the need of plasma treatment for the optimal transfer of the cell adhesion protein to the PMMA surface.

The hydrophilic zone was biochemically functionalized with either fibronectin or collagen in order to achieve cell adhesion. Collagen is the main structural protein of the extracellular matrix and promotes cell adhesion to the substrates [18]. Fibronectin is another extracellular matrix protein and plays a major role in cell adhesion through the generation of focal adhesions [19]. Adhesion of colorectal cancer cells HCT116 to the functionalized zones was studied. Adhesion to the hydrophilic zone without biochemical functionalization was also studied. After drop deposition, all PMMA slides were adhered and aligned to a PDMS channel using a middle layer of pressure sensitive adhesive, a double-sided tape that allows the attachment between the PDMS and the PMMA by pressure. This allowed the generation of a simple microfluidic device that contained the cell suspension drop and the hydrophilic zone on the center of its channel, **Figure 3 A**. After incubation,

culture medium was flowed through the channel to rinse any non-adhered cell. In the case of the samples that did not undergo any biochemical functionalization with cell adhesion proteins, almost all cells flowed away after rinsing, indicating that the treatment with plasma does not induce the generation of focal adhesion points for proper cell adhesion dynamics by itself, see **Figure 3 B**.

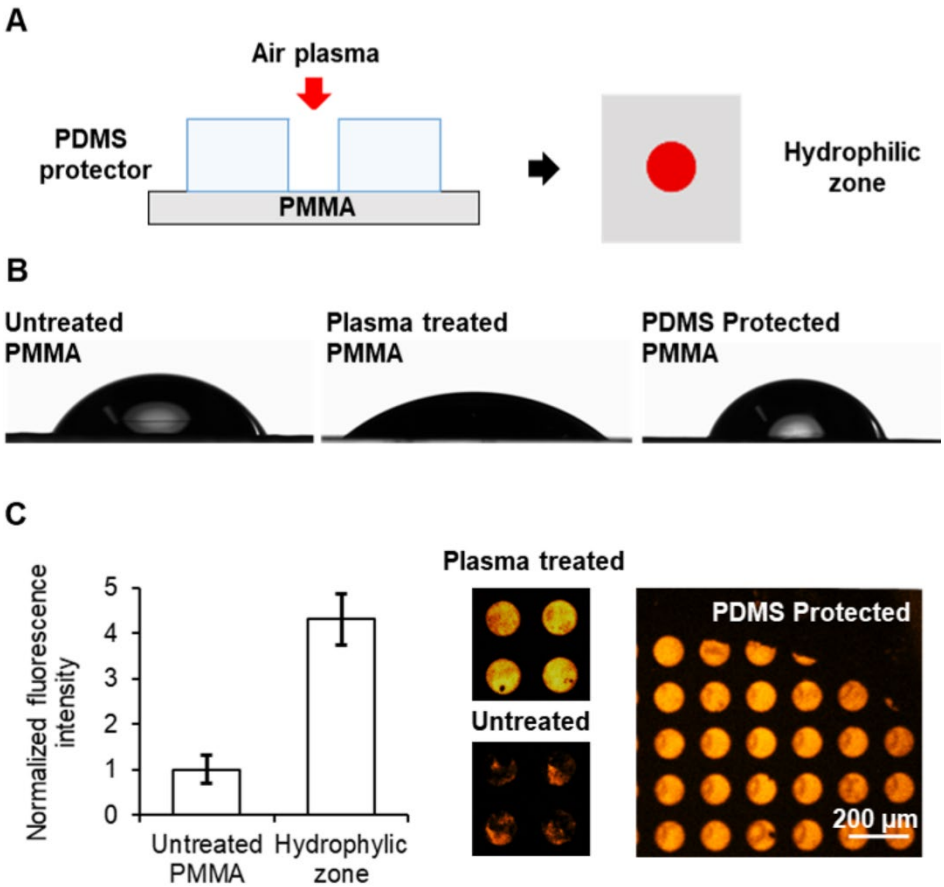


**Figure 2. Localized oxidation of PMMA.** A) Drawing of the oxidation of a single zone of the PMMA surface to generate a discrete hydrophilic zone. B) Drop spreading on PMMA surfaces under different treatments. C) Plot of the normalized fluorescence intensity (left) and fluorescence images of micropatterned BSA-TAMRA dots on PMMA under different surface treatments.

Contrary to that, cell adhesion could be observed in the samples treated with either collagen or fibronectin after only 1 hour of incubation. In the case of the collagen samples, approximately 1000 cells could be observed in the substrate after rinsing, indicating that 45% of cells incubated successfully attached to the PMMA. However, 24 hours after the incubation, the number of cells decreased by 25%, with the remaining cells displaying rounded morphology and lack of spreading, indicating that cells were not producing optimal interactions with the substrate (**Figure 3 C and D**). In the samples treated with fibronectin, approximately 2100 cells could be found successfully attached to the substrate, corresponding to a 85% of the total number of cells incubated. In the case of samples incubated with fibronectin, cell number on the surface increased in the course of 24 hours, approximately 2200 cells, and presented a more elongated shape relating with a better interaction and adhesion of the cells with the PMMA. This indicated that biochemical functionalization of PMMA is a key factor in order to achieve cell adhesion to this material.

Out of the two proteins tested, fibronectin showcased overall better results than collagen, as more cells adhered under the same conditions and incubation time and the culture proliferated over the course of 24 h. For such reason, fibronectin was chosen as the cell adhesion protein for further experiments.

### *3.2. Patterning of cells on hydrophilic PMMA surfaces*

Once demonstrated the improved cell adhesion properties of PMMA after selective plasma and fibronectin coating, and the capability to produce fibronectin patterns on the PMMA surface, the next objective was to achieve controlled cell adhesion in the form of patterns on the PMMA substrate. This was achieved through μCP, a methodology that allows the dry transfer of a protein from a PDMS stamp with engraved features to the surface of the substrate.

An array of 100 μm fibronectin dots was produced. The adhesion of three different cell types was evaluated, including the previously mentioned

HCT116 cells, prostate cancer PC3 cells and human mesenchymal stem cells hHF-MSCs, **Figure 4 A**.

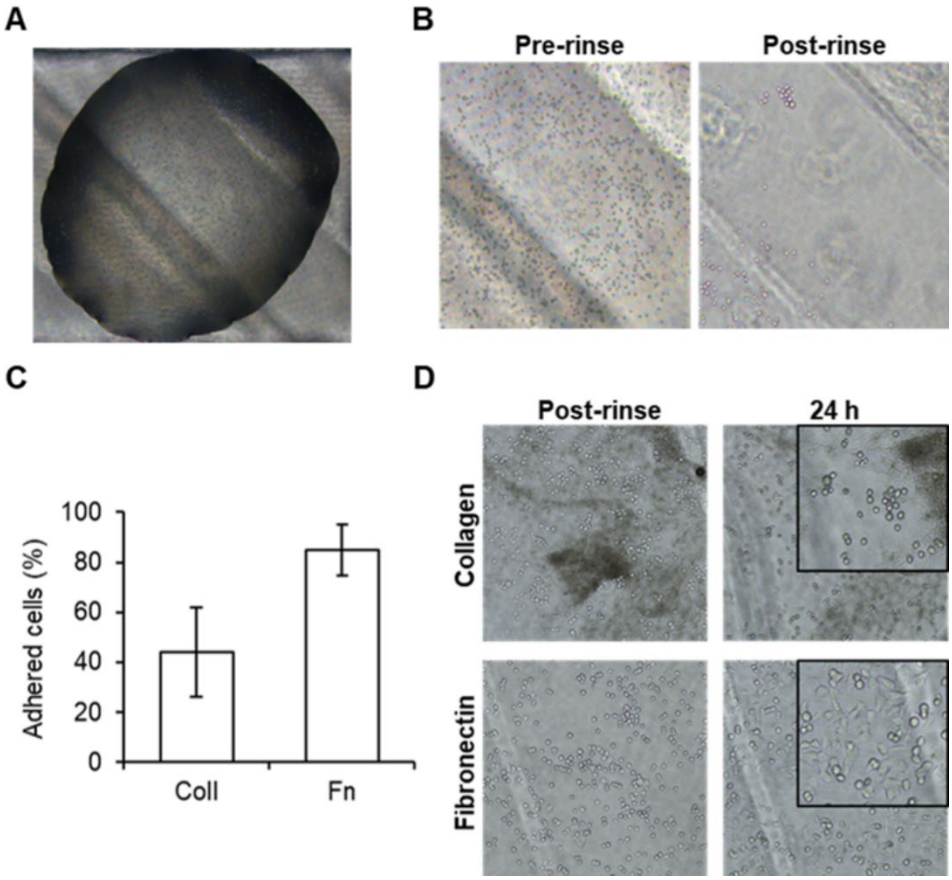


**Figure 3. Adhesion of HCT116 cells on PMMA treated surface.** A) Brightfield microscopy image of the cell suspension drop on the middle of the PDMS channel. B) Brightfield microscopy images of HCT116 cells cultured before flow (left) and after flow (right). C) Plot of the percentage of cell adhered to collagen (CG) and fibronectin (FN) treated hydrophilic zones in the PMMA. Error bars mean ± SD (n = 3 samples per experimental condition). D) Brightfield microscopy images of cells adhered to collagen (top row) and fibronectin (bottom row) after flow (left column) and 24 hours afterwards (right column).

The pattern of small cell-colonies for all three types of cells was successfully obtained, obtaining dozens of individual cell events in a single sample. This confirmed the possibility to control cell adhesion and cell localization in PMMA through simple surface manipulation and micropatterning. The number of cells per spot was directly correlated with the size of the cell type itself, as the cells attach and expand as much as the fibronectin spot allows them, where 5 ± 2, 15 ± 3 and 22 ± 6 cells could be found per spot for the patterns with hHF-MSCs, PC3 and HCT116 respectively. This assay implied that this patterning methodology, and therefore the subsequent microfluidic device is, *in principle,* suitable for different cell types and can be adapted to a wide range of scenarios. Different fibronectin patterns, including 50 µm dots, 100 µm dots and lollipop-like features were printed on PMMA slides and incubated with PC3. For all three types of fibronectin arrays studied the corresponding array of PC3 was obtained, demonstrating the capabilities of the methodology to control cell localization and cell-cell interactions, **Figure 4 B**.

Cell patterning on conventional cell culture substrates, such as polystyrene well-plates and glass substrates, require blockage of non-printed areas with a blocking agent, such as bovine serum albumin, and usually needs the retrieval of the serum from the medium in order to avoid cell migration outside of the pattern. In contrast, patterning of PC3 was highly specific in the PMMA substrate see Supporting Information 4, Figure SI-4. Due to the high contrast between hydrophilic cell adhesion areas and the rest of the hydrophobic surface, adhesion and migration of the cells outside of their pattern was supressed.

The fact that blocking agents are not required for the arrays studied in this assay presents a huge advantage over cell patterning on conventional cell culture substrates, as avoiding the blocking step allows to speed up the production and fabrication process of the platform and improves its direct applicability and scalability potential. Our previous works on the use of cell patterns for the optical based monitoring of cell behaviours could immensely benefit from these advantages to evolve from quick cell monitoring methodologies to fully formed devices with manufacturing and commercialization prospect [20–22].

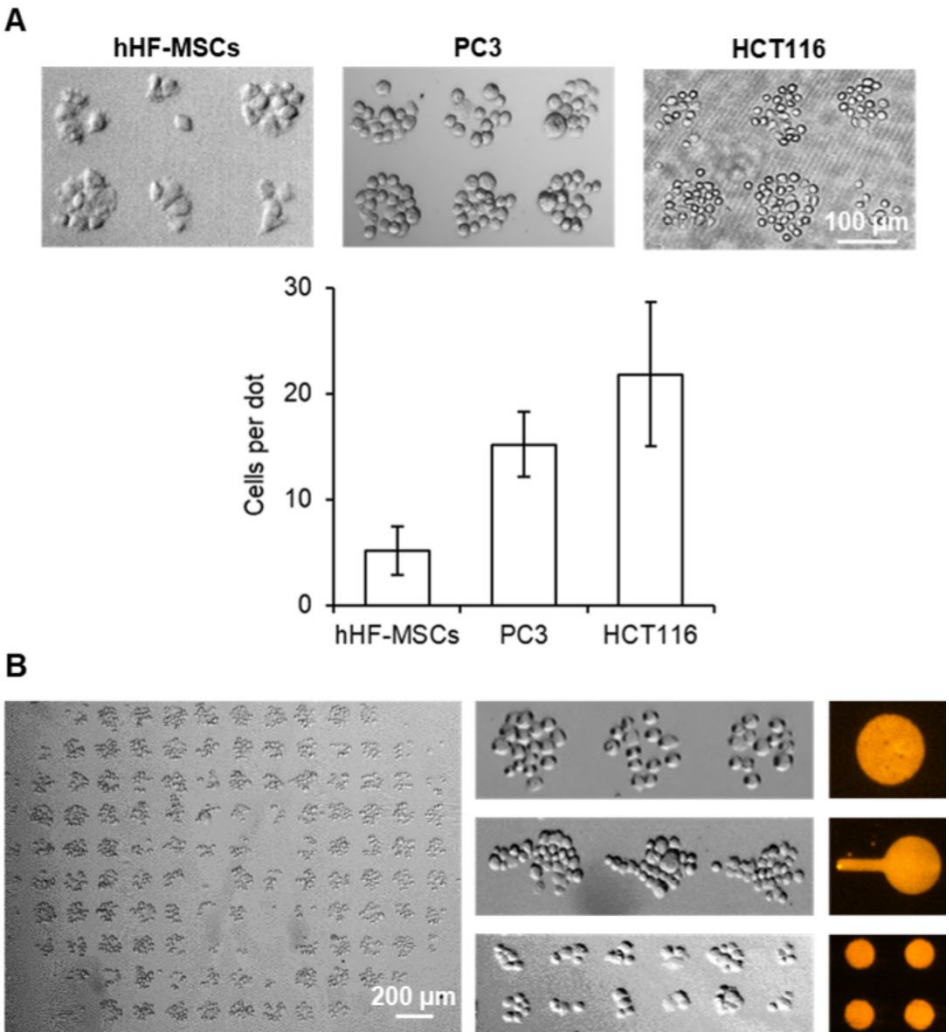


**Figure 4.** A) Brightfield images of the arrays of small cell-colonies for each of the three different cell types studied (top) and graphical representation of the number of cells per spot (bottom). Error bars mean ± SD (n = 3 samples per experimental condition). B) Brightfield microscopy images of full PC3 array on 100µm fibronectin dot patterns (left), pattern of PC3 on 100µm dots, lollipop-like features and 50µm dots (middle column, top to bottom) and fluorescence images fluorescent BSA printing of the same features (right column).

### *3.3. Maintenance of PC3 patterns under flow conditions*

Fluids-related mechanic forces, such as shear stress, are known to influence cell behavior on physiological conditions, affecting their attachment dynamics and proliferation rates among others [23–25]. For such reasons, there is an increasing interest in developing microfluidic devices that allows to study and monitor cell patterns under controlled flow conditions.

PC3 patterns in 50 µm fibronectin dots were maintained in a constant flow of 10 µL $min^{-1}$ overnight, see **Figure 5 A and B** for setup specifications. While some cells detached during the process, cells were still concealed in their respective dot and the patterns remained similar to their original state, see **Figure 5 C**.

These results indicate that the cell arrays can be directly integrated and studied inside of a microfluidic device under controlled flow conditions, giving direct applicability to the platform. It should be noted that both cell adhesion and the overnight incubation were performed using cell culture medium supplemented with serum. The growth and migration factors contained in the serum may cause the cells to move and proliferate outside of the patterns in conventional cell culture substrates. However, the PMMA samples did not present unspecific attachment or cell migration outside of the pattern. This is a consequence of the strong cytophobic characteristic of non-treated PMMA, which prevents cells from moving or attaching outside of the discrete cell adhesion spots, resulting in yet another advantage of PMMA over conventional cell culture materials.

### *3.4 Single-PC3 patterning on PMMA surface*

While different types of cell arrays were obtained on PMMA surfaces following the methodology presented in this chapter, single cell arrays couldn't be obtained with this procedure, observing no cell adhesion after washing steps. This could be attributed to the interactions between cells, formed during the static incubation of cell suspension with the hydrophilic zone, being stronger than the interaction a single cell can achieve with the tiny fibronectin spot in

which they can attach. This resulted in the total removal of all cells in the washing steps and not only the non-adhered ones.

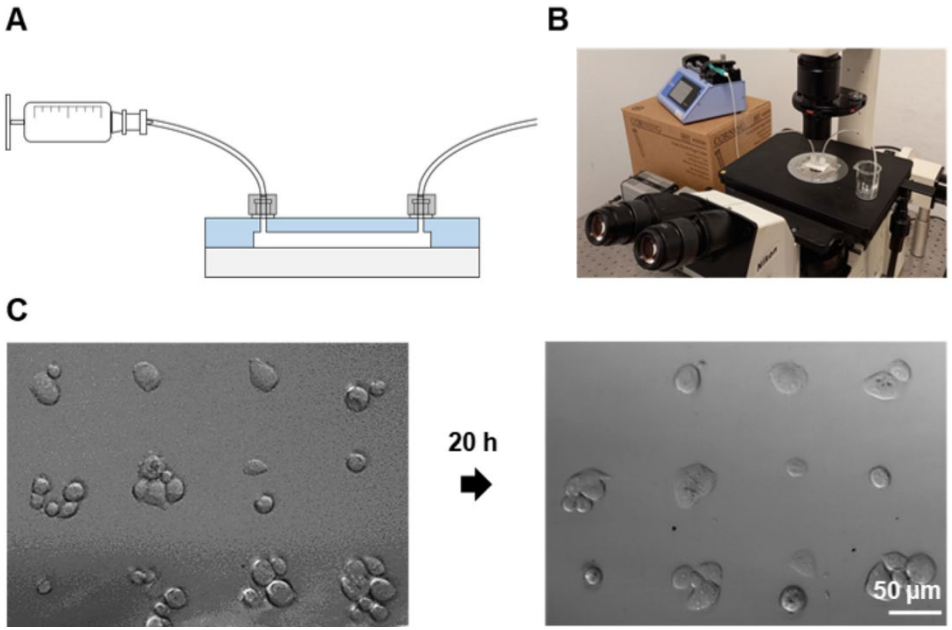


**Figure 5. Maintenance of cell patterns under flow conditions.** A) Schematic drawing of the syringe-device connection. B) Photograph of the setup. C) Brightfield microscopy images of PC3 on 50 um patterns after patterning and after 20 h on flow (10 µL $min^{-1}$).

For such reason, a different µCP protocol was applied. PMMA wells were fabricated and 20 µm fibronectin arrays were produced through µCP on fully oxidized PMMA surface. Cell suspension was incubated with the fibronectin arrays on constant oscillation in order to move the cells throughout the surface and avoid the accumulation of them in a single point and avoid cell-cell interaction as much as possible.

With this procedure, single PC3 could be observed after the washing steps, see Supporting Information 5. This results indicates that static *versus* motion conditions on the incubation of cells with the fibronectin patterns plays a significant role on the formation of single cell patterns. Adapting a flow-based

attachment of cells into the methodology explored in this chapter could not only be beneficial but necessary for the formation of single cell patterns. However, unlike the previous assays in PMMA surfaces, zones with no cells and zones with non-specific attachment could be observed. Optimization on incubation time, protein and cell concentration should be considered for the future.

## 4. Conclusions

In the recent years, new microfluidic devices have been developed for a wide variety of areas. New cell culture microfluidic devices and platforms aim to improve control over different cell interactions and refine cell monitoring, searching for a real-time, low invasive analysis of a high number of events at the same time. Among all the materials, PMMA is highly used in the development of microfluidic devices because of its versatility and easy manipulation. While the material itself present good biocompatibility, it does not have very good properties for cell adhesion. In this chapter, PMMA was physicochemical modified with localized air plasma in order to improve PMMA surface hydrophilicity. Cell adhesion was tested using biochemical functionalization with collagen and fibronectin. Finally, microcontact printing was used for the patterning of different cell types with controlled cell localization and cell-cell contact.

The exploration of PMMA surface functionalization and cell-material interactions has allowed to improve the cell adhesion capabilities of the polymer, allowing no only the conversion of PMMA from cytophobic to cytophilic but the generation of controlled patterns of cells. Furthermore, this has also allowed to reduce the production time of the cell arrays when compared to the patterning on conventional cell culture materials and directly adapt the patterns into a simple proof-of-concept microfluidics device, making the process much more user-friendly. Combined with the SCADA or the transfection efficiency monitoring methods, this approach of cell patterning could contribute to the development of products for monitoring cell behaviour.

## 5.5. Supporting Information

*SI-1. PDMS channel specifications*

A PDMS channel was fabricated and adhered directly on top to the cell patterns through pressure sensitive adhesive, **Figure SI-1**.

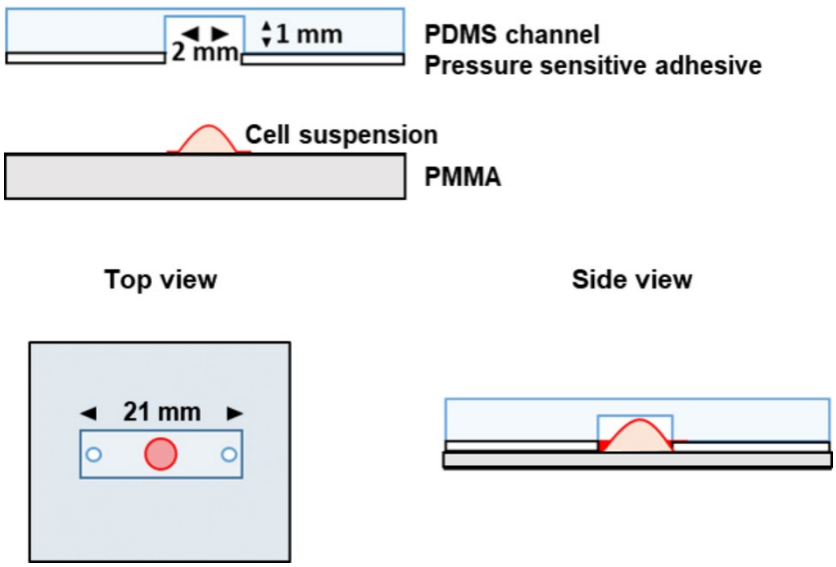


**Figure SI-1.** PDMS channel specifications.

### *SI-2. PMMA wells specifications*

In order to generate wells (2 cm) made of PMMA, three PMMA layers (4 mm) were cut with a laser and pasted both between them and with the glass cover with pressure sensitive adhesive (PSA). **Figure SI-2**.

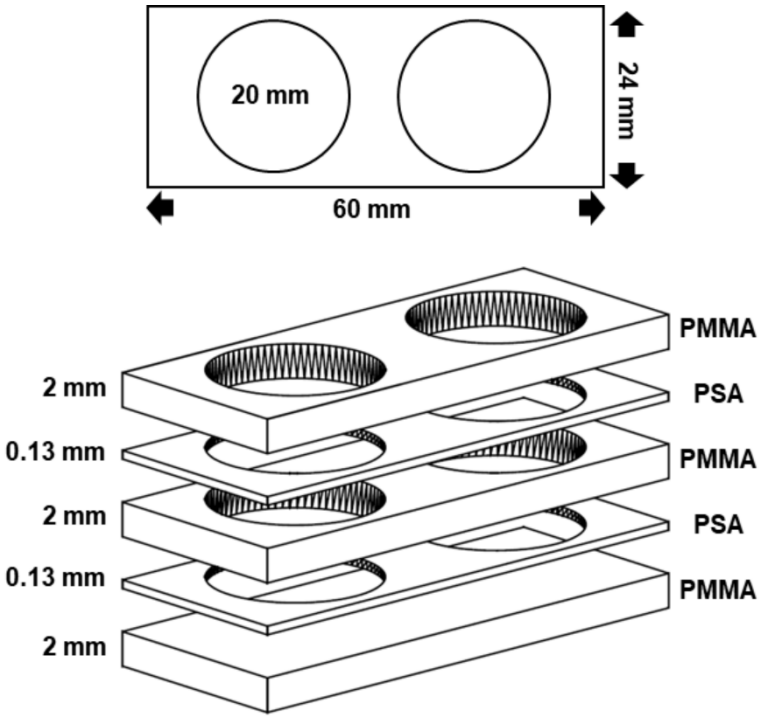


**Figure SI-2.** PMMA wells specifications.

*SI-3. Printed fibronectin features*

For the patterning of cells with different cell-cell contact and cell confluences, different arrays of fibronectin features were printed, **Figure SI-3**.

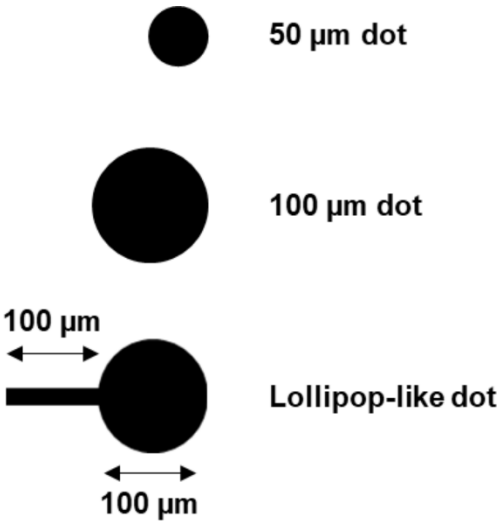


**Figure SI-3.** Fibronectin features printed for cell adhesion.

*SI-4. Patterning of PC3 on cell culture wells, glass covers and PMMA*

PDMS slabs containing a 3 mm hole were put on intimate contact with the bottom of cell culture polystyrene wells, glass covers and PMMA slides. The PDMS protected surfaces were oxidized using air plasma inside of a plasma cleaner with a power of 29.6 W for 150 seconds.

Microcontact printing of fibronectin was carried out. PDMS stamps, containing arrays of pillars of 100 μm dots, were wetted with 50 μL of a solution of fibronectin 50 μg $mL^{-1}$, BSA-TAMRA 6.25 μg $mL^{-1}$, for 30 minutes. Afterwards, the ink was removed and the PDMS stamps were rinsed with DI water and dried with compressed air. Each PDMS stamp was put in contact on top of the hydrophilic zones in the cell culture well, the glass cover or the PMMA surface. Finally, PDMS stamps were retrieved after 30 min.

Drops of 1 μL of PC3 cell suspension $10^6$ cells $mL^{-1}$ were put on top of the hydrophilic zones with the fibronectin patterns and incubated at 37º and 5% $CO_2$ inside a cell culture incubator for 1 hour with high humidity environment. Afterwards, 200 μL of their corresponding cell culture medium were flown three times through hydrostatic pressure in order to rinse non-adhere cells. Brightfield microscopy images were taken after rinsing.

Cells incubated on the cell culture wells and the glass covers adhered unspecifically throughout the surface, due to the lack of addition of a blocking agent, **Figure SI-4**. Contrary to that, patterns on the PMMA surface were highly specific, where cells did not adhered nor migrated outside of their respective dots due to the high contrast between the cytophilic fibronectin dot and the cytophobic PMMA.

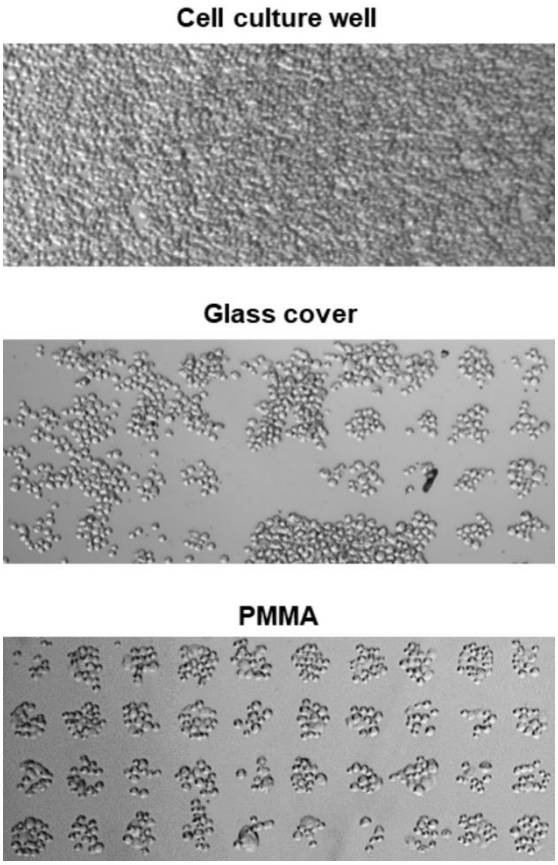


**Figure SI-4.** Brightfield images of PC3 on 100 µm dots fibronectin patterns with prior hydrophilic zone generation on cell culture polystyrene wells (top), glass cover (middle) and PMMA surface (bottom).

### *SI-5. Single PC3 cell patterning on PMMA*

In order to obtain single cell patterns on PMMA surfaces, a more conventional approach to μCP was tested.

PDMS stamps containing arrays of 20 μm dots separated by 50 μm were wetted with 50 μL of a fibronectin solution 50 μg $mL^{-1}$. Afterwards, the ink was removed and the PDMS stamps were rinsed with DI water and dried with compressed air. Each PDMS stamp was put in contact with the PMMA wells for 30 min. PMMA wells were previously oxidized using air plasma inside of a plasma cleaner with a power of 29.6 W for 150 seconds. PDMS stamps were retrieved, and wells were directly loaded with 750 mL of PC3 suspension $10^5$ cells $mL^{-1}$. Samples were left for 2 h on constant oscillation in a rocker inside an incubator at 37 ºC and 5 % $CO_2$ air atmosphere. Afterwards, samples were rinsed three times with PBS.

Single cells could be observed on the surface on the PMMA, see **Figure SI-5**. It should be noted that zones with no cells and zones with non-specific attachment could be observed, indicating that further optimization of the methodology is required.

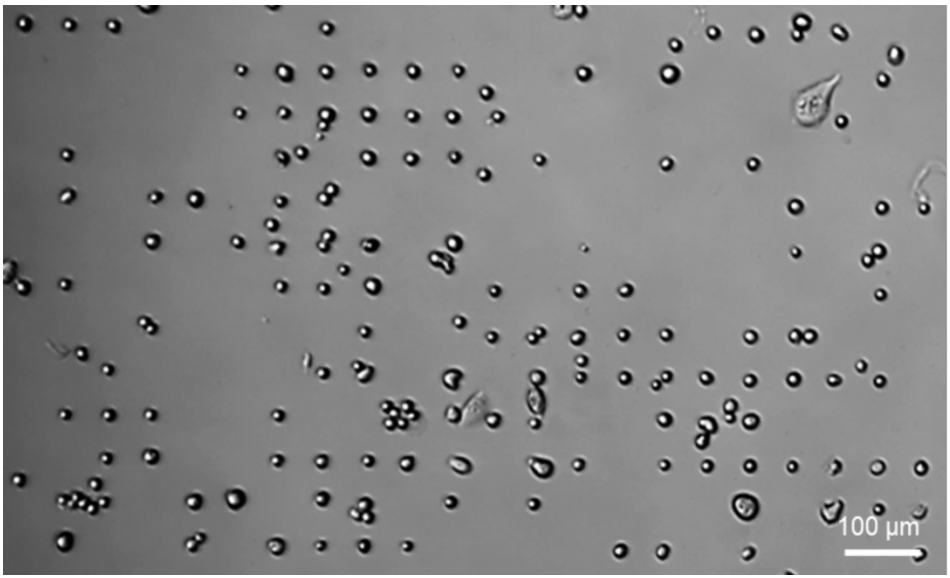


**Figure SI-5.** Brightfield microscopy image of single cell patterning of PC3 on PMMA surface.

## 5.6. References

(1) Streets, A. M.; Huang, Y. Chip in a Lab: Microfluidics for next Generation Life Science Research. *Biomicrofluidics* **2013**, *7* (1), 011302.

(2) Azuaje-Hualde, E.; García-Hernando, M.; Etxebarria-Elezgarai, J.; De Pancorbo, M.; Benito-Lopez, F.; Basabe-Desmonts, L. Microtechnologies for Cell Microenvironment Control and Monitoring. *Micromachines* **2017**, *8* (6), 166.

(3) Coluccio, M. L.; Perozziello, G.; Malara, N.; Parrotta, E.; Zhang, P.; Gentile, F.; Limongi, T.; Raj, P. M.; Cuda, G.; Candeloro, P.; Di Fabrizio, E. Microfluidic Platforms for Cell Cultures and Investigations. *Microelectron. Eng.* **2019**, *208*, 14–28.

(4) Matellan, C.; del Río Hernández, A. E. Cost-Effective Rapid Prototyping and Assembly of Poly(Methyl Methacrylate) Microfluidic Devices. *Sci. Rep.* **2018**, *8* (1), 6971.

(5) Liga, A.; Morton, J. A. S.; Kersaudy-Kerhoas, M. Safe and Cost-Effective Rapid-Prototyping of Multilayer PMMA Microfluidic Devices. *Microfluid. Nanofluidics* **2016**, *20* (12), 164.

(6) Rega, R.; Gennari, O.; Mecozzi, L.; Pagliarulo, V.; Mugnano, M.; Oleandro, E.; Nazzaro, F.; Ferraro, P.; Grilli, S. Pyro-Electrification of Freestanding Polymer Sheets: A New Tool for Cation-Free Manipulation of Cell Adhesion in Vitro. *Front. Chem.* **2019**, *7*, 429.

(7) Mecozzi, L.; Gennari, O.; Rega, R.; Grilli, S.; Bhowmick, S.; Gioffrè, M. A.; Coppola, G.; Ferraro, P. Spiral Formation at the Microscale by μ-Pyro-Electrospinning. *Soft Matter* **2016**, *12* (25), 5542–5550.

(8) Jaganjac, M.; Milković, L.; Cipak, A.; Mozetič, M.; Recek, N.; Žarković, N.; Vesel, A. Cell Adhesion On Hydrophobic Polymer Surfaces. *Mater. Tehnol.* **2012**, *1*, 53–56.

(9) Cai, S.; Wu, C.; Yang, W.; Liang, W.; Yu, H.; Liu, L. Recent Advance in Surface Modification for Regulating Cell Adhesion and Behaviors. *Nanotechnol. Rev.* **2020**, *9* (1), 971–989.

(10) Apostol, M.; Mironava, T.; Yang, N.-L.; Pernodet, N.; Rafailovich, M. H. Cell Sheet Patterning Using Photo-Cleavable Polymers. *Polym. J.* **2011**, *43* (8), 723–732.

(11) Riau, A. K.; Mondal, D.; Yam, G. H. F.; Setiawan, M.; Liedberg, B.; Venkatraman, S. S.; Mehta, J. S. Surface Modification of PMMA to Improve Adhesion to Corneal Substitutes in a Synthetic Core–Skirt Keratoprosthesis. *ACS Appl. Mater. Interfaces* **2015**, *7* (39), 21690–21702.

(12) Patel, S.; Thakar, R. G.; Wong, J.; McLeod, S. D.; Li, S. Control of Cell Adhesion on Poly(Methyl Methacrylate). *Biomaterials* **2006**, *27* (14), 2890–2897.

(13) Welle, A.; Gottwald, E. UV-Based Patterning of Polymeric Substrates for Cell Culture Applications. *Biomed. Microdevices* **2002**, *4*, 33–41.

(14) Kanioura, A.; Constantoudis, V.; Petrou, P.; Kletsas, D.; Tserepi, A.; Gogolides, E.; Chatzichristidi, M.; Kakabakos, S. Oxygen Plasma Micro-Nanostructured PMMA Plates and Microfluidics for Increased Adhesion and Proliferation of Cancer versus Normal Cells: The Role of Surface Roughness and Disorder. *Micro Nano Eng.* **2020**, *8*, 100060.

(15) Detrait, E.; Lhoest, J.-B.; Knoops, B.; Bertrand, P.; van den Bosch de Aguilar, P. Orientation of Cell Adhesion and Growth on Patterned Heterogeneous Polystyrene Surface. *J. Neurosci. Methods* **1998**, *84* (1–2), 193–204.

(16) Schmalenberg, K. E.; Uhrich, K. E. Micropatterned Polymer Substrates Control Alignment of Proliferating Schwann Cells to Direct Neuronal Regeneration. *Biomaterials* **2005**, *26* (12), 1423–1430.

(17) Schmalenberg, K. E.; Buettner, H. M.; Uhrich, K. E. Microcontact Printing of Proteins on Oxygen Plasma-Activated Poly(Methyl Methacrylate). *Biomaterials* **2004**, *25* (10), 1851–1857.

(18) Heino, J. The Collagen Family Members as Cell Adhesion Proteins. *Bioessays* **2007**, *29* (10), 1001–1010.

(19) Hsiao, C.-T.; Cheng, H.-W.; Huang, C.-M.; Li, H.-R.; Ou, M.-H.; Huang, J.-R.; Khoo, K.-H.; Yu, H. W.; Chen, Y.-Q.; Wang, Y.-K.; Chiou, A.; Kuo, J.-C. Fibronectin in Cell Adhesion and Migration via N-Glycosylation. *Oncotarget* **2017**, *8* (41), 70653–70668.

(20) Gonzalez-Pujana, A.; Santos-Vizcaino, E.; García-Hernando, M.; Hernaez-Estrada, B.; M. de Pancorbo, M.; Benito-Lopez, F.; Igartua, M.; Basabe-Desmonts, L.; Hernandez, R. M. Extracellular Matrix Protein Microarray-Based Biosensor with Single Cell Resolution: Integrin Profiling and Characterization of Cell-Biomaterial Interactions. *Sensors Actuators B Chem.* **2019**, *299*, 126954.

(21) Garcia-Hernando, M.; Calatayud-Sanchez, A.; Etxebarria-Elezgarai, J.; de Pancorbo, M. M.; Benito-Lopez, F.; Basabe-Desmonts, L. Optical Single Cell Resolution Cytotoxicity Biosensor Based on Single Cell Adhesion Dot Arrays. *Anal. Chem.* **2020**, *92* (14), 9658–9665.

(22) Azuaje-Hualde, E.; Rosique, M.; Calatayud-Sanchez, A.; Benito-Lopez, F.; M de Pancorbo, M.; Basabe-Desmonts, L. Continuous Monitoring of Cell Transfection Efficiency with Micropatterned Substrates. *Biotechnol. Bioeng.* **2021**, bit.27783.

(23) Zhang, X.; Jones, P.; Haswell, S. Attachment and Detachment of Living Cells on Modified Microchannel Surfaces in a Microfluidic-Based Lab-on-a-Chip System. *Chem. Eng. J.* **2008**, *135*, S82–S88.

(24) Murthy, S. K.; Radisic, M. Cell Adhesion and Detachment. *Encycl. Microfluid. Nanofluidics* **2013**, 1–9.

(25) Salvi, J. D.; Lim, J. Y.; Donahue, H. J. Finite Element Analyses of Fluid Flow Conditions in Cell Culture. *Tissue Eng. Part C Methods* **2010**, *16* (4), 661–670.

Los apéndices 6 y 7 están sujetos a confidencialidad por el autor

# Section 4

## Acknowledgements

**Acknowledgements to the financial support**

Enrique Azuaje Hualde acknowledges funding from the Basque Government, Department of Education, for predoctoral fellowship 2016. Authors of the experimental works acknowledge funding support from Basque Government, under Grupos Consolidados with Grant No. IT1271-19, from Gobierno de España, Ministerio de Economia y Competitividad, with Grant No. BIO2016-80417-P (AEI/FEDER, UE) and from the DNASURF (H2020-MSCA-RISE-778001) project.

**Acknowledgements to the technical assistance**

Authors of the experimental works thank for technical and human support provided by PhD Maite Alvarez from DNA Bank Service (SGIker) of the University of the Basque Country (UPV/EHU) and European funding (ERDF and ESF). The authors also thank for technical and human support provided by “Analytical and High-Resolution Microscopy in Biomedice” SGIker (UPV/EHU/ ERDF, EU). Authors wish to thank the intellectual and technical assistance from the ICTS “NANBIOSIS”, more specifically by the Drug Formulation Unit (U10) of the CIBER in Bioengineering, Biomaterials & Nanomedicine (CIBER-BBN). Authors thank Dr. Alberto Gorrochategui from “Clínica Dermatológica Ercilla (Bilbao)” for providing the hair follicles from where hHF-MSCs were extracted. Authors thank the technical assistance of the Finally, authors also wish to thank the technical assistance from the Nanopharmagene research group at the University of the Basque Country (UPV/EHU).

**Acknowledgements to the editorials**

Authors thank the editorials MDPI, Elsevier and Wiley for granting the permission to reuse the published articles in this thesis.

# Section 5

## Scientific outputs

## Published peer-reviewed scientific articles

3 scientific articles have been published from the results of this thesis:

1. *Azuaje-Hualde, E.; García-Hernando, M.; Etxebarria-Elezgarai, J.; De Pancorbo, M.; Benito-Lopez, F.; Basabe-Desmonts, L. Microtechnologies for Cell Microenvironment Control and Monitoring. Micromachines 2017, 8 (6), 166. https://doi.org/10.3390/mi8060166.*

2. *Azuaje-Hualde, E.; Arroyo-Jimenez, S.; Garai-Ibabe, G.; de Pancorbo, M. M.; Benito-Lopez, F.; Basabe-Desmonts, L. Naked Eye Y Amelogenin Gene Fragment Detection Using DNAzymes on a Paper-Based Device. Anal. Chim. Acta 2020, 1123, 1–8. https://doi.org/10.1016/j.aca.2020.05.010.*

3. *Azuaje-Hualde, E.; Rosique, M.; Calatayud-Sanchez, A.; Benito-Lopez, F.; M de Pancorbo, M.; Basabe-Desmonts, L. Continuous Monitoring of Cell Transfection Efficiency with Micropatterned Substrates. Biotechnol. Bioeng. 2021, bit.27783. https://doi.org/10.1002/bit.27783.*

## Manuscripts in preparation

Currently, 5 scientific manuscripts are in preparation for their future publication in international journals from the results of this thesis:

1. *Azuaje-Hualde, E.; De Pancorbo, M; Benito-Lopez, F.; Basabe-Desmonts, L. Integrated Cell Culture Systems for the Biosensing of Cell Secretion: Critical Review.*

2. *Azuaje-Hualde, E.; De Pancorbo, M; Benito-Lopez, F.; Basabe-Desmonts, L. Paper based microfluidic analytical device for single-step detection of mesenchymal stromal cells secreted VEGF.*

3. *Azuaje-Hualde, E.; Komen, J.; den Berg, A.; De Pancorbo, M; Benito-Lopez, F.; der Meer, A.; Basabe-Desmonts, L. Cell patterning on polymethyl methacrylate through controlled physicochemical and biochemical functionalization.*

4. *Azuaje-Hualde, E.; Alvarez-Braña, Y.; De Pancorbo, M; Benito-Lopez, F.; Basabe-Desmonts, L. Highly efficient presentation of FGF-2 to small cell-colonies through microbead patterns.*

5. *Azuaje-Hualde, E.; De Pancorbo, M; Benito-Lopez, F.; Basabe-Desmonts, L. Highly efficient detection of VEGF secretion from small colonies of adherent cells*

## Published peer-reviewed proceedings

3 scientific proceedings have been published from the results of this thesis:

1. *Azuaje-Hualde, E.; Arroyo-Jimenez, S.; de Pancorbo, M. M.; Garai-Ibabe, G.; Benito-Lopez, F.; Basabe-Desmonts, L. Low-Cost Paper Device for Fast Gender Identification on Crime Scenes. 21st International Conference on Miniaturized Systems for Chemistry and Life Sciences, MicroTAS 2017.*

2. *Azuaje-Hualde, E.; de Pancorbo, M. M.; Benito-Lopez, F.; Basabe-Desmonts, L. Topographical and Chemical Patterning of Cell Culture Substrates. 21st International Conference on Miniaturized Systems for Chemistry and Life Sciences, MicroTAS 2017.*

3. *Azuaje-Hualde, E.; de Pancorbo, M. M.; Benito-Lopez, F.; Basabe-Desmonts, L. Paper Microfluidics Device for Label-Free Detection of Mesenchymal Stem Cells Secreted Vascular Endothelial Growth Factor. 24th International Conference on Miniaturized Systems for Chemistry and Life Sciences, MicroTAS 2020.*

## Conference presentations

4 written presentation (poster) and 1 oral presentation were presented in international conferences from results of this thesis:

1. *Azuaje-Hualde, E.; Arroyo-Jimenez, S.; de Pancorbo, M. M.; Garai-Ibabe, G.; Benito-Lopez, F.; Basabe-Desmonts, L. Low-Cost Paper Device for Fast Gender Identification on Crime Scenes. 21st International Conference on Miniaturized Systems for Chemistry and Life Sciences, MicroTAS 2017. (Poster).*

2. *Azuaje-Hualde, E.; de Pancorbo, M. M.; Benito-Lopez, F.; Basabe-Desmonts, L. Topographical and Chemical Patterning of Cell Culture Substrates. 21st International Conference on Miniaturized Systems for Chemistry and Life Sciences, MicroTAS 2017. (Poster).*

3. *Azuaje-Hualde, E.; Arroyo-Jimenez, S.; Garai-Ibabe, G.; de Pancorbo, M. M.; Benito-Lopez, F.; Basabe-Desmonts, L. Naked Eye Y Amelogenin Gene Fragment Detection Using DNAzymes on a Paper Device. 28th Congress of the International Society for Forensic Genetics, ISFG 2019. (Poster).*

4. *Azuaje-Hualde, E.; Rosique, M.; Calatayud-Sanchez, A.; Ojeda, E.; Benito-Lopez, F.; M de Pancorbo, M.; Basabe-Desmonts, L. Microtechnologies for Cell Transfection with Controlled Cell-Cell Contact. 8th International Congress of Histology and Tissue Engineering, SEHIT 2019. (Oral).*

5. *Azuaje-Hualde, E.; de Pancorbo, M. M.; Benito-Lopez, F.; Basabe-Desmonts, L. Paper Microfluidics Device for Label-Free Detection of Mesenchymal Stem Cells Secreted Vascular Endothelial Growth Factor. 24th International Conference on Miniaturized Systems for Chemistry and Life Sciences, MicroTAS 2020. (Poster).*